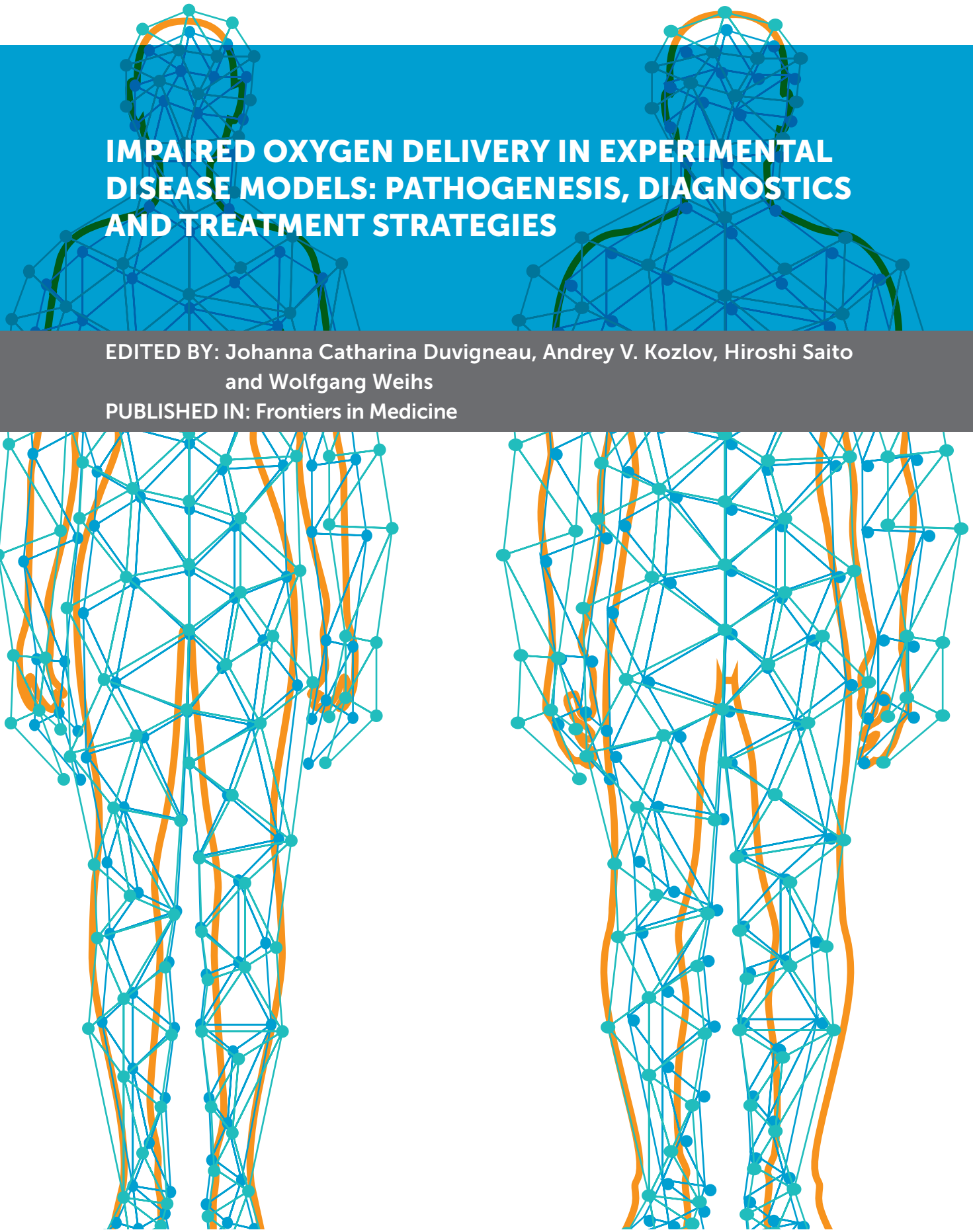

IMPAIRED OXYGEN DELIVERY IN EXPERIMENTAL DISEASE MODELS: PATHOGENESIS, DIAGNOSTICS AND TREATMENT STRATEGIES

EDITED BY: Johanna Catharina Duvigneau, Andrey V. Kozlov, Hiroshi Saito and Wolfgang Weihs

PUBLISHED IN: Frontiers in Medicine

frontiers Research Topics

frontiers

ISSN 1664-8714
ISBN 978-2-83250-171-9
DOI 10.3389/978-2-83250-171-9

About Frontiers

Frontiers is more than just an open-access publisher of scholarly articles: it is a pioneering approach to the world of academia, radically improving the way scholarly research is managed. The grand vision of Frontiers is a world where all people have an equal opportunity to seek, share and generate knowledge. Frontiers provides immediate and permanent online open access to all its publications, but this alone is not enough to realize our grand goals.

Frontiers Journal Series

The Frontiers Journal Series is a multi-tier and interdisciplinary set of open-access, online journals, promising a paradigm shift from the current review, selection and dissemination processes in academic publishing. All Frontiers journals are driven by researchers for researchers; therefore, they constitute a service to the scholarly community. At the same time, the Frontiers Journal Series operates on a revolutionary invention, the tiered publishing system, initially addressing specific communities of scholars, and gradually climbing up to broader public understanding, thus serving the interests of the lay society, too.

Dedication to Quality

Each Frontiers article is a landmark of the highest quality, thanks to genuinely collaborative interactions between authors and review editors, who include some of the world's best academicians. Research must be certified by peers before entering a stream of knowledge that may eventually reach the public - and shape society; therefore, Frontiers only applies the most rigorous and unbiased reviews.
Frontiers revolutionizes research publishing by freely delivering the most outstanding research, evaluated with no bias from both the academic and social point of view. By applying the most advanced information technologies, Frontiers is catapulting scholarly publishing into a new generation.

What are Frontiers Research Topics?

Frontiers Research Topics are very popular trademarks of the Frontiers Journals Series: they are collections of at least ten articles, all centered on a particular subject. With their unique mix of varied contributions from Original Research to Review Articles, Frontiers Research Topics unify the most influential researchers, the latest key findings and historical advances in a hot research area! Find out more on how to host your own Frontiers Research Topic or contribute to one as an author by contacting the Frontiers Editorial Office: frontiersin.org/about/contact

IMPAIRED OXYGEN DELIVERY IN EXPERIMENTAL DISEASE MODELS: PATHOGENESIS, DIAGNOSTICS AND TREATMENT STRATEGIES

Topic Editors:
Johanna Catharina Duvigneau, University of Veterinary Medicine Vienna, Austria
Andrey V. Kozlov, Institute for Experimental and Clinical Traumatology (LBG), Austria
Hiroshi Saito, University of Kentucky, United States
Wolfgang Weihs, Medical University of Vienna, Austria

Citation: Duvigneau, J. C., Kozlov, A. V., Saito, H., Weihs, W., eds. (2022). Impaired Oxygen Delivery in Experimental Disease Models: Pathogenesis, Diagnostics and Treatment Strategies. Lausanne: Frontiers Media SA.
doi: 10.3389/978-2-83250-171-9

Table of Contents

frontiers | Frontiers in Medicine

TYPE Editorial
PUBLISHED 25 August 2022
DOI 10.3389/fmed.2022.995958

OPEN ACCESS

EDITED AND REVIEWED BY
Ata Murat Kaynar,
University of Pittsburgh, United States

*CORRESPONDENCE
Johanna Catharina Duvigneau
catharina.duvigneau@vetmeduni.ac.at

SPECIALTY SECTION
This article was submitted to Intensive Care Medicine and Anesthesiology, a section of the journal Frontiers in Medicine

RECEIVED 16 July 2022
ACCEPTED 18 July 2022
PUBLISHED 25 August 2022

CITATION
Weihs W, Kozlov AV, Saito H and Duvigneau JC (2022) Editorial: Impaired oxygen delivery in experimental disease models: Pathogenesis, diagnostics and treatment strategies. *Front. Med.* 9:995958. doi: 10.3389/fmed.2022.995958

Editorial: Impaired oxygen delivery in experimental disease models: Pathogenesis, diagnostics and treatment strategies

Wolfgang Weihs[1], Andrey V. Kozlov[2,3], Hiroshi Saito[4] and Johanna Catharina Duvigneau[5]*

[1]Department of Emergency Medicine, Medical University of Vienna, Vienna, Austria, [2]Ludwig Boltzmann Institute for Traumatology, The Research Center in Cooperation With Allgemeine Unfallversicherungsanstalt (AUVA), Vienna, Austria, [3]Austrian Cluster for Tissue Regeneration, Vienna, Austria, [4]Department of Surgery, University of Kentucky, Lexington, KY, United States, [5]Department of Biomedical Sciences, University of Veterinary Medicine, Vienna, Austria

KEYWORDS

oxygen delivery, hemorrhagic shock, systemic inflammatory response, ischemia reperfusion injury, metabolism, hypoxia, hypothermia

Editorial on the Research Topic
Impaired oxygen delivery in experimental disease models: Pathogenesis, diagnostics and treatment strategies

This Research Topic is aimed at collecting contributions that help to shed more light on pathogenesis, diagnostics, and prospective therapeutic tools in critical clinical conditions resulting from impaired oxygen availability, such as cardiac arrest, hypoxia, ischemia, and sepsis. Emphasizing translational research, we invited the scientific community to contribute studies conducted with experimental animal models, as these allow the detailed analysis of the complex pathophysiological processes for developing new therapeutic strategies. Here we present nine contributions. Seven studies describe experimental results, mainly animal experiments, and two are reviews that expand our knowledge of the physiological and pathophysiological events associated with impaired oxygen delivery.

The review of Hof, Marcus et al. offers a "tool-box," comprising a combination of analyses to determine structural and functional changes of the microcirculation and of mitochondria that are applicable in studies using experimental animals for modeling septic complications and hemorrhagic shock. In order to accurately assess the consequences of impaired oxygen delivery on organ function, cell metabolism, and inflammatory processes, the authors further suggest magnetic resonance imaging as a non-invasive method.

The review of Bjertnæs et al. gives us a well-written overview about the physiological consequences of accidental hypothermia, a medical condition, which still has a high mortality rate. The authors describe guidelines for the rewarming procedure, which are

of relevance not only for the treatment of victims of accidental hypothermia, but may also interest those considering hypothermia as a therapeutic approach.

An additional insight in the association of hypothermia and hypoxia is given in the *in-vitro* study presented by Woyke et al., describing the combined effect of lowering temperature and increasing CO_2 levels on the oxygen dissociation curve in unbuffered human whole blood. The authors found that decreasing temperature leads to an increased oxygen affinity to hemoglobin. However, this temperature effect is outweighed by the CO_2-effect, inducing a right shift of the oxygen dissociation curve. Interestingly, the relative CO_2-effect was higher with decreasing temperature, indicating a significant interaction of temperature and pCO_2. Additionally, the CO_2-effect was diminished at higher CO_2 levels suggesting saturation effect. The study further suggests that levels of pCO_2 exceeding 40 mmHg may result in a too poor oxygen binding and an insufficient oxygen delivery within the system.

This study presented by Hof, Truse et al. compared the effect of locally applied CO_2 and O_2 on gastric and oral microcirculation in dogs subjected to hemorrhagic shock. The idea behind it was, that when applied locally, CO_2 at high concentrations increases the oxygen release from hemoglobin locally, which can be used to intentionally improve the oxygenation of hypoxic tissue. Indeed, local hypercapnia improved microvascular oxygenation and was associated with a continuous blood flow. Thus, local CO_2-application is able to improve oxygen saturation of hypoxic tissues better than application of oxygen and represents an interesting new minimally invasive approach to improve gastric microcirculation during hemorrhagic shock.

A deeper insight into the cellular metabolism associated with insufficient oxygen supply is given by the contribution of Graf et al. They used succinyl phosphonate as an inhibitor of 2-oxoglutarate dehydrogenase complex (OGDHC) in cerebellar tissue of pregnant and non-pregnant rats. Both, OGDHC inhibition by limiting NADH, and hypobaric hypoxia by limiting oxygen supply, perturb the respiratory chain function. OGDHC inhibition produced similar changes in the cerebellar amino acid pools, which were different between pregnant and non-pregnant rats. The authors suggest that chemical OGDHC inhibition is suitable for mimicking the metabolic changes induced by insufficient oxygen supply.

The study by Rutai et al. used a clinically relevant porcine model for mimicking human sepsis and septic shock and developed a standardized research protocol that allowed characterizing the progression of sepsis-related events. Their approach is to cluster the host responses into sepsis and septic shock groups using a specific porcine SOFA score including quantitative and qualitative assessment of blood CFUs along with the measurement of macro- and microcirculatory variables.

The study by Denoix et al. used a porcine long-term model of hemorrhagic shock and resuscitation with pre-existing atherosclerosis to investigate whether sodium thiosulfate, an H_2S releasing compound, exerts neuroprotective effects. However, despite its lung-protective efficacy in this model, neuro-histopathological analysis revealed no differences between groups, possibly because the blood brain barrier remained intact and neuronal tissue appeared relatively unaffected by the induced hemorrhagic shock. This research group additionally examined H_2S as a potential therapeutic in mice with deleted H_2S-producing cystathionine-γ-lyase (CSE). In a previous study, they could demonstrate sodium thiosulfate-mediated protection against traumatic/hemorrhagic shock induced injury (1).

Using the same model, the group next investigated the role of sodium thiosulfate in the CSE knock-out mice challenged with an underlying co-morbidity, such as diabetes. The data, which are presented by Gröger et al., show that traumatic/hemorrhagic shock in streptozotocin-induced diabetic mice led to severe circulatory failure, strong manifestation of an inflammatory response, and an increased tissue expression of typical stress response markers, however, none was prevented by the application of sodium thiosulfate. These findings are of translational significance, since they show that an underlying co-morbidity not only worsens the shock induced pathophysiological changes, but may also diminish efficacy of the therapeutic approach.

Finally, the contribution of Szabó-Biczók et al. dealt with the side effects of therapeutic restoration of oxygen supply using veno-venous extracorporeal membrane oxygenation (ECMO). Although ECMO can save lives in respiratory distress, it has serious side-effects as it frequently induces acute kidney injury. Therefore, the group developed a clinically relevant model using Vietnamese minipigs for a prolonged ECMO protocol (30 h). The described protocol induced acute renal impairment, which was demonstrated by a significantly decreased renal function with signs of structural damage and impaired mitochondrial function. It is therefore a good tool to further study therapeutic interventions for decreasing acute kidney injury introduced by ECMO.

Author contributions

JCD and WW planned the Editorial. WW wrote the first draft. JCD and AVK performed major revisions of the text. All authors contributed and approved the submitted version of the article.

Conflict of interest

The authors declare that the research was conducted in the absence of any commercial or financial relationships that could be construed as a potential conflict of interest.

Publisher's note

References

1. Gröger M, Hogg M, Abdelsalam E, Kress S, Hoffmann A, Stahl B, et al. Effects of sodium thiosulfate during resuscitation from trauma-and-hemorrhage in cystathionine gamma lyase (CSE) knockout mice. *Shock*. (2022) 57:131–9. doi: 10.1097/SHK.0000000000001828

frontiers in Medicine

BRIEF RESEARCH REPORT
published: 17 December 2021
doi: 10.3389/fmed.2021.751639

Inhibition of 2-Oxoglutarate Dehydrogenase as a Chemical Model of Acute Hypobaric Hypoxia

Anastasia Graf[1,2,3], *Alexander Ksenofontov*[3] *and Victoria Bunik*[3,4,5]*

[1] *Faculty of Biology, Lomonosov Moscow State University, Moscow, Russia,* [2] *Faculty of Nano-, Bio-, Informational and Cognitive and Socio-Humanistic Sciences and Technologies, Moscow Institute of Physics and Technology, Moscow, Russia,* [3] *Andrey Nikolaevich (A. N.) Belozersky Institute of Physicochemical Biology, Lomonosov Moscow State University, Moscow, Russia,* [4] *Faculty of Bioengineering and Bioinformatics, Lomonosov Moscow State University, Moscow, Russia,* [5] *Biochemistry Department, Sechenov University, Moscow, Russia*

Both hypoxia and inhibition of 2-oxoglutarate dehydrogenase complex (OGDHC) are known to change cellular amino acid pools, but the quantitative comparison of the metabolic and physiological outcomes has not been done. We hypothesize that OGDHC inhibition models metabolic changes caused by hypoxia, as both perturb the respiratory chain function, limiting either the NADH (OGDHC inhibition) or oxygen (hypoxia) supply. In the current study, we quantify the changes in the amino acid metabolism after OGDHC inhibition in the highly sensitive to hypoxia cerebellum and compare them to the earlier characterized changes after acute hypobaric hypoxia. In addition, the associated physiological effects are characterized and compared. A specific OGDHC inhibitor succinyl phosphonate (SP) is shown to act similar to hypoxia, increasing levels of many amino acids in the cerebellum of non-pregnant rats, without affecting those in the pregnant rats. Compared with hypoxia, stronger effects of SP in non-pregnant rats are observed on the levels of cerebellar amino acids, electrocardiography (ECG), and freezing time. In pregnant rats, hypoxia affects ECG and behavior more than SP, although none of the stressors significantly change the levels of cerebellar amino acids. The biochemical differences underlying the different physiological actions of SP and hypoxia are revealed by correlation analysis of the studied parameters. The negative correlations of cerebellar amino acids with OGDHC and/or tryptophan, shown to arise after the action of SP and hypoxia, discriminate the overall metabolic action of the stressors. More negative correlations are induced in the non-pregnant rats by hypoxia, and in the pregnant rats by SP. Thus, our findings indicate that the OGDHC inhibition mimics the action of acute hypobaric hypoxia on the cerebellar amino acid levels, but a better prediction of the physiological outcomes requires assessment of integral network changes, such as increases in the negative correlations among the amino acids, OGDHC, and/or tryptophan.

Keywords: brain metabolism of amino acids, hypoxia, 2-oxoglutarate dehydrogenase, pregnancy, succinyl phosphonate

OPEN ACCESS

Edited by:
Wolfgang Weihs,
Medical University of Vienna, Austria

Reviewed by:
Ivana Budic,
University of Niš, Serbia
Alisdair Fernie,
Max Planck Institute of Molecular Plant Physiology, Germany

***Correspondence:**
Victoria Bunik
bunik@belozersky.msu.ru

Specialty section:
This article was submitted to Intensive Care Medicine and Anesthesiology, a section of the journal Frontiers in Medicine

Received: *01 August 2021*
Accepted: *15 November 2021*
Published: *17 December 2021*

Citation:
Graf A, Ksenofontov A and Bunik V (2021) Inhibition of 2-Oxoglutarate Dehydrogenase as a Chemical Model of Acute Hypobaric Hypoxia. Front. Med. 8:751639. doi: 10.3389/fmed.2021.751639

INTRODUCTION

Molecular mechanisms of complex pathophysiological phenomena are often studied in their chemical models. For instance, pentylenetetrazol is widely employed to model epilepsy (1), while mitochondrial impairment in neurodegenerative diseases is often modeled by exposure of animals to inhibitors of the respiratory chain (2, 3). The high sensitivity of mitochondrial complex II to inhibition by malonate and 3-nitropropionic acid (3-NP) is used to model Huntington's disease (2, 4). Bioactivation of 1-methyl-4-phenyl-1,2,3,6-tetrahydropyridine (MPTP) to its toxic 1-methyl-4-phenylpyridinium cation by glial monoamine oxidase B (5) may contribute to Parkinson's-disease-like localization of the damage, making this inhibitor of complex I useful to create the disease models (6). However, interpretations of similar models employing another such inhibitor, rotenone, are complicated by its side effects, not considered in the original model suggestion. As revealed by now, some of the rotenone actions may be caused not only by targeting complex I of the respiratory chain (3, 7). Thus, translational value of the results obtained in the chemical models of pathologies essentially depends on the knowledge of molecular features of the complex pathophysiology, which are reproduced by the model, and those which characterize the substance-specific action. In particular, although mitochondrial impairment occurs upon inhibition of either complex I or II, different downstream pathways are activated by each of specific mitochondrial inhibitors, potentially reproducing the symptoms specific for particular neurodegenerative diseases (8).

Hypoxic damage to cells, tissues, and organisms is widely studied because hypoxia is a component of many different pathologies. The higher the oxygen dependence of a tissue or an organism, the higher their sensitivity to hypoxia and the more deleterious the consequences. For instance, as a major oxygen consumer, the brain is prone to increased risk of hypoxia-induced insults. Many diseases of the central nervous system (CNS), such as stroke, encephalopathies, and Parkinson's or Alzheimer's diseases, are associated with hypoxia. On the other hand, pregnancy imposes additional oxygen demands to support the mother and growing fetus, which is manifested in a higher sensitivity to hypoxia of pregnant vs. non-pregnant women (9). Hypoxia during pregnancy has profound adverse effects on maternal and fetal health, being the main cause of pregnancy complications, such as preeclampsia and intrauterine growth restriction. A challenging question is to what extent these specific physiological features are addressed by this or that model of hypoxia. However, very often, this question is ignored, whereas the usage of specific chemical models of hypoxia is hidden under the definition "hypoxic stress" (10, 11). For instance, a rather high concentration of $CoCl_2$ (0.15 mM) is used to model hypoxia (11), although it is known that, despite the similarity in some changes induced by hypoxia or $CoCl_2$ administration, their causes are disparate (12). Hypoxia perturbs the oxygen-requiring terminal step of the respiratory chain, i.e., the reaction catalyzed by cytochrome oxidase (complex IV of the respiratory chain). This perturbation decreases the mitochondrial capacity to produce energy through oxidative phosphorylation. The question arises, how similar the metabolic changes induced by hypoxia are to those induced by other perturbations of mitochondrial energy production? In a wider context, the question applies to the treatment of diseases having convergent symptoms yet induced by different molecular causes. We and others have shown that hypoxic damage to an organism includes perturbations in the amino acid pools (9, 13). Remarkably, this action of hypoxia is not reproduced in the $CoCl_2$ models of hypoxia (12) but is highly reminiscent of the perturbations in the amino acid profiles by specific inhibition of the mitochondrial 2-oxoglutarate dehydrogenase multienzyme complex (OGDHC), observed in different biosystems *in situ* and *in vivo* (13). Apart from its involvement in amino acid metabolism, the OGDHC inhibition decreases the production of NADH to be oxidized by the respiratory chain. We, therefore, hypothesized that Succinyl phosphonate (SP) administration may be a fruitful model of hypoxia, reproducing not only the energetic impairments but also the metabolic action of hypoxia on the amino acid pool. As free amino acids are involved in protein synthesis, energy production, neurotransmission, and immunity, changes in cellular amino acid pools may be important mediators of the pathological cascades induced by hypoxia.

The goal of the current study is to characterize the inhibition of the Tricarboxylic Acid (TCA) cycle flux through OGDHC as a chemical model of hypoxia. To achieve this goal, we quantify the changes in the amino acid metabolism, induced by a short-term inhibition of OGDHC, and compare them to those after acute hypobaric hypoxia, characterized in our previous study (9). We reveal qualitatively similar, physiological-state-dependent consequences of the OGDHC inhibition and hypoxia for the levels of free amino acids. Using a previously developed sensitive approach to quantify metabolic changes beyond the steady-state concentration of metabolites (9, 14, 15), we show that the induced homeostatic responses, manifested in the insult-specific sets of changed metabolic correlations, are not necessarily the same for SP and hypoxia. As a result, the biochemical actions of SP and hypoxia are more similar in the non-pregnant than pregnant rats. The characterized physiological effects of OGDHC inhibition and hypoxia are shown to depend not only on the changed levels of amino acids but also on the induction of negative interdependences between amino acids and OGDHC and/or tryptophan by SP or hypoxia.

MATERIALS AND METHODS

Animals

All the experiments were in accordance with the Guide for the Care and Use of Laboratory Animals (European Union Directives 86/609/EEC and 2010/63/EU), and approved by the Bioethics Committee of Lomonosov Moscow State University (protocol number 69-o from 09.06.2016). The animals were kept at 21 ± 2°C and relative humidity 53 ± 5% with the 12/12 h light/dark cycle (lights on 9:00 and lights off 21:00). The rats were purchased from the State Research Center of the

Russian Federation—Institute for Biomedical Problems, Russian Academy of Sciences, and were adapted to our conditions for 2 weeks before they entered experimental settings. Five to six animals were kept in one T/4K cage. Standard rodent pellet food (laboratorkorm.ru) and tap water were available *ad libitum*.

Wistar female rats, pregnant ($n = 29$) and non-pregnant ($n = 38$), of about 250–300 g (2.5–3.0 months) were used in the experiment. Two virgin female rats were located in a cage with one male. After 24 h, vaginal smears were analyzed. The first day of pregnancy was considered to be the day of the sperm detection in the vaginal smear. After that, the male rats were removed from the cage.

Six groups of female rats were used for comparison: (1) normoxic non-pregnant, $n = 17$; (2) hypoxic non-pregnant, $n = 8$; (3) non-pregnant with intranasal administration of SP, $n = 13$; (4) normoxic pregnant, $n = 8$; (5) hypoxic pregnant, $n = 10$; and (6) pregnant with intranasal application SP, $n = 11$. The animals from several independent experiments were pooled. The animals were decapitated after the physiological assessment was completed, 24 h after the treatments. Cerebella were quickly excised and stored at −70°C prior to the biochemical analyses. A half of each cerebellum was used to prepare the homogenates for enzymatic assays, the other half—to prepare the methanol-acetic acid extracts for the amino acid analysis.

Acute Hypobaric Hypoxia

Female rats were exposed to hypobaric hypoxia in a decompression (altitude) chamber by decreasing the atmospheric pressure, as described previously (9). The pregnant rats were exposed to hypoxia at the 9–10th day of pregnancy, roughly corresponding to the first trimester of human pregnancy (16, 17). This period is critical for organogenesis.

Administration of the OGDH Inhibitor SP to Animals

The animals received SP at 5 mg/kg by intranasal application of the water solution of the trisodium salt, with 0.9% NaCl substituting for SP in all reference groups. Intranasal administration was applied as it provided high bioavailability of the administered substances to the brain (18, 19). Administration of SP to pregnant rats was done on the 9–10th day of pregnancy.

Behavioral Parameters

The "Open Field" test ("OpenScience", Moscow, Russia) was used to quantify anxiety level, exploratory, and locomotor activities 24 h after exposure to SP or hypoxia. Exploratory activity and anxiety were assessed cumulatively as described previously (20).

Electrocardiography

Electrocardiography (ECG) was registered as described previously (20) using non-invasive ECG recording. The balance of autonomous regulation of heart rate was assessed according to the published method (21) by calculating the following parameters: average R–R interval in a sample, ms; parasympathetic, or relaxation, index of the state of the nervous system—RMSSD; sympathetic, or stress, index of the state of the nervous system—SI (21, 22).

OGDHC Assays

We used euthanasia by decapitation 24 h after a treatment (0.9% sodium chloride, SP, or hypoxia). The cerebella were quickly excised on ice, frozen in liquid nitrogen, and stored at −70°C. Homogenization of cerebella and assays of their OGDHC activity were performed as described earlier (23) with the recent modifications introduced in (22).

Ninhydrine Quantification of Amino Acids

Methanol/acetic acid extracts of cerebella were prepared according to a published protocol (24) and stored at −70°C. Amino acids were quantified in 50 μl of the extracts injected to an ion-exchange column 2622SC(PH) (Hitachi, Ltd., P/N 855-3508, 4.6 × 80 mm, Japan), eluted by the step gradient of sodium-acetate buffers according to the published procedure (9).

Data Acquisition and Statistics

Statistical analysis was performed using the GraphPad Prism 7.0 software (GraphPad Software Inc., CA, USA) and Statistica 10.0 (StatSoft Inc., Tulsa, OK, USA). The values are presented as means ± SEM. Statistical significance of differences upon the comparison of more than the two experimental groups was assessed using two-way ANOVA with Tukey's *post-hoc* test. The Pearson′s correlations between the levels of different amino acids or between the levels of amino acids and OGDHC activity were characterized by the correlation coefficients and *p*-values of the correlation. Statistical significance of differences in the elaborated earlier parameters to characterize metabolic interactions between the levels of OGDHC activity and/or amino acids (9, 14, 15), was assessed by the Wilcoxon signed-rank test. Differences with $p \leq 0.05$ were considered significant. Differences with $0.05 < p \leq 0.1$ were considered as trends.

RESULTS

Changes in the Levels of Free Amino Acids in Cerebella of the SP-Exposed vs. Control Female Rats Depend on Pregnancy, Similar to the Changes After Acute Hypobaric Hypoxia

Figure 1 (NP) shows that exposures of non-pregnant female rats to either SP or acute hypobaric hypoxia have similar effects, increasing the levels of many amino acids in the cerebellum. In most cases, the levels of the amino acids are increased more by SP than hypoxia. This feature is evident by comparison of not only the corresponding mean values but also the values of p characterizing the statistical significance of the differences to the control groups.

As shown earlier, pregnant rats mostly do not differ from non-pregnant rats in their cerebellar amino acid levels, with only glutamate and tryptophan being higher in the pregnant

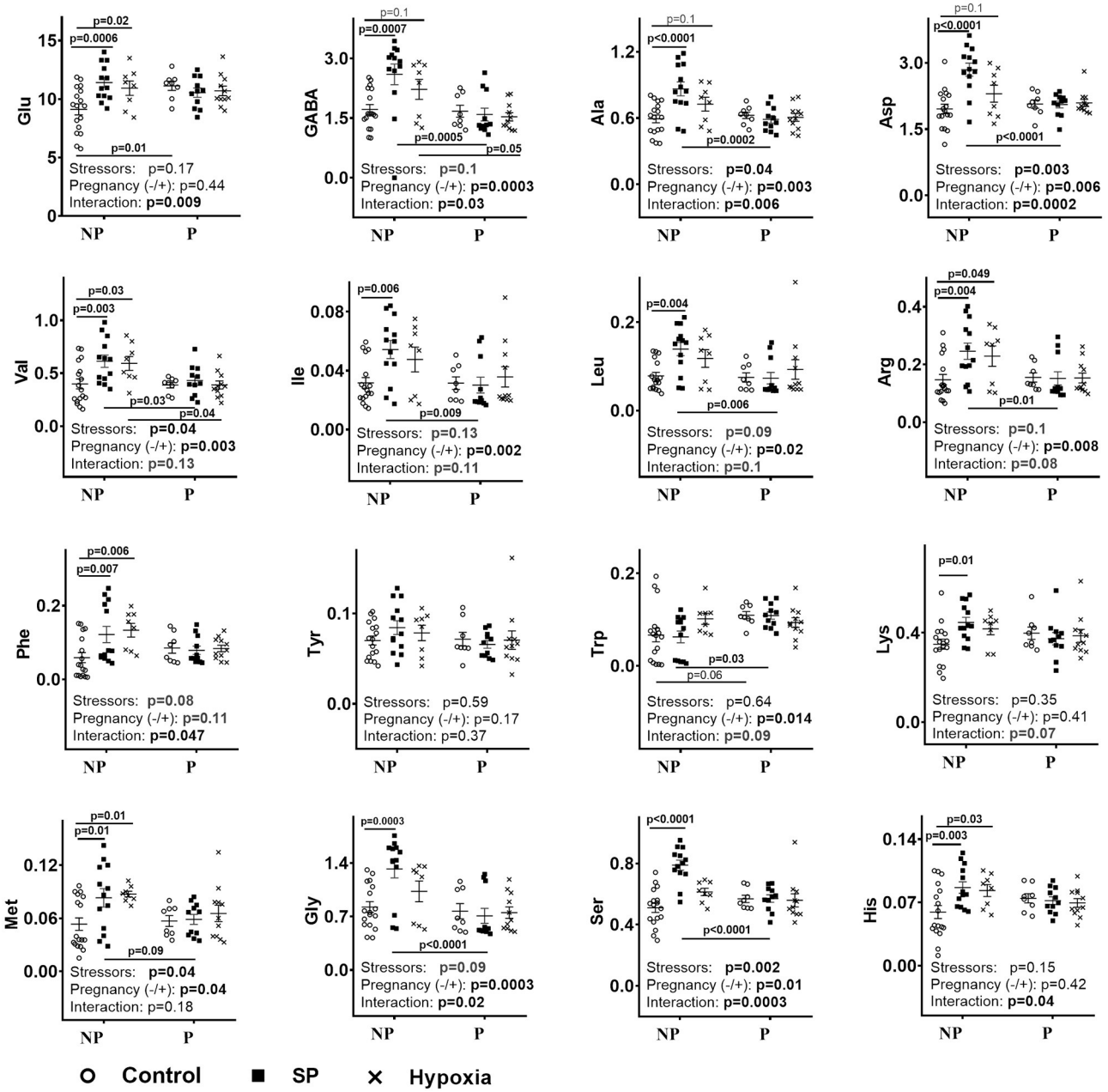

FIGURE 1 | Influence of succinyl phosphonate (SP) on the cerebellar levels of amino acids in the non-pregnant (NP) and pregnant (P) rats and comparison of the SP effects to those of acute hypobaric hypoxia. The content of free amino acids indicated on *Y*-axes is shown in micromoles per grams of fresh tissue weight. NP—non-pregnant rats: control $n = 17$, SP $n = 13$, hypoxia $n = 8$. P—pregnant rats: control $n = 8$, SP $n = 11$, hypoxia $n = 10$. The comparison of the effects of SP and hypoxia employs the data on hypoxic rats obtained earlier (9). Statistical analysis by two-way ANOVA is described in Methods. Statistically significant differences between the groups determined by the *post-hoc* test, and significance of the factors (stressors SP or hypoxia and pregnancy) and their interaction determined by ANOVA, are given on the graphs.

vs. non-pregnant rats (9). However, neither hypoxia nor SP changes the cerebellar amino acids in pregnant rats (**Figure 1**, P). Due to these disparate effects on the non-pregnant and pregnant rats, both SP and hypoxia induce differences between these rat groups in cerebellar levels of many amino acids, which are absent before the treatments. Regarding the pre-existing differences, both treatments eliminate the difference in the glutamate levels, whereas the difference in the tryptophan level is preserved after SP treatment, but lost after hypoxia (**Figure 1**, NP vs. P).

TABLE 1 | Analysis of the succinyl phosphonate SP-induced changes in interdependence of the levels of amino acids and OGDHC activity in cerebella of the NP and P rats.

Groups	Non-pregnant rats (NP)								Pregnant rats (P)							
	∑		X		+		–		∑		X		+		–	
Parameter	Control	SP	Control	SP	Control	SP	Control	SP	Control	SP	Control	SP	Control	SP	Control	SP
OGDHC	4.27	6.96	0.27	0.43	1	0	0	6	6.04	5.08	0.38	0.32	0	0	0	1
ALA	9.45	11.78	0.59	0.74	10	12	0	1	8.95	11.06	0.60	0.69	3	9	0	0
ARG	10.89	11.73	0.68	0.73	13	12	0	0	10.19	11.47	0.68	0.72	5	11	0	1
ASP	8.65	8.99	0.54	0.56	9	8	0	1	9.12	6.97	0.61	0.44	0	2	0	1
GABA	10.21	9.93	0.64	0.62	11	10	0	1	9.29	11.70	0.62	0.73	5	11	0	1
GLU	10.59	10.40	0.66	0.65	14	11	0	1	5.28	4.89	0.35	0.31	0	1	0	1
GLY	9.62	11.25	0.60	0.70	10	11	0	0	9.28	11.59	0.62	0.72	4	10	0	1
HIS	9.61	11.62	0.60	0.73	11	12	0	0	5.82	9.44	0.39	0.59	1	7	0	0
ILE	10.59	11.69	0.66	0.73	12	12	0	1	9.81	11.68	0.65	0.73	6	11	0	1
LEU	10.39	11.58	0.65	0.72	12	12	0	1	9.95	11.70	0.66	0.73	6	11	0	1
LYS	7.24	10.81	0.45	0.68	4	11	0	0	9.72	10.27	0.65	0.64	2	8	0	1
MET	8.42	6.29	0.53	0.39	9	5	0	0	5.67	9.97	0.38	0.62	0	9	0	2
PHE	9.89	7.84	0.62	0.49	8	8	0	0	9.21	11.70	0.61	0.73	1	12	0	1
SER	8.16	8.76	0.51	0.55	12	9	0	0	7.78	8.06	0.52	0.50	1	3	0	1
TRP	4.49	5.97	0.28	0.37	2	3	0	0	6.13	10.32	0.41	0.65	0	0	0	10
TYR	9.18	11.77	0.57	0.74	11	13	0	0	10.49	9.05	0.70	0.57	5	8	0	0
VAL	10.63	6.92	0.66	0.43	13	7	0	0	5.09	9.70	0.34	0.61	1	7	0	1
Sum or Average	**152.28**	**164.27**	**0.56**	**0.60**	**162**	**156**	**0**	**12**	**137.82**	**164.67**	**0.54**	**0.61**	**40**	**120**	**0**	**24**
p vs. control	*0.11*		*0.12*				**0.018**		**0.05**		**0.04**		**0.0007**		**0.0014**	
p NP vs. P													**0.05**	**0.0009**	*0.14*	

For the 2-oxoglutarate dehydrogenase complex (OGDHC) activity (OGDHC) and each of the amino acids, the arithmetic sum of its correlation coefficients (absolute values) to other amino acids (Σ), average correlation coefficient (X) calculated from the absolute values, and the total number of statistically significant positive (+) and negative (–) correlations are shown. At the bottom, the sum (in case of Σ, positive and negative correlations) or average (in case of X) of all the values in the row are presented, along with p values of the differences between these parameters in the control and SP groups (p vs. control), or between NP and P rats (p NP vs. P), estimated by the Wilcoxon signed rank test. NP rats: control n = 17. SP n = 13; P rats: control n = 8. SP n = 11. The parameters exhibiting statistically significant differences and the corresponding p-values are marked in bold. The p-values at the level of a trend are shown in italic.

Correlation Analysis of Changes in Metabolic Interdependence Between the Cerebellar OGDHC Activity and/or Amino Acids Levels in the Female Rats

Correlation analysis characterizing the relationships between the quantified parameters is a powerful tool to unravel integral changes in metabolic networks, which may be hidden upon analysis of the mean values because of homeostatic mechanisms, effected to stabilize these values (9, 14, 15). The correlations of **Supplementary Table 1** form the condition- and physiological-state-dependent patterns which may be quantified by the summarized and mean correlation coefficients, and the number of positive and negative correlations, presented in **Table 1**. This analysis reveals a significant difference in the correlation patterns of the non-pregnant and pregnant rats (**Table 1**, **Supplementary Table 1**), reciprocating the different reactivity of the amino acid levels in these rats to SP exposure (**Figure 1**). SP induces negative correlations between the OGDHC activity and several amino acids in the non-pregnant rats (**Supplementary Table 1A**), with the effect not pronounced in the pregnant rats (**Supplementary Table 1B**). Instead, in the cerebella of pregnant rats, SP induces negative correlations between tryptophan and several amino acids (**Supplementary Table 1B**). This metabolic action is specific to SP, as it is not observed in the pregnant rats exposed to hypoxia (9). The summarized correlations show the degree of interdependence between the components of the metabolic network, characterizing the network state (9, 15). In particular, the sum and average of the correlation coefficients tend to increase interdependence in the SP-treated non-pregnant rats vs. the control group ($p \sim 0.1$), but only the difference in the number of negative correlations in these groups is statistically significant ($p = 0.018$) (**Table 1**). In contrast, in pregnant rats, SP strongly increases all the parameters characterizing the interdependence between OGDHC activity and/or amino acids levels (**Table 1**). A higher increase in interdependence of amino acids in the SP-exposed pregnant vs. non-pregnant rats, compared with the respective control groups, manifests greater reorganization of the metabolic network in response to SP in the pregnant vs. non-pregnant rats. This is in good accord with the higher stabilization of the amino acid levels in the cerebella of the pregnant vs. non-pregnant rats (**Figure 1**).

Thus, the stabilization of the amino acid levels in the cerebellum of SP-treated pregnant rats (**Figure 1**, P) is achieved along with their increased interdependence (**Table 1**). In the non-pregnant rats, where the less prominent perturbation in

TABLE 2 | Induction by SP or acute hypobaric hypoxia of negative correlations of OGDHC or tryptophan with amino acids in the cerebella of NP or P rats.

Groups	Non-pregnant rats (NP)						Pregnant rats (P)					
	∑ OGDHC			∑ TRP			∑ OGDHC			∑ TRP		
Parameter	**Control**	**SP**	**Hypoxia**	**Control**	**SP**	**Hypoxia**	**Control**	**SP**	**Hypoxia**	**Control**	**SP**	**Hypoxia**
TRP or OGDHC	0.71	0.46	0.53	0.71	0.46	0.53	0.85	−0.32	0.05	0.85	−0.32	0.05
ALA	0.12	−0.58	−0.94	0.39	0.15	−0.68	−0.35	−0.34	−0.17	−0.21	−0.58	−0.02
ARG	−0.3	−0.45	−0.94	−0.14	0.25	−0.66	−0.33	−0.25	−0.03	−0.45	−0.77	−0.52
ASP	−0.47	−0.66	−0.9	−0.4	*−0.44*	−0.33	−0.04	−0.67	−0.06	0.01	−0.04	0.58
GABA	−0.4	−0.61	−0.95	−0.3	−0.32	−0.56	−0.55	−0.21	−0.12	−0.55	−0.73	−0.45
GLU	0.06	−0.72	−0.84	0.3	−0.36	−0.39	0.33	*−0.58*	−0.22	0.64	0.52	0.89
GLY	−0.4	−0.35	−0.95	−0.41	0.39	−0.56	−0.51	−0.23	−0.15	−0.59	−0.78	−0.49
HIS	−0.11	−0.39	−0.94	−0.05	0.40	−0.58	0.76	−0.32	0.03	0.53	−0.43	0.3
ILE	−0.35	−0.58	−0.95	−0.1	0.04	−0.56	−0.44	−0.21	0.14	−0.46	−0.8	−0.39
LEU	−0.31	−0.64	−0.95	−0.17	−0.04	−0.6	−0.42	−0.24	0.19	−0.48	−0.78	−0.27
LYS	0.28	−0.29	−0.69	0.62	0.39	−0.67	0.07	0.27	0.24	−0.08	−0.84	0.33
MET	0	0	−0.65	−0.05	0.77	−0.43	−0.15	0.24	0.63	−0.63	−0.91	−0.31
PHE	−0.24	−0.17	−0.95	−0.25	0.06	−0.6	−0.04	−0.11	0.08	−0.43	−0.81	−0.64
SER	0.03	−0.5	−0.19	0.01	−0.34	−0.11	0.36	0.42	0.44	0.02	−0.66	0.12
TYR	0.32	−0.45	−0.89	0.47	0.69	−0.63	−0.08	−0.32	0.13	−0.26	−0.57	0.09
VAL	−0.18	0.35	0.11	−0.11	0.024	0.69	0.76	0.48	0.36	0.79	0.22	−0.79
Sum	**−1.24**	**−5.58**	**−11.09**	**0.52**	**2.12**	**−6.14**	**0.22**	**−2.39**	**1.54**	**−1.3**	**−8.28**	**−1.52**
p vs. control	**0.008**	**0.0008**			**0.005**						**0.0004**	
p SP vs. hypoxia		***0.002***			***0.01***			***0.001***			***0.006***	
p P vs. NP							**0.007**	**0.0006**		**0.006**	**0.003**	

∑ *OGDHC—the algebraic sum of correlation coefficients of the OGDHC activity and each of the amino acids.*

∑ *TRP—the algebraic sum of correlation coefficients of tryptophan and each of the other amino acids or OGDHC activity.*

NP rats: control n = 17, SP n = 13, hypoxia n = 8. P rats: control n = 8, SP n = 11, hypoxia n = 10.

The three bottom lines show p values of the statistically significant ($p < 0.05$) differences between the indicated groups, estimated by the Wilcoxon signed rank test.

The strength of the negative correlations is estimated by the algebraic sum of correlation coefficients of OGDHC or tryptophan with other components. The algebraic sums for the hypoxic rats have been calculated using the published data (9). The parameters exhibiting statistically significant differences and the corresponding p-values are marked in bold. The p-values at the level of a trend are shown in italic.

the metabolic interdependence between OGDHC and/or amino acids is observed in the SP-treated vs. control rats (**Table 1**), the levels of amino acids increase (**Figure 1**, NP).

Comparison of the Changes in the Amino Acid Metabolism, Induced by SP or Hypoxia

The impact of SP on the metabolic interdependencies between OGDHC and/or amino acids in both the non-pregnant and pregnant rats is most robustly observed from the increased number of the negative correlations (**Table 1** and **Supplementary Table 1**). However, this effect of SP involves different components in different metabolic networks. In the non-pregnant rats, it is the OGDHC activity that becomes negatively correlated with multiple amino acids, whereas in the pregnant rats it is the tryptophan level that becomes negatively correlated with many amino acids (**Supplementary Table 1**).

Thus, in addition to the levels of free amino acids (**Figure 1**) or arithmetic sums characterizing the metabolic interdependencies in general (i.e., both positive and negative ones) (9, 14, 15), the abundance of negative metabolic interdependencies of amino acids with the OGDHC activity or tryptophan levels is estimated in this work to compare the metabolic actions of SP and acute hypobaric hypoxia. **Table 2** shows that both SP and hypoxia induce negative interdependencies. However, this change occurs to different degrees, dependent on specific perturbation (SP or hypoxia) or physiological state (pregnant or non-pregnant). In the non-pregnant rats, hypoxia increases negative interdependencies of both OGDHC and tryptophan, while SP does so with the OGDHC interdependencies only. Moreover, the algebraic sum of the correlation coefficients (**Table 2**) indicates that the increase in the negative interdependencies by SP is less pronounced than the one by hypoxia. Thus, in the non-pregnant rats, SP increases the negative correlations less than hypoxia does, while the opposite is observed in the pregnant rats (**Table 2**).

Comparison of the Physiological Effects of SP and Hypoxia

The data presented in **Figure 2** compare the physiological actions of SP or hypoxia. First of all, similar to the biochemical parameters (**Figure 1**), the physiological ones (**Figure 2**) show different reactivities to SP and/or hypoxia in the non-pregnant and pregnant rats. The RMSSD and SI are changed

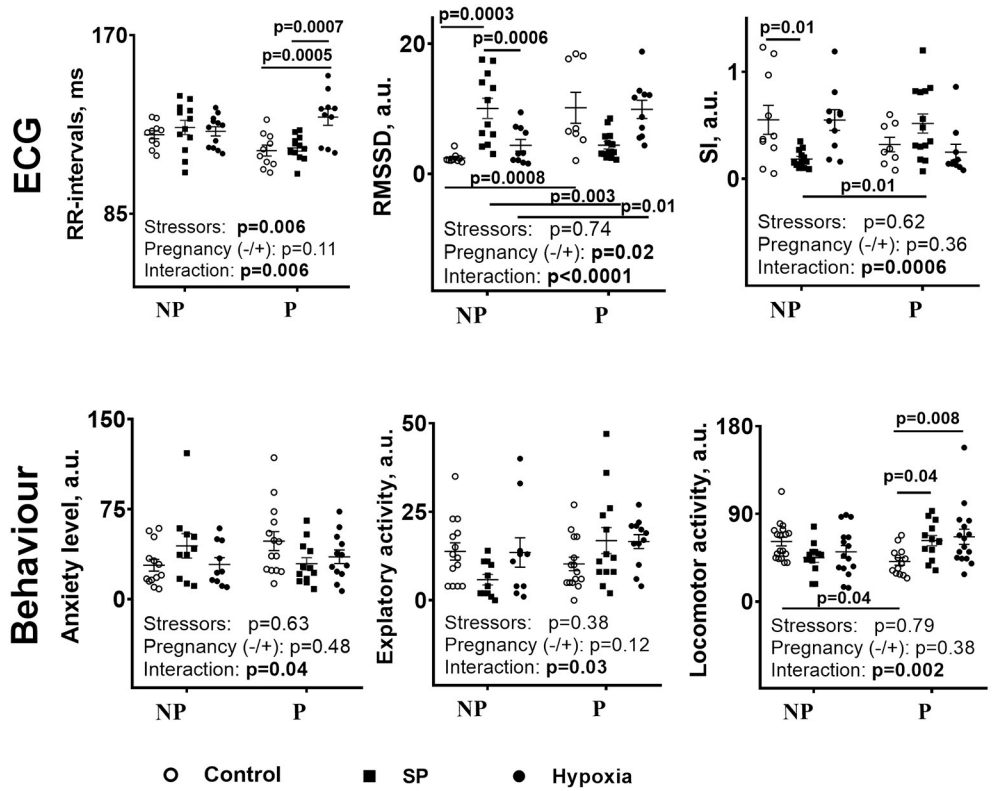

FIGURE 2 | Comparison of the influence of SP or acute hypobaric hypoxia on physiological parameters of the NP and P rats. NP—the non-pregnant rats: control $n = 17$, SP $n = 13$, hypoxia $n = 12$. P—pregnant rats: control $n = 10$, SP $n = 13$, and hypoxia $n = 10$. Statistical analysis by two-way ANOVA is described in Methods. Both the *post-hoc*-test-determined statistically significant differences between the groups and ANOVA-determined significance of the factors (stressors SP or hypoxia and pregnancy) and their interaction are given on the graphs.

by SP and/or hypoxia in the non-pregnant rats, whereas the R–R intervals, anxiety, and locomotion—in the pregnant rats. As a result, differences in the ECG and behavioral parameters between the non-pregnant and pregnant rats arise, (**Figure 2**, SI), disappear (**Figure 2**, locomotion, anxiety), or reverse (**Figure 2**, RMSSD), similar to the differences in the cerebellar amino acids content (**Figure 1**). Second, in the non-pregnant rats, a more pronounced, compared with hypoxia, the action of SP on animal physiology is seen in RMSSD and SI (**Figure 2**), similar to the more pronounced action of SP vs. hypoxia on the cerebellar amino acids content (**Figure 1**). In the pregnant rats, anxiety is decreased and locomotion is increased by SP, not hypoxia (**Figure 2**), in good accord with the SP-specific induction of the negative correlations of tryptophan with amino acids and OGDHC (**Table 2**). Finally, the different actions of SP and hypoxia on the tryptophan correlations in the pregnant rats (**Table 2**), associated with the disappearance of the difference in the tryptophan levels between the pregnant and non-pregnant rats after hypoxia (**Figure 1**), corresponds to the hypoxia-specific action on R–R interval in the pregnant rats (**Figure 2**, R–R interval).

Thus, the actions of SP and hypoxia on the non-pregnant and pregnant rats demonstrate several common features when the cerebellar amino acid content (**Figure 1**) and metabolic interactions (**Table 2**) are compared. The physiological responses (**Figure 2**) correspond to quantitative differences between the SP- and hypoxia-induced changes.

DISCUSSION

In this study, we have established a chemical model of acute hypoxia by showing high similarity in the actions of a specific inhibitor of OGDHC (SP) and acute hypobaric hypoxia on the cerebellar amino acid pool. The similarity is obvious from quantifications of the average levels of the cerebellar amino acids, and change reactivities of the amino acids to SP or hypoxia with pregnancy (**Figure 1**). Similar physiological consequences of animal exposure to acute hypobaric hypoxia or SP are also known from our previous studies, where the dependence of such responses on physiological differences imposed by sex has been shown upon exposure to SP or hypoxia of the adult animals (25) and in utero (26). From the metabolic viewpoint, the similarity is based on the fact that mitochondrial NADH oxidation by oxygen in the respiratory chain may be impaired both by inhibition of OGDHC and hypoxia. In the former case, the impairment is due to the limited NADH production

in the tricarboxylic acid cycle, whereas in the latter case it is due to the limited oxygen availability. Remarkably, similarity in the action of the perturbed OGDHC function and hypoxia has been recently characterized by the stabilization of the hypoxia-inducible factor (HIF) in both cases (27). Thus, in good accord with the intimate relationship between metabolic perturbations and signaling systems whose action is always directed to normalize the perturbation, similar consequences of the OGDHC inhibition and hypoxia are revealed at both the metabolic and signaling levels.

More specific insights in the SP- or hypoxia-induced changes in the amino acid metabolic network are revealed by correlation analysis of the interdependencies between the network components (9, 15). In particular, this analysis pinpoints another common feature of the action of SP and hypoxia, which is the reversal of the correlation sign from positive to negative for many correlations of OGDHC or tryptophan with amino acids. The appearance of the negative correlations between OGDHC and amino acids may be interpreted as increased degradation of amino acids through OGDHC. The appearance of the negative correlations between amino acids and tryptophan, associated with preservation of the difference in the tryptophan levels between the non-pregnant and pregnant rats, implies that the levels of tryptophan upon the action of SP in pregnant rats are stabilized at the expense of other amino acids.

Compared with SP, hypoxia induces more negative metabolic interdependences in the non-pregnant rats (**Table 2**), associated with a higher stabilization of the levels of amino acids in the non-pregnant rats after hypoxia than after SP (**Figure 1**, NP). In contrast, in pregnant rats, hypoxia affects the interdependencies of either OGDHC or tryptophan much less than SP does, which is especially obvious regarding tryptophan (**Table 2**). As mentioned above, the SP-changed correlations of tryptophan in the pregnant rats presumably preserve the difference in the tryptophan levels between the pregnant and non-pregnant rats. Indeed, the difference is lost after hypoxia not affecting the tryptophan correlations in the pregnant rats (**Table 2**, **Supplementary Table 1**, **Figure 1**, Trp). It thus appears that the OGDHC- or tryptophan-involving pathways of the female rat cerebellum are the pathways with the highest reorganization during the perturbations induced by SP or hypoxia. Yet the reorganization of these pathways may occur to a different degree depending on physiological settings (pregnancy) and perturbation type (SP or hypoxia). These quantitative differences (**Table 2**) manifest in the stressor-specific physiological outcomes (**Supplementary Table 1**).

Supplementary Table 2 compares the overall changes in the amino acids/OGDHC metabolic network, induced by SP (characterized in the current study), and acute hypobaric hypoxia [studied previously in reference (9)]. The comparison indicates that the SP action is more similar to that of hypoxia in the non-pregnant than pregnant rats (**Supplementary Table 2**). Although increases in the summarized and average correlation coefficients are less pronounced after SP treatment ($p = 0.1$) compared with hypoxia ($p < 0.01$) (**Supplementary Table 2A**), the number of the negative correlations of the amino acid levels with the OGDHC activity is significantly increased by both SP and hypoxia (**Supplementary Table 2B**). This analysis confirms the leading role of the reorganization of the OGDHC-involving pathways in the SP- or hypoxia-induced perturbations. In the pregnant rats, the consequences of the actions of SP and hypoxia on the free amino acid levels are similar (**Figure 1**), yet this similarity is achieved through different adaptations of the metabolic network to the insults (**Table 2** and **Supplementary Table 2**). The difference is due to the fact that SP strongly affects the tryptophan-involving pathways only in the pregnant rats, while hypoxia exerts such an effect in the non-pregnant rats. The finding that in the non-pregnant rats, hypoxia strongly affects both the OGDHC and tryptophan interdependencies with amino acids, corresponds to a higher impact of hypoxia vs. SP on the amino acid metabolic network in this animal group (**Supplementary Table 2**). In contrast, in the pregnant rats, it is the SP-induced perturbation in the tryptophan metabolic network, not observed after hypoxia, that provides for a higher network impact of SP vs. hypoxia (**Supplementary Table 2**). These quantitative differences between the SP and hypoxia network action in pregnant rats manifest in the physiological effects of SP on the anxiety and locomotor activity, absent in the hypoxic rats (**Figure 2**).

In view of the critical contribution of tryptophan metabolism to the cerebellar response to SP or hypoxia (**Figure 1**; **Table 2**), multiple studies pointing to the pregnancy-changed tryptophan metabolism are worth noting. This change is important both for fetus and mother, associated with the pregnancy-increased metabolic, energy, and oxygen demands (28–32). In pregnant rats, serotonin (33) and NAD (34) syntheses from tryptophan are increased, with the kinurenine pathway of the tryptophan degradation being critical for early embryonic brain development (35). The preservation by SP of the differences in the tryptophan levels in the pregnant vs. non-pregnant rats, which is not observed after hypoxia (**Figure 1**), may contribute to the SP-exerted protection from the action of hypoxia, known from our earlier studies of the effects of SP and/or hypoxia on adult animals and offspring (22, 23, 25, 26). The importance of amino-acids-related metabolism and signaling in pregnancy is underlined by the mTOR-controlled interaction between fetal growth and maternal supply (36). As discussed in our previous work (9), pregnancy-imposed changes in the mTOR signaling may be linked to the degradation of amino acids through the OGDHC-limited tricarboxylic acid cycle. This is supported by the critical difference in responses of the OGDHC-related amino acid metabolism to SP and hypoxia between the non-pregnant and pregnant rats, shown in our current work.

CONCLUSIONS

Regarding the cerebellar metabolism of amino acids, specific inhibition of OGDHC mimics acute hypobaric hypoxia, with the similarity of the metabolic actions higher in the non-pregnant

than pregnant rats. The highest impact of the OGDHC inhibition and hypoxia is shown on the pathways involving OGDHC and tryptophan.

DATA AVAILABILITY STATEMENT

The original contributions presented in the study are included in the article/**Supplementary Material**, further inquiries can be directed to the corresponding author/s.

ETHICS STATEMENT

The animal study was reviewed and approved by the Ethics Committee of Lomonosov Moscow State University (protocol number 69-o from 09.06.2016).

AUTHOR CONTRIBUTIONS

VB: conceptualization, writing—original draft preparation, supervision, project administration, and funding acquisition. AG and AK: methodology, software, and validation. AG: formal analysis, investigation, data curation, and visualization. AG, AK, and VB: resources and writing—review and editing. All authors read and agreed to the published version of the manuscript.

FUNDING

This research was funded by the Russian Science Foundation grant number N 18-14-00116 to VB.

ACKNOWLEDGMENTS

We thank Dr. L. Trofimova (MSU, Biology Department) for participation in the preparation of cerebellar extracts. Dr. A. Kazantsev and Prof. N. Lukashev (MSU, Chemistry Dept.) for synthesis and purification of SP.

SUPPLEMENTARY MATERIAL

The Supplementary Material for this article can be found online at: https://www.frontiersin.org/articles/10.3389/fmed.2021.751639/full#supplementary-material

REFERENCES

1. Lisgaras CP, Mikroulis A, Psarropoulou C. Region-specific effects of early-life status epilepticus on the adult hippocampal CA3–medial entorhinal cortex circuitry *in vitro*: focus on interictal spikes and concurrent high-frequency oscillations. *Neuroscience.* (2021) 466:235-47. doi: 10.1016/j.neuroscience.2021.04.030
2. Yang L, Shi Q, Ho DJ, Starkov AA, Wille EJ, Xu H, et al. Mice deficient in dihydrolipoyl succinyl transferase show increased vulnerability to mitochondrial toxins. *Neurobiol Dis.* (2009) 36:320–30. doi: 10.1016/j.nbd.2009.07.023
3. Innos J, Hickey MA. Using rotenone to model parkinson's disease in mice: a review of the role of pharmacokinetics. *Chem Res Toxicol.* (2021) 34:1223–39. doi: 10.1021/acs.chemrestox.0c00522
4. Stavrovskaya AV, Voronkov DN, Yamshchikova NG, Ol'shanskiy AS, Khudoerkov RM, Illarioshkin SN. Experience of experimental modelling of huntington's disease. *Hum Physiol.* (2016) 42:898–904. doi: 10.1134/S0362119716080120
5. Kupsch A, Sautter J, Götz ME, Breithaupt W, Schwarz J, Youdim MBH, et al. Monoamine oxidase-inhibition WH, and MPTP-induced neurotoxicity in the non-human primate: comparison of rasagiline (TVP 1012) with selegiline. *J Neural Transm.* (2001) 108:985-1009. doi: 10.1007/s007020170018
6. Frim DM, Uhler TA, Galpern WR, Beal MF, Breakefield XO, Isacson O. Implanted fibroblasts genetically engineered to produce brain-derived neurotrophic factor prevent 1-methyl-4-phenylpyridinium toxicity to dopaminergic neurons in the rat. *Proc Natl Acad Sci.* (1994) 91:5104–08. doi: 10.1073/pnas.91.11.5104
7. Bisbal M, Sanchez M. Neurotoxicity of the pesticide rotenone on neuronal polarization: a mechanistic approach. *Neural Regen Res.* (2019) 14:762–6. doi: 10.4103/1673-5374.249847
8. Ranganayaki S, Jamshidi N, Aiyaz M, Rashmi S-K, Gayathri N, Harsha PK, et al. Inhibition of mitochondrial complex II in neuronal cells triggers unique pathways culminating in autophagy with implications for neurodegeneration. *Sci Rep.* (2021) 11:1483. doi: 10.1038/s41598-020-79339-2
9. Graf A, Trofimova L, Ksenofontov A, Baratova L, Bunik V. Hypoxic adaptation of mitochondrial metabolism in rat cerebellum decreases in pregnancy. *Cells.* (2020) 9:139. doi: 10.3390/cells9010139
10. Al-Rasheed NM, Fadda LM, Al-Rasheed NM, Attia H, Ali HM, El-Agami H. Role of natural antioxidants in the modulation of plasma amino acid pattern in rats exposed to hemic hypoxia. *Brazilian Arch Biol Technol.* (2015) 58:184–202. doi: 10.1590/S1516-89132015050224
11. Shahulhameed S, Swain S, Jana S, Chhablani J, Ali MJ, Pappuru RR, et al. A robust model system for retinal hypoxia: live imaging of calcium dynamics and gene expression studies in primary human mixed retinal culture. *Front Neurosci.* (2020) 13:1445. doi: 10.3389/fnins.2019.01445
12. Gleason JE, Corrigan DJ, Cox JE, Reddi AR, McGinnis LA, Culotta VC. Analysis of hypoxia and hypoxia-like states through metabolite profiling. *PLoS ONE.* (2011) 6:e2474. doi: 10.1371/journal.pone.0024741
13. Araújo WL, Trofimova L, Mkrtchyan G, Steinhauser D, Krall L, Graf A, et al. On the role of the mitochondrial 2-oxoglutarate dehydrogenase complex in amino acid metabolism. *Amino Acids.* (2013) 44:683-700. doi: 10.1007/s00726-012-1392-x
14. Aleshin VA, Mkrtchyan GV, Kaehne T, Graf AV, Maslova MV, Bunik VI. Diurnal regulation of the function of the rat brain glutamate dehydrogenase by acetylation and its dependence on thiamine administration. *J Neurochem.* (2020) 153:80-102. doi: 10.1111/jnc.14951
15. Tsepkova PM, Artiukhov AV, Boyko AI, Aleshin VA, Mkrtchyan GV, Zvyagintseva MA, et al. Thiamine induces long-term changes in amino acid profiles and activities of 2-oxoglutarate and 2-oxoadipate dehydrogenases in rat brain. *Biochemistry.* (2017) 82:723-36. doi: 10.1134/S0006297917060098
16. Zhao M, Liu T, Pang G. Intercellular wireless communication network between mother and fetus in rat pregnancy-a study on directed and weighted network. *Reprod Biol Endocrinol.* (2019) 17:40. doi: 10.1186/s12958-019-0485-8
17. Patten AR, Fontaine CJ, Christie BR. A comparison of the different animal models of fetal alcohol spectrum disorders and their use in studying complex behaviors. *Front Pediatr.* (2014) 2:93. doi: 10.3389/fped.2014.00093
18. Badhan RKS, Kaur M, Lungare S, Obuobi, S. Improving brain drug targeting through exploitation of the nose-to-brain route: a physiological and pharmacokinetic perspective. *Curr Drug Deliv.* (2014) 11:458–71. doi: 10.2174/1567201811666140321113555
19. Djupesland PG, Messina JC, Mahmoud RA. The nasal approach to delivering treatment for brain diseases: an anatomic, physiologic, and delivery technology overview. *Ther Deliv.* (2014) 5:709–33. doi: 10.4155/tde.14.41

20. Aleshin VA, Graf AV, Artiukhov AV, Boyko AI, Ksenofontov AL, Maslova MV, et al. Physiological and biochemical markers of the sex-specific sensitivity to epileptogenic factors, delayed consequences of seizures and their response to vitamins B1 and B6 in a rat model. *Pharmaceuticals.* (2021) 14:737. doi: 10.3390/ph14080737
21. Baevsky RM, Chernikova AG. Heart rate variability analysis: physiological foundations and main methods. *Cardiometry.* (2017) 10:66-76. doi: 10.12710/cardiometry.2017.10.6676
22. Graf A, Trofimova L, Loshinskaja A, Mkrtchyan G, Strokina A, Lovat M, et al. Up-regulation of 2-oxoglutarate dehydrogenase as a stress response. *Int J Biochem Cell Biol.* (2013) 45:175–89. doi: 10.1016/j.biocel.2012.07.002
23. Trofimova L, Lovat M, Groznaya A, Efimova E, Dunaeva T, Maslova M, et al. Behavioral impact of the regulation of the brain 2-oxoglutarate dehydrogenase complex by synthetic phosphonate analog of 2-oxoglutarate: implications into the role of the complex in neurodegenerative diseases. *Int J Alzheimers Dis.* (2010) 3:1–8. doi: 10.4061/2010/749061
24. Ksenofontov AL, Boyko AI, Mkrtchyan GV, Tashlitsky VN, Timofeeva AV, Graf AV, et al. Analysis of free amino acids in mammalian brain extracts. *Biochemistry.* (2017) 82:1183-92.. doi: 10.1134/S000629791710011X
25. Artiukhov AV, Graf AV, Bunik VI. Directed regulation of multienzyme complexes of 2-oxo acid dehydrogenases using phosphonate and phosphinate analogs of 2-oxo acids. *Biochemistry.* (2016) 81:1498-521. doi: 10.1134/S0006297916120129
26. Graf A, Kabysheva M, Klimuk E, Trofimova L, Dunaeva T, Zündorf G, et al. Role of 2-oxoglutarate dehydrogenase in brain pathologies involving glutamate neurotoxicity. *J Mol Catal B Enzym.* (2009) 61:80-7. doi: 10.1016/j.molcatb.2009.02.016
27. Burr SP, Costa ASH, Grice GL, Timms RT, Lobb IT, Freisinger P, et al. Mitochondrial protein lipoylation and the 2-oxoglutarate dehydrogenase complex controls hif1α stability in aerobic conditions. *Cell Metab.* (2016) 24:740-52. doi: 10.1016/j.cmet.2016.09.015
28. Xu K, Liu H, Bai M, Gao J, Wu X, Yin Y. Redox properties of tryptophan metabolism and the concept of tryptophan use in pregnancy. *Int J Mol Sci.* (2017) 18:1595. doi: 10.3390/ijms18071595
29. Groer M, Fuchs D, Duffy A, Louis-Jacques A, D'Agata A, Postolache TT. Associations among obesity, inflammation, and tryptophan catabolism in pregnancy. *Biol Res Nurs.* (2018) 20:284-91. doi: 10.1177/1099800417738363
30. Badawy AA-B, Namboodiri AMA, Moffett JR. The end of the road for the tryptophan depletion concept in pregnancy and infection. *Clin Sci.* (2016) 130:1327-33. doi: 10.1042/CS20160153
31. van Lee L, Cai S, Loy SL, Tham EKH, Yap FKP, Godfrey KM, et al. Relation of plasma tryptophan concentrations during pregnancy to maternal sleep and mental well-being: the GUSTO cohort. *J Affect Disord.* (2018) 225:523-9. doi: 10.1016/j.jad.2017.08.069
32. Badawy AA-B. Tryptophan metabolism, disposition and utilization in pregnancy. *Biosci Rep.* (2015) 35:e00261. doi: 10.1042/BSR20150197
33. Russo S, Kema I, Bosker F, Haavik J, Korf J. Tryptophan as an evolutionarily conserved signal to brain serotonin: molecular evidence and psychiatric implications. *World J Biol Psychiatry.* (2009) 10:258-68. doi: 10.3109/15622970701513764
34. Wertz AW, Lojkin ME, Bouchard BS, Derby MB. Tryptophan-niacin relationships in pregnancy. *J Nutr.* (1958) 64:339–53. doi: 10.1093/jn/64.3.339
35. Pisar M, Forrest CM, Khalil OS, McNair K, Vincenten MCJ, Qasem S, et al. Modified neocortical and cerebellar protein expression and morphology in adult rats following prenatal inhibition of the kynurenine pathway. *Brain Res.* (2014) 1576:1-17. doi: 10.1016/j.brainres.2014.06.016
36. Gupta MB, Jansson T. Novel roles of mechanistic target of rapamycin signaling in regulating fetal growth†. *Biol Reprod.* (2019) 100:872-84. doi: 10.1093/biolre/ioy249

Conflict of Interest: The authors declare that the research was conducted in the absence of any commercial or financial relationships that could be construed as a potential conflict of interest.

Publisher's Note: All claims expressed in this article are solely those of the authors and do not necessarily represent those of their affiliated organizations, or those of the publisher, the editors and the reviewers. Any product that may be evaluated in this article, or claim that may be made by its manufacturer, is not guaranteed or endorsed by the publisher.

frontiers in Medicine

ORIGINAL RESEARCH
published: 07 February 2022
doi: 10.3389/fmed.2021.808025

Effects of Carbon Dioxide and Temperature on the Oxygen-Hemoglobin Dissociation Curve of Human Blood: Implications for Avalanche Victims

Simon Woyke[1,2], *Hermann Brugger*[1,2], *Mathias Ströhle*[1]*, *Thomas Haller*[3], *Hannes Gatterer*[2], *Tomas Dal Cappello*[2] *and Giacomo Strapazzon*[1,2]

[1] *Department of Anaesthesiology and Critical Care Medicine, Medical University of Innsbruck, Innsbruck, Austria,* [2] *Institute of Mountain Emergency Medicine, Eurac Research, Bolzano, Italy,* [3] *Institute of Physiology, Medical University of Innsbruck, Innsbruck, Austria*

OPEN ACCESS

Edited by:
Hiroshi Saito, University of Kentucky, United States

Reviewed by:
Lars Jakob Bjertnæs, Arctic University of Norway, Norway
Jason Qu, Massachusetts General Hospital and Harvard Medical School, United States

***Correspondence:**
Mathias Ströhle
Mathias.Stroehle@tirol-kliniken.at

Specialty section:
This article was submitted to Intensive Care Medicine and Anesthesiology, a section of the journal Frontiers in Medicine

Received: *02 November 2021*
Accepted: *20 December 2021*
Published: *07 February 2022*

Citation:
Woyke S, Brugger H, Ströhle M, Haller T, Gatterer H, Dal Cappello T and Strapazzon G (2022) Effects of Carbon Dioxide and Temperature on the Oxygen-Hemoglobin Dissociation Curve of Human Blood: Implications for Avalanche Victims. Front. Med. 8:808025. doi: 10.3389/fmed.2021.808025

Completely avalanche-buried patients are frequently exposed to a combination of hypoxia and hypercapnia with a risk of normothermic cardiac arrest. Patients with a long burial time and an air pocket are exposed to a combination of hypoxia, hypercapnia, and hypothermia which may lead to the development of the "triple H syndrome". This specific combination has several pathophysiological implications, particularly on the cardiovascular system and oxygen transport (oxygen supply and oxygen consumption). To examine the effects on hemoglobin oxygen affinity, we investigated venous blood samples from 15 female and 15 male healthy subjects. In a factorial design of four different carbon dioxide partial pressure (PCO_2) levels (20, 40, 60, and 80 mmHg) and five different temperature levels (13.7°C, 23°C, 30°C, 37°C, and 42°C), 30 unbuffered whole blood samples were analyzed in a newly developed *in vitro* method for high-throughput oxygen dissociation curve (ODC) measurements. P50s, Hill coefficients, CO_2-Bohr coefficients, and temperature coefficients were analyzed using a linear mixed model (LMM). Mean P50 at baseline (37°C, 40 mmHg PCO_2) was 27.1 ± 2.6 mmHg. Both CO_2-Bohr ($p < 0.001$) and temperature coefficients ($p < 0.001$) had a significant effect on P50. The absolute CO_2 effect was still pronounced at normothermic and febrile temperatures, whereas at low temperatures, the relative CO_2 effect (expressed by CO_2-Bohr coefficient; $p < 0.001$, interaction) was increased. The larger impact of PCO_2 on oxygen affinity at low temperature may be caused by the competition of 2,3-BPG with PCO_2 and the exothermic binding characteristic of 2,3-BPG. In a model of an avalanche burial, based on published data of CO_2 levels and cooling rates, we calculated the resulting P50 for this specific condition based on the here-reported PCO_2 and temperature effect on ODC. Depending on the degree of hypercapnia and hypothermia, a potentially beneficial increase in hemoglobin oxygen affinity in the hypoxic condition might ensue.

Keywords: oxygen affinity, oxygen dissociation curve, carbon dioxide, temperature, avalanche burial, hypoxia, hypothermia, hypercapnia

INTRODUCTION

A completely avalanche-buried patient who is still able to breathe into an air pocket (any space in front of mouth and nose) may cool down during a long burial time and suffer from cardiovascular and respiratory changes that are not exclusively explainable by the effect of decreased core temperature. In the early phase of burial, acute hypoxia is associated with high carbon dioxide (CO_2) levels due to rebreathing exhaled air (dead space ventilation) (1, 2). Without a sufficient supply of O_2 and removal of CO_2, hypoxia and hypercapnia increase the risk of normothermic cardiac arrest. After a long burial time but with sufficient supply or removal of respiratory gases, the patient is exposed to a combination of hypoxia, hypercapnia, and hypothermia (3). This combination of hypoxia, hypercapnia, and hypothermia has been defined as the triple H syndrome (1). Experimental studies showed that when human participants breathed into snow air pockets, the inspiratory CO_2-fraction rapidly increased and stabilized at a level of approximately 5–6% of CO_2 (1, 4, 5). Despite hypercapnia can speed up the cooling rate (6), the combination of hypothermia with hypoxia and hypercapnia may result in a worse neurological outcome in completely avalanche-buried patients compared to patients suffering solely from hypothermic cardiac arrest (7–9). Such outcome is determined by the temporal sequence of the events, as a decrease in oxygen supply and CO_2 removal usually proceed the development of hypothermia.

The oxygen dissociation curve (ODC) describes the reversible binding of four molecules of oxygen to Hb (10–12). The ODC is usually described by the P50 value, that is, the value of O_2 partial pressure, PO_2 at which 50% of Hb is saturated with oxygen, and by the Hill coefficient (HC), a parameter that describes maximum steepness in the Hill plot and that reflects the cooperativity of ligand binding. Temperature, pH, 2,3-bisphosphoglycerate (2,3-BPG), and PCO_2 are the four main factors that affect the ODC. Based on Severinghaus' equation, ODC should be corrected for the effects of the different factors (11). Specifically, exposing blood to CO_2 results in a decrease of oxygen affinity *via* two ways, first a decrease in pH resulting in a decrease of oxygen affinity (Bohr effect) and second a direct binding to the oxygen-linked CO_2 binding site and carbamino-Hb formation (CO_2 effect) (12, 13). The combined effect with temperature as another independent factor can result in a combination of three of the four main effectors to the ODC. However, the effects of the association of hypercapnia with hypothermia on the oxygen cascade, that is, uptake, transportation, and delivery of oxygen to tissues, defined by the hemoglobin (Hb) oxygen affinity, are not fully understood. Interactions of CO_2 and temperature may affect cellular oxygenation *via* several different pathways. In blood, the solubility of O_2 and CO_2 is affected by temperature and pH. In the tissues and at a cellular level, oxygen consumption and CO_2 and also metabolic acid production decrease at lower temperatures. The possible interaction of CO_2-Bohr coefficient (CO_2-BC), a function of P50 CO_2 dependency, with temperature coefficient (TC), a function of P50 temperature dependency, was studied with contradictory results in humans and animals (14–16).

The aim of this study was to describe single and combined effects of CO_2 and temperature on the ODC in unbuffered whole blood to better understand the pathophysiology of oxygen transport in pathophysiological situations characterized by changes in temperature and levels of respiratory gases.

METHODS

This study was approved by the Ethical Board of the Medical University of Innsbruck (vote nr. 1123/2019) and is registered with clinicaltrials.gov (NCT04041531). Written informed consent was obtained from all participants.

Inclusion criteria were the age between 18 and 40 years, no recent history of acute or chronic illness, blood loss, or sojourn at high altitude (>3,000 m a.s.l.) within the past 28 days. All participants were at fasting (6 h) before blood collection. Blood was taken from nonsmoking volunteers from an antecubital vein with a minimum of stasis period. The blood samples were split into two aliquots: one was immediately analyzed by a blood gas analyzer (ABL 800 flex, Radiometer, Denmark), and another aliquot of the sample was placed on ice for the ODC experiment and analyzed within 5 h.

ODC Experiments

Oxygen dissociation curve experiments were performed with a modification of a recently published method (17). In this method, PO_2 is continuously decreased from 140 mmHg to 0 mmHg, and data points of PO_2 and SO_2 are acquired every minute to record the ODC. Within the study setting, different aliquots of the same sample can be simultaneously exposed up to four different gas mixtures. Specifically, four different PCO_2 levels (20, 40, 60, and 80 mmHg) were applied and combined in consecutive measurements with five different temperatures (13.7, 23, 30, 37, and 42°C) that were chosen based on previously publications related to hypothermia and avalanche burial, to maximize comparability and clinical relevance (14–16, 18–20). To quantify the relative effect of temperature (TC) and CO_2 (CO_2-BC) on P50, coefficients were calculated [Eqs. 1, 2; (12)].

$$Eq.1: CO_2 - BC = \frac{\Delta \log_{10} P50}{\Delta \log_{10} PCO_2}$$

$$Eq.2: TC = \frac{\Delta \log_{10} P50}{\Delta temperature}$$

In a 4 × 5 factorial design, every blood sample was exposed to all 20 combinations of four PCO_2 levels and five temperature levels, starting with the lowest temperature level, followed by heating the entire experimental setup to the next higher temperature level. To address the increase of water vapor saturation pressure with temperature, gas mixtures were prepared volumetrically from dry, pure gases (CO_2, N_2 and O_2) in gas-tight sampling bags, according to the Magnus equation (21). The temperature management of the fluorescence plate reader instrument (Tecan 200 Infinite Pro, Tecan Genios Corp., Switzerland) ensured correct temperature in the measurement chamber, whereas temperature of the conducting Viton tubes, gas mixtures, humidifiers, and temperature of the whole experimental setup

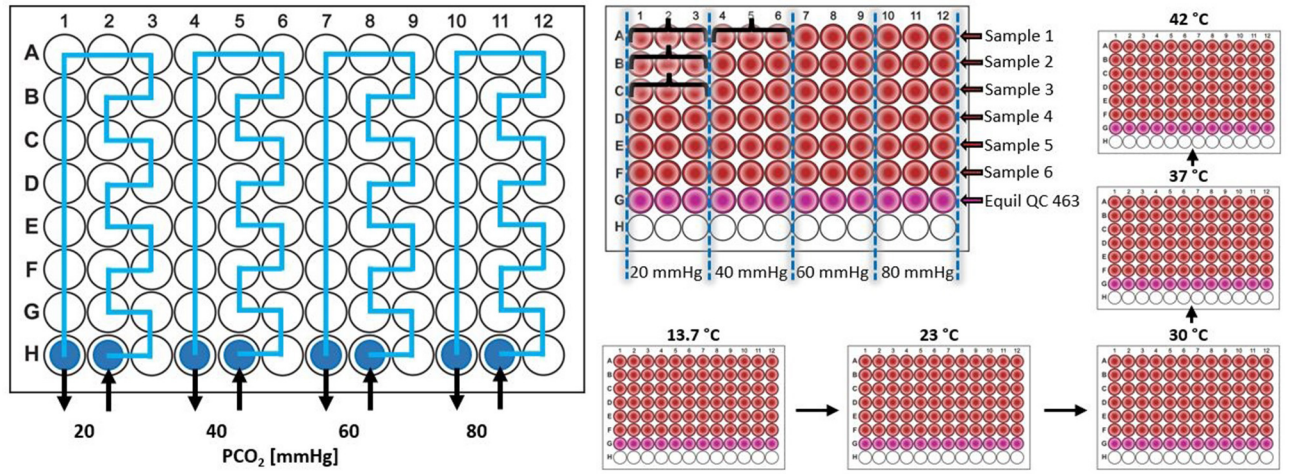

FIGURE 1 | Scheme of the four channel Oxygen Dissociation Curve (ODC) plate [see (17) for further descriptions of plate design and the measurement principles]. The gas supply was randomized throughout the study, here exemplary shown for increasing PCO_2 levels from left to right. Participant's blood samples were pipetted in rows (e.g., participant 1 in row A, participant 2 in row B, …) and triplet measurement were obtained for all combinations (e.g., for participant 1: 3 ODC measurements in wells A1, A2, and A3 for the combination of gas system 20 mmHg and applied temperature X, 3 ODC measurements in wells A4, A5, and A6 for the combination of gas system 40 mmHg and applied temperature X, …, indicated by the curly brackets). Different temperature levels were achieved by heating between the experiments, thus temperature effect measured in consecutive experiments. PCO_2, carbon dioxide partial pressure.

was monitored and strictly controlled. The supply of the four different gas mixtures to the four gas systems in the four-channel ODC plate was randomized (**Figure 1**). Up to six participant's blood samples were analyzed per experiment (rows). The average of triplet measurements for every combination and sample (**Figure 1**) was used for analysis. Additionally, an internal standard Hb solution (Equil QC 463 Level 2, RNA medical, USA) was analyzed in each test to check and adjust for accuracy of the measurements as described before (17).

Statistical Analysis

Student's *t*-test was used to detect sex differences in P50 and HC at baseline. Factors that affect P50, HC, CO_2-BC, and TC were analyzed by means of a linear mixed model (LMM). The factors investigated were the following.

- For P50 and HC: sex, age (two levels: <30 and ≥30 years), temperature (13.7, 23, 30, 37, and 42°C), PCO_2 (20, 40, 60, and 80 mmHg), and interactions of temperature with PCO_2, sex with temperature, sex with PCO_2, and sex with age.
- For CO_2-BC: sex, age, temperature, and interactions of sex with temperature and sex with age.
- For TC: sex, age, PCO_2, and interactions of sex with PCO_2 and sex with age.

The covariance structure for the residuals of the LMM was chosen by means of the Schwarz's Bayesian Criterion among diagonal, compound symmetry, unstructured and first-order autoregression. The Holm–Bonferroni method was used to correct *p*-values for multiple comparisons. Considering ΔT as difference of temperature from 37°C (baseline temperature), ΔPCO_2 as difference of PCO_2 from 40 mmHg (baseline PCO_2), and ΔP50 as difference from P50 at 37°C and 40 mmHg, a LMM was also performed to calculate an equation to predict ΔP50 from ΔT and ΔPCO_2. For the calculation, ΔT and ΔPCO_2 were inserted in the LMM as covariates in a model without intercept.

TABLE 1 | Results of blood gas analysis for women and men as mean ± standard deviation (Student's *t*-test).

	All	Women	Men	*p*-value
pH	7.36 ± 0.03	7.37 ± 0.04	7.35 ± 0.02	0.070
PCO_2 [mmHg]	46.5 ± 6.5	42.7 ± 5.8	50.6 ± 4.8	<0.001
HCO_3 [mmol/l]	23.6 ± 1.5	22.9 ± 1.0	24.3 ± 1.6	0.006
Hb [g/dl]	14.9 ± 1.5	13.7 ± 0.8	16.0 ± 1.0	<0.001
Hct [%]	45.6 ± 4.5	42.0 ± 2.4	49.0 ± 3.1	<0.001
Cl^- [mmol/l]	106.8 ± 1.9	107.7 ± 1.5	106.1 ± 1.9	0.017
Glucose [mg/dl]	94.4 ± 6.8	91.9 ± 7.5	95.9 ± 4.6	0.094
Lactate [mg/dl]	9.9 ± 5.4	8.9 ± 5.1	10.9 ± 5.8	0.326
COHb [%]	1.4 ± 0.6	1.4 ± 0.5	1.4 ± 0.6	0.926
MetHb [%]	1.0 ± 0.1	1.0 ± 0.1	1.0 ± 0.1	0.112

PCO_2, carbon dioxide partial pressure; HCO_3, bicarbonate; Hb, hemoglobin concentration; Hct, hematocrit; Cl^-, chloride concentration; COHb, carboxyhemoglobin; MetHb, methemoglobin.

Data are shown as mean ± standard deviation, whereas LMM estimated means as mean (95% confidence interval; CI). $p < 0.05$ (two-sided) was considered statistically significant. Excel (Microsoft Office 2016, Microsoft Corp.) and SPSS version 25 (IBM Corp., Armonk, NY, USA) were used for data collection, calculation, and analysis.

RESULTS

Thirty participants (15 women and 15 men) were recruited and 30 blood samples were analyzed. Participants' mean age was 30.6 ± 3.9 years. Results of blood gas analysis, measured immediately

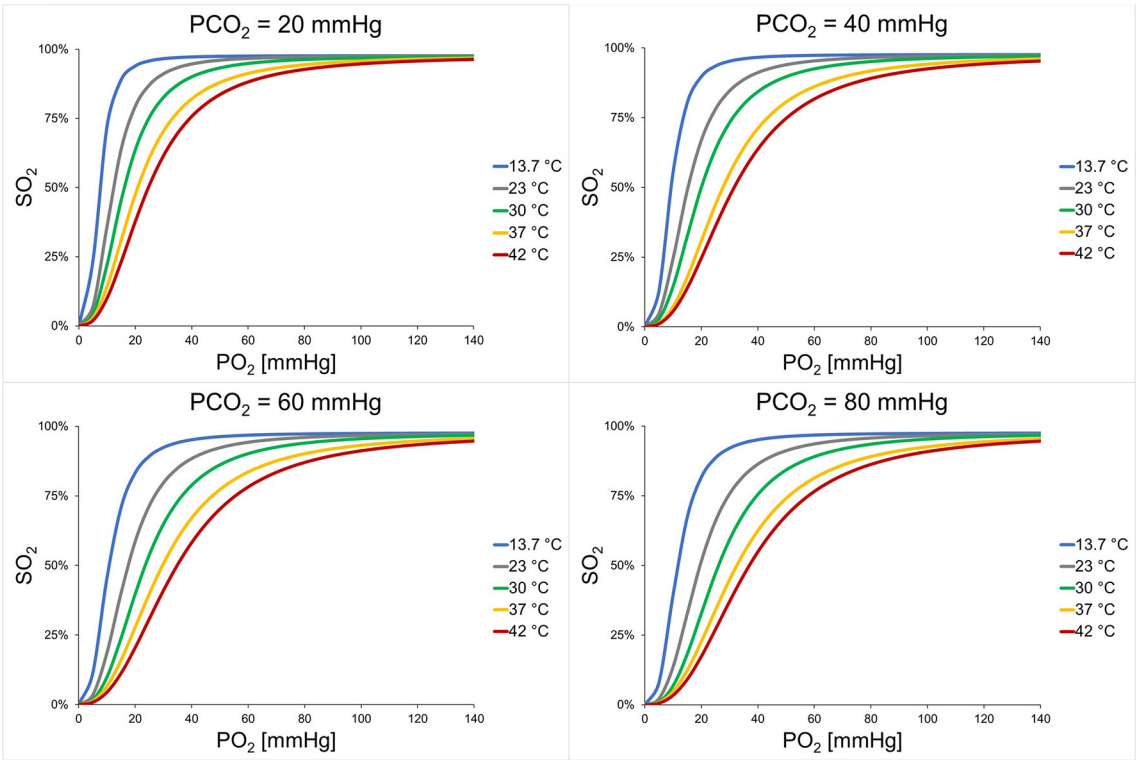

FIGURE 2 | Mean ODCs of all participants. The temperature effect is shown for each PCO_2 level. For each combination, mean P50s and mean Hill coefficient were inserted in the Hill equation [see Eq. 4 in (17)]. Each graph represents the mean of 30 participants and triplet measurements. P50, oxygen partial pressure at which 50% of hemoglobin is saturated with oxygen; SO_2, oxygen saturation; PCO_2, carbon dioxide partial pressure.

TABLE 2 | *p*-Values of the factors inserted in the LMMs.

Dependent variable	Intercept	Sex	Age	Temperature	PCO_2	Temperature * PCO_2	Sex * Temperature	Sex * PCO_2	Sex * Age
P50	<0.001	<0.001	<0.001	<0.001	<0.001	<0.001	0.001	1.000	1.000
Temperature coefficient	<0.001	0.576	1.000	–	0.034	–	–	1.000	0.543
CO_2-Bohr coefficient	<0.001	1.000	0.063	<0.001	–	–	0.554	–	1.000
Hill coefficient	<0.001	0.002	1.000	<0.001	<0.001	0.002	1.000	0.096	1.000

*The p-values are corrected by means of the Holm–Bonferroni method. P50, oxygen partial pressure at which 50% of hemoglobin is saturated with oxygen; PCO_2, carbon dioxide partial pressure. * An asterisk between two factors indicates the effect of interaction of the two factors. - A dash indicates that the factor was not inserted in the LMM.*

after blood sampling, are shown in **Table 1**. At baseline (37°C and 40 mmHg PCO_2), P50s in women were not significantly higher than in men (28.0 ± 2.8 and 26.2 ± 2.2 mmHg; $p = 0.061$) and HCs were 2.53 ± 0.14 and 2.56 ± 0.16 ($p = 0.641$), respectively.

Factors Affecting P50

Mean ODCs in relation to different PCO_2 and temperature levels are shown in **Figure 2**. A significant effect of PCO_2, temperature, and sex on P50 could be detected ($p < 0.001$ for all parameters; **Table 2**). The effect of the interaction of temperature and PCO_2 on P50 was also significant ($p < 0.001$). At temperatures lower than 37°C, PCO_2 increased P50 in an almost linear relationship, whereas at higher temperatures, this linearity was lost (**Figure 3**). An effect of age and of the interaction of sex and temperature on P50 was also significant ($p < 0.001$ and $p = 0.001$, respectively).

The estimated means of P50 were higher for participants <30 years in comparison with participants ≥30 years old [21.3 (95% CI 21.1–21.5) vs. 20.7 (95% CI 20.5–20.9)]. The effect of the interaction of temperature and PCO_2 on P50 was quantified in Eq. 3 and plotted in **Figure 4**.

$$Eq.3: \Delta P50 = 0.733 \times \Delta T + 0.214 \times \Delta PCO_2 - 0.002 \times \Delta PCO_2{}^2 + 0.004 \times \Delta T \times \Delta PCO_2$$

$\Delta P50 = P50\text{-}P50_{(PCO_2=40mmHg;\,temperature=37°C)}$; $\Delta PCO_2 = PCO_2\text{-}40\ mmHg$ and $\Delta T = temperature\text{-}37°C$.

Factors Affecting CO_2-Bohr Coefficient

With LMM, an effect of temperature on CO_2-BC could be detected ($p < 0.001$; **Table 2**). CO_2-BCs progressively decreased

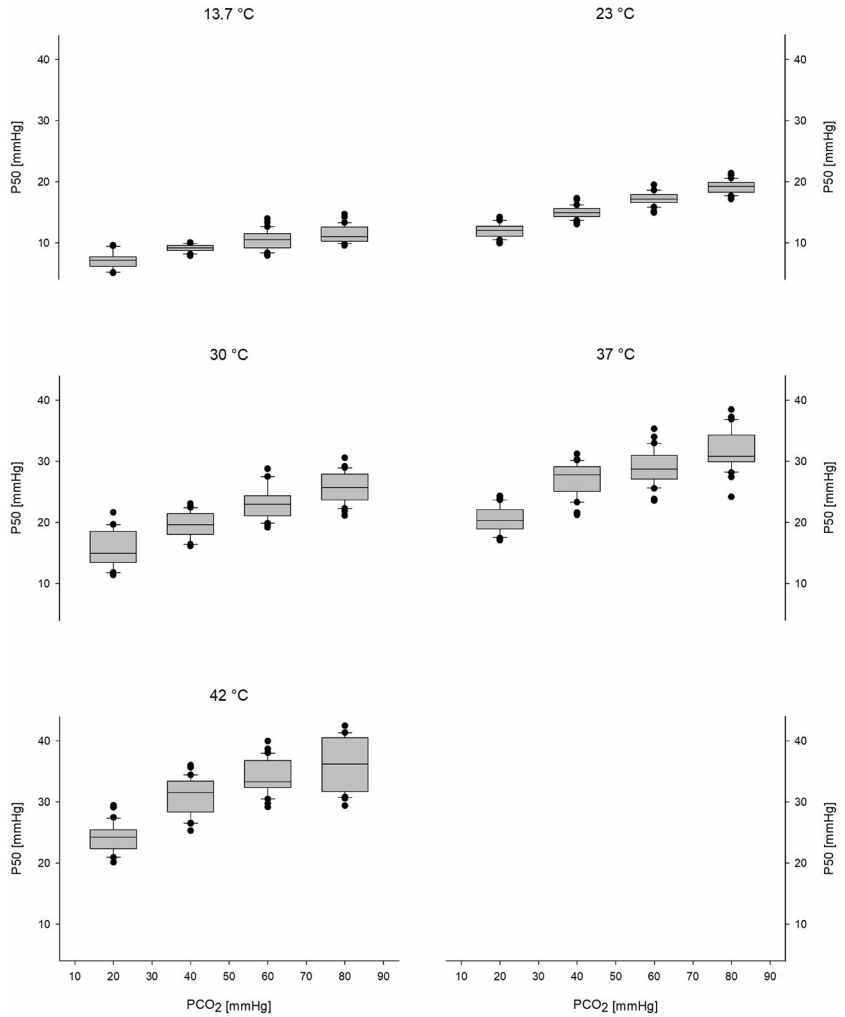

FIGURE 3 | Boxplots of the P50s of all participants show the CO_2-Bohr effect for each temperature level. Black circles represent outliers. P50, oxygen partial pressure at which 50% of hemoglobin is saturated with oxygen; PCO_2, carbon dioxide partial pressure.

with the increase of temperature (**Figure 5A**). The differences were significant between 13.7 and 37°C ($p = 0.001$), 13.7 and 42°C ($p < 0.001$), and also between 23 and 42°C ($p = 0.044$) and between 30 and 42°C ($p = 0.001$).

Factors Affecting Temperature Coefficient

Only an effect of PCO_2 ($p = 0.034$; **Table 2**) was detected on TC. There was an indication that TCs at 40 mmHg (baseline PCO_2 level) were higher than at 80 mmHg PCO_2 ($p = 0.051$; **Figure 5B**).

Factors Affecting Hill Coefficient

There was an effect on HC by PCO_2, temperature, sex, and the interaction of temperature and PCO_2 ($p \leq 0.002$ for all parameters; **Table 2**). HCs were different at different P50s (**Figure 6A**) with a typical flattening of the ODC when shifted to the right. Mean HCs changed in relation to the different combinations of PCO_2 and temperature (**Figure 6B**). Overall, HCs were higher at PCO_2 80 mmHg compared to PCO_2 60 mmHg for a specific temperature (i.e., a right-shifted, but steeper ODC). The estimated mean of HC at 60 mmHg was significantly lower in comparison with 20, 40, and 80 mmHg [2.73 (95% CI 2.66–2.80) at 20 mmHg; 2.69 (95% CI 2.65–2.72) at 40 mmHg; 2.60 (95% CI 2.56–2.63) at 60 mmHg; and 2.72 (95% CI 2.68–2.75) at 80 mmHg] (i.e., an extended ODC shape).

DISCUSSION

We describe a significant interaction of the CO_2-Bohr effect and the temperature effect on the ODC in unbuffered whole blood samples. At temperatures lower than 37°C, the effect of temperature seems to outweigh the effect of even high CO_2 levels. There was a left-shifted ODC that could facilitate oxygen uptake in the lungs but might possibly limit deoxygenation at tissue level. Such modification could be protective against excessive hypoxia in a state of hypercapnia and hypothermia, as in the triple H

syndrome. At temperatures higher than 37°C and high CO_2 levels, the effect of CO_2-BC on the ODC decreased. Such findings may be due to an excess of respiratory gases (i.e., saturation effect). An increase in PCO_2 up to 80 mmHg resulted in right-shifted but also slightly steeper ODCs compared to those at PCO_2 60 mmHg, indicated by higher HCs, for example, at 42°C. Due to the great extent of both effects, this finding might be of clinical impact for the oxygen transport from the lungs to the tissue in hypoxic situations where both parameters are out of physiological range and pulmonary oxygen supply, oxygen transport capacity, or cardiac output is deteriorated (e.g., critical illness, acute respiratory distress syndrome, COVID-19, sepsis, and hypothermic major trauma).

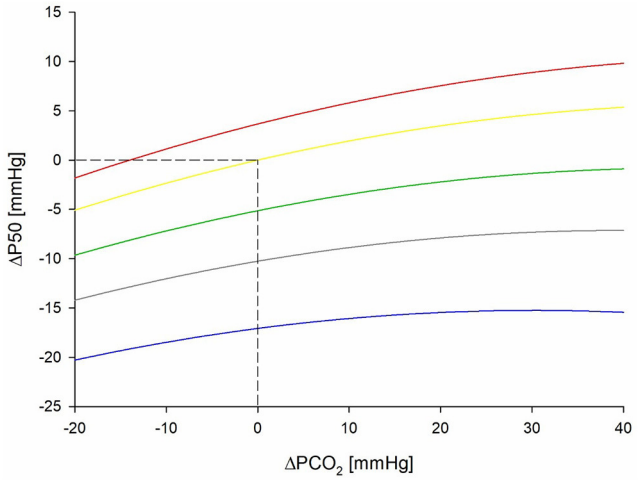

FIGURE 4 | Graphical presentation in form of a nomogram for the equation of ΔP50 dependency to ΔPCO_2 and different levels of temperature. ΔPCO_2 denotes difference from 40 mmHg (baseline PCO_2) and ΔP50 denotes difference from P50 at 37°C (baseline temperature) and 40 mmHg. Blue line represents 13.7°C, gray line 23°C, green line 30°C, yellow line 37°C, and red line 42°C. P50, oxygen partial pressure at which 50% of hemoglobin is saturated with oxygen; PCO_2, carbon dioxide partial pressure.

Our data showed that CO_2-Bohr effect decreased with increasing temperatures from hypothermic to normothermic conditions which is supported by some of the available literature. Differences in the methodological approaches and results in studies investigating the interaction of the CO_2-Bohr and temperature effect in human and animal studies caused inconsistencies. In 1961, Callaghan studied blood of dogs under hypothermic conditions (15, 23, 30, and 37°C) at various CO_2 levels (20, 40, 60, and 70 mmHg) with a self-constructed instrument (16). When analyzing their published data using Eq. 1, CO_2-Bohr effect showed a decrease with increasing temperatures from hypothermic to normothermic conditions. Such results are consistent with our data in humans. In 1977, Hlastala studied the interactions between all four main parameters affecting ODC on 93 humans (14) using an instrument presented by Duvelleroy (22). They also studied different combinations of temperature (23, 30, 37, and 44°C) and CO_2 levels (2.5, 5.8, and 8.5%). Hlastala reported an even increased CO_2-Bohr effect with increasing temperature from hypothermic to normothermic conditions. In 1980, Reeves also studied temperature levels from 13 to 43°C and CO_2 levels from 1 to 8% (15) using a self-constructed instrument for rapid ODC measurements in a blood film (23). Reeves reported neither variations in the shape of the ODC with temperature nor an interaction of CO_2-Bohr effect with temperature and also rejected the finding reported by Hlastala that the TC varies with oxygen saturation (15). Overall, we assume that the main reason for the contradictory results is the different approaches in calculating the CO_2-BC. Hlastala calculated CO_2-BC using pH and base excess. pH and base excess are not only difficult to be exactly measured in a blood film, but pH

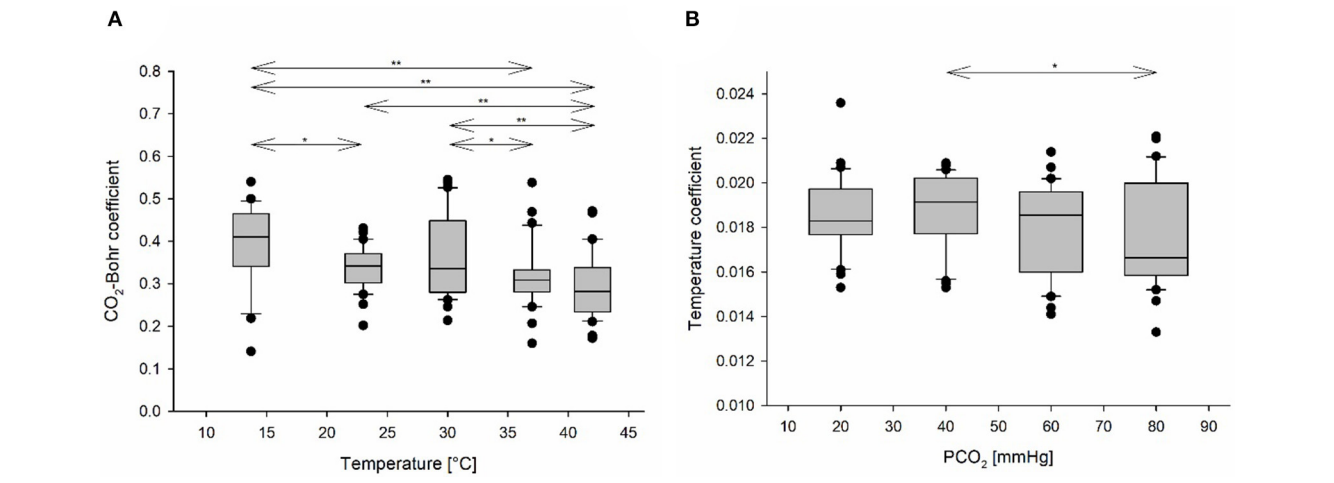

FIGURE 5 | (A) CO_2-Bohr coefficients (CO_2-BCs) in relation to temperature, presented as boxplots. CO_2-BC, a measure of relative CO_2-Bohr effect, decreases with increasing temperature. **(B)** Temperature coefficients (TCs) in relation to PCO_2, presented as boxplots. Black circles represent outliers. A line with arrows and asterisks indicates a pairwise comparison which was detected as statistically significant by the LMM; one asterisk denotes $0.05 \leq p < 0.1$, and two asterisks denote $p < 0.05$.

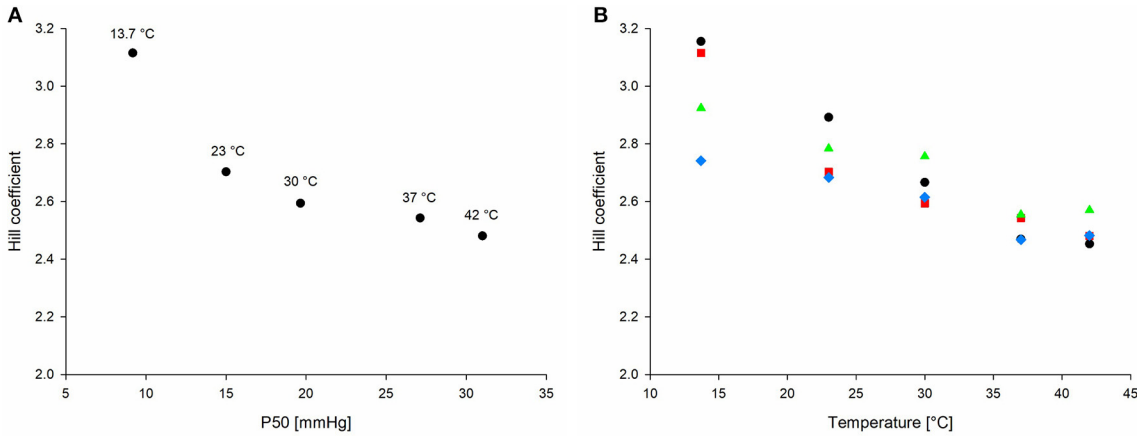

FIGURE 6 | (A) Correlation of Hill coefficient (HC) with P50. HCs decrease with increasing P50. **(B)** Mean Hill coefficient over all 20 combinations of PCO_2 and temperature (black circle 20 mmHg, red square 40 mmHg, blue rhombus 60 mmHg, and green triangle 80 mmHg). P50, oxygen partial pressure at which 50% of hemoglobin is saturated with oxygen.

itself is temperature-dependent by definition (24). In our study, only PCO_2 values were used for calculations. Unfortunately, raw data are not published by Hlastala, so a direct comparison by recalculating their results using our equation is not possible. Hlastala also used an oxygenation protocol, whereas both Callaghan (15) and our group worked with deoxygenation for the determination of ODCs (17). As the solubility of CO_2 increases with a decrease of temperature, and CO_2 and O_2 are competing agents in binding to hemoglobin (Haldane effect), the way of the oxygen ramp might be of importance as this could interfere with the measurement results. Both methods are working with blood films, and thus, the impact of solubility changes due to temperature changes should be neglectable. Our method might be of advantage for clinical insights when compared to an oxygenation protocol. It simulates more the pathological changes, as at the beginning, full saturation is expected.

Our data showed that the effect of CO_2 was diminished at higher CO_2 levels and the relative effect, expressed by the CO_2-BC, decreased with increasing temperature. Benesch showed that the binding of 2,3-BPG to hemoglobin is an exothermic reaction (25), reducing the amount of 2,3-BPG bound to hemoglobin at higher temperatures. CO_2 binding to hemoglobin and carbamino group formation is favored, as 2,3-BPG and CO_2 are competing agents to the binding to Hb (13, 14). Such data suggest that there is a strong competition between CO_2 and 2,3-BPG at lower temperatures, resulting in a strong effect of PCO_2 on P50. Conversely, at higher temperatures (e.g., 42°C), the majority of 2,3-BPG is dissociated from hemoglobin, lowering the impact of the competition with CO_2, and emphasizing the effect of lower PCO_2 levels (e.g., 20 mmHg or 40 mmHg). A further increase of PCO_2 (60 mmHg or 80 mmHg) seems to cause a reduction of the impact on P50, because the N-terminal binding sites of the Hb β-chains may be already occupied by CO_2 (26). Christiansen described that at lower PCO_2 levels, CO_2 uptake is facilitated, whereas at higher PCO_2 levels, the curve flattens and may indicate a further increase of CO_2 uptake only by physically solved CO_2 (26). As Hb binding sites for CO_2 are limited by the amount of Hb, we assume that at some point, a state of saturation in the combination of CO_2 and O_2 binding to Hb exists, and a further increase in PCO_2 does not lead to an additional right-shift of the ODC. The human body might not benefit of an improved oxygen delivery to the tissue at P50 levels exceeding 40 mmHg. If the oxygen affinity of Hb is too low, a sufficient binding and thereby transportation of oxygen cannot be provided any more.

Böning also reported an interaction of the Bohr effect and TC and a sex dependency of both effects regarding P50 (27). Our data also show that the temperature effect on P50 is sex-dependent, but the difference almost disappeared at temperature <23°C.

When oxygen content in the inspiratory air is limited, a left-shifted ODC, which increases oxygen uptake in the lungs, is beneficial. For instance, P50 in humans exposed to extreme altitude is reduced due to hypocapnia, resulting in increased SO_2. In the placenta, PaO_2 is very low (30 mmHg) and ODC of the fetus is shift to the left due to fetal hemoglobin (P50 about 20 mmHg) (28). Such status can be observed also in accidentally hypothermic patients and can explain better outcome after hypothermic cardiac arrest. Completely avalanche-buried patients with long burial can develop accidental hypothermia, but they are also exposed to a combination of hypoxia and hypercapnia that can lead to a worse outcome (2, 24). Human experimental studies showed that smaller air pockets and higher density of the surrounding avalanche debris can impair respiratory gas supply or removal and lead to a more severe level of hypoxia and hypercapnia (1, 4, 5). The effects of the combination of the three factors could only be tested in animal models (29, 30). A porcine study on the triple H syndrome experimentally showed a decrease in brain tissue PO_2, cerebral venous SO_2 and regional cerebral SO_2 at a core

TABLE 3 | A model for P50 in an avalanche burial model.

	PCO_2		
	41 mmHg	**47 mmHg**	**75 mmHg**
28°C	20.7	21.7	24.3
34°C	25.1	26.2	29.5
36.4°C	26.9	28	31.6

Calculations based on mean P50 of this study (P50 = 27.1 mmHg) with PCO_2 levels (4) and cooling rates (32–34) from other studies, respectively. Temperature is denoted in columns and PCO_2 in rows. P50, oxygen partial pressure at which 50% of hemoglobin is saturated with oxygen; PCO_2, carbon dioxide partial pressure.

temperature of 28°C. The reduced FiO_2 and increased CO_2 caused a mismatch between metabolic oxygen consumption and oxygen delivery (30). In sole deep hypothermia, cerebrovascular reactivity (cerebral autoregulation) was impaired in pigs (31). Interestingly, whereas mean arterial pressure and cerebral perfusion pressure were decreased at 28.8°C, brain oxygenation was increased (31). Our study suggests that there can be an ODC shift to the left in spite of moderate elevated CO_2 level, due to hypothermia.

Based on measured CO_2 levels from a human experimental study (4) and cooling rates from observational studies of avalanche victims (32–34), the expected P50s in avalanche-buried victims were simulated in a model (**Table 3**). The calculated P50 (**Table 3**, P50 at 36.4°C and PCO_2 of 47 mmHg) suggests an increased tissue oxygen unloading that might contribute to outcome (e.g., better cerebral oxygenation). Such status could be found in the early stage of triple H syndrome (5) when the patients is still not hypothermic. In the presence of an air pocket and sufficient exchange of respiratory gases, arterial PCO_2 might remain stable, whereas the progressive cooling could allow a further left-shift (i.e., a core temperature <35°C; **Table 3**, P50 at 34°C or 28°C and PCO_2 of 47 mmHg). In case of insufficient exchange of respiratory gases, there could be higher $PaCO_2$ levels (e.g., 75 mmHg, see **Table 3**) without a left-shift.

In other hypothermic patients, oxygen consumption is decreased and thereby also CO_2 production. The relevance of the interaction of PCO_2 and temperature may thus also have an impact of the fields of therapeutic hypothermia, ARDS, pulmonary oedema, in cardio-anesthesiology, and intensive care medicine. In hypothermic circulatory arrest, acid-base management is based on two different approaches: pH-stat or alpha-stat. Whether one of the two approaches is superior to the other is under debate, yet an age-dependent approach seems preferable (35). The present findings of an interaction effect of PCO_2 and temperature on the ODC might add a small piece of the puzzle in this debate. In an in-hospital setting, P50 as a therapeutic target plays nowadays a tangential role, despite possible treatment options (36, 37).

Limitations

CO_2-BC was established as a function of PCO_2, as pH is temperature-dependent and hard to measure in a small volume of blood sample, whereas PCO_2 is a parameter measured routinely *in vivo* in a clinical setting. Due to the small volumes of blood (15 μl) in single cell layer films, there was neither a pH measurement nor a measurement of base excess feasible. Thus, a definition and calculation of CO_2-BC based on pH and base excess could not be carried out, which results in a limitation of comparability to other published data (14). The supply of the different PCO_2 levels to the 3H plate was randomized, but we started always with the lowest temperature and then increased the temperature for practical reasons. Thus, at lower temperature, the blood was fresher than at higher temperature. This possible bias should be neglectable as the correct storage of the blood samples on ice was a main focus and the metabolic parameters were shown to remain stable within hours after blood sampling (17). The presented equation that can be used for exact P50, PCO_2, and temperature correction is obtained from one sample of participants ($n = 30$), and another independent study evaluating this interaction is necessary to validate the proposed equation. In this study, the interactions of CO_2-BC and TC were studied in an *in vitro* experiment. Direct transfer of study findings in an *in vivo* scenario should be done cautiously. Due to the difficulties in feasibility and transfer from animal studies (38–41), the *in vitro* ODC determination is advantageous under these conditions. Further studies are needed to investigate the reasons for the here-reported interaction of CO_2-Bohr effect with temperature effect. The saturation dependency of Bohr effect (42) was not accounted for in this study.

CONCLUSION

We describe a significant interaction of the CO_2-Bohr effect and the temperature effect on the ODC in unbuffered whole blood samples. At temperatures lower than 37°C, the effect of temperature seems to outweigh the effect of even high CO_2 high levels. There was a left-shifted ODC that could result in an increased oxygen uptake in the lungs. At temperatures higher than 37°C and high CO_2 levels, the effect of CO_2-BC on the ODC decreased. Depending on the degree of hypercapnia and hypothermia in a completely avalanche-buried patient, there could be a left-shift of the ODC with a potential benefit when oxygen content in the inspiratory air is limited (i.e., hypoxia and hypercapnia) and oxygen consumption of the brain is decreased (i.e., hypothermia). Further studies are needed to investigate *in vivo* the current *ex vivo* results and the systemic effects of the reported interaction effect of CO_2-Bohr effect and TC, and the clinical use of P50 could allow to better triage avalanche.

DATA AVAILABILITY STATEMENT

The raw data supporting the conclusions of this article will be made available by the authors upon reasonable request.

ETHICS STATEMENT

The studies involving human participants were reviewed and approved by Ethikkommission der Medizinischen Universität Innsbruck, Innrain 43, Innsbruck, Austria. The participants provided their written informed consent to participate in this study.

AUTHOR CONTRIBUTIONS

SW prepared original draft. SW and TDC conducted data curation, formal analysis, and visualization. HB, MS, TH, and GS have done supervision and project administration. All authors performed conceptualization, methodology, validation, involved in writing, reviewing, editing, and approved the submitted version.

FUNDING

This study was funded by equity capital of the Medical University of Innsbruck, Austria, and Eurac Research, Bolzano, Italy.

ACKNOWLEDGMENTS

We thank Martin Streicher for the valuable technical support in the experimental setup. The authors thank the Department of Innovation, Research, University and Museums of the Autonomous Province of Bozen/Bolzano for covering the Article Processing Fee.

REFERENCES

1. Brugger H, Sumann G, Meister R, Adler-Kastner L, Mair P, Gunga HC, et al. Hypoxia and hypercapnia during respiration into an artificial air pocket in snow: implications for avalanche survival. *Resuscitation.* (2003) 58:81–8. doi: 10.1016/S0300-9572(03)00113-8
2. Kottmann A, Pasquier M, Strapazzon G, Zafren K, Ellerton J, Paal P. Quality indicators for avalanche victim management and rescue. *Int J Environ Res Public Health.* (2021) 18:9570. doi: 10.3390/ijerph18189570
3. Strapazzon G, Brugger H. On-site treatment of snow avalanche victims: from bench to mountainside. *High Alt Med Biol.* (2018) 19:307–15. doi: 10.1089/ham.2018.0036
4. Strapazzon G, Paal P, Schweizer J, Falk M, Reuter B, Schenk K, et al. Effects of snow properties on humans breathing into an artificial air pocket-an experimental field study. *Sci Rep.* (2017) 7:17675. doi: 10.1038/s41598-017-17960-4
5. Strapazzon G, Gatterer H, Falla M, Dal Cappello T, Malacrida S, Turner R, et al. Hypoxia and hypercapnia effects on cerebral oxygen saturation in avalanche burial: a pilot human experimental study. *Resuscitation.* (2021) 158:175–82. doi: 10.1016/j.resuscitation.2020.11.023
6. Grissom CK, Radwin MI, Scholand MB, Harmston CH, Muetterties MC, Bywater TJ. Hypercapnia increases core temperature cooling rate during snow burial. *J Appl Physiol.* (1985) 96:1365–70. doi: 10.1152/japplphysiol.00531.2003
7. Boue Y, Payen JF, Torres JP, Blancher M, Bouzat P. Full neurologic recovery after prolonged avalanche burial and cardiac arrest. *High Alt Med Biol.* (2014) 15:522–3. doi: 10.1089/ham.2014.1082
8. Hilmo J, Naesheim T, Gilbert M. "Nobody is dead until warm and dead": prolonged resuscitation is warranted in arrested hypothermic victims also in remote areas–a retrospective study from northern Norway. *Resuscitation.* (2014) 85:1204–11. doi: 10.1016/j.resuscitation.2014.04.029
9. Mair P, Brugger H, Mair B, Moroder L, Ruttmann E. Is extracorporeal rewarming indicated in avalanche victims with unwitnessed hypothermic cardiorespiratory arrest? *High Alt Med Biol.* (2014) 15:500–3. doi: 10.1089/ham.2014.1066
10. Barcroft J, Camis M. The dissociation curve of blood. *J Physiol.* (1909) 39:118–42. doi: 10.1113/jphysiol.1909.sp001330
11. Severinghaus JW. Simple, accurate equations for human blood O2 dissociation computations. *J Appl Physiol Respir Environ Exerc Physiol.* (1979) 46:599–602. doi: 10.1152/jappl.1979.46.3.599
12. Mairbäurl H, Weber RE. Oxygen transport by hemoglobin. *Compr Physiol.* (2012) 2:1463–89. doi: 10.1002/cphy.c080113
13. Imai K. *Allosteric Effects in Haemoglobin*. Cambridge: Cambridge University Press (1982).
14. Hlastala MP, Woodson RD, Wranne B. Influence of temperature on hemoglobin-ligand interaction in whole blood. *J Appl Physiol Respir Environ Exerc Physiol.* (1977) 43:545–50. doi: 10.1152/jappl.1977.43.3.545
15. Reeves RB. The effect of temperature on the oxygen equilibrium curve of human blood. *Respir Physiol.* (1980) 42:317–28. doi: 10.1016/0034-5687(80)90122-X
16. Callaghan PB, Lister J, Paton BC, Swan H. Effect of varying carbon dioxide tensions on the oxyhemoglobin dissociation curves under hypothermic conditions. *Ann Surg.* (1961) 154:903–10.
17. Woyke S, Ströhle M, Brugger H, Strapazzon G, Gatterer H, Mair N, et al. High-throughput determination of oxygen dissociation curves in a microplate reader-A novel, quantitative approach. *Physiol Rep.* (2021) 9:e14995. doi: 10.14814/phy2.14995
18. Astrup P, Engel K, Severinghaus JW, Munson E. The influence of temperature and pH on the dissociation curve of oxyhemoglobin of human blood. *Scand J Clin Lab Invest.* (1965) 17:515–23. doi: 10.3109/00365516509083359
19. Musi ME, Sheets A, Zafren K, Brugger H, Paal P, Hölzl N, et al. Clinical staging of accidental hypothermia: the revised swiss system: recommendation of the international commission for mountain emergency medicine (ICAR MedCom). *Resuscitation.* (2021) 162:182–7. doi: 10.1016/j.resuscitation.2021.02.038
20. Gilbert M, Busund R, Skagseth A, Nilsen PA, Solbo JP. Resuscitation from accidental hypothermia of 13. 7 degrees C with circulatory arrest. *Lancet.* (2000) 355:375–6. doi: 10.1016/S0140-6736(00)01021-7
21. Kraus H. Die Luftfeuchtigkeit. In: Kraus H, editor. *Die Atmosphäre der Erde.* Springer, Berlin, Heidelberg (2004).
22. Duvelleroy MA, Buckles RG, Rosenkaimer S, Tung C, Laver MB. An oxyhemoglobin dissociation analyzer. *J Appl Physiol.* (1970) 28:227–33. doi: 10.1152/jappl.1970.28.2.227
23. Reeves RB. A rapid micro method for obtaining oxygen equilibrium curves on whole blood. *Respir Physiol.* (1980) 42:299–315. doi: 10.1016/0034-5687(80)90121-8
24. Paal P, Gordon L, Strapazzon G, Brodmann Maeder M, Putzer G, Walpoth B, et al. Accidental hypothermia-an update : the content of this review is endorsed by the international commission for mountain emergency medicine (ICAR MEDCOM). *Scand J Trauma Resusc Emerg Med.* (2016) 24:111. doi: 10.1186/s13049-016-0303-7
25. Benesch R, Benesch R. The oxygenation of hemoglobin in the presence of 2,3 diphosphoglycerate. Effect of temperature, pH, ionic strength, and hemoglobin concentration. *Biochemistry.* (1969) 8:2567–71. doi: 10.1021/bi00834a046
26. Christiansen J, Douglas CG, Haldane JS. The absorption and dissociation of carbon dioxide by human blood. *J Physiol.* (1914) 48:244–71. doi: 10.1113/jphysiol.1914.sp001659
27. Böning D, Draude W, Trost F, Meier U. Interrelation between Bohr and temperature effects on the oxygen dissociation curve in men and women. *Respir Physiol.* (1978) 34:195–207. doi: 10.1016/0034-5687(78)90028-2
28. Delivoria-Papadopoulos M, Morrow G IIIrd, Oski FA. Exchange transfusion in the newborn infant with fresh and "old" blood: the role of storage on

2,3-diphosphoglycerate, hemoglobin-oxygen affinity, and oxygen release. *J Pediatr.* (1971) 79:898–903. doi: 10.1016/S0022-3476(71)80181-6
29. Paal P, Strapazzon G, Braun P, Ellmauer PP, Schroeder DC, Sumann G, et al. Factors affecting survival from avalanche burial–a randomised prospective porcine pilot study. *Resuscitation.* (2013) 84:239–43. doi: 10.1016/j.resuscitation.2012.06.019
30. Strapazzon G, Putzer G, Dal Cappello T, Falla M, Braun P, Falk M, et al. Effects of hypothermia, hypoxia, and hypercapnia on brain oxygenation and hemodynamic parameters during simulated avalanche burial: a porcine study. *J Appl Physiol.* (1985) 130:237–44. doi: 10.1152/japplphysiol.00498.2020
31. Gaasch M, Putzer G, Schiefecker AJ, Martini J, Strapazzon G, Ianosi B, et al. Cerebral autoregulation is impaired during deep hypothermia-a porcine multimodal neuromonitoring study. *Ther Hypothermia Temp Manag.* (2020) 10:122–7. doi: 10.1089/ther.2019.0009
32. Locher T, Walpoth BH. [Differential diagnosis of circulatory failure in hypothermic avalanche victims: retrospective analysis of 32 avalanche accidents]. *Praxis.* (1996) 85:1275–82.
33. Van Tilburg C, Grissom CK, Zafren K, McIntosh S, Radwin MI, Paal P, et al. Wilderness medical society practice guidelines for prevention and management of avalanche and nonavalanche snow burial accidents. *Wilderness Environ Med.* (2017) 28:23–42. doi: 10.1016/j.wem.2016.10.004
34. Mittermair C, Foidl E, Wallner B, Brugger H, Paal P. Extreme cooling rates in avalanche victims: case report and narrative review. *High Alt Med Biol.* (2021) 22:235–40. doi: 10.1089/ham.2020.0222
35. Abdul Aziz KA, Meduoye A. Is pH-stat or alpha-stat the best technique to follow in patients undergoing deep hypothermic circulatory arrest? *Interact Cardiovasc Thorac Surg.* (2010) 10:271–82. doi: 10.1510/icvts.2009.214130
36. Srinivasan AJ, Morkane C, Martin DS, Welsby IJ. Should modulation of p50 be a therapeutic target in the critically ill? *Expert Rev Hematol.* (2017) 10:449–58. doi: 10.1080/17474086.2017.1313699
37. Woyke S, Rauch S, Strohle M, Gatterer H. Modulation of Hb-O2 affinity to improve hypoxemia in COVID-19 patients. *Clin Nutr.* (2020) 40:38–9. doi: 10.1016/j.clnu.2020.04.036
38. Brugger H, Paal P, Falk M. Outcry stopped approved pig study of avalanche survival. *Nature.* (2010) 463:877. doi: 10.1038/463877a
39. Condò SG, Corda M, Sanna MT, Pellegrini MG, Ruiz MP, Castagnola M, et al. Molecular basis of low-temperature sensitivity in pig hemoglobins. *Eur J Biochem.* (1992) 209:773–6. doi: 10.1111/j.1432-1033.1992.tb17347.x
40. Willford DC, Hill EP. Modest effect of temperature on the porcine oxygen dissociation curve. *Respir Physiol.* (1986) 64:113–23. doi: 10.1016/0034-5687(86)90035-6
41. Paal P, Braun P, Brugger H, Strappazzon G, Falk M. How the media and animal rights activists put avalanche burial study on ice. *BMJ.* (2010) 341:c3778. doi: 10.1136/bmj.c3778
42. Böning D, Littschwager A, Hütler M, Beneke R, Staab D. Hemoglobin oxygen affinity in patients with cystic fibrosis. *PLoS ONE.* (2014) 9:e97932. doi: 10.1371/journal.pone.0097932

Conflict of Interest: The authors declare that the research was conducted in the absence of any commercial or financial relationships that could be construed as a potential conflict of interest.

Publisher's Note: All claims expressed in this article are solely those of the authors and do not necessarily represent those of their affiliated organizations, or those of the publisher, the editors and the reviewers. Any product that may be evaluated in this article, or claim that may be made by its manufacturer, is not guaranteed or endorsed by the publisher.

frontiers in Medicine

REVIEW
published: 23 February 2022
doi: 10.3389/fmed.2022.824395

Physiological Changes in Subjects Exposed to Accidental Hypothermia: An Update

Lars J. Bjertnæs[1,2], Torvind O. Næsheim[2,3], Eirik Reierth[4], Evgeny V. Suborov[5], Mikhail Y. Kirov[6], Konstantin M. Lebedinskii[7,8] and Torkjel Tveita[1,2]*

[1] Department of Clinical Medicine, Faculty of Health Sciences, Anesthesia and Critical Care Research Group, University of Tromsø, UiT The Arctic University of Norway, Tromsø, Norway, [2] Division of Surgical Medicine and Intensive Care, University Hospital of North Norway, Tromsø, Norway, [3] Department of Clinical Medicine, Faculty of Health Sciences, Cardiovascular Research Group, University of Tromsø, UiT The Arctic University of Norway, Tromsø, Norway, [4] Science and Health Library, University of Tromsø, UiT The Arctic University of Norway, Tromsø, Norway, [5] The Nikiforov Russian Center of Emergency and Radiation Medicine, St. Petersburg, Russia, [6] Department of Anesthesiology and Intensive Care, Northern State Medical University, Arkhangelsk, Russia, [7] Department of Anesthesiology and Intensive Care, North-Western State Medical University named after I.I. Mechnikov, St. Petersburg, Russia, [8] Federal Research and Clinical Center of Intensive Care Medicine and Rehabilitology, Moscow, Russia

OPEN ACCESS

Edited by:
Andrey V. Kozlov,
Institute for Experimental and Clinical Traumatology (LBG), Austria

Reviewed by:
Sebastian Brandt,
University of Lübeck, Germany
Wolfgang Sipos,
University of Veterinary Medicine Vienna, Austria

***Correspondence:**
Lars J. Bjertnæs
lars.bjertnaes@uit.no

Specialty section:
This article was submitted to Intensive Care Medicine and Anesthesiology, a section of the journal Frontiers in Medicine

Received: *29 November 2021*
Accepted: *28 January 2022*
Published: *23 February 2022*

Citation:
Bjertnæs LJ, Næsheim TO, Reierth E, Suborov EV, Kirov MY, Lebedinskii KM and Tveita T (2022) Physiological Changes in Subjects Exposed to Accidental Hypothermia: An Update. Front. Med. 9:824395. doi: 10.3389/fmed.2022.824395

Background: Accidental hypothermia (AH) is an unintended decrease in body core temperature (BCT) to below 35°C. We present an update on physiological/pathophysiological changes associated with AH and rewarming from hypothermic cardiac arrest (HCA).

Temperature Regulation and Metabolism: Triggered by falling skin temperature, Thyrotropin-Releasing Hormone (TRH) from hypothalamus induces release of Thyroid-Stimulating Hormone (TSH) and Prolactin from pituitary gland anterior lobe that stimulate thyroid generation of triiodothyronine and thyroxine (T4). The latter act together with noradrenaline to induce heat production by binding to adrenergic β3-receptors in fat cells. Exposed to cold, noradrenaline prompts degradation of triglycerides from brown adipose tissue (BAT) into free fatty acids that uncouple metabolism to heat production, rather than generating adenosine triphosphate. If BAT is lacking, AH occurs more readily.

Cardiac Output: Assuming a 7% drop in metabolism per °C, a BCT decrease of 10°C can reduce metabolism by 70% paralleled by a corresponding decline in CO. Consequently, it is possible to maintain adequate oxygen delivery provided correctly performed cardiopulmonary resuscitation (CPR), which might result in approximately 30% of CO generated at normal BCT.

Liver and Coagulation: AH promotes coagulation disturbances following trauma and acidosis by reducing coagulation and platelet functions. Mean prothrombin and partial thromboplastin times might increase by 40–60% in moderate hypothermia. Rewarming might release tissue factor from damaged tissues, that triggers disseminated intravascular coagulation. Hypothermia might inhibit platelet aggregation and coagulation.

Kidneys: Renal blood flow decreases due to vasoconstriction of afferent arterioles, electrolyte and fluid disturbances and increasing blood viscosity. Severely deranged renal function occurs particularly in the presence of rhabdomyolysis induced by severe AH combined with trauma.

Conclusion: Metabolism drops 7% per °C fall in BCT, reducing CO correspondingly. Therefore, it is possible to maintain adequate oxygen delivery after 10°C drop in BCT provided correctly performed CPR. Hypothermia may facilitate rhabdomyolysis in traumatized patients. Victims suspected of HCA should be rewarmed before being pronounced dead. Rewarming avalanche victims of HCA with serum potassium >12 mmol/L and a burial time >30 min with no air pocket, most probably be futile.

Keywords: accidental hypothermia, cardiopulmonary resuscitation, hypothermic cardiac arrest, temperature regulation, extracorporeal life support, hibernating animals, oxygen-saving mechanisms, systemic inflammatory response syndrome

INTRODUCTION

Accidental hypothermia (AH) is a fall in body core temperature (BCT) to below 35°C after exposure to cold or decrease in metabolic rate (1, 2). Volunteers subjected to hypothermia may present with reduced consciousness when approaching a BCT of 33.5°C. Simultaneously, the electroencephalogram (EEG) shifts to less alpha activity and more theta and beta frequencies. Most people lose consciousness at a BCT of 30°C and EEG mostly appears isoelectric below 20°C (3, 4).

Humans react to mild hypothermia (BCT of 35–32°C) with tachypnea, peripheral vasoconstriction and increased tendency of atrial fibrillation. Arrhythmia risk increases as the temperature drops further. Severe hypothermia (below 28°C) is associated with falling respiratory rate, increased tidal volumes, reduced oxygen consumption and increased risks of more severe cardiac dysrhythmias (atrioventricular block, ventricular fibrillation, asystole, or pulseless electrical activity). Estimated mortality rate after AH varies between 30 and 80%. In deep AH (below 20°C), nearly all patients present with asystole (5–7).

In a historical perspective, AH has contributed to the outcome of wars. While crossing the Alps during his siege of Italy (218–203 BC), Carthaginian general Hannibal lost an estimated half of his army of more than 100.000, and Napoleon when attacking Russia in 1812, left behind more than half a million men in battle, or because of malnourishment and hypothermia combined. Nearly one million German soldiers perished during the battle of Stalingrad in World War II, and the subsequent retreat in February 1943 (8, 9).

The lowest BCT noticed in survivors of HCA, is 11.8°C in a 2½ year old boy and 13.7°C in a 29 year old female skier, respectively (10, 11). However, the temperature limit, to which the human body can be actively cooled, followed by hours of hypothermic cardiac arrest (HCA), and still with a maintained potential of successful resuscitation, is unknown. Hypothermia with BCT of 9 and 4.2°C, followed by 1 hour of cardiac arrest (CA), was induced as adjunct therapy in two patients suffering from cancer. Although HCA had no beneficial effects on the malignancies, the patients underwent successful resuscitations with no sequela due to the cooling *per se* (12, 13).

Prognosis of hypothermic cardiac arrest (HCA) depends on the circumstances causing AH, the quality and length of cardiopulmonary resuscitation (CPR, and the types of treatments given from the scene of accident to a tertiary hospital providing rewarming by means of extracorporeal life support (ECLS) (14, 15). However, if such a hospital could not be reached, survival from HCA has been reported even after 6½ h of manually performed cardiopulmonary resuscitation (CPR) at a local hospital (16). Notably, survival rate differs between victims of witnessed CA being able to breathe while gradually loosing body temperature, and those developing asphyxia and acidosis before the heart stops (17–19). Particularly high mortality rates were reported in traumatized patients with a BCT below 32°C, in whom mortality reached nearly 100% (20).

As activities in circumpolar areas increase, AH affects not only the poor and the elderly, but also tourists, hikers, skiers, mountain climbers and workers exploiting natural resources. Often taking place on remote locations, these activities necessitate that health personnel have a good knowledge of the physiology and pathophysiology of AH and update themselves about logistics and treatment algorithms and train together as teams (21). Our aim is to update the readers on physiological changes occurring in various organ systems, as a knowledge basis for rewarming victims of AH and HCA. Although the topic recently was reviewed by one of us, the different emphasis should make this paper be considered as complementary (22).

BACKGROUND AND METHODS

In April 2016, we started a collaboration in studying the management of accidental hypothermia between Anesthesia and Critical Care Research Group, Department of Clinical Medicine, Faculty of Heath Sciences, The Arctic University of Norway, Tromsø, Norway and The Department of Anesthesiology and Intensive Care Medicine, North-Western State Medical University named after I.I. Mechnikov, St. Petersburg and

Department of Anesthesiology and Intensive Care, Northern State Medical University, Arkhangelsk, Russia. We agreed on starting the collaboration with publishing our local Norwegian guidelines for rewarming victims of HCA in Anesteziologia and Reanimatologia, the official Journal of the Russian Society of Anesthesiologists (23). Moreover, we aimed at authoring a review and meta-analysis on rewarming victims of HCA by means of extracorporeal life support (ECLS) (24), and the present update on the physiology and pathophysiology of accidental hypothermia and HCA. The latter two projects are registered in PROSPERO international prospective register of systematic reviews (registration no. 47,934). These projects spawned a systematic search for references across two databases (Medline and EMBASE), resulting in close to 1,600 references of interest, made available for all co-authors by use of Endnote (Endnote TM 97.4; Thompson Reuters. Toronto, ON, Canada). In addition, we performed a directed and goal-oriented search for additional references in the same databases, using key scientific phrases from each of the headline partitioning in this update. References were screened before making a discretionary consensus-based selection of which of them we found relevant to include in each individual paper.

The present update originates from our collective experiences from clinical practice and experimental activities. Six of the authors have a background as consultants in anesthesia with cardiothoracic anesthesia and intensive care medicine, including extracorporeal membrane oxygenation (ECMO), as main fields of interest. Two of the authors, additionally have worked as consultants in the governmental Norwegian air ambulance system (LB and TN). All the authors have doctoral degrees or have spent several years in experimental physiology and/or pathophysiology research.

The following key search phrases were used in combination with hypothermia, in the additional directed and goal-oriented search for additional references: temperature regulation, myocardial function*, drug*, CPR, cardiopulmonary resuscitation, respiration, respiratory, breath holding, acidosis, coagulation, fibrinolysis, kidney, liver function. For complete information on search methodology [see (24)].

HYPOTHERMIA-INDUCED CHANGES IN ORGAN FUNCTIONS

Temperature Regulation and Metabolism

Temperature homeostasis is a thoroughly regulated balance between heat production and dissipation. AH occurs when heat loss is greater than heat production. The drop in BCT either results from decreased metabolic rate or exposure to cold without capability of increasing heat production sufficiently, giving rise to "chronic hypothermia" (2). Patients abusing drugs and alcohol or suffering from cancer or sepsis are often disposed to malabsorption and endangered by AH due to decreased thermogenesis. In some countries, particularly the elderly are prone to AH because of poor living quarters, malnourishment, neglected illnesses and lack of physical activity (25, 26).

Skeletal muscles generate heat under physical activity and by shivering thermogenesis, which might increase heat production by up to five times. An integrated response to cold triggers formation of Thyrotropin-Releasing Hormone (TRH) in the preoptic area of hypothalamus. Acting *via* secretion of Thyroid stimulating hormone (TSH), TRH promotes synthesis and release of triiodothyronine (T_3) and its prohormone, thyroxine (T_4) in the thyroid gland. These hormones work in concert with increasing noradrenergic stimulation to enhance heat production (27).

Neonates of seals that are born on the ice, generate heat under adrenergic stimulation of metabolism of brown adipose tissue (BAT) (28). This is localized in the regions of the back and shoulders (29). When exposing babies to cold, noradrenaline binds to adrenergic β_3-receptors of fat cells that trigger degradation of triglycerides into free fatty acids (FFA). The latter interact with mitochondrial uncoupling protein-1 (UCP1), which uncouples metabolism to produce heat, rather than adenosine triphosphate (ATP). Therefore, if BAT is lacking, for instance, in premature babies, hypothermia occurs more easily (30, 31). In adults, metabolic rate normally rises by increasing metabolism in skeletal muscles (shivering thermogenesis), and in various other tissues as the liver and the intestines. However, the last few years, investigators have shown that BAT also plays an important role in heat generation in adults, as demonstrated by means of ^{18}F - FDG-positron emission tomography/computed tomography (PET/CT) imaging (32, 33).

According to recent investigators, the amount of BAT can be linked to the body mass index (BMI) and the season of conception. By transferring these ideas to an experimental model on mice, the authors showed that cold exposure of males before mating resulted in increased systemic metabolism and protection of male offspring from diet-induced obesity (34). The investigators suggested that the improved metabolic condition of the offspring was due to enhanced BAT formation, increased neurogenesis, and noradrenaline release into BAT during cold exposure. They concluded that epigenetic changes might occur that can even improve cold-adaption of future generations in sperms of individuals exposed to cold climate (34).

Fur animals reduce heat dissipation by means of piloerection, which widens the air layer insulating the skin. This α_1-adrenergic and phylogenetically old heat conservation mechanism also occurs in humans, although being of little practical significance (35).

Researchers have suggested to increase body temperature of victims of immersion or exposure to cold by supplying them with a pill that can increase heat production, such as 3,4-methylenedioxymethamphetamine (MDMA, "Ecstasy") (36). Clinical experiments indicate that the MDMA-induced elevation of human body temperature partially depend on release of norepinephrine, which involves enhanced metabolic heat generation concomitant with cutaneous vasoconstriction, resulting in impaired heat dissipation. However, use of this recreational drug in an emergency should be strongly discouraged.

Can We Learn From Hibernating Animals?

Mammals, such as hedgehogs, bats, hamsters, squirrels and bears hibernate to save energy. The ground squirrel, for instance, hibernates through seven months of freezing temperatures, during which its heart rate and body temperature drops to approximately one beat per minute and nearly −3°C below the freezing point of water, respectively, while brain temperature remains above +0.7°C. During hibernation, circadian clock function is inhibited for periods of up to 13 days (37). Why blood does not freeze when undercooled remains a puzzle. Some experts believe that ground squirrels are able to remove nucleators from circulation that generate ice crystals in blood (38). However, although the mechanism behind this super cooler remains grossly unclear (39), it could be of potential use both for preservation of donated organs for transplantations and for provoking a state of "suspended animation" in severely traumatized patients while awaiting blood transfusion or organ transplantation (40, 41).

Myocardial Changes During Hypothermia and After Rewarming

Hypothermia is frequently associated with myocardial dysfunction. Previous researchers noticed that when dogs were cooled to a BCT of 21°C, cardiac output (CO) decreased exponentially to 20% of its value at normal BCT and recovered to significantly below its control value upon rewarming whereas myocardial blood flow (MBF) returned to pre-hypothermic values (42). Tveita et al. reported a 37% decrease in CO upon cooling of dogs to 25°C, but in their experiments neither CO nor MBF returned to their pre-hypothermic control values upon rewarming (43). By lowering the aortic arch temperature in rats to 13–15°C, Tveita et al. observed that CO fell to 13% of its control value. Assuming a 7% drop in metabolism per °C fall in BCT a spontaneously breathing patient should experience approximately a 75% reduction of metabolism following a fall in BCT to 26°C and a corresponding decrease in CO (44). Consequently, if cardiac arrest occurs at or below this temperature, it is possible to maintain adequate oxygen delivery by means of external CPR. In dogs, correctly performed heart-lung resuscitation resulted in 42% of the CO measured with Fick's principle prior to ventricular fibrillation (45). In patients with cardiac arrest, Fodden and coworkers obtained a median cardiac index (CI) of 3.2 L $min^{-1} \cdot m^{-2}$ as assessed by Doppler aortovelography during external cardiac compression performed by experienced personnel as opposed to 1.2 L min^{-1} m^{-2} when CPR was carried out by unexperienced operators (46). The electrocardiogram (ECG) changes characteristically during hypothermia. Patients may present with sinus bradycardia, AV-block, widened QRS complex, QT prolongation or pulseless electrical activity (PEA) (47, 48). Higuchi and co-workers analyzed the prevalence of so-called Osborne J waves (hypothermia-associated notches on the QRS complex) in 60 AH patients. In 50% of the patients, the investigators found Osborne J waves that disappeared upon rewarming to pre-hypothermic BCT. The J waves tended to occur with higher frequency and amplitude in patients with the lowest BCT. However, the authors found no associations between J waves and fatal arrhythmias (49).

In 2012, Shattock and Tipton introduced the concept "autonomic conflict," which is a potential mechanism of arrhythmias that frequently causes unexpected deaths in cold water due to simultaneous powerful stimulation of both the sympathetic and the parasympathetic nervous systems (50, 51). According to the authors, "autonomic conflict" occurs suddenly upon rapid submersion and breath holding in water at temperatures <15°C. This activates two powerful autonomic responses, the cold shock response, and the diving response. The former consists of reflexes driven by cutaneous cold-receptors and is characterized by sympathetically mediated tachycardia, a respiratory gasp, uncontrollable hyperventilation, peripheral vasoconstriction, and hypertension. The latter reflex triggers a strong excitation of cardiac vagal motor neurons *via* M_2 acetylcholine receptors causing sinus bradycardia and expiratory apnea. Reflex inhibition of central respiratory neurons and excitation of sympathetic vasoconstrictor neurons make up the complete picture. These responses generate vasoconstriction mainly in the trunk and the limbs, thereby prioritizing cerebral blood flow and oxygenation (50).

Despite the fact that cardiac contractility is partially restored after rewarming, cardiac function may be a limiting factor for survival after AH (52). The reduced contractility in deep hypothermia (BCT<15°C) is believed to be caused by reduced myocyte calcium (Ca^{2+}) - sensitivity in association with increased phosphorylation of Troponin I (52–54). According to Kondratiev et al. alterations in Ca^{2+}-handling resulted in Ca^{2+} - overload during hypothermia/rewarming, which may contribute to myocardial failure during and after rewarming (55). In contrast, in mild hypothermia in pigs (33°C), left ventricular contractility increases, as compared to the situation at 37°C, and diastolic relaxation appeared to be delayed independent of heart rate (56). However, another porcine study failed to show increased contractility, as determined by echocardiography and preload recruitable stroke work relationship. By contrast, in that investigation the heart showed increased duration of systole on the account of reduced ventricular filling and shortening of the diastole (57). Thus, apparently the increased contractility in mild hypothermia does not depend on increased Ca^{2+}-transients in myocytes, but rather on increased myofilament responsiveness to calcium (58).

Inotropic, Vasoactive and Antiarrhythmic Drugs in Hypothermic Subjects

Evidence is sparse concerning the effects of vasoactive-, antiarrhythmic- and inotropic drugs in victims of AH. Therefore, most recommendations are derived from animal experiments (59). After rewarming from deep AH, an acute cardiac failure, called "rewarming shock" threatens the patients. This is a progressive reduction of cardiac output (CO) in association with a decrease in arterial blood pressure. Inotropic drugs have been tested in attempts on preventing rewarming shock (60). However, the effect of anti-arrhythmic and inotropic medicines in victims

of HCA seems ambiguous. Therefore, international guidelines are reluctant to recommend their use (61, 62).

Clinical experience indicates that the hypothermic heart is relatively unresponsive to defibrillation, pacing and vasoactive – and anti-arrhythmic drugs below a BCT of 30°C (62). Tveita and Sieck report from experiments on rats that adrenalin, given during normothermia, in doses that increased CO without affecting vascular resistance, gave rise to vasoconstriction, but failed to elevate a low CO when injected on hypothermic animals (60). In contrast, a recent meta-analysis of investigations aimed at studying return of spontaneous circulation (ROSC) in severely hypothermic animals with ventricular fibrillation, revealed that success rates were higher with application of vasopressor medications (i.e., adrenaline or vasopressin), as compared with placebo (63).

In normothermic conditions, adrenaline affects cardiac contractility by stimulating myocyte sarcolemmal β-adrenoceptors *via* cyclic adenosine monophosphate (cAMP) and protein kinase A pathways. This allows for a greater trans-sarcolemmal Ca^{2+} influx with each depolarization, which is partly responsible for the positive inotropic effect of adrenaline during normothermia. Relaxation is caused by re-uptake of Ca^{2+} into the sarcoplasmic reticulum by means of sarcolemmal ATPase and Na^{+}/Ca^{2+} exchange (64). In pigs exposed to dopamine infusion during surface cooling to a BCT of 25°C, left ventricle stroke volume fell and systemic vascular resistance and heart rate increased concomitant with a four-fold rise in dopamine plasma concentration, as compared with the condition after rewarming (65).

Concerning antiarrhythmic therapy, hypothermic dogs with ventricular fibrillation treated with either amiodarone or bretylium demonstrated no significant difference in survival rate as compared with placebo-treated controls (66). Interestingly, researchers studying HCA in rats reported that the combined calcium sensitizer and phosphodiesterase 3 (PDE3) inhibitor, levosimendan, exerted positive inotropic effects during hypothermia and rewarming from a core temperature of 15°C (67, 68). However, in spite of documentation of promising effects on rats, we found only an anecdotal report confirming similar effects of levosimendan on cardiac function in humans (69). Thus, according to recent studies, administration of adrenaline might be futile during resuscitation of individuals with BCT below 30°C. Indications for dopamine and levosimendan as inotropic and vasoactive support for resuscitation of patients with HCA need to be further elucidated in experimental and clinical studies (70).

Continuity of CPR in Victims of HCA

Prehospital, resuscitation of hypothermic patients should be rejected only if the cause of CA is attributable to a lethal injury, fatal illness, prolonged asphyxia, or incompressible chest stiffness (61). If diagnosed without pulses after checking for 1 min, CPR of a hypothermic patient should start immediately, and preferentially continue with a mechanical chest-compression device to avoid interruption during transport (71, 72). The European Resuscitation Council recommend the same technique for chest compression and ventilation rates for patients of HCA as for normothermic victims of CA. Moreover, if ventricular fibrillation (VF) persists after three attempts of defibrillation, further attempts should be postponed until the patient is warmed to a BCT above 30°C. Adrenaline injections also should be avoided when BCT is below 30°C. When BCT raises above 30°C, adrenaline administration intervals of 6–10 min during normothermia should be doubled (61). In patients with a BCT of between 28 and 20°C, or with unknown BCT, CPR should go on continuously for periods of at least 5 min, alternating with periods of no longer than 5 min without CPR. In victims of HCA with a BCT below 20°C, CPR should be interrupted maximally for 10 min p (73).

Oxygen–Saving Mechanisms

In victims of asphyxia, like drowning and avalanches, respiration might be hampered before the heart stops, due to aspiration of liquids into the airways, or compression of the chest hindering lung ventilation. On the other hand, according to forensic investigators, 10–15% of drowned victims have "dry" airways because laryngeal spasm has prevented water from intruding into the airways (74–76). More than 80 years ago, Irwin and Scholander suggested that in diving animals, breath-holding triggers cardiovascular mechanisms that are established for saving oxygen by preferentially redistributing circulation to the myocardium and the brain, the organs most in need of continuous oxygen supply (77, 78). A heart catheterization study in humans showed that intermittent periods of apnea and face immersion (AFI) more than halved cardiac output (CO) concomitant with a doubling of systemic vascular resistance during ergometer bicycling at constant workload (79). While bicycling at the same workload, one of the test subjects demonstrated a 85% reduction in average blood velocity (ABV) in a radial artery concomitant with a 67% increase in ABV in a vertebral artery during exposure to AFI, as determined with a Doppler ultrasound velocity meter (80). Correspondingly, Kjeld et al. noticed that middle cerebral artery ABV more than doubled during AFI when exercising at 100 Watt (81). In 1999, Lindholm et al. found a correlation between cardiovascular responses and oxyhemoglobin desaturation rate, indicating a causal relationship between intensity of the cardiovascular responses to apnea and O_2 -conservation, as reflected by a less steep decline in SaO_2, as determined by pulse oximetry during breath-holding (82). An increase in vertebral artery ABV also might be triggered by a rise in $PaCO_2$ secondary to apnea. In a real drowning situation, the increase in vertebral artery blood flow could potentially increase the rate of brain cooling due to heat exchange in the lungs concomitantly reducing the cerebral metabolic oxygen demand, thus prompting a more successful outcome from drowning, as suggested by Golden and recently demonstrated in the seal by Blix and co-workers (83, 84).

The AFI-induced increase in systemic arterial pressure (79), which is also observed in diving ducks, differs from that experienced in seals in whom there is no such increase while cardiac output decreases to ∼1/10 of its value during normal breathing (85). We cannot decide to what extent the diving response protects people exposed to drowning or burial by avalanche from brain anoxia. However, case reports of successful

resuscitation after more than 40 min of HCA after submersion, make such contributions likely (50, 86–88).

Respiratory Effects of Hypothermia

In victims of AH, respiratory rate and depth decrease with falling BCT. Evolving hypoventilation causes CO_2 accumulation, which gives rise to hypoxia and respiratory acidosis. Mucociliary function of the respiratory epithelium and the cough reflexes are depressed, thus predisposing for secrete stagnation and pneumonia (89). Studies in sheep cooled on femoral veno-arterial bypass revealed that lung mechanics are affected during cooling and rewarming. During deep hypothermia lung compliance dropped transiently, but normalized upon rewarming to 24–30°C, and decreased again on further warming (90). A retrospective study of mechanically ventilated patients exposed to therapeutic hypothermia after cardiac arrest, showed significant decreases in $PaCO_2$ and airway pressure and increased lung compliance, as compared with normothermic controls (91). In full term infants subjected to whole body cooling because of hypoxic ischemic encephalopathy, PaO_2/FIO_2 ratio increased in concert with a decrease in $PaCO_2$, which was interpreted as a result of reduced oxygen consumption and CO_2 production at unchanged ventilation and constant PEEP levels during hypothermia (92, 93).

Hypothermia-Induced Changes in pH

A neutral solution is defined as one containing equal numbers of $[H^+]$ and $[OH^-]$ ions, not as a solution of a pH of 7. In any solution, pH changes with temperature since the dissociation of H_2O into $[H^+]$ and $[OH^-]$ions is an endothermic reaction. When the temperature decreases, the concentration of $[H^+]$ falls in parallel with a raising pH. However, the ratio between $[H^+]$ and $[OH^-]$, remains unchanged and acid/base neutrality is maintained (94). The ratio of protonated to non-protonated intracellular proteins depends on neutrality rather than pH, and therefore remains constant, independent of temperature changes. In hypothermic patients, correction of pH by adjusting an apparent respiratory alkalosis at normal BCT, might lead to disruption of the normal extracellular/intracellular pH-gradient. This might cause distortion of intracellular neutrality, and derangement of cellular function.

As the solubility of O_2 and CO_2 in water increases with decreasing temperature, gaseous partial pressures above the liquid level fall as the temperature drops. Hemoglobin's affinity for oxygen also increases when the temperature falls. This results in a discrepancy between gaseous partial pressures and the contents of gases in blood. Ashwood and co-workers demonstrated that the oxygen content of blood is constant over a wide range of temperatures although PaO_2 varies (95). Temperature corrections of partial pressures of O_2 and CO_2 in hypothermic patients might therefore lead to interventions that will induce unphysiological blood gas concentrations.

Before measuring blood gases, the blood gas analyzer warms the blood sample to 37°C. If BCT of the patient is below 37°C, PaO_2, $PaCO_2$ and pH will change during heating of the sample to 37°C. Thus, the values will not reflect the actual levels in the cold patient. Correcting formulas, allow us to use the values determined at 37°C for correction of any blood gas abnormalities. This kind of correction is named the pH-stat-strategy. However, such corrections can be physiologically delusive. Alternatively, according to the so-called alpha-stat strategy, we accept the values measured at 37°C without any correction, When we use the pH-stat strategy, gaseous CO_2 often must be added to the inspiration gas mixture to achieve normal $PaCO_2$ and pH values, as compared with the α-stat strategy (96).

Carbon dioxide (CO_2) is a cerebral vasodilator. Increased levels of CO_2 have a potential of increasing cerebral perfusion beyond metabolic requirements by offsetting cerebral autoregulation (CAR). When using CPB, the increased cerebral blood flow is associated with an increased risk of cerebral emboli (97). Reduced pH and increased CO_2-levels counteract a leftward shift of the oxyhemoglobin dissociation curve, facilitating release of O_2 to the tissues. (98, 99). Gaasch and co-workers noticed impaired CAR during deep hypothermia in pigs. However, despite a decrease in MAP and CPP, brain oxygenation increased, most likely due to a decrease in brain metabolism (100).

Rats subjected to transient closure of the middle cerebral artery at normal BCT, subsequently followed by reperfusion for 5 h at 33°C, and treatment according to the pH-stat- strategy, had significantly better outcome as compared with animals exposed to an α-stat policy. These findings also were confirmed in piglets cooled to a brain temperature of 19°C and subsequently subjected to profound HCA for 90 min before being resuscitated on CPB (101, 102). In patients undergoing combined valve surgery with $pH/PaCO_2$ - management following the pH-stat policy, investigators reported that CPB at BCT $\leq$32°C resulted in higher central venous oxygen saturation, but decreased cerebral tissue oxygenation, oxygen delivery and oxygen consumption, as compared with normothermic CPB (103). Abdul Aziz and Meduoye stratified outcome results from 16 best evidence reports. They suggested that the best management of acid-base balance in patients undergoing deep HCA during cardiac surgery depends upon the age of the patient. The authors concluded that the pH-stat protocol should be used in children and the alpha-stat strategy in adults (104).

Blood Coagulation and Fibrinolysis

Victims of HCA often present with changes in the coagulation system. However, there is no consensus on whether these changes are due to asphyxia, acidosis, or hypothermia *per se*, or to a combination. Traumatized patients may suffer increased blood loss because of deranged coagulation. The mechanisms include activation of protein C, platelet dysfunction, fibrinogen depletion, and endothelial glycocalyx disruption. Hypothermia and acidosis that often accompany trauma, may amplify the coagulopathy. Researchers have demonstrated significant reductions in platelet function and coagulation system activity even after mild hypothermia (105, 106). However, evidence is conflicting and there is still a need to elucidate the effect on platelet function of hypothermia *per se*. Some investigators suggest that platelet aggregation even increases in mild hypothermia (107, 108). They believe that the increased

bleeding rather results from coagulopathy, consistent with impaired thrombin generation (109).

In a cohort of 58 traumatized patients, the investigators found that half of them presented with life-threatening coagulopathy characterized by prothrombin time and partial thromboplastin time that were the double of those of the controls. Multiple logistic regression revealed four significant risk factors, (1) pH <7.10 with odds ratio (OR 12.3), (2) temperature <34°C (OR 8.7), (3) Injury Severity Score (ISS) >25 (OR 7.7) and (4) systolic blood pressure <70 mm Hg (OR 5.8). With all risk factors present, incidence of coagulopathy amounted to 98%. This indicates that in traumatized patients, even mild hypothermia may increase bleeding. Thus, protective measures against heat loss should have high priority already from the site of accident.

Tissue hypoxia can induce expression of tissue factor (TF) (110), thereby triggering the coagulation system. According to Østerud and Bjørklid, TF originates from TF-rich micro particles shedded from monocytes (111). Deep hypothermia followed by rewarming can lead to tissue factor (TF) release from damaged tissues, which triggers the formation of fulminant disseminated intravascular coagulation (DIC), as reported by Mahajan and co-workers (112). These investigators argue that hypothermia inhibits both platelet aggregation and coagulation in cases in which hypothermia occurs prior to asphyxia and cardiac arrest.

Liver Function

In patients with HCA, liver function tests, such as serum aspartate aminotransferase (ASAT) and alanine aminotransferase (ALAT were used as markers for liver damage. Both increased significantly albeit without significant difference between survivors and non-survivors (113). The liver produces most of the coagulation factors. Hepatocytes synthesize fibrinogen, prothrombin, coagulation factors V, VII, IX, X, XI, XII, proteins C and S and antithrombin, and sinusoidal endothelial cells produce von Willebrand factor and factor VIII (114). Recently, researchers examined the effect of hypothermia on the coagulation cascade and found that mean prothrombin time and partial thromboplastin time increased significantly by ∼40 and 60%, respectively. The authors conclude that hypothermia strongly inhibits the enzymatic reactions of the coagulation cascade even when coagulation factor levels were normal (115).

The liver also plays an important role in the metabolism and clearance of drugs from circulation, but displays reduced capability in patients undergoing therapeutic hypothermia (116). Let us, for instance, assess the metabolism of midazolam. In a study, eight patients were subjected to mild therapeutic hypothermia for 48 hrs, with seven normothermic controls (117). Each subject received midazolam 5 μg/kg/min intravenously. Normothermic subjects obtained steady state plasma concentration of ∼1500 ng/mL. The hypothermic patients did not achieve steady state, but obtained a five-fold increase in midazolam plasma concentrations when BCT fell <35°C. Pharmacokinetic analysis showed a >100-fold decrease in systemic clearance of midazolam when BCT fell <35°C. Since midazolam degradation depends on CYP3A4 and CYP3A5 activities, the marked increase in midazolam concentration were due to depressed activity of the cytochrome P450 family of detoxification enzymes. These enzymes are responsible for the clearance of a great variety of commonly used drugs (118).

Kidney Function, Electrolytes and Fluid Balance

By lowering BCT of rats by 10°C, renal blood flow (RBF) decreased by nearly 50% followed by an almost complete restoration of control values after rewarming (119). Systemic blood pressure remained unchanged throughout the experiment. The reduced RBF was due to a 75% increase in vascular resistance, due to constriction of afferent arterioles, combined with increased blood viscosity. A decrease in glomerular capillary pressure during cooling changed into an excessive pressure after rewarming. The glomerular filtration rate (GFR) decreased by almost 50 % during hypothermia and increased to nearly baseline values after rewarming. The fall in GFR assumingly resulted from a decrease in filtration net driving pressure at unchanged filtration coefficient. Both proximal and distal tubular fluid flow decreased, but fractional reabsorption remained unchanged. Interestingly, urine flow increased by more than 200% during hypothermia, mainly as a result of reduced fluid reabsorption in the distal tubules, and returned to slightly above baseline after rewarming (119). These observations were consistent with findings in dogs cooled to 21°C of 73 and 80% reductions of renal cortical and medullary blood flows, respectively, as reported by Anzai et al. (42).

Based on a meta-analysis of data from patients who underwent thoracic aortic surgery in deep hypothermic circulatory arrest, the authors found no evidence that hypothermia *per se* damage the kidneys (120). Another study showed that therapeutic hypothermia prevented neither the development of acute kidney injury nor the requirement of dialysis (121). Recently, Arnaoutakis et al. showed that patients undergoing elective ascending aortic hemiarch repair, showed no difference in rates of acute kidney injury between one group, operated under moderate HCA and anterograde cerebral perfusion, and another group exposed to deep HCA and retrograde cerebral perfusion (122). On the other hand, after injuries, rhabdomyolysis, characterized by increased serum levels of myoglobin, creatine kinases (CK and CK-MB) and transaminases (ASAT and ALAT), often presents with acute renal injury. Evidence is accumulating that even therapeutic hypothermia may facilitate rhabdomyolysis in injured patients (123, 124). To reduce the risks of rhabdomyolysis, experts recommend increased administration of isotonic fluids from the site of accident, and in case of myoglobinuria, sodium bicarbonate solution should be administered for urine alkalinization (123).

Lactic acidosis and electrolyte and fluid disturbances characterize non-survivors of AH. Elevated serum potassium concentration, traditionally a marker of asphyxia, has been considered a limiting factor of successful resuscitation in victims of HCA (18). Attempts on resuscitating HCA patients with serum potassium exceeding 9 mmol/L were considered futile until Dobson and Burgess successfully resuscitated a girl aged 31 months with a serum potassium concentration of 11.8 mmol/L. She had unattended locked herself out from home

(outdoor temperature −22°C) after her father had left for work at 02:30 in the morning. Her mother found her pulseless without respiration at 08:10. Two nurse residents provided CPR, and ambulance personnel intubated her at 09:15. Then, ECG showed bradycardia (< 10 beats/minute) without palpable pulses. She arrived at hospital at 09:38 with a rectal temperature of 14.2°C and was connected to CPB for rewarming at 10:10. After successful resuscitation, her condition complicated with gangrene of left leg, necessitating amputation. When followed up at 3 years of age, she was able to walk with a prosthesis. Her development was otherwise unremarkable (125).

Recently, investigators resuscitated a 7 year old boy after an estimated submersion time of at least 83 min in icy sea water presenting on admission to hospital with a potassium of 11.3 mmol/L and a pH of 6.6 (126). However, despite these rare reports, most authors still agree that high potassium values might identify HCA victims in whom death occurred before cooling (127).

A few years ago, investigators reported median potassium concentrations in survivors of HCA of 5.9 mmol/L against 7.7 mmol/L in non-survivors (14). In a retrospective study of avalanche victims, Locher et al. reported a serum potassium concentration of 6.4 mmol/L in one of the patients, which is the highest ever registered in a survivor of avalanche (128). Arterial lactate concentration also has been suggested a role as prognostic factor of AH with refractory cardiac arrest, but no consensus has been reached concerning its concentration limit with a maintained possibility of surviving.

Generally, AH patients with poor outcomes present with lower pH and higher concentrations of potassium, creatinine, sodium and lactate in parallel with more severe coagulation disorders (127). However, according to Mair and co-workers, moderate and severe hyperkalemia in victims of cardiac arrest after prolonged exposure to cold need not necessarily indicate postmortem autolysis. Consequently, decisions to continue or terminate CPR should not base solely on laboratory parameters (129).

Hypothermia-Induced Microvascular Changes

Victims of severe AH usually present with increases in hemoglobin, hematocrit and blood viscosity (4, 130). Experimental studies reveal that induction of hypothermia is associated with extravasation of water and proteins independent of whether hypothermia is due to surface cooling or core cooling. Investigators have shown that fluids and proteins shifting from the intravascular to the interstitial compartment might result in edema of most organs, except for the lungs, in which fulminant edema often is seen first after rewarming from HCA (131–133). Therefore, investigators recently wondered if hypothermia-induced increase in pulmonary vascular resistance (PVR) could explain this difference (134). They compared fluid filtration rate in normothermic rat lungs perfused with blood at constant flow with two groups of blood-perfused lungs cooled to 15°C; one group perfused at constant flow and one group perfused at constant pulmonary artery inflow pressure (PPA). Increased fluid filtration rate and fulminant edema appeared in hypothermic lungs perfused at constant flow, but significantly less so in lungs perfused at constant PPA that responded more like normothermic controls perfused at constant flow. The findings were interpreted as the result of a more-fold increase in pulmonary vascular resistance (PVR) in the constant PPA group, which reduced microvascular pressure and fluid filtration rate. A similar mechanism could possibly also provide an early protection against lung edema in humans exposed to AH (134).

The mechanisms responsible for hypothermia-induced fluid shifts are poorly understood. Two theories have been proposed; the first states that the decrease in plasma volume could be explained by trapping of plasma within certain parts of the vasculature (135); the second suggests that a net trans-capillary fluid filtration takes place, thus giving rise to hemoconcentration and decreased circulatory volume (17, 136, 137).

In addition to fluid extravasation, water and electrolytes are lost due to "cold diuresis" resulting from peripheral vasoconstriction with increased central pooling of blood and reduced release of antidiuretic hormone. During rewarming vasodilation may add to the hemodynamic effects of fluid loss (138). However, to prevent further heat loss, fluid replacement should only take place with liquids heated to 38–42°C prior to intravenous administration. In a cold pre-hospital environment, intravenous fluids cool rapidly, and cold fluids can exacerbate hypothermia. Moreover, vasodilatation usually accompanies rewarming. Therefore, warm crystalloid fluids should be administered based on general principles for fluid replacement, such as volume status, plasma glucose, electrolyte concentrations and pH measurements. Health personnel also should bear in mind that resuscitation with large volumes of isotonic saline might aggravate acidosis. Vasopressors should be used with caution to antagonize hypotension (59). Notably, these agents can also provoke arrhythmias and compromise peripheral circulation, which is particularly unfortunate in patients at risk for frostbite (139, 140).

Interaction Between Blood – and Membrane Surfaces in Cooling and Rewarming

Endothelial glycocalyx is a meshwork of glycoproteins with a thickness of from 20 to several hundred nanometers, which plays an essential role for maintaining cell junction integrity (141). Glycocalyx consists of three building blocks, hyaluronan, heparan sulfate and syndecan and separates endothelial cells from the blood stream. By interacting with plasma proteins and lipids, it constitutes an integral part of blood rheology, hemostasis, and defense against intruders. Hyaluronan, a main component of extracellular matrix, is an anionic non-sulphated glycosaminoglycan of significant importance for cell migration and proliferation. Based on experiments on umbilical vein endothelium, investigators recently suggested that increased shear stress augments the storage of hyaluronan in the glycocalyx (142). Heparan sulfate is a native proteoglycan, attached with HS-bridges to cell surface or extracellular matrix. When activated, heparan sulfate displays heparin-like anticoagulant properties

(143). Syndecans have strong associations with the actin cytoskeleton with consequences for regulation of cell adhesion and migration. According to Afratis et al., syndecans interact with cell surface receptors, such as growth factor and integrins leading to activation of signaling pathways that are critical for cellular behavior. Syndecans also play a key role in intracellular calcium regulation and homeostasis (144).

Glycocalyx derangement precedes damage to the endothelium (145). In patients undergoing major surgery employing CPB, investigators found more-fold increments in syndecan−1 and heparan sulfate concentrations indicating that these proteoglycans could serve as markers of glycocalyx shedding (146). Studies of coronary vascular permeability concluded that preventing damage to the glycocalyx should be a prioritized goal for cardioprotection in many clinical conditions, including myocardial ischemia, hypoxia and inflammation (147). The glycocalyx degradation products syndecan-1, heparan sulfate and hyaluronan increased as part of the post-cardiac arrest syndrome. Not surprisingly, syndecan-1 and heparan sulfate levels were higher in non-survivors than in survivors of CA (148).

Coronary artery bypass grafting (CABG) is associated with increased glycocalyx shedding if the surgery is performed with CPB as compared with off-pump (149). However, other investigators failed to show differences in peak syndecan-1 concentrations depending on whether patients underwent CABG on- or off-pump, but found that degradation of glycocalyx was preceded by increased levels of atrial natriuretic peptide (150). Rehm et al. also reported increased syndecan-1 and heparan sulfate degradation products after global ischemia during aortic surgery (146). In children, glycocalyx shedding occurred particularly when CPB, aortic clamping and deep hypothermic CA were combined. In contrast, when performed under beating heart conditions, CPB failed to provoke glycocalyx shedding (151). However, so far, no one study has focused specifically on the influence on endothelial glycocalyx of AH *per se*. Thus, the topic needs further elucidation, both experimentally and clinically.

Tissue Factor (TF) triggers the extrinsic coagulation pathway. During exposure to ECLS, complement activation can stimulate release of TF from monocytes. Additionally, TNF-α and IL-6 trigger generation of soluble TF in endothelial cells (152, 153). Moreover, activation of factor X to Xa provokes cleavage of prothrombin to thrombin and subsequently of fibrinogen to fibrin, the ultimate step in clot formation. Thrombin also promotes inflammation through neutrophil activation, and adherence to endothelial cells mediated by adhesion-molecules E-selectin and P-selectin (154). Activated platelets adhere to fibrin deposited on the endothelial surface and stimulate leukocytes to cytokine secretion and TF-expression (152). Endothelial cells generate platelet activating factor (PAF), which activates neutrophils and their generation of inflammatory cytokines (155). Conventional CPB activates the classical complement pathway, the alternative pathway, and the lectin pathway The lectin pathway activates the adaptive and the innate immune systems. The latter systems defend the body against hostile intruders by direct cell lysis or modulation of leucocytes through opsonisation or generation of pro-inflammatory anaphylatoxins. CPB or ECMO with biocompatible membranes, such as the heparin-coating, seems to reduce the intensity of complement activation *in vivo* (156).

Initiation of ECLS causes generation and release of pro- and anti-inflammatory cytokines. Reactive oxygen species (ROS) and cytokines act in concert with complement to stimulate endothelial cells to secrete pro-inflammatory cytokines that interact with leukocytes through adhesion molecules. Expression of P-selectin dominates the early activation of endothelial cells after complement stimulation. Subsequently, TNF-α and interleukin – 1β (IL-1β), overshadow the process, resulting in neutrophil transmigration and tissue infiltration (152). After initiation of ECLS, a slower monocyte activation follows the peak activation of neutrophils. The latter cells degranulate and release cytotoxic enzymes, like elastases, peroxidases, lysozymes, and ROS, causing widespread tissue damage. These constituents appear at high concentrations in bronco-alveolar lavage during ECMO. Monocytes generate pro-inflammatory cytokines that stimulate the extrinsic coagulation system *via* activation of cytosolic TF (152).

Investigators studying the influence of CPB on inflammatory markers during CABG at BCTs of 32 and 36°C, showed no differences in timing or increments in the levels of IL-6, IL-8, IL-10, cortisol, or CRP, within the first 44 h after the start of operation. Postoperatively, bleeding was less in the normothermic group, but transfusion requirements were the same (157). At variance, Grünenfelder et al. showed higher levels of E-selectin, ICAM, IL-6 and IL-8 after 24 h in CABG-patients treated with CPB at a BCT of 34 °C as compared to 24–26°C (158).

Following HCA, the rewarming technique might also affect the inflammatory reaction. *In vitro*, cooling and rewarming of blood from 21 to 38.5°C showed increased neutrophil elastase activity, in parallel with increments in IL-1β, IL-8 and TNF-α (159). A porcine model of HCA assessing rapid vs. slow ECLS rewarming, showed no difference between groups as regards IL-6, TNF-α and neuron-specific enolase (NSE). Moreover, receptor for advanced glycation end products (RAGE), which is a marker of alveolar epithelial injury, was elevated in the rapidly rewarmed group (160).

In their studies of therapeutic hypothermia, Sipos and co-workers evaluated the impact of different intra-arrest hypothermia levels on the expression of selected cytokines and their prognostic value for 9-day survival in pigs. Interestingly, these investigators found that the systemic inflammatory response syndrome after cardiac arrest is characterized by marked increments in plasma IL-6 and TNF-α levels. As a prognostic marker for 9-Day survival of CA, IL-10 was identified with decreasing mRNA levels (161). Moreover, Meybohm et al. also observed a significant reduction in cerebral cortex inflammatory cytokine mRNA expression after HCA, as compared with animals who underwent CA when normothermic. Thus, mild therapeutic hypothermia resulted in decreased expression of typical cerebral inflammatory mediators after CPR (162).

Immune Modulation/Suppression–Lessons Learned From Therapeutic Hypothermia

Brain injury may occur both after CA ("ischemia"; I) and after ROSC when brain perfusion is reestablished ("reperfusion injury"; R). According to a review by Tahsili-Fahadan and co-workers, inflammatory processes after ischemia-reperfusion (I/R) injury play an important role in the development of neurological damage. For these conditions, therapeutic hypothermia (TH) has documented beneficial effects (163). After I/R injury, several proinflammatory chemokines, and matrix metalloproteinases (MMPs) aggravate brain injury by increasing permeability of the blood brain barrier, thereby increasing brain edema. In animals, increased levels of IL-10, enhanced expression of tumor growth factor β (TGF-β) and insulin-like growth factor-1 (IGF-1), suppress the activities of Th1 and Th2 lymphocytes after ischemia, thereby inducing neuroprotection. However, the role of this kind of immune suppressive therapy in human HCA is still unknown (163). Mitochondrial permeability transition pore (PTP), which is regulated by the matrix protein cyclophilin D (CypD), plays a key role in the pathophysiology of post-cardiac arrest (CA) syndrome. Recently, Jahandiez et al. demonstrated in rabbits who underwent 15 min of CA followed by 120 min of reperfusion, that therapeutic hypothermia limited post-cardiac arrest (CA) syndrome by preventing mitochondrial permeability transition, mainly through a CypD -dependent mechanism (164).

Cho et al. recently reviewed the evidence after hypoxic-ischemic brain injury of neuroprotective effects of immunomodulation, in addition to cooling. These investigators found encouraging results of stem cell therapy in small animals, suggesting augmented hypothermic neuroprotection. However, still the evidence of these effects are conflicting and the authors recommend rigorous testing in translational animal models (165).

Resuscitation From HCA With ECLS

In 1967 investigators independently reported successful rewarming from AH of two intoxicated patients by means of veno-arterial CPB (166, 167). Since then, rewarming by ECLS has become an established treatment, especially for those presenting with HCA. Compared with other rewarming modalities, ECLS ensures perfusion and oxygenation in addition to core rewarming. The rate of rewarming is also superior to any other technique (168). Swiss and Austrian physicians operating in close proximity to the Alps have worked out protocols integrating rewarming and trauma management from the site of accident and throughout the whole hospital stay (169–171).

ECLS during HCA activates host defense, including both the complement, coagulation, kinin - kallikrein and the fibrinolytic systems, in addition to leucocytes, platelets and inflammatory cytokines (152, 159, 172–176). The magnitude of these combined responses might affect the extent and degree of multiorgan failure and the outcome after rewarming. Surface contact between the ECLS system, coagulation factors XII, XI and high molecular weight kininogens (HMWK), constituting the contact system, activates production of vasodilator bradykinin *via* the kallikrein-kinin system (177). The activated forms have pro-coagulant and pro-inflammatory effects and can potentially stimulate the release of cytokines and interleukins, like TNF-α and IL-10, and the nitric oxide synthase/nitric oxide (NOS/NO) pathway (152). Upon contact with blood, the ECLS surface activates factor XII (Hageman factor) to XIIa and XIIf. The former triggers the intrinsic coagulation pathway and assists factor XIIf in converting pre-kallikrein to kallikrein and with HMWK to bradykinin. Amplification of factors IX, X and XI, activates the common coagulation pathway.

ECLS can be carried out with conventional cardiopulmonary bypass (CPB), a miniaturized CPB (MCPB) or an ECMO system. The choice of ECLS technique depends on the availability, competence, and clinical judgment. Each method has its advantages and pitfalls (178). ECMO and MCPB share the theoretical advantages of active venous drainage, small priming volumes and minimal hemodilution. Most likely, limited blood-surface-exposure, and possibly, the elimination of a blood-air interface attenuate the inflammatory response to ECLS (152, 179, 180). A review discussing interventions aimed at reducing inflammatory responses to CPB identified eight randomized controlled trials (RCT) comparing CPB with MCPB (181). Six of the RCTs using MCPB showed reduced activation of one or more of the inflammatory markers, IL-8, IL-6, activated complement factor 3 (C3a), the cytolytic component of the complement pathway activation C5b-9, integrin CD11b, TNF-α, neuron-specific enolase (NSE), and thromboxane B2. Additionally, three studies showed reduction of one or more of the clinical endpoints: ICU stay, ventilator time and cardiac troponin I (cTnI) plasma concentration (181).

Of note, in hypothermic piglets, CPB caused greater extravasation as compared to normothermic controls (137). Hyperoncotic priming solutions, like hydroxyethyl starch, and anti-inflammatory drugs, such as methylprednisolone, vitamin C, or α-tri-inositol given as pretreatment, were unable to prevent the increased fluid extravasation rate during hypothermic CPB (182, 183). However, in dogs resuscitated from HCA, addition of the oxidant scavenger N-acetylcysteine (NAC) to the CPB priming solution, reduced the inflammatory response during rewarming. Following exposure to deep hypothermia and ischemia-reperfusion combined, lungs pretreated with NAC demonstrated increased glutathione concentration with less deterioration of lung mechanics and gas exchange (184).

In comparison with CPB, ECMO has the additional advantage of extending cardiopulmonary support for days if the patient displays cardiopulmonary insufficiency after rewarming. In pigs, rewarming with ECMO restored MAP, CO, $\dot{D}O_2$, and blood flow to the heart and parts of the brain. Perfusion of the kidneys, stomach, liver, and spleen remained significantly reduced. In comparison, during CPR oxygen delivery ($\dot{D}O_2$) and O_2 uptake ($\dot{V}O_2$) fell to critically low levels, although, a small increase in lactate and a modest drop in pH indicated the presence of maintained aerobic metabolism (185). A few years ago, Ruttmann and co-workers retrospectively compared 34 patients with HCA rewarmed with CPB and 25 patients rewarmed with ECMO. Multivariate analysis showed a 6.6-fold ($95_{CI\%}$ 1.2–49.3) increased chance of surviving with ECMO in comparison

with CPB (186). Recently, we confirmed the early finding of Farstad et al. that a woman has a greater chance of surviving HCA as compared to a man. Moreover, that rewarming with ECMO increases the chance of surviving as compared with CPB. However, in a subset of patients from whom we found individual data, serum potassium ($n = 177$) was significantly higher in the CPB group as compared with the ECMO group. By removing 10 patients with s-$K^+ \geq 11.8$ mmol/L from the analysis, differences in survival between ECMO-treated and CPB-treated patients vanished, which is consistent with recent findings of Pasquier et al. (15, 24).

SUMMARY

- The update surveys physiological changes associated with AH, HCA and rewarming on various organ systems.
- In hypothermic individuals, a decrease in metabolic rate of 6–7 % per °C fall in body temperature, makes it possible to cover the requirement for oxygen even during manually performed CPR over a sizeable period.
- AH hampers the coagulation, the kinin–kallikrein, and the fibrinolytic systems.
- AH inhibits liver enzymes involved in the coagulation cascade, causing reduced prothrombin generation, which gives rise to increased bleeding after injuries.
- During hypothermia, clearance of drugs from the circulation may be hampered, as characterized by reduced elimination of midazolam secondary to declined activity of the P450 enzyme family.
- During hypothermia, renal blood flow and glomerular filtration rate decrease, but urine flow increases, because of reduced fluid reabsorption in the distal tubules.
- In hypothermic subjects, defibrillation and the use of inotropic or vasoactive drugs is not recommended until BCT rises to > 30°C after rewarming.
- After rewarming from AH or HCA, acute myocardial failure might occur, called "rewarming shock."
- Adjustment of acid-base balance in hypothermic children should follow the "pH-stat strategy", i.e., correcting pH and blood gases analyzed at 37°C back to the patient's BCT.
- Adjustment of acid-base balance in hypothermic adults with HCA should follow the "alpha-stat strategy," i.e., employing the values measured at 37°C directly without correcting to the actual BCT.
- The chance of surviving HCA is significantly higher after rewarming with ECMO, as compared to CPB, and in patients with witnessed compared to unwitnessed HCA.
- Male sex, high initial body temperature, low pH, and high s-K+ are factors associated with low surviving chances HCA.
- Avalanche victims have the lowest probability of surviving HCA.
- Rewarming victims of HCA with a serum potassium exceeding 12 mmol/L and a burial time of >30 min after avalanches with no air pocket, most probably be futile.

AUTHOR CONTRIBUTIONS

Colleagues at UiT The Arctic University of Norway (TN, ER, TT, and LB), Tromsø, Norway and at the Department of Anesthesiology and Intensive Care, the North-Western State Medical University (KL), St. Petersburg, the Nikiforov Russian Center of Emergency and Radiation Medicine (ES), St. Petersburg and the Northern State Medical University (MK), Arkhangelsk, Russia, collaborated on writing this update on physiological changes in accidental hypothermia and rewarming. LB drafted the manuscript together with TN. ER performed and updated the literature searches, as outlined in Methods. All authors made important contributions to the study, revised the manuscript, read, and approved the final version.

FUNDING

The study was supported by grants provided by the Norwegian Center for International Cooperation in Education, Project Number CPRU-2015/10021.

ACKNOWLEDGMENTS

We appreciate the kind assistance of Senior Librarian Grete Overvaag, Science and Health Library, University of Tromsø, The Arctic University of Norway, Tromsø, Norway.

REFERENCES

1. Brown DJA, Brugger H, Boyd J, Paal P. Accidental hypothermia. *N Engl J Med.* (2012) 367:1930–8. doi: 10.1056/NEJMra1114208
2. Ranhoff AH. Accidental hypothermia in the elderly. *Int J Circumpolar Health.* (2000) 59:255–9.
3. FitzGibbon T, Hayward JS, Walker D. EEG and visual evoked potentials of conscious man during moderate hypothermia. *Electroencephalogr Clin Neurophysiol.* (1984) 58:48–54. doi: 10.1016/0013-4694(84)90199-8
4. Mallet ML. Pathophysiology of accidental hypothermia. *QJM.* (2002) 95:775–85. doi: 10.1093/qjmed/95.12.775
5. Wollenek G, Honarwar N, Golej J, Marx M. Cold water submersion and cardiac arrest in treatment of severe hypothermia with cardiopulmonary bypass. *Resuscitation.* (2002) 52:255–63. doi: 10.1016/S0300-9572(01)00474-9
6. Tsuei BJ, Kearney PA. Hypothermia in the trauma patient. *Injury.* (2004) 35:7–15. doi: 10.1016/S0020-1383(03)00309-7
7. Giesbrecht GG. Emergency treatment of hypothermia. *Emerg Med.* (2001) 13:9–16. doi: 10.1046/j.1442-2026.2001.00172.x
8. Davis PR, Byers M. Accidental hypothermia. *J R Army Med Corps.* (2005) 151:223–33. doi: 10.1136/jramc-151-04-03
9. Guly H. History of accidental hypothermia. *Resuscitation.* (2011) 82:122–5. doi: 10.1016/j.resuscitation.2010.09.465
10. Mroczek T, Gladki M, Skalski J. Successful resuscitation from accidental hypothermia of 11.8°C: where is the lower bound for human beings? *Eur J Cardiothorac Surg.* (2020) 58:1091–2. doi: 10.1093/ejcts/ezaa159
11. Gilbert M, Busund R, Skagseth A, Nilsen PA, Solbo JP. Resuscitation from accidental hypothermia of 13.7 degrees C with circulatory arrest. *Lancet.* (2000) 355:375–6. doi: 10.1016/S0140-6736(00)01021-7

12. Stephen CR, Dent SJ, Hall KD, Smith WW. Physiologic reactions during profound hypothermia with cardioplegia. *Anesthesiology.* (1961) 22:873–81. doi: 10.1097/00000542-196111000-00001
13. Niazi SA, Lewis FJ. Profound hypothermia in man; report of a case. *Ann Surg.* (1958) 147:264–6. doi: 10.1097/00000658-195802000-00019
14. Hilmo J, Naesheim T, Gilbert M. "Nobody is dead until warm and dead": prolonged resuscitation is warranted in arrested hypothermic victims also in remote areas - a retrospective study from northern Norway. *Resuscitation.* (2014) 85:1204–11. doi: 10.1016/j.resuscitation.2014.04.029
15. Pasquier MHO, Paal P, Daroza T, Paal P, Darocha T, Blancherd M, et al. Hypothermia outcome prediction after extracorporeal life support for hypothermic cardiac arrest patients: the HOPE score. *Resuscitation.* (2018) 126:58–64. doi: 10.1016/j.resuscitation.2018.02.026
16. Lexow K. Severe accidental hypothermia: survival after 6 hours 30 minutes of cardiopulmonary resuscitation. *Arctic Med Res.* (1991) 50(Suppl. 6):112–4.
17. Farstad M, Andersen KS, Koller ME, Grong K, Segadal L, Husby P. Rewarming from accidental hypothermia by extracorporeal circulation. A retrospective study. *Eur J Cardiothorac Surg.* (2001) 20:58–64. doi: 10.1016/S1010-7940(01)00713-8
18. Locher T, Walpoth B, Pfluger D, Althaus U. [Accidental hypothermia in Switzerland (1980–1987)–case reports and prognostic factors]. *Schweiz Med Wochenschr.* (1991) 121:1020–8.
19. Mair P, Frimmel C, Vergeiner G, Hohlrieder M, Moroder L, Hoesl P, et al. Emergency medical helicopter operations for avalanche accidents. *Resuscitation.* (2013) 84:492–5. doi: 10.1016/j.resuscitation.2012.09.010
20. Jurkovich GJ, Greiser WB, Luterman A, Curreri PW. Hypothermia in trauma victims: an ominous predictor of survival. *J Trauma.* (1987) 27:1019–24. doi: 10.1097/00005373-198709000-00011
21. Hill JG, Hardekopf SJ, Chen JW, Krieg JC, Bracis RB, Petrillo RJ, et al. Successful resuscitation after multiple injuries in the wilderness. *J Emerg Med.* (2013) 44:440–3. doi: 10.1016/j.jemermed.2012.08.016
22. Tveita T, Sieck GC. Physiological impact of hypothermia: the good, the bad and the ugly. *Physiology.* (2021). doi: 10.1152/physiol.00025.2021
23. Filset OM, Fredriksen K, Gamst TM, Gilbert M, Hesselberg N, Naesheim T. Guidelines for management of accidental hypothermia in a university hospital in Northern Norway. *Anesteziol Reanimatol.* (2016) 61:479–82. doi: 10.18821/0201-7563-2016-6-479-482
24. Bjertnæs LJ, Hindberg K, Næsheim TO, Suborov EV, Reierth E, Kirov MY, et al. Rewarming from hypothermic cardiac arrest applying extracorporeal life support: a systematic review and meta-analysis. *Front Med.* (2021) 8:641633. doi: 10.3389/fmed.2021.641633
25. Lee HA, Ames AC. Haemodialysis in severe barbiturate poisoning. *Br Med J.* (1965) 1:1217–9. doi: 10.1136/bmj.1.5444.1217
26. Duguid H, Simpson RG, Stowers JM. Accidental hypothermia. *Lancet.* (1961) 2:1213–9. doi: 10.1016/S0140-6736(61)92588-0
27. Silva JE. Thermogenic mechanisms and their hormonal regulation. *Physiol Rev.* (2006) 86:435–64. doi: 10.1152/physrev.00009.2005
28. Blix AS. Arctic Animals and Their Adaptations to Life on the Edge. Trondheim: Tapir Academic Press (2005) p. 296.
29. Bianco AC, McAninch EA. The role of thyroid hormone and brown adipose tissue in energy homoeostasis. *Lancet Diabetes Endocrinol.* (2013) 1:250–8. doi: 10.1016/S2213-8587(13)70069-X
30. Lunze K, Hamer DH. Thermal protection of the newborn in resource-limited environments. *J Perinatol.* (2012) 32:317–24. doi: 10.1038/jp.2012.11
31. Asakura H. Fetal and neonatal thermoregulation. *J Nippon Med Sch.* (2004) 71:360–70. doi: 10.1272/jnms.71.360
32. Cohade C, Osman M, Pannu HK, Wahl RL. Uptake in supraclavicular area fat ("USA-Fat"): description on 18F-FDG PET/CT. *J Nucl Med.* (2003) 44:170–6.
33. van der Lans AA, Wierts R, Vosselman MJ, Schrauwen P, Brans B, van Marken Lichtenbelt WD. Cold-activated brown adipose tissue in human adults: methodological issues. *Am J Physiol Regul Integr Comp Physiol.* (2014) 307:R103–113. doi: 10.1152/ajpregu.00021.2014
34. Sun W, Dong H, Becker AS, Dapito DH, Modica S, Grandl G, et al. Publisher correction: cold-induced epigenetic programming of the sperm enhances brown adipose tissue activity in the offspring. *Nat Med.* (2018) 24:1777. doi: 10.1038/s41591-018-0163-y
35. Tansey EA, Johnson CD. Recent advances in thermoregulation. *Adv Physiol Educ.* (2015) 39:139–48. doi: 10.1152/advan.00126.2014
36. Liechti ME. Effects of MDMA on body temperature in humans. *Temperature.* (2014) 1:192–200. doi: 10.4161/23328940.2014.955433
37. Williams CT, Barnes BM, Richter M, Buck CL. Hibernation and circadian rhythms of body temperature in free-living Arctic ground squirrels. *Physiol Biochem Zool.* (2012) 85:397–404. doi: 10.1086/666509
38. Barnes BM. Freeze avoidance in a mammal: body temperatures below 0 degree C in an Arctic hibernator. *Science.* (1989) 244:1593–5. doi: 10.1126/science.2740905
39. Singhal NS, Bai M, Lee EM, Luo S, Cook KR, Ma DK. Cytoprotection by a naturally occurring variant of ATP5G1 in Arctic ground squirrel neural progenitor cells. *Elife.* (2020) 9:1–18. doi: 10.7554/eLife.55578
40. Andrews MT. Advances in molecular biology of hibernation in mammals. *Bioessays.* (2007) 29:431–40. doi: 10.1002/bies.20560
41. Mohiyaddin S, Nanjaiah P, Saad AO, Acharya MN, Khan TA, Davies RH, et al. Suspended animation: the past, present and future of major cardiothoracic trauma. *ANZ J Surg.* (2018) 88:678–82. doi: 10.1111/ans.14313
42. Anzai T, Turner MD, Gibson WH, Neely WA. Blood flow distribution in dogs during hypothermia and posthypothermia. *Am J Physiol.* (1978) 234:H706–710. doi: 10.1152/ajpheart.1978.234.6.H706
43. Tveita T, Mortensen E, Hevrøy O, Refsum H, Ytrehus K. Experimental hypothermia: effects of core cooling and rewarming on hemodynamics, coronary blood flow, and myocardial metabolism in dogs. *Anesth Analg.* (1994) 79:212–8. doi: 10.1213/00000539-199408000-00002
44. Tveita T, Ytrehus K, Skandfer M, Oian P, Helset E, Myhre ES, et al. Changes in blood flow distribution and capillary function after deep hypothermia in rat. *Can J Physiol Pharmacol.* (1996) 74:376–81. doi: 10.1139/y96-028
45. Silver DI, Murphy RJ, Babbs CF, Geddes LA. Cardiac output during CPR: a comparison of two methods. *Crit Care Med.* (1981) 9:419–20. doi: 10.1097/00003246-198105000-00034
46. Fodden DI, Crosby CA, Channer KS. Doppler measurement of cardiac output during cardiopulmonary resuscitation. *J Accid Emerg Med.* (1996) 13:379–82. doi: 10.1136/emj.13.6.379
47. Lins M, Petersen B, Tiroke A, Simon R. Reversible electrocardiographic changes in hypothermia. *Z Kardiol.* (2004) 93:630–3. doi: 10.1007/s00392-004-0110-4
48. Boue Y, Payen JF, Brun J, Thomas S, Levrat A, Blancher M, et al. Survival after avalanche-induced cardiac arrest. *Resuscitation.* (2014) 85:1192–6. doi: 10.1016/j.resuscitation.2014.06.015
49. Higuchi S, Takahashi T, Kabeya Y, Hasegawa T, Nakagawa S, Mitamura H. J waves in accidental hypothermia - body temperature and its clinical implications. *Circulation Journal.* (2014) 78:128–34. doi: 10.1253/circj.CJ-13-0704
50. Shattock MJ, Tipton MJ. 'Autonomic conflict': a different way to die during cold water immersion? *J Physiol.* (2012) 590:3219–30. doi: 10.1113/jphysiol.2012.229864
51. Harris KM, Creswell LL, Haas TS, Thomas T, Tung M, Isaacson E, et al. Death and cardiac arrest in U.S. triathlon participants, 1985 to 2016: a case series. *Ann Intern Med.* (2017) 167:529–35. doi: 10.7326/M17-0847
52. Han YS, Tveita T, Prakash YS, Sieck GC. Mechanisms underlying hypothermia-induced cardiac contractile dysfunction. *Am J Physiol Heart Circ Physiol.* (2010) 298:H890–7. doi: 10.1152/ajpheart.00805.2009
53. Schaible N, Han YS, Hoang T, Arteaga G, Tveita T, Sieck G. Hypothermia/rewarming disrupts excitation-contraction coupling in cardiomyocytes. *Am J Physiol Heart Circ Physiol.* (2016) 310:H1533–40. doi: 10.1152/ajpheart.00840.2015
54. Stowe DF, Fujita S, An J, Paulsen RA, Varadarajan SG, Smart SC. Modulation of myocardial function and [Ca2+] sensitivity by moderate hypothermia in guinea pig isolated hearts. *Am J Physiol.* (1999) 277:H2321–32. doi: 10.1152/ajpheart.1999.277.6.H2321
55. Kondratiev TV, Wold RM, Aasum E, Tveita T. Myocardial mechanical dysfunction and calcium overload following rewarming from experimental hypothermia in vivo. *Cryobiology.* (2008) 56:15–21. doi: 10.1016/j.cryobiol.2007.09.005
56. Alogna A, Manninger M, Schwarzl M, Zirngast B, Steendijk P, Verderber J, et al. Inotropic effects of experimental hyperthermia and hypothermia on left

ventricular function in pigs-comparison with dobutamine. *Crit Care Med.* (2016) 44:e158–7. doi: 10.1097/CCM.0000000000001358
57. Kerans V, Espinoza A, Skulstad H, Halvorsen PS, Edvardsen T, Bugge JF. Systolic left ventricular function is preserved during therapeutic hypothermia, also during increases in heart rate with impaired diastolic filling. *Intensive Care Med Exp.* (2015) 3:41. doi: 10.1186/s40635-015-0041-6
58. Kusuoka H, Ikoma Y, Futaki S, Suga H, Kitabatake A, Kamada T, et al. Positive inotropism in hypothermia partially depends on an increase in maximal Ca(2+)-activated force. *Am J Physiol.* (1991) 261:H1005–10. doi: 10.1152/ajpheart.1991.261.4.H1005
59. Dietrichs ES, Sager G, Tveita T. Altered pharmacological effects of adrenergic agonists during hypothermia. *Scand J Trauma Resusc Emerg Med.* (2016) 24:143. doi: 10.1186/s13049-016-0339-8
60. Tveita T, Sieck GC. The physiologic responses to epinephrine during cooling and after rewarming *in vivo*. *Crit Care*. (2011) 15:R225. doi: 10.1186/cc10465
61. Truhlar A, Deakin CD, Soar J, Khalifa GE, Alfonzo A, Bierens JJ, et al. European resuscitation council guidelines for resuscitation 2015: section 4. Cardiac arrest in special circumstances. *Resuscitation.* (2015) 95:148–201. doi: 10.1016/j.resuscitation.2015.07.017
62. Vanden Hoek TL, Morrison LJ, Shuster M, Donnino M, Sinz E, Lavonas EJ, et al. Part 12: cardiac arrest in special situations: 2010 American heart association guidelines for cardiopulmonary resuscitation and emergency cardiovascular care. *Circulation*. (2010) 122(18 Suppl. 3):S829–61. doi: 10.1161/CIRCULATIONAHA.110.971069
63. Wira CR, Becker JU, Martin G, Donnino MW. Anti-arrhythmic and vasopressor medications for the treatment of ventricular fibrillation in severe hypothermia: a systematic review of the literature. *Resuscitation*. (2008) 78:21–9. doi: 10.1016/j.resuscitation.2008.01.025
64. Bers DM, Despa S. Cardiac myocytes Ca2+ and Na+ regulation in normal and failing hearts. *J Pharmacol Sci.* (2006) 100:315–22. doi: 10.1254/jphs.CPJ06001X
65. Filseth OM, How OJ, Kondratiev T, Gamst TM, Sager G, Tveita T. Changes in cardiovascular effects of dopamine in response to graded hypothermia *in vivo*. *Crit Care Med.* (2012) 40:178–86. doi: 10.1097/CCM.0b013e31822d78de
66. Stoner J, Martin G, O'Mara K, Ehlers J, Tomlanovich M. Amiodarone and bretylium in the treatment of hypothermic ventricular fibrillation in a canine model. *Acad Emerg Med.* (2003) 10:187–91. doi: 10.1197/aemj.10.3.187
67. Dietrichs ES, Haheim B, Kondratiev T, Sieck GC, Tveita T. Cardiovascular effects of levosimendan during rewarming from hypothermia in rat. *Cryobiology.* (2014) 69:402–10. doi: 10.1016/j.cryobiol.2014.09.007
68. Rungatscher A, Hallstrom S, Giacomazzi A, Linardi D, Milani E, Tessari M, et al. Role of calcium desensitization in the treatment of myocardial dysfunction after deep hypothermic circulatory arrest. *Critical care (London, England).* (2013) 17:R245. doi: 10.1186/cc13071
69. Braun JP, Schneider M, Kastrup M, Liu J. Treatment of acute heart failure in an infant after cardiac surgery using levosimendan. *Eur J Cardiothorac Surg.* (2004) 26:228–30. doi: 10.1016/j.ejcts.2004.03.034
70. Polderman KH. Of ions and temperature: the complicated interplay of temperature, fluids, and electrolytes on myocardial function. *Crit Care.* (2013) 17:1018. doi: 10.1186/cc13139
71. Holmstrom P, Boyd J, Sorsa M, Kuisma M. A case of hypothermic cardiac arrest treated with an external chest compression device (LUCAS) during transport to re-warming. *Resuscitation.* (2005) 67:139–41. doi: 10.1016/j.resuscitation.2005.04.013
72. Putzer G, Braun P, Zimmermann A, Pedross F, Strapazzon G, Brugger H. LUCAS compared to manual cardiopulmonary resuscitation is more effective during helicopter rescue-a prospective, randomized, cross-over manikin study. *Am J Emerg Med.* (2013) 31:384–9. doi: 10.1016/j.ajem.2012.07.018
73. Gordon L, Paal P, Ellerton JA, Brugger H, Peek GJ, Zafren K. Delayed and intermittent CPR for severe accidental hypothermia. *Resuscitation.* (2015) 90:46–9. doi: 10.1016/j.resuscitation.2015.02.017
74. Lunetta P, Modell JH, Sajantila A. What is the incidence and significance of "dry-lungs" in bodies found in water? *Am J Forensic Med Pathol.* (2004) 25:291–301. doi: 10.1097/01.paf.0000146240.92905.7e
75. Lunetta P, Penttila A, Sajantila A. Circumstances and macropathologic findings in 1590 consecutive cases of bodies found in water. *Am J Forensic Med Pathol.* (2002) 23:371–6. doi: 10.1097/00000433-200212000-00015
76. Modell JH, Bellefleur M, Davis JH. Drowning without aspiration: is this an appropriate diagnosis? *J Forensic Sci.* (1999) 44:1119–23. doi: 10.1520/JFS14580J
77. Elsner R. The irving-scholander legacy in polar physiology. *Comp Biochem Physiol A Mol Integr Physiol.* (2000) 126:137–42. doi: 10.1016/S1095-6433(00)00207-5
78. Scholander PF. The master switch of life. *Sci Am.* (1963) 209:92–106. doi: 10.1038/scientificamerican1263-92
79. Bjertnaes L, Hauge A, Kjekshus J, Soyland E. Cardiovascular responses to face immersion and apnea during steady state muscle exercise. A heart catheterization study on humans. *Acta Physiol Scand.* (1984) 120:605–12. doi: 10.1111/j.1748-1716.1984.tb07427.x
80. Bjertnaes LJ, Hauge A, Thoresen M, Walløe L. Prioritized brain circulation during ergometer cycling with apnea and face immersion in ice-cold water: a case report. *Int Med Case Rep J.* (2021) 14:675–81. doi: 10.2147/IMCRJ.S317404
81. Kjeld T, Pott FC, Secher NH. Facial immersion in cold water enhances cerebral blood velocity during breath-hold exercise in humans. *J Appl Physiol.* (2009) 106:1243–8. doi: 10.1152/japplphysiol.90370.2008
82. Lindholm P, Sundblad P, Linnarsson D. Oxygen-conserving effects of apnea in exercising men. *J Appl Physiol.* (1999) 87:2122–7. doi: 10.1152/jappl.1999.87.6.2122
83. Golden F. Mechanisms of body cooling in submersed victims. *Resuscitation.* (1997) 35:107–9. doi: 10.1016/S0300-9572(97)00065-8
84. Blix AS, Walløe L, Messelt EB, Folkow LP. Selective brain cooling and its vascular basis in diving seals. *J Exp Biol.* (2010) 213(Pt 15):2610–6. doi: 10.1242/jeb.040345
85. Hollenberg NK, Uvnas B. The role of the cardiovascular response in the resistance to asphyxia of avian divers. *Acta Physiol Scand.* (1963) 58:150–61. doi: 10.1111/j.1748-1716.1963.tb02637.x
86. Kvittingen TD, Naess A. Recovery from drowning in fresh water. *Br Med J.* (1963) 1:1315–7. doi: 10.1136/bmj.1.5341.1310-a
87. Siebke H, Rod T, Breivik H, Lind B. Survival after 40 minutes; submersion without cerebral sequeae. *Lancet.* (1975) 1:1275–7. doi: 10.1016/S0140-6736(75)92554-4
88. Antretter H, Dapunt OE, Mueller LC. Survival after prolonged hypothermia. *N Engl J Med.* (1994) 330:219. doi: 10.1056/NEJM199401203300318
89. Giesbrecht GG. The respiratory system in a cold environment. *Aviat Space Environ Med.* (1995) 66:890–902.
90. Deal CW, Warden JC, Monk I. Effect of hypothermia on lung compliance. *Thorax.* (1970) 25:105–9. doi: 10.1136/thx.25.1.105
91. Karnatovskaia LV, Festic E, Freeman WD, Lee AS. Effect of therapeutic hypothermia on gas exchange and respiratory mechanics: a retrospective cohort study. *Ther Hypothermia Temp Manag.* (2014) 4:88–95. doi: 10.1089/ther.2014.0004
92. Dassios T, Austin T. Respiratory function parameters in ventilated newborn infants undergoing whole body hypothermia. *Acta Paediatrica.* (2014) 103:157–61. doi: 10.1111/apa.12476
93. Aslami H, Binnekade JM, Horn J, Huissoon S, Juffermans NP. The effect of induced hypothermia on respiratory parameters in mechanically ventilated patients. *Resuscitation.* (2010) 81:1723–5. doi: 10.1016/j.resuscitation.2010.09.006
94. Yagasaki T, Iwahashi K, Saito S, Ohmine I. A theoretical study on anomalous temperature dependence of pKw of water. *J Chem Phys.* (2005) 122:144504. doi: 10.1063/1.1878712
95. Ashwood ER, Kost G, Kenny M. Temperature correction of blood-gas and pH measurements. *Clin Chem.* (1983) 29:1877–85. doi: 10.1093/clinchem/29.11.1877
96. Kofstad J. Blood gases and hypothermia: some theoretical and practical considerations. *Scand J Clin Lab Invest Suppl.* (1996) 224:21–6. doi: 10.3109/00365519609088622
97. Nollert G, Reichart B. Cardiopulmonary bypass and cerebral injury in adults. *Shock.* (2001) 16(Suppl. 1):16–9. doi: 10.1097/00024382-200116001-00004

98. Arora S, Tantia P. Physiology of oxygen transport and its determinants in intensive care unit. *Indian J Crit Care Med.* (2019) 23:S172–7. doi: 10.5005/jp-journals-10071-23246
99. Mairbäurl H. Red blood cells in sports: effects of exercise and training on oxygen supply by red blood cells. *Front Physiol.* (2013) 4:332. doi: 10.3389/fphys.2013.00332
100. Gaasch M, Putzer G, Schiefecker AJ, Martini J, Strapazzon G, Ianosi B, et al. Cerebral autoregulation is impaired during deep hypothermia-a porcine multimodal neuromonitoring study. *Ther Hypothermia Temp Manag.* (2020) 10:122–7. doi: 10.1089/ther.2019.0009
101. Kollmar R, Frietsch T, Georgiadis D, Schabitz WR, Waschke KF, Kuschinsky W, et al. Early effects of acid-base management during hypothermia on cerebral infarct volume, edema, and cerebral blood flow in acute focal cerebral ischemia in rats. *Anesthesiology.* (2002) 97:868–74. doi: 10.1097/00000542-200210000-00018
102. Priestley MA, Golden JA, O'Hara IB, McCann J, Kurth CD. Comparison of neurologic outcome after deep hypothermic circulatory arrest with alpha-stat and pH-stat cardiopulmonary bypass in newborn pigs. *J Thorac Cardiovasc Surg.* (2001) 121:336–43. doi: 10.1067/mtc.2001.112338
103. Lenkin AI, Zaharov VI, Lenkin PI, Smetkin AA, Bjertnaes LJ, Kirov MY. Normothermic cardiopulmonary bypass increases cerebral tissue oxygenation during combined valve surgery: a single-centre, randomized trial. *Interact Cardiovasc Thorac Surg.* (2013) 16:595–601. doi: 10.1093/icvts/ivt016
104. Abdul Aziz KA, Meduoye A. Is pH-stat or alpha-stat the best technique to follow in patients undergoing deep hypothermic circulatory arrest? *Interact Cardiovasc Thorac Surg.* (2010) 10:271–82. doi: 10.1510/icvts.2009.214130
105. Simmons JW, Powell MF. Acute traumatic coagulopathy: pathophysiology and resuscitation. *Br J Anaesth.* (2016) 117(Suppl. 3):iii31–43. doi: 10.1093/bja/aew328
106. Wolberg AS, Meng ZH, Monroe DM, Hoffman M. A systematic evaluation of the effect of temperature on coagulation enzyme activity and platelet function. *J Trauma.* (2004) 56:1221–8. doi: 10.1097/01.TA.0000064328.97941.FC
107. Kander T, Schött U. Effect of hypothermia on haemostasis and bleeding risk: a narrative review. *J Int Med Res.* (2019) 47:3559–68. doi: 10.1177/0300060519861469
108. Scharbert G, Kalb ML, Essmeister R, Kozek-Langenecker SA. Mild and moderate hypothermia increases platelet aggregation induced by various agonists: a whole blood in vitro study. *Platelets.* (2010) 21:44–8. doi: 10.3109/09537100903420269
109. Mitrophanov AY, Rosendaal FR, Reifman J. Computational analysis of the effects of reduced temperature on thrombin generation: the contributions of hypothermia to coagulopathy. *Anesth Analg.* (2013) 117:565–74. doi: 10.1213/ANE.0b013e31829c3b22
110. Cosgriff N, Moore EE, Sauaia A, Kenny-Moynihan M, Burch JM, Galloway B. Predicting life-threatening coagulopathy in the massively transfused trauma patient: hypothermia and acidoses revisited. *J Trauma.* (1997) 42:857–61; discussion 861–52. doi: 10.1097/00005373-199705000-00016
111. Osterud B, Bjorklid E. Tissue factor in blood cells and endothelial cells. *Front Bioscience.* (2012) 4:289–99. doi: 10.2741/e376
112. Mahajan SL, Myers TJ, Baldini MG. Disseminated intravascular coagulation during rewarming following hypothermia. *JAMA.* (1981) 245:2517–8. doi: 10.1001/jama.245.24.2517
113. Brunet J, Valette X, Ivascau C, Lehoux P, Sauneuf B, Dalibert Y, et al. Extracorporeal life support for refractory cardiac arrest or shock: a 10-year study. *ASAIO J.* (2015) 61:676–81. doi: 10.1097/MAT.0000000000000282
114. Heinz S, Braspenning J. Measurement of blood coagulation factor synthesis in cultures of human hepatocytes. *Methods Mol Biol.* (2015) 1250:309–16. doi: 10.1007/978-1-4939-2074-7_23
115. Rohrer MJ, Natale AM. Effect of hypothermia on the coagulation cascade. *Crit Care Med.* (1992) 20:1402–5. doi: 10.1097/00003246-199210000-00007
116. Wood T, Thoresen M. Physiological responses to hypothermia. *Semin Fetal Neonatal Med.* (2015) 20:87–96. doi: 10.1016/j.siny.2014.10.005
117. Fukuoka N, Aibiki M, Tsukamoto T, Seki K, Morita S. Biphasic concentration change during continuous midazolam administration in brain-injured patients undergoing therapeutic moderate hypothermia. *Resuscitation.* (2004) 60:225–30. doi: 10.1016/j.resuscitation.2003.09.017
118. Tortorici MA, Kochanek PM, Poloyac SM. Effects of hypothermia on drug disposition, metabolism, and response: a focus of hypothermia-mediated alterations on the cytochrome P450 enzyme system. *Crit Care Med.* (2007) 35:2196–204. doi: 10.1097/01.CCM.0000281517.97507.6E
119. Broman M, Kallskog O. The effects of hypothermia on renal function and haemodynamics in the rat. *Acta Physiol Scand.* (1995) 153:179–84. doi: 10.1111/j.1748-1716.1995.tb09849.x
120. Englberger L, Suri RM, Greason KL, Burkhart HM, Sundt TM 3rd, Daly RC, et al. Deep hypothermic circulatory arrest is not a risk factor for acute kidney injury in thoracic aortic surgery. *J Thorac Cardiovasc Surg.* (2011) 141:552–8. doi: 10.1016/j.jtcvs.2010.02.045
121. Susantitaphong P, Alfayez M, Cohen-Bucay A, Balk EM, Jaber BL. Therapeutic hypothermia and prevention of acute kidney injury: a meta-analysis of randomized controlled trials. *Resuscitation.* (2012) 83:159–67. doi: 10.1016/j.resuscitation.2011.09.023
122. Arnaoutakis GJ, Vallabhajosyula P, Bavaria JE, Sultan I, Siki M, Naidu S, et al. The impact of deep versus moderate hypothermia on postoperative kidney function after elective aortic hemiarch repair. *Ann Thorac Surg.* (2016) 102:1313–21. doi: 10.1016/j.athoracsur.2016.04.007
123. Cervellin G, Comelli I, Lippi G. Rhabdomyolysis: historical background, clinical, diagnostic and therapeutic features. *Clin Chem Lab Med.* (2010) 48:749–56. doi: 10.1515/CCLM.2010.151
124. Ciapetti M, di Valvasone S, Spina R, Peris A. Rhabdomyolysis following therapeutic hypothermia after traumatic cardiac arrest. *Resuscitation.* (2011) 82:493. doi: 10.1016/j.resuscitation.2010.10.032
125. Dobson JA, Burgess JJ. Resuscitation of severe hypothermia by extracorporeal rewarming in a child. *J Trauma.* (1996) 40:483–5. doi: 10.1097/00005373-199603000-00032
126. Romlin BS, Winberg H, Janson M, Nilsson B, Bjork K, Jeppsson A, et al. Excellent outcome with extracorporeal membrane oxygenation after accidental profound hypothermia (13.8degreeC) and drowning. *Crit Care Med.* (2015) 43:e521–5. doi: 10.1097/CCM.0000000000001283
127. Debaty G, Moustapha I, Bouzat P, Maignan M, Blancher M, Rallo A, et al. Outcome after severe accidental hypothermia in the French Alps: a 10-year review. *Resuscitation.* (2015) 93:118–23. doi: 10.1016/j.resuscitation.2015.06.013
128. Locher T, Walpoth BH. [Differential diagnosis of circulatory failure in hypothermic avalanche victims: retrospective analysis of 32 avalanche accidents]. *Praxis.* (1996) 85:1275–82.
129. Mair P, Kornberger E, Furtwaengler W, Balogh D, Antretter H. Prognostic markers in patients with severe accidental hypothermia and cardiocirculatory arrest. *Resuscitation.* (1994) 27:47–54. doi: 10.1016/0300-9572(94)90021-3
130. Danzl DF, Pozos RS. Accidental hypothermia. *N Engl J Med.* (1994) 331:1756–60. doi: 10.1056/NEJM199412293312607
131. Hammersborg SM, Farstad M, Haugen O, Kvalheim V, Onarheim H, Husby P. Time course variations of haemodynamics, plasma volume and microvascular fluid exchange following surface cooling: an experimental approach to accidental hypothermia. *Resuscitation.* (2005) 65:211–9. doi: 10.1016/j.resuscitation.2004.11.020
132. Hammersborg SM, Brekke HK, Haugen O, Farstad M, Husby P. Surface cooling versus core cooling: comparative studies of microvascular fluid- and protein-shifts in a porcine model. *Resuscitation.* (2008) 79:292–300. doi: 10.1016/j.resuscitation.2008.06.008
133. Bjertnæs L. New developments in the treatment of accidental hypothermia. In: *Acta Anaesth Scand.* Munksgaard Int Publ LTD 35 Norre Søgade, PO Box 2148, DK-1016 Copenhagen, Denmark (1987).
134. Halsoy K, Kondratiev T, Tveita T, Bjertnaes LJ. Effects of constant flow vs. constant pressure perfusion on fluid filtration in severe hypothermic isolated blood-perfused rat lungs. *Front Med.* (2016) 3:70. doi: 10.3389/fmed.2016.00070
135. Chen RY, Chien S. Plasma volume, red cell volume, and thoracic duct lymph flow in hypothermia. *Am J Physiol.* (1977) 233:H605–12. doi: 10.1152/ajpheart.1977.233.5.H605
136. Heltne JK, Farstad M, Lund T, Koller ME, Matre K, Rynning SE, et al. Determination of plasma volume in anaesthetized piglets using the carbon monoxide (CO) method. *Lab Anim.* (2002) 36:344–50. doi: 10.1258/002367702320162333

137. Farstad M, Heltne JK, Rynning SE, Lund T, Mongstad A, Eliassen F, et al. Fluid extravasation during cardiopulmonary bypass in piglets–effects of hypothermia and different cooling protocols. *Acta Anaesthesiol Scand.* (2003) 47:397–406. doi: 10.1034/j.1399-6576.2003.00103.x
138. Soar J, Perkins GD, Abbas G, Alfonzo A, Barelli A, Bierens JJ, et al. European resuscitation council guidelines for resuscitation 2010 section 8. Cardiac arrest in special circumstances: electrolyte abnormalities, poisoning, drowning, accidental hypothermia, hyperthermia, asthma, anaphylaxis, cardiac surgery, trauma, pregnancy, electrocution. *Resuscitation.* (2010) 81:1400–33. doi: 10.1016/j.resuscitation.2010.08.015
139. Lacey AM, Nygaard RM, Deisler R, Calcaterra D, Schmitz KR, Fey RM, et al. 388 case study: severe hypothermia and frostbite requiring ecmo and four limb amputations. *J Burn Care Res.* (2018) 39:S165. doi: 10.1093/jbcr/iry006.310
140. Reamy BV. Frostbite: review and current concepts. *J Am Board Fam Pract.* (1998) 11:34–40. doi: 10.3122/15572625-11-1-34
141. Pries AR, Secomb TW, Gaehtgens P. The endothelial surface layer. *Pflugers Arch.* (2000) 440:653–66. doi: 10.1007/s004240000307
142. Gouverneur M, Spaan JA, Pannekoek H, Fontijn RD, Vink H. Fluid shear stress stimulates incorporation of hyaluronan into endothelial cell glycocalyx. *Am J Physiol Heart Circ Physiol.* (2006) 290:H458–2. doi: 10.1152/ajpheart.00592.2005
143. Liu J, Pedersen LC. Anticoagulant heparan sulfate: structural specificity and biosynthesis. *Appl Microbiol Biotechnol.* (2007) 74:263–72. doi: 10.1007/s00253-006-0722-x
144. Afratis NA, Nikitovic D, Multhaupt HA, Theocharis AD, Couchman JR, Karamanos NK. Syndecans - key regulators of cell signaling and biological functions. *FEBS J.* (2017) 284:27–41. doi: 10.1111/febs.13940
145. Schott U, Solomon C, Fries D, Bentzer P. The endothelial glycocalyx and its disruption, protection and regeneration: a narrative review. *Scand J Trauma Resusc Emerg Med.* (2016) 24:48. doi: 10.1186/s13049-016-0239-y
146. Rehm M, Bruegger D, Christ F, Conzen P, Thiel M, Jacob M, et al. Shedding of the endothelial glycocalyx in patients undergoing major vascular surgery with global and regional ischemia. *Circulation.* (2007) 116:1896–906. doi: 10.1161/CIRCULATIONAHA.106.684852
147. Becker BF, Chappell D, Jacob M. Endothelial glycocalyx and coronary vascular permeability: the fringe benefit. *Basic Res Cardiol.* (2010) 105:687–701. doi: 10.1007/s00395-010-0118-z
148. Grundmann S, Fink K, Rabadzhieva L, Bourgeois N, Schwab T, Moser M, et al. Perturbation of the endothelial glycocalyx in post cardiac arrest syndrome. *Resuscitation.* (2012) 83:715–20. doi: 10.1016/j.resuscitation.2012.01.028
149. Koning NJ, Vonk AB, Vink H, Boer C. Side-by-side alterations in glycocalyx thickness and perfused microvascular density during acute microcirculatory alterations in cardiac surgery. *Microcirculation.* (2016) 23:69–74. doi: 10.1111/micc.12260
150. Svennevig K, Hoel T, Thiara A, Kolset S, Castelheim A, Mollnes T, et al. Syndecan-1 plasma levels during coronary artery bypass surgery with and without cardiopulmonary bypass. *Perfusion.* (2008) 23:165–71. doi: 10.1177/0267659108098215
151. Bruegger D, Brettner F, Rossberg I, Nussbaum C, Kowalski C, Januszewska K, et al. Acute degradation of the endothelial glycocalyx in infants undergoing cardiac surgical procedures. *Ann Thorac Surg.* (2015) 99:926–31. doi: 10.1016/j.athoracsur.2014.10.013
152. Millar JE, Fanning JP, McDonald CI, McAuley DF, Fraser JF. The inflammatory response to extracorporeal membrane oxygenation (ECMO): a review of the pathophysiology. *Crit Care.* (2016) 20:387. doi: 10.1186/s13054-016-1570-4
153. Szotowski B, Antoniak S, Poller W, Schultheiss HP, Rauch U. Procoagulant soluble tissue factor is released from endothelial cells in response to inflammatory cytokines. *Circ Res.* (2005) 96:1233–9. doi: 10.1161/01.RES.0000171805.24799.fa
154. Binder FP, Ernst B. E- and P-selectin: differences, similarities and implications for the design of P-selectin antagonists. *Chimia.* (2011) 65:210–3. doi: 10.2533/chimia.2011.210
155. Wan S, LeClerc JL, Vincent JL. Inflammatory response to cardiopulmonary bypass: mechanisms involved and possible therapeutic strategies. *Chest.* (1997) 112:676–92. doi: 10.1378/chest.112.3.676
156. Moen O, Fosse E, Brockmeier V, Andersson C, Mollnes TE, Hogasen K, et al. Disparity in blood activation by two different heparin-coated cardiopulmonary bypass systems. *Ann Thorac Surg.* (1995) 60:1317–23. doi: 10.1016/0003-4975(95)00777-I
157. Rasmussen BS, Sollid J, Knudsen L, Christensen T, Toft E, Tonnesen E. The release of systemic inflammatory mediators is independent of cardiopulmonary bypass temperature. *J Cardiothorac Vasc Anesth.* (2007) 21:191–6. doi: 10.1053/j.jvca.2006.02.030
158. Grunenfelder J, Zund G, Schoeberlein A, Schmid ER, Schurr U, Frisullo R, et al. Expression of adhesion molecules and cytokines after coronary artery bypass grafting during normothermic and hypothermic cardiac arrest. *Eur J Cardiothorac Surg.* (2000) 17:723–8. doi: 10.1016/S1010-7940(00)00401-2
159. Tang M, Zhao XG, He Y, Gu JY, Mei J. Aggressive re-warming at 38.5 degrees C following deep hypothermia at 21 degrees C increases neutrophil membrane bound elastase activity and pro-inflammatory factor release. *Springerplus.* (2016) 5:495. doi: 10.1186/s40064-016-2084-x
160. Debaty G, Maignan M, Perrin B, Brouta A, Guergour D, Trocme C, et al. Deep hypothermic cardiac arrest treated by extracorporeal life support in a porcine model: does the rewarming method matter? *Acad Emerg Med.* (2016) 23:665–73. doi: 10.1111/acem.12893
161. Sipos W, Duvigneau C, Sterz F, Weihs W, Krizanac D, Bayegan K, et al. Changes in interleukin-10 mRNA expression are predictive for 9-day survival of pigs in an emergency preservation and resuscitation model. *Resuscitation.* (2010) 81:603–8. doi: 10.1016/j.resuscitation.2010.01.014
162. Meybohm P, Gruenewald M, Zacharowski KD, Albrecht M, Lucius R, Fösel N, et al. Mild hypothermia alone or in combination with anesthetic post-conditioning reduces expression of inflammatory cytokines in the cerebral cortex of pigs after cardiopulmonary resuscitation. *Crit Care.* (2010) 14:R21. doi: 10.1186/cc8879
163. Tahsili-Fahadan P, Farrokh S, Geocadin RG. Hypothermia and brain inflammation after cardiac arrest. *Brain Circ.* (2018) 4:1–13. doi: 10.4103/bc.BC_4_18
164. Jahandiez V, Cour M, Bochaton T, Abrial M, Loufouat J, Gharib A, et al. Fast therapeutic hypothermia prevents post-cardiac arrest syndrome through cyclophilin D-mediated mitochondrial permeability transition inhibition. *Basic Res Cardiol.* (2017) 112:35. doi: 10.1007/s00395-017-0624-3
165. Cho KH, Davidson JO, Dean JM, Bennet L, Gunn AJ. Cooling and immunomodulation for treating hypoxic-ischemic brain injury. *Pediatr Int.* (2020) 62:770–8. doi: 10.1111/ped.14215
166. Davies DM, Millar EJ, Miller IA. Accidental hypothermia treated by extracorporeal blood warming. *Lancet.* (1967) 1:1036–7. doi: 10.1016/S0140-6736(67)91546-2
167. Kugelberg J, Schuller H, Berg B, Kallum B. Treatment of accidental hypothermia. *Scand J Thorac Cardiovasc Surg.* (1967) 1:142–6. doi: 10.3109/14017436709131858
168. Morita S, Inokuchi S, Yamagiwa T, Iizuka S, Yamamoto R, Aoki H, et al. Efficacy of portable and percutaneous cardiopulmonary bypass rewarming versus that of conventional internal rewarming for patients with accidental deep hypothermia. *Crit Care Med.* (2011) 39:1064–8. doi: 10.1097/CCM.0b013e31820edd04
169. Brodmann Maeder M, Dunser M, Eberle B, Loetscher S, Dietler R, Englberger L, et al. The bernese hypothermia algorithm: a consensus paper on in-hospital decision-making and treatment of patients in hypothermic cardiac arrest at an alpine level 1 trauma centre. *Injury.* (2011) 42:539–43. doi: 10.1016/j.injury.2010.11.037
170. Paal P, Gordon L, Strapazzon G, Brodmann Maeder M, Putzer G, Walpoth B, et al. Accidental hypothermia–an update. *Scand J Trauma Resusc Emerg Med.* (2016) 24:111. doi: 10.1186/s13049-016-0303-7
171. Brugger H, Durrer B, Elsensohn F, Paal P, Strapazzon G, Winterberger E, et al. Resuscitation of avalanche victims: evidence-based guidelines of the international commission for mountain emergency medicine (ICAR MEDCOM): intended for physicians and other advanced life support personnel. *Resuscitation.* (2013) 84:539–46. doi: 10.1016/j.resuscitation.2012.10.020
172. Kagawa H, Morita K, Uno Y, Ko Y, Matsumura Y, Kinouchi K, et al. Inflammatory response to hyperoxemic and normoxemic cardiopulmonary bypass in acyanotic pediatric patients. *World J Pediatr Congenit Heart Surg.* (2014) 5:541–5. doi: 10.1177/2150135114551029

173. Rossaint J, Berger C, Van Aken H, Scheld HH, Zahn PK, Rukosujew A, et al. Cardiopulmonary bypass during cardiac surgery modulates systemic inflammation by affecting different steps of the leukocyte recruitment cascade. *PLoS ONE.* (2012) 7:e45738. doi: 10.1371/journal.pone.0045738
174. Christen S, Finckh B, Lykkesfeldt J, Gessler P, Frese-Schaper M, Nielsen P, et al. Oxidative stress precedes peak systemic inflammatory response in pediatric patients undergoing cardiopulmonary bypass operation. *Free Radic Biol Med.* (2005) 38:1323–32. doi: 10.1016/j.freeradbiomed.2005.01.016
175. Boyle EM Jr, Pohlman TH, Johnson MC, Verrier ED. Endothelial cell injury in cardiovascular surgery: the systemic inflammatory response. *Ann Thorac Surg.* (1997) 63:277–84.
176. McBride WT, Armstrong MA, Crockard AD, McMurray TJ, Rea JM. Cytokine balance and immunosuppressive changes at cardiac surgery: contrasting response between patients and isolated CPB circuits. *Br J Anaesth.* (1995) 75:724–33. doi: 10.1093/bja/75.6.724
177. Wu Y. Contact pathway of coagulation and inflammation. *Thromb J.* (2015) 13:17. doi: 10.1186/s12959-015-0048-y
178. Nollert G, Schwabenland I, Maktav D, Kur F, Christ F, Fraunberger P, et al. Miniaturized cardiopulmonary bypass in coronary artery bypass surgery: marginal impact on inflammation and coagulation but loss of safety margins. *Ann Thorac Surg.* (2005) 80:2326–32. doi: 10.1016/j.athoracsur.2005.05.080
179. Kiaii B, Fox S, Swinamer SA, Rayman R, Higgins J, Cleland A, et al. The early inflammatory response in a mini-cardiopulmonary bypass system: a prospective randomized study. *Innovations.* (2012) 7:23–32. doi: 10.1097/imi.0b013e3182552ade
180. Schoenebeck J, Haddad M, Wegscheider K, Joubert-Huebner E, Reichenspurner H, Detter C. Prospective, randomized study comparing two different minimized versus conventional cardiopulmonary bypass systems. *Innovations.* (2010) 5:270–7. doi: 10.1177/155698451000500405
181. Landis RC, Brown JR, Fitzgerald D, Likosky DS, Shore-Lesserson L, Baker RA, et al. Attenuating the systemic inflammatory response to adult cardiopulmonary bypass: a critical review of the evidence base. *J Extra Corpor Technol.* (2014) 46:197–211. Available online at: http://www.ncbi.nlm.nih.gov/pmc/articles/pmc4566828/
182. Farstad M, Heltne JK, Rynning SE, Onarheim H, Mongstad A, Eliassen F, et al. Can the use of methylprednisolone, vitamin C, or alpha-trinositol prevent cold-induced fluid extravasation during cardiopulmonary bypass in piglets? *J Thorac Cardiovasc Surg.* (2004) 127:525–34. doi: 10.1016/S0022-5223(03)01028-6
183. Farstad M, Haugen O, Kvalheim VL, Hammersborg SM, Rynning SE, Mongstad A, et al. Reduced fluid gain during cardiopulmonary bypass in piglets using a continuous infusion of a hyperosmolar/hyperoncotic solution. *Acta Anaesthesiol Scand.* (2006) 50:855–62. doi: 10.1111/j.1399-6576.2006.01064.x
184. Cakir O, Oruc A, Kaya S, Eren N, Yildiz F, Erdinc L. N-acetylcysteine reduces lung reperfusion injury after deep hypothermia and total circulatory arrest. *J Card Surg.* (2004) 19:221–5. doi: 10.1111/j.0886-0440.2004.04059.x
185. Nilsen JH, Schanche T, Valkov S, Mohyuddin R, Haaheim B, Kondratiev TV, et al. Effects of rewarming with extracorporeal membrane oxygenation to restore oxygen transport and organ blood flow after hypothermic cardiac arrest in a porcine model. *Sci Rep.* (2021) 11:18918. doi: 10.1038/s41598-021-98044-2
186. Ruttmann E, Weissenbacher A, Ulmer H, Müller L, Höfer D, Kilo J. Prolonged extracorporeal membrane oxygenation-assisted support provides improved survival in hypothermic patients with cardiocirculatory arrest. *J Thorac Cardiovasc Surg.* (2007) 134:594–600. doi: 10.1016/j.jtcvs.2007.03.049

Conflict of Interest: The authors declare that the research was conducted in the absence of any commercial or financial relationships that could be construed as a potential conflict of interest.

Publisher's Note: All claims expressed in this article are solely those of the authors and do not necessarily represent those of their affiliated organizations, or those of the publisher, the editors and the reviewers. Any product that may be evaluated in this article, or claim that may be made by its manufacturer, is not guaranteed or endorsed by the publisher.

GLOSSARY

ADP	Adenosine diphosphate
AH	Accidental hypothermia
ALAT	Alanine aminotransferase
ASAT	Aspartate aminotransferase
ATP	Adenosine triphosphate
ATPase	Group of enzymes catalyzing hydrolysis of ATP to ADP
BAT	Brown adipose tissue
BC	Before Christ
BCT	Body core temperature
°C	Degree(s) Celcius
CA	Cardiac arrest
CAR	Cerebral autoregulation
Ca^{2+}	Calcium ion
CABG	Coronary artery bypass grafting
cAMP	Cyclic adenosine monophosphate
CI	Confidence interval
CO	Cardiac output
CO^2	Carbon dioxide
CPB	Cardiopulmonary bypass
CPP	Cerebral perfusion pressure
CPR	Cardiopulmonary resuscitation
CypD	Matrix protein cyclophilin D
$\dot{D}O^2$	Oxygen delivery
ECLS	Extracorporeal life support
ECG	Electrocardiogram
ECMO	Extracorporeal membrane oxygenation
EEG	Electroencephalogram
HCA	Hypothermic cardiac arrest
HMWK	High molecular weight kininogens
hr(s)	Hour(s)
ICU	Intensive Care Unit
IGF-1	Insulin-like growth factor-1
IL-6	Interleukin 6
IL-8	Interleukin 8
ISS	Injury Severity Score
MAP	Mean arterial pressure
MMPs	Matrix metalloproteinases
NSE	neuron-specific enolase
OR	Odds ratio
PaO^2	Arterial partial pressure of oxygen
PaO^2/FiO^2	Ratio of arterial oxygen tension to inspired gas oxygen fraction
PEA	Pulseless electrical activity
PEEP	Positive end-expiratory pressure
PET/CT	Positron emission tomography/computed tomography
pH	$= -\log^{10}[H^+]$; literally, the negative logarithm base 10 of the hydrogen ion concentration in a solution
PPCPB	Portable percutaneous cardiopulmonary bypass system
PTP	Mitochondrial permeability transition pore
PVR	Pulmonary vascular resistance
PROSPERO	International Prospective Register of Systematic Reviews
PVR	Pulmonary vascular resistance
RAGE	Receptor for advanced glycation end products
RR	Relative risk ratio
RBF	Renal blood flow
RCT	Randomized controlled trial
ROSC	Return of spontaneous circulation
SD	Standard deviation
$s\text{-}K^+$	Serum potassium
s-Na	Serum sodium
TGF-β	Tumor growth factor -β
Th-1 and Th-2	Lymphocytes providing immune protection against intra – and extracellular intruders
TRH	Thyrotropin-Releasing Hormone
VF	Ventricular fibrillation
VO^2	Oxygen uptake

frontiers | Frontiers in Medicine

ORIGINAL RESEARCH
published: 28 April 2022
doi: 10.3389/fmed.2022.866667

Veno-Venous Extracorporeal Membrane Oxygenation in Minipigs as a Robust Tool to Model Acute Kidney Injury: Technical Notes and Characteristics

Antal Szabó-Biczók[1†], Gabriella Varga[2†], Zoltán Varga[2], Gábor Bari[1], Gyöngyvér Vigyikán[2], Ámos Gajda[2], Noémi Vida[2], Ádám Hodoniczki[2], Attila Rutai[2], László Juhász[2], Anna Nászai[2], Máté Gyöngyösi[2], Sándor Turkevi-Nagy[3], Dániel Érces[2‡] and Mihály Boros[2‡]*

[1] Division of Cardiac Surgery, Second Department of Internal Medicine and Cardiology Center, University of Szeged, Szeged, Hungary, [2] Institute of Surgical Research, University of Szeged, Szeged, Hungary, [3] Department of Pathology, University of Szeged, Szeged, Hungary

Objective: Veno-venous extracorporeal membrane oxygenation (vv-ECMO) can save lives in severe respiratory distress, but this innovative approach has serious side-effects and is accompanied by higher rates of iatrogenic morbidity. Our aims were, first, to establish a large animal model of vv-ECMO to study the pathomechanism of complications within a clinically relevant time frame and, second, to investigate renal reactions to increase the likelihood of identifying novel targets and to improve clinical outcomes of vv-ECMO-induced acute kidney injury (AKI).

Methods: Anesthetized Vietnamese miniature pigs were used. After cannulation of the right jugular and femoral veins, vv-ECMO was started and maintained for 24 hrs. In Group 1 (n = 6) ECMO was followed by a further 6-hr post-ECMO period, while (n = 6) cannulation was performed without ECMO in the control group, with observation maintained for 30 h. Systemic hemodynamics, blood gas values and hour diuresis were monitored. Renal artery flow (RAF) was measured in the post-ECMO period with an ultrasonic flowmeter. At the end of the experiments, renal tissue samples were taken for histology to measure myeloperoxidase (MPO) and xanthine oxidoreductase (XOR) activity and to examine mitochondrial function with high-resolution respirometry (HRR, Oroboros, Austria). Plasma and urine samples were collected every 6 hrs to determine neutrophil gelatinase-associated lipocalin (NGAL) concentrations.

Results: During the post-ECMO period, RAF dropped (96.3 ± 21 vs. 223.6 ± 32 ml/min) and, similarly, hour diuresis was significantly lower as compared to the control group (3.25 ± 0.4 ml/h/kg vs. 4.83 ± 0.6 ml/h/kg). Renal histology demonstrated significant structural damage characteristic of ischemic injury in the tubular system. In the vv-ECMO group NGAL levels, rose significantly in both urine (4.24 ± 0.25 vs. 2.57 ± 0.26 ng/ml) and plasma samples (4.67 ± 0.1 vs.

OPEN ACCESS

Edited by:
Wolfgang Weihs, Medical University of Vienna, Austria

Reviewed by:
András Lovas, Kiskunhalas Semmelweis Hospital, Hungary
Rene H. Tolba, University Hospital RWTH Aachen, Germany

***Correspondence:**
Mihály Boros
boros.mihaly@med.u-szeged.hu

† These authors have contributed equally to this work and share first authorship

‡ These authors have contributed equally to this work and share last authorship

Specialty section:
This article was submitted to Intensive Care Medicine and Anesthesiology, a section of the journal Frontiers in Medicine

Received: *31 January 2022*
Accepted: *08 April 2022*
Published: *28 April 2022*

Citation:
Szabó-Biczók A, Varga G, Varga Z, Bari G, Vigyikán G, Gajda Á, Vida N, Hodoniczki Á, Rutai A, Juhász L, Nászai A, Gyöngyösi M, Turkevi-Nagy S, Érces D and Boros M (2022) Veno-Venous Extracorporeal Membrane Oxygenation in Minipigs as a Robust Tool to Model Acute Kidney Injury: Technical Notes and Characteristics. Front. Med. 9:866667. doi: 10.3389/fmed.2022.866667

3.22 ± 0.2 ng/ml), while tissue XOR (5.88 ± 0.8 vs. 2.57 ± 0.2 pmol/min/mg protein) and MPO (11.93 ± 2.5 vs. 4.34 ± 0.6 mU/mg protein) activity was elevated. HRR showed renal mitochondrial dysfunction, including a significant drop in complex-I-dependent oxidative capacity (174.93 ± 12.7 vs. 249 ± 30.07 pmol/s/ml).

Conclusion: Significantly decreased renal function with signs of structural damage and impaired mitochondrial function developed in the vv-ECMO group. The vv-ECMO-induced acute renal impairment in this 30-hr research protocol provides a good basis to study the pathomechanism, biomarker combinations or possible therapeutic possibilities for AKI.

Keywords: extracorporeal membrane oxygenation, kidney injury, renal artery flow, mitochondrial function, ischemia, inflammation

INTRODUCTION

Extracorporeal membrane oxygenation (ECMO) is a temporary, life-saving support therapy for patients with respiratory or circulatory failure. Two main configurations of ECMO are veno-arterial and veno-venous (vv-ECMO). Vv-ECMO provides respiratory support and alternative gas exchange when the possibilities for conventional mechanical ventilation are exhausted, and thus patients gain time in which the gas exchange function of the damaged lungs can return. If there is no improvement in lung function, further ECMO support is reasonable only if lung transplantation is indicated.

Despite the benefits of ECMO therapy, continuous extracorporeal circulation has several adverse effects, including bleeding, thrombosis and infections (1, 2). Many organ complications are also documented, but acute kidney injury (AKI) is perhaps the most frequent phenomenon, developing in 70–85% of ECMO patients (1, 3–6), with up to 78% of adults requiring vv-ECMO support (3, 7). It has also been shown that 45% of patients who develop renal failure require some modality of renal replacement therapy and that mortality is 3.7 times higher in these cases (6). Further, renal function may not return to normal in 58% of patients weaned from ECMO treatment following hospital discharge (4, 6), with 19% of patients possibly requiring some form of chronic renal replacement therapy (8).

A number of theories have been put forward to date, but the underlying pathophysiology of renal impairment is still not fully understood. The proposed mechanisms include hemodynamic changes, humoral and hormonal imbalance, and a combination of systemic inflammatory reactions and volume overload following the initiation of ECMO therapy (9). The main problem is that investigation of the effects of a vv-ECMO-induced process on undamaged kidneys is impossible in clinical scenarios, even though identification of elements involved in lung-related effects can help us to explain the controversial results and consequences. Therefore, the aim of our study was to develop a well-controlled large animal model that is suited to characterizing vv-ECMO-induced AKI and may contribute to the exploration of background pathophysiological processes. Such models can be useful to identify triggering factors or targeted specific therapies to prevent the development of EMCO-related AKI or to reduce severity, thus lowering its morbidity and mortality.

MATERIALS AND METHODS

The experiments were performed on female (n = 5) and castrated male (n = 7) outbred Vietnamese minipigs (n = 12; 46.5 ± 4.5 kg bw) in accordance with the National Institutes of Health guidelines on the handling of and care for experimental animals and EU Directive 2010/63 on the protection of animals used for scientific purposes (approval number: V.1480.2019).

Animals and Anesthesia

Outbred Vietnamese minipigs (n = 12; weighing 46.5 ± 4.5 kg), obtained from a local, licensed breeder, were used. The animals were kept in the licensed, conventional hygienic level animal house of the Institute for an acclimatization period of 7–10 days with natural circadian light and free access to water and food. Prior to the experiments, the animals were fasted for 12 hrs with free access to tap water. At the beginning of the experiments, anesthesia was induced with an intramuscularly administered mixture of tiletamine-zolazepam (5 mg/kg im; Zoletil, Virbac, Carros, France) and xylazine (2 mg/kg im; Produlab Pharma, Raamsdonksveer, The Netherlands). After endotracheal intubation, mechanical ventilation was started with a tidal volume of 8–10 ml/kg, the respiratory rate was adjusted to maintain the end-tidal pressure of carbon dioxide in the 35–45 mmHg range, and the fraction of inspired oxygen (FiO_2) was set to keep arterial partial pressure of oxygen (PaO_2) between 80 and 100 mmHg. Anesthesia was maintained with a continuous infusion of propofol (6 mg/kg/h iv; Fresenius Kabi, Bad Homburg, Germany), midazolam (1.2 mg/kg/h; Torrex Chiesi Pharma, Vienna, Austria) and fentanyl (0.02 mg/kg/h; Richter Gedeon, Budapest, Hungary). Ringer's lactate (RL) infusion was administered at a rate of 10 ml/kg/h. The depth of anesthesia was regularly controlled by monitoring the jaw tone and the absence of the interdigital reflex.

Surgical Preparations

The anesthetized animals were placed in the supine position on a heating pad to maintain body temperature between 36 and 37°C. The left jugular vein was cannulated for fluid and drug administration, and the left femoral artery was cannulated for invasive hemodynamic monitoring and to measure cardiac output (CO) by transpulmonary thermodilution (PULSION

Medical Systems, Munich, Germany). A urinary catheter was surgically placed in the bladder *via* the femoral incision.

To establish the ECMO circuit, the access cannula was inserted into the right femoral vein and the return cannula was introduced into the right jugular vein (21 Fr, HLS cannulas; Maquet, Rastatt, Germany). The position of the cannulas (access: proximal of the hepatic artery; return: orifice of the superior vena cava) was checked using an X-ray image intensifier (Ziehm SOLO; Ziehm Imaging GmbH, Nuremberg, Germany).

Before setting up the ECMO circuit, CO was directly measured with the PiCCO system *via* thermodilution, and the flow settings were initially adjusted accordingly at the start of ECMO circulation. Lung-safe ventilation was initiated during ECMO. Sweep gas and circuit blood flow rates were refined according to the arterial partial pressure of the carbon dioxide ($PaCO_2$; 35–45 mmHg) and PaO_2 (70–100 mmHg) values of the arterial blood gas samples, drawn from the left femoral artery. Transmembrane pressure was monitored, and the blood flow in the circuit was measured with the inline ultrasound flow probe of the pump. Mean arterial pressure (MAP) was monitored continuously and kept over 60 mmHg. As a positive inotropic treatment, norepinephrine was administered if necessary (0.05–0.35 μg/kg/h iv; Arterenol; Sanofi-Aventis, Frankfurt am Main, Germany).

The ECMO circulation was stopped after 24 h, and the ECMO cannulas were removed. Ventilation was set to the pre-ECMO settings. If necessary, oxygen and breathing rates were set according to the blood gas values.

After median laparotomy, the right renal artery was dissected free, and a perivascular flow probe was placed around it (Transonic Systems Inc., Ithaca, NY, United States) to measure the renal blood flow. The wound cut in the abdominal wall was then temporarily closed with clips.

Experimental Protocol

Prior to the experiments, the animals underwent a general health check and if no outer injuries, discharge from body orifices or any signs of inflammations (swelling, edema, epithelial hyperemia) could be observed they were included in the study. The animals (n = 12) were randomly allocated into two experimental groups (n = 6, each group; the female-castrated male ratio: 0.5 for vv-ECMO and 0.33 for control group). In the vv-ECMO group, extracorporeal circulation was maintained for 24 h. After 24 h, ECMO was abandoned, the cannulas were removed, and the cannulation entry points were surgically closed. A further six-hour post-ECMO observation followed. For technical reasons, renal artery flow was measured in this phase only. In the control group, identical ECMO cannulation was completed, but extracorporeal circulation was not initiated. The same interventions and time frames were applied as in the vv-ECMO group. No animals were excluded from the study for any reasons.

During the 30-hour total observation, blood samples were taken every hour for blood gas analysis and for determination of total haemoglobin concentration (tHb) and hematocrit (Hct; Cobas b 123, Roche Ltd., Basel, Switzerland) and every 6 h (at baseline and hours 6, 12, 18, 24, and 30) to measure neutrophil gelatinase-associated lipocalin (NGAL) values. The urine was collected and measured hourly during the observation period to calculate the average hour diuresis, and further urine samples were taken for NGAL determination every 6 h (baseline and hours 6, 12, 18, 24, and 30).

At the end of the observation period, kidney tissue biopsies were taken to measure myeloperoxidase (MPO), xanthine oxidoreductase (XOR) enzyme activity and mitochondrial oxygen consumption as well as for histological examinations (**Figure 1**). After removal of tissue samples the animals were over anesthetized through the jugular vein cannula with a single 120 mg/kg dose of sodium pentobarbital (Sigma-Aldrich Inc, St. Louis, MO, United States).

Hemodynamic Measurements

Mean arterial pressure and heart rate (HR) were monitored continuously and registered hourly, while transpulmonary thermodilution was used to measure CO hourly during the observation period (PiCCO Plus monitoring system; PULSION Medical Systems; Munich, Germany) and based on this CO value pulse contour analysis was used to continuously monitor (registered hourly) the stroke volume (SV). Blood flow signals (T206 Animal Research Flowmeter; Transonic Systems Inc., Ithaca, NY, United States) were recorded and registered every hour during the post-ECMO period with a computerized data acquisition system (SPELL Haemosys; Experimetria, Budapest, Hungary).

Measurement of Mitochondrial Respiratory Function

Mitochondrial oxygen (O_2) consumption (or volume-specific O_2 flux) was assessed in kidney homogenates using High-Resolution FluoRespirometry (Oxygraph-2k, Oroboros Instruments, Innsbruck, Austria). After renal decapsulation, approx. 300 mg tissue samples were cut into smaller pieces, washed in phosphate-buffered saline (PBS) three times and then homogenized with a Potter–Elvehjem tissue grinder in Mir05 medium (pH 7.1).

Calibration and measurements were performed with continuous stirring (750 rpm) at 37°C in a 2 mL Mir05 respiration medium. After stabilization of the baseline respiration, NADH- and $FADH_2$-supported LEAK respiration and complex I- and II-linked capacities of oxidative phosphorylation (OXPHOS) were measured in the presence of substrates ($LEAK_{GM}$; 10 mmol/l glutamate, 2 mmol/l malate; and $LEAK_S$; 10 mmol/l succinate) and saturating concentration of ADP (2.5 mmol/l). Rotenone (0.5 μmol/l; complex I inhibitor) was administered prior to succinate to block reverse electron transport-derived ROS formation and oxaloacetate accumulation (a known endogenous inhibitor of complex II). Following stimulation of OXPHOS, the integrity of the outer mitochondrial membrane was tested with exogenous cytochrome c (10 μ mol/l).

Complex V (or ATP synthase) was inhibited by oligomycin (2.5 μmol/l) to evaluate LEAK respiration in a non-phosphorylating state ($LEAK_{Omy}$). The respiratory control ratio (RCR), an index of coupling between respiration and phosphorylation, was expressed as a ratio of OXPHOS to the $LEAK_{Omy}$ state. The electron transport system-independent

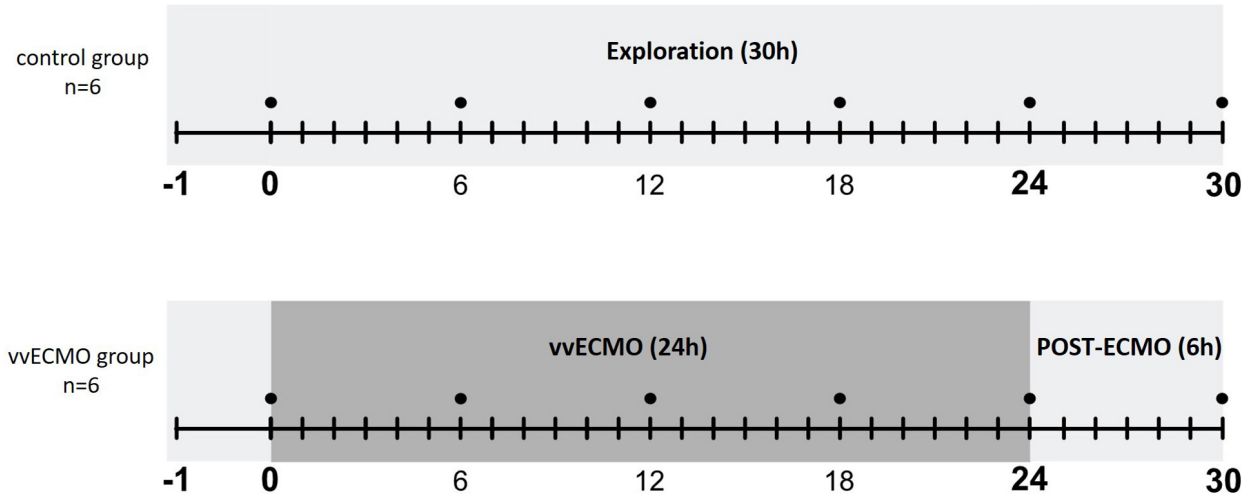

FIGURE 1 | Scheme of experimental protocol.

respiration (or residual O_2 consumption) was assessed following complex III inhibition with antimycin A (2.5 μ mol/l).

The DatLab software (Oroboros Instruments, Innsbruck, Austria) was used for online display, respirometry data acquisition and analysis. Oxygen flux normalized to 8 mg wet weight expressed in pmol/s/ml.

Kidney Histology

Kidney samples were fixed in 4% neutral buffered formalin. Tissue slices were embedded in paraffin using a Thermo Shandon PathCentre tissue processor. 3-μm-thick sections were cut with a Leica RM2125 rotary microtome. After deparaffinization and re-hydration, the sections were routinely stained for haematoxylin-eosin (HE) and periodic acid Schiff (PAS). The extent of tubular cell edema, apical cytoplasm vacuolization, tubular cell vacuolization, tubular lumen irregularity, loss of brush border, sloughing of tubular cells, tubular dilation, tubular cell necrosis, flattened and simplified tubular epithelium, and denudement of tubular basal membrane was assessed by a renal pathologist in a blinded way. To quantify these changes, we set up a kidney injury score, based on the extent of the histological changes noted above (0 points = 0%; 1 point = 1–20%; 2 points = 21–40%; 3 points = 41–60%; 4 points = 61–80%; and 5 points = 81–100%). The values of the tubular cell necrosis and denuded basement membranes were weighted by a factor of two.

Measurement of Neutrophil Gelatinase Associated Lipocalin

Four-milliliter blood samples were drawn from the jugular vein into chilled polypropylene tubes containing EDTA (1 mg/mL) and 4-ml urine samples were collected in Eppendorf tubes at baseline and hours 6, 12, 18, 24 and 30. The blood samples were centrifuged at 1,200*g* for 10 min at 4°C. The plasma samples were then collected and stored at −70°C until assay. The urine samples were kept at −70°C until assay.

The plasma and urine concentration of NGAL was measured with a commercially available ELISA kit (Quantikine ELISA for Human Lipocalin-2/NGAL Immunoassay, United States R&D Systems, Minneapolis, MN, United States).

Measurement of Tissue Xanthine-Oxidoreductase and Myeloperoxidase Enzyme Activities

Tissue samples were harvested immediately after the animals were sacrificed. A circular 1–2.5-cm-thick sample was excised from the distal pole of the left kidney. After saline rinsing, the sample was stored in liquid nitrogen for further analysis. Tissue biopsies kept on ice were homogenized in a phosphate buffer (pH 7.4) containing 50 mM Tris–HCl (Reanal, Budapest, Hungary), 0.1 mM EDTA, 0.5 mM dithiothreitol, 1 mM phenylmethylsulfonyl fluoride, 10 μg/ml soybean trypsin inhibitor and 10 μg/ml leupeptin (Sigma-Aldrich GmbH, Germany). The homogenate was centrifuged at 4°C for 20 min at 2,4000 *g*, and the supernatant was loaded into centrifugal concentrator tubes (Amicon Centricon-100; 100 000 MW cut-off ultrafilter).

Xanthine oxidoreductase activity was determined in the ultrafiltered, concentrated supernatant with a fluorometric kinetic assay based on the conversion of pterine to isoxanthopterine in the presence (total XOR) or absence (xanthine oxidase activity) of the electron acceptor methylene blue (10).

Myeloperoxidase activity was measured on the pellet of the homogenate (11). Briefly, the pellet was resuspended in a K_3PO_4 buffer (0.05 M; pH 6.0) containing 0.5% hexa-1,6-bis-decyltriethylammonium bromide. After three repeated freeze-thaw procedures, the material was centrifuged at 4°C for 20 min at 24,000 *g*, and the supernatant was used for MPO determination. Next, 0.15 ml of 3,3′,5,5′-tetramethylbenzidine (dissolved in DMSO; 1.6 mM) and 0.75 ml of hydrogen

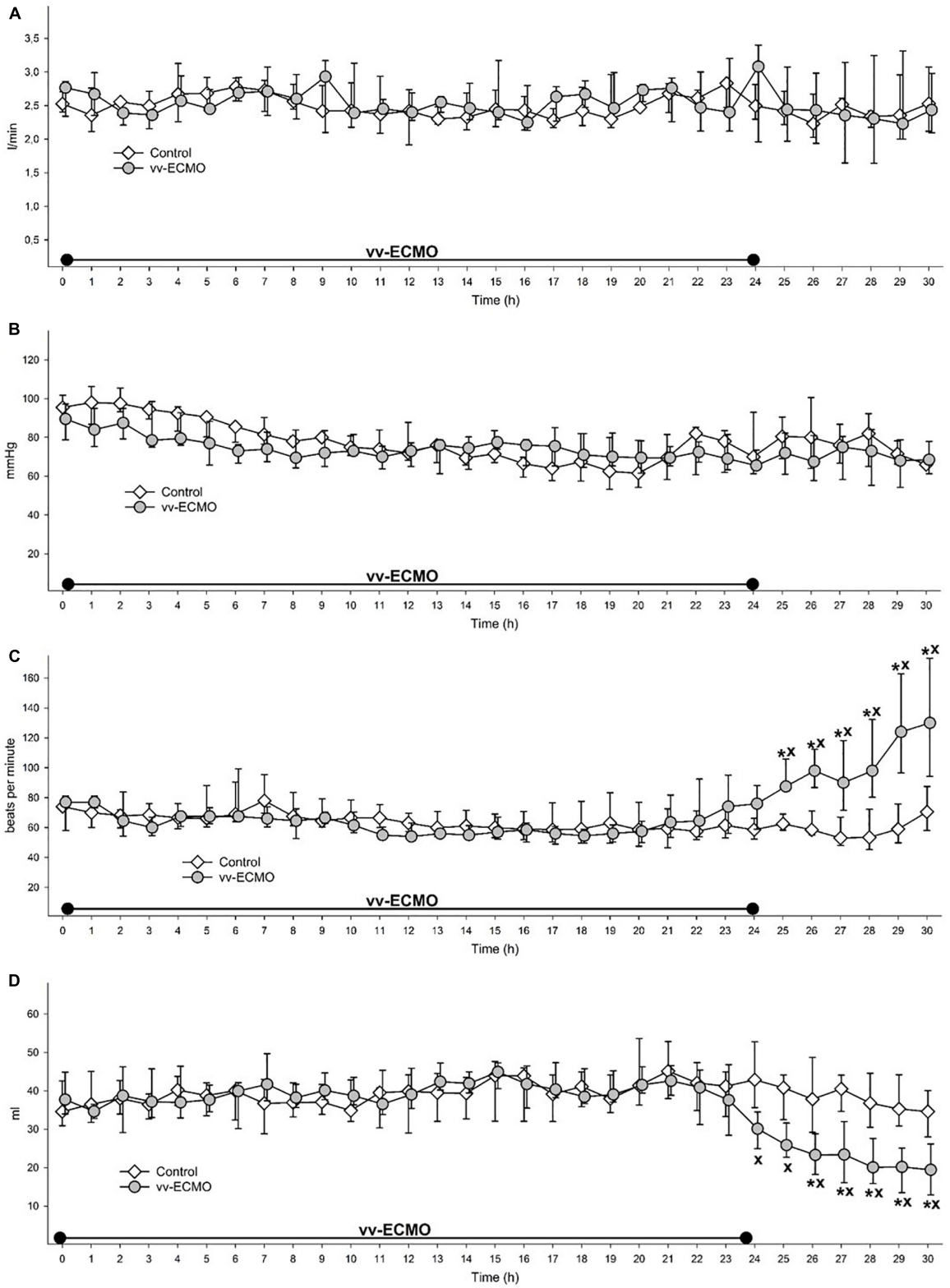

FIGURE 2 | Changes in cardiac output **(A)**, mean arterial pressure **(B),** heart rate **(C)** and stroke volume **(D)** during the whole observation period in the control group (empty diamonds joined by a thin continuous line) and vv-ECMO group (gray circles joined by a continuous line). The plots demonstrate the median and the 25th (lower whisker) and 75th (upper whisker) percentiles. $^{*}P < 0.05$ for the groups vs. baseline values (Friedman and Dunn tests). $^{x}P < 0.05$ for the vv-ECMO vs. control group values (Mann–Whitney test).

peroxide (dissolved in K_3PO_4 buffer; 0.6 mM) were added to 0.1 ml of the sample. The reaction led to the hydrogen peroxide-dependent oxidation of tetramethylbenzidine, which was detected spectrophotometrically at 450 nm (UV-1601 spectrophotometer; Shimadzu, Kyoto, Japan). MPO activity was measured at 37°C; then the reaction was halted after 5 min with the addition of 0.2 ml of H_2SO_4 (2 M). The data were expressed in terms of protein content.

Statistical Analysis

Data analysis was performed with a statistical software package (SigmaStat for Windows; Jandel Scientific, Erkrath, Germany). Normality of data distribution was analyzed with the Shapiro–Wilk test. Friedman repeated-measures analysis of variance on ranks was applied within groups. Time-dependent differences from the baseline for each group were assessed by Dunn's method. Differences between groups were analyzed with the Mann–Whitney test. Median values and 75th and 25th percentiles are provided in the figures; *P*-values <0.05 were considered significant. The sample sizes were estimated with PS: Power and Sample Size Calculation 3.1 software (12), and for sample size estimation the differences in the tissue XOR activity were the primary outcome measures.

RESULTS

Changes in Systemic Hemodynamics

During the ECMO and post-ECMO period, we could not identify differences in CO (**Figure 2A**) and MAP between the two groups (**Figure 2B**). However, HR started to rise in the vv-ECMO group after 20 h and reached significantly higher values at 25 h compared to the control group (**Figure 2C**). The SV decreased significantly after 24 h compared to the control group (**Figure 2D**).

Changes in Renal Hemodynamics and Function

During the post-ECMO period, the RAF (**Figure 3A**) significantly decreased in the vv-ECMO group relative to the control group. Parallel to the drop in the renal arterial flow, the average hour diuresis fell during the observation period (**Figure 3B**).

Changes in Total Hemoglobin Concentration and Hematocrit

The tHb and Hct values decreased early, by the 6th of vv-ECMO treatment and remained significantly lower as compared to the control group until the end of the observation period (**Table 1**).

Histological Changes in the Kidneys

Changes in renal hemodynamics and function were accompanied by histological changes in the kidneys. The occurrence ratio of all the histological features under examination was significantly higher in the vv-ECMO group (**Figure 4A**). A kidney-specific injury score was used to summarize and quantify the qualitative histological alterations, which demonstrated significantly increased injury in the vv-ECMO group (**Figure 4B**), pointing to the net damage of the renal tissue.

Renal Tissue Damage: Biochemical Markers

Renal tissue damage was also characterized by a rise in NGAL levels in both the urine (**Figure 5A**) and plasma samples

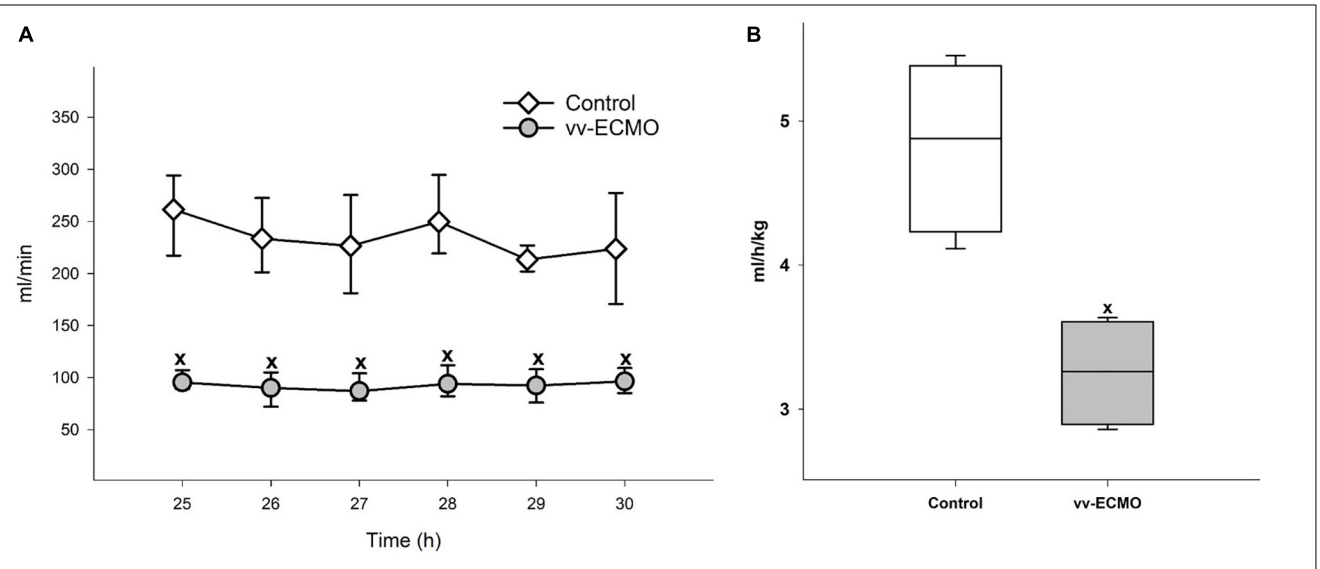

FIGURE 3 | Changes in renal artery flow **(A)** in the control group (empty diamonds joined by a thin continuous line) and vv-ECMO group (gray circles joined by a continuous line). The plots demonstrate the median and the 25th (lower whisker) and 75th (upper whisker) percentiles. $^{x}P < 0.05$ for the vv-ECMO vs. control group values (Mann–Whitney test). Changes in average hour diuresis **(B)** in the control group (empty box) and vv-ECMO group (striped gray box). The plots demonstrate the median (horizontal line in the box), the 25th and 75th percentiles, and the range of data (whiskers). $^{x}P < 0.05$ for the vv-ECMO vs. control group values (Mann–Whitney test).

TABLE 1 | The effects of vv-ECMO on blood total hemoglobin concentration (tHb) [g/dL] and hematocrit (Hct) [%]. The table demonstrates the median values and the 25th and 75th percentiles.

tHb			
Time (h)	**Parameters**	**Control**	**vv-ECMO**
0	Median	11.3	10.7
	p25; p75	9.8; 11.8	8.9; 11.5
6	Median	9.3	6.4 x
	p25; p75	8.6; 10.9	5.5; 6.8
12	Median	9.3	7.1 x
	p25; p75	8.3; 10	6.2; 8.1
18	Median	9.2	6.4 *x
	p25; p75	8.1; 9.3	5.5; 7.2
24	Median	8.9	5.5 *x
	p25; p75	8.7; 1.40	4.2; 6.8
30	Median	9.6	5.5 *x
	p25; p75	9.2; 10.4	4.2; 6.7
Hct			
0	Median	32.7	30.9
	p25; p75	28.4; 34	30.1; 34.1
6	Median	26	17.8 x
	p25; p75	25.4; 33.1	15.2; 18.3
12	Median	24.5	17.6 x
	p25; p75	23.2; 30.7	16.9; 21.1
18	Median	22	15.1 *x
	p25; p75	20.8; 23	13.9; 17.9
24	Median	23	14.7 *x
	p25; p75	22; 27,3	9.9; 19.3
30	Median	25.7	14.7 *x
	p25; p75	23; 27	11.5; 17.9

$p < 0.05$ vs. baseline values; x $p < 0.05$ vs. control group.

(**Figure 5B**). Compared to the control group, this kidney injury marker increased from the sixth hour of vv-ECMO and remained elevated during the post-ECMO phase until the end of the observation period.

We also demonstrated a significant growth in enzyme activity in two enzymes, which may greatly contribute to oxidative stress in the kidneys. Notably, relative to the control group, both XOR (**Figure 6A**) and MPO (**Figure 6B**) activity was elevated in kidney tissue samples that were taken at the end of the experiments.

Changes in Mitochondrial Oxygen Consumption

In comparison with the controls, vv-ECMO tissue samples showed a significant drop in complex I- and complex II-linked OXPHOS capacities and in RCR values (**Figures 7A,B**). In addition, outer membrane permeability rose in these animals, indicated by significantly higher O_2 flux following addition of cytochrome c (Cytc%; **Figures 7C,D**). However, baseline respiration or respiration in the presence of complex I- and complex II-linked substrates ($LEAK_{GM}$ and LEAKs; in a non-phosphorylating resting state) did not change significantly (**Figures 7A,B**).

DISCUSSION

The clinical use of vv-ECMO is a subject of ongoing debate. Although the improved mortality of patients with severe ARDS and vv-ECMO treatment has been demonstrated (during both the H1N1 and COVID-19 pandemics) (13), the technique still suffers from shortcomings and is accompanied by serious complications, including AKI (13). Nevertheless, it is difficult to outline the direct role of vv-ECMO treatment in clinical setups, as patients already have serious underlying diseases and investigations in healthy humans are impossible. An important aim of preclinical research is to recapitulate the human situation with model experiments. In this study, we have therefore focused on the establishment of a large animal model that makes the

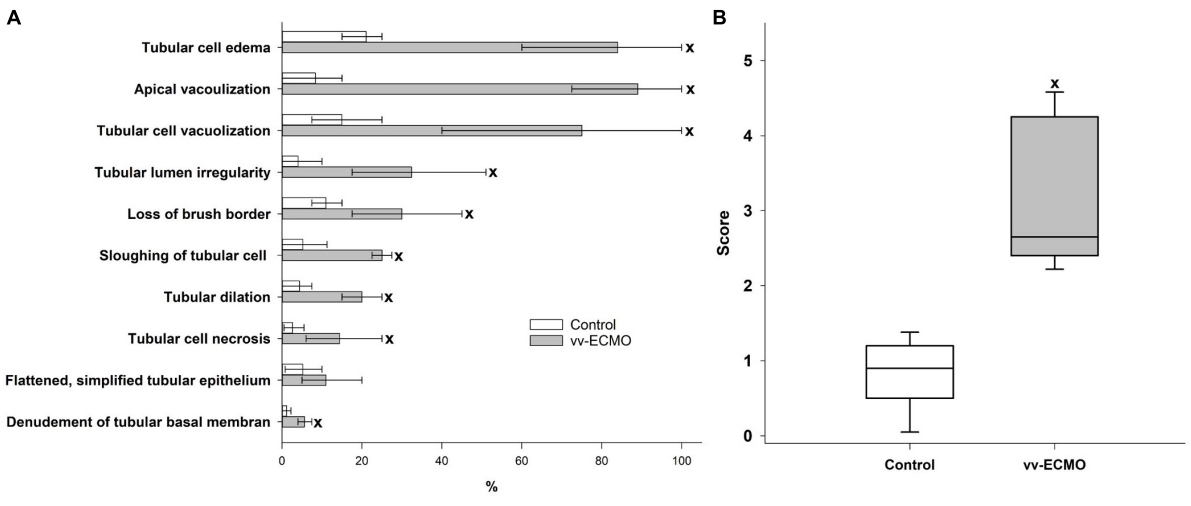

FIGURE 4 | The extent of the renal histological changes **(A)** in the control group (empty column) and vv-ECMO group (gray column). The plots demonstrate the median (top line of the column) and the 25th and 75th percentiles (whiskers). $^{x}P < 0.05$ for the vv-ECMO vs. control group values (Mann–Whitney test). Changes in the renal histology score **(B)** in the control group (empty box) and vv-ECMO group (gray box). The plots demonstrate the median (horizontal line in the box), the 25th and 75th percentiles, and the range of data (whiskers). $^{x}P < 0.05$ for the vv-ECMO vs. control group values (Mann–Whitney test).

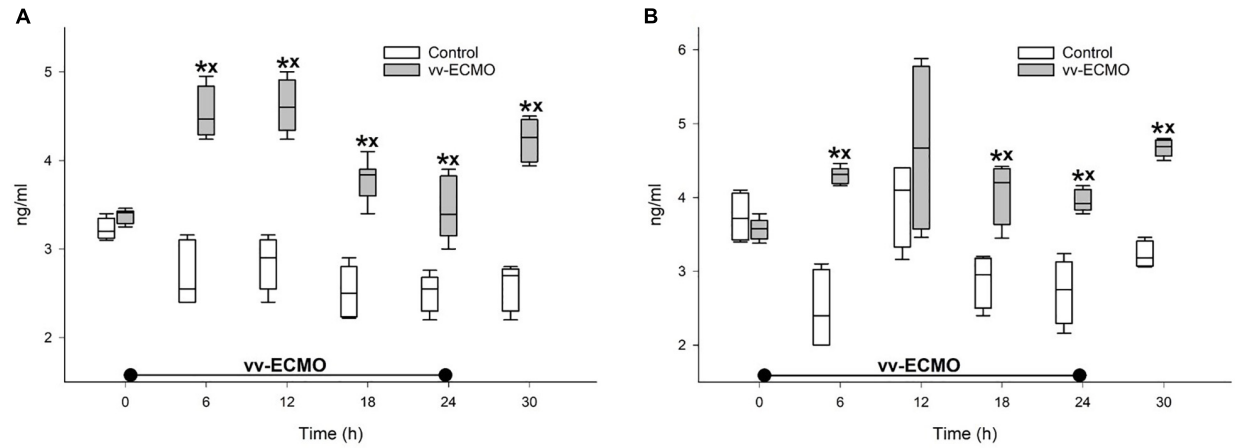

FIGURE 5 | Changes in the neutrophil gelatinase-associated lipocalin levels in the urine **(A)** and plasma **(B)** in the control group (empty box) and vv-ECMO group (gray box). The plots demonstrate the median (horizontal line in the box), the 25th and 75th percentiles, and the range of data (whiskers). $^{*}P < 0.05$ for groups vs. baseline values (Friedman and Dunn tests), $^{x}P < 0.05$ for the vv-ECMO vs. control group values (Mann–Whitney test).

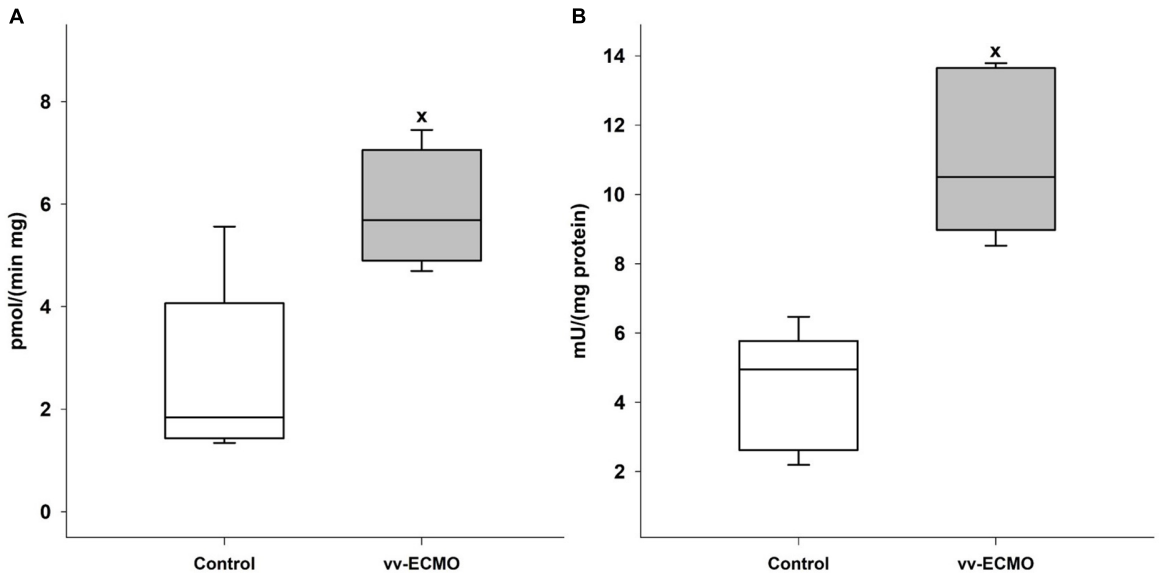

FIGURE 6 | Changes in the xanthine-oxidoreductase **(A)** and myeloperoxidase **(B)** enzyme activities in the renal tissue in the control group (empty box) and vv-ECMO group (gray box). The plots demonstrate the median (horizontal line in the box), the 25th and 75th percentiles, and the range of data (whiskers). $^{x}P < 0.05$ for the vv-ECMO vs. control group values (Mann–Whitney test).

examination of the pathomechanism of vv-ECMO-induced AKI feasible. We chose pigs due to the translational similarities to humans, including comparable respiratory physiology and activity of pro-inflammatory enzymes. We also selected AKI as a primary subject, as it can be an important component of multiorgan failure and one of the most important risk factors of mortality among vv-ECMO patients (6, 14).

We were unable to show any differences in MAP and CO between the vv-ECMO-treated and non-treated groups in our model. Nonetheless, HR started to increase in the later phase, including the whole post-ECMO period, in the vv-ECMO group and this was, as expected, accompanied by a decrease in the SV from the 24th hour of the observation period. These changes may point to the initiation of hemodynamic compensatory mechanisms to maintain adequate CO, but this process may also be related to the systemic inflammatory activation induced by the ECMO system. Data from previous *in vitro* studies suggest that IL-1β might be a key component of the process (15). IL-1β affects myocardial contractility in multiple ways, such as modulation of inducible nitric oxide synthase (iNOS) activity (16) and alteration of L-type Ca^{2+} current (17).

The lower average hour diuresis in the vv-ECMO group points to an impaired renal function, which may be the result of a reduced filtration rate caused by the decreased renal perfusion.

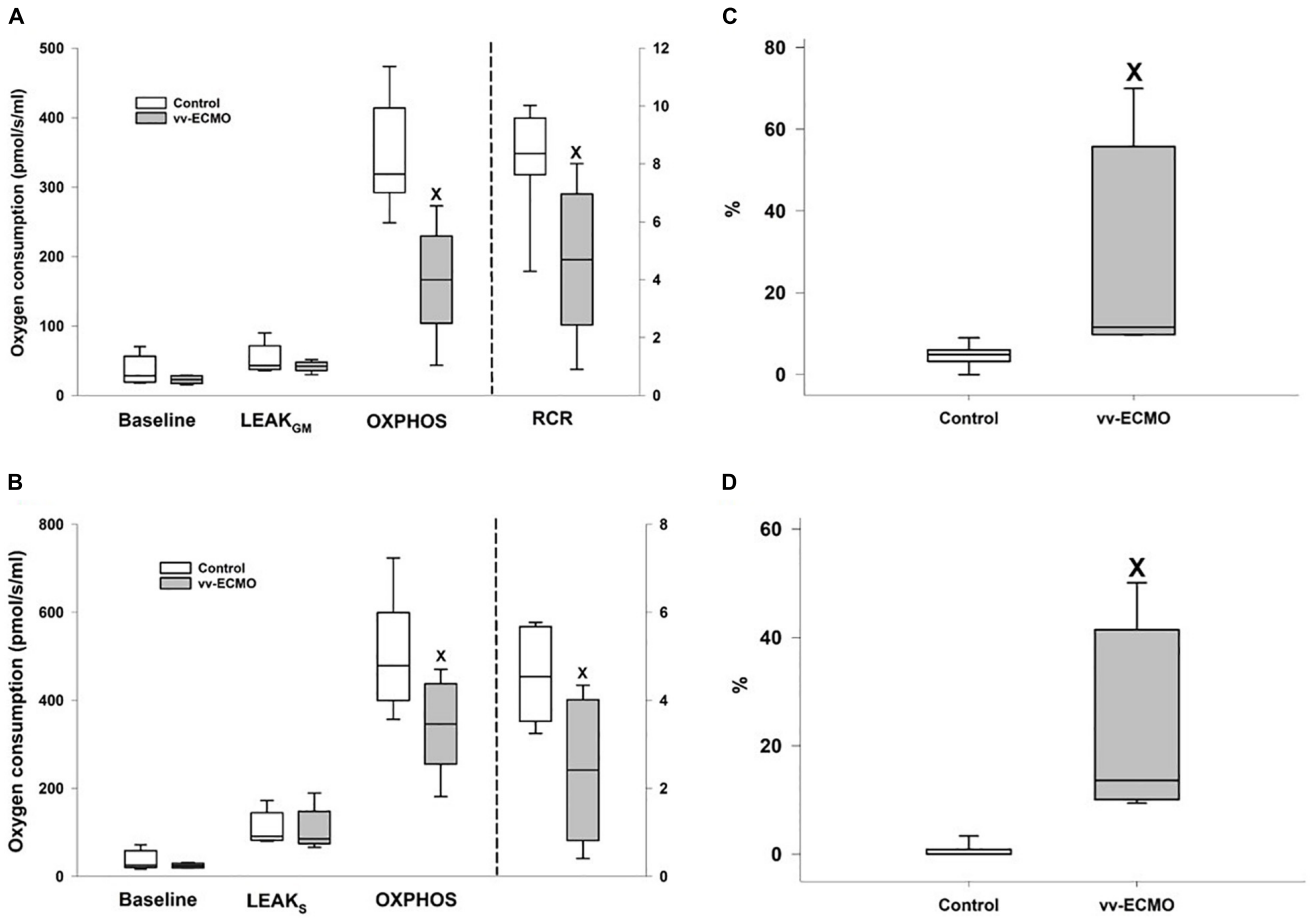

FIGURE 7 | Changes in baseline and LEAK$_{GM}$ respirations, complex I-linked oxidative phosphorylation capacities (OXPHOS; left axis) and respiratory acceptor control ratios (RCR; right axis) in the control (empty box) and vv-ECMO (gray box) groups **(A)**. Changes in baseline and LEAK$_S$ respirations, complex II-linked oxidative phosphorylation capacities (OXPHOS; left axis) and respiratory acceptor control ratios (RCR; right axis) in the control (empty box) and vv-ECMO (gray box) groups **(B)**. Changes in the complex I-linked **(C)** and complex II-linked **(D)** oxygen flux following addition of cytochrome c in the control (empty box) and vv-ECMO (gray box) groups. The plots demonstrate the median (horizontal line in the box), the 25th and 75th percentiles, and the range of data (whiskers). $^{x}P < 0.05$ for the vv-ECMO vs. control group values (Mann–Whitney test).

Indeed, RAF was reduced during the post-ECMO period after vv-ECMO treatment, although there was no difference in CO and MAP values between the two experimental groups. MAP was also kept over 60 mmHg, which is the lowest MAP value necessary to maintain renal function (18). We were not able to obtain RAF data during the ECMO phase for technical reasons. The anticoagulation during ECMO and the need for surgical intervention for the placement of perivascular flow probes around the renal artery would have raised the risk of bleeding. We therefore cut the invasive interventions to a minimum before and during ECMO. Nonetheless, we collected plasma and urine samples during the ECMO phase to measure the levels of kidney injury marker NGAL (19, 20), which provided us with an insight into the condition of the kidneys. These data demonstrate an early increase in both urine and plasma NGAL at 6 h after ECMO initiation. This suggests that the development of AKI starts at a very early stage and precedes systemic hemodynamic changes. Therefore, humoral, inflammatory factors may play a far more important role in the emergence of vv-ECMO-induced AKI than hemodynamic factors.

It should be added that we have already provided evidence for the fall in RAF in another, short-term cardiopulmonary bypass model (21). We explained the phenomenon with the role of superoxide anion generation, as it can raise Ca^{2+} influx into the smooth muscle cells of the renal afferent arterioles, causing vasoconstriction and subsequently reduced renal flow (21, 22). This hypothesis is supported by the heightened activity of MPO and XOR enzymes, which may which greatly contributes to the development of oxidative stress in the renal tissue.

The deterioration of renal tissue perfusion resulted in tubular damage. The histological changes in the kidney samples in the vv-ECMO group correspond to those observed in ischemic kidneys (23). The reduced tHb and Hct could aggravate the effect of the decreased RAF as these factors are key components of the local, tissue oxygen delivery (DO_2). However, the development of tubular damage is multifactorial, and other causes besides

an impaired renal DO_2, including inflammatory activation and mitochondrial damage, are significant inducers of AKI of other origins (24, 25). Indeed, our study is the first to demonstrate vv-ECMO-linked mitochondrial functional impairment in non-cardiac tissue. Structural and functional changes in cardiac mitochondria have previously been confirmed in pigs following vv-ECMO (26), and now we have found that both complex I- and complex II-linked OXPHOS capacities (an indicator of ATP synthesis) and RCR (respiration coupled to OXPHOS) values were markedly lower in the kidney. Moreover, the integrity of the outer membrane was impaired, indicated by elevated respiration following addition of cytochrome c. The ECMO-related mitochondrial dysfunction may also be linked to the release of pro-inflammatory cytokines, such as TNF-α, IL-1β and IL-6 (27). Ligation of TNF receptors with TNF-α is associated with (1) increased mitochondrial ROS formation at complex I and complex III, (2) inhibition of OXPHOS and ATP depletion *via* tyrosine phosphorylation at subunit I of cytochrome c oxidase, (3) decreased mitochondrial membrane potential and (4) altered mitochondrial integrity (28, 29). Dysfunctional mitochondria generate a high level of reactive oxygen species (ROS), release cell-free mitochondrial DNA (cf-mtDNA) and multiply damage-associated molecular patterns (DAMPs), such as cardiolipin, ATP and cytochrome c (30); all these events may ultimately lead to further mitochondrial and kidney damage. There is also evidence that ECMO affects metabolic flexibility and upregulates pyruvate dehydrogenase kinase-4 (PDK4), a crucial enzyme responsible for the suppression of pyruvate dehydrogenase complex (PDC) (31, 32). PDK4 plays a decisive role in the metabolic shift from OXPHOS to glycolysis; PDK4 downregulation lowered lactate level and boosted ATP generation, whereas PDK4 over-expression increased lactate and reduced ATP level *in vitro* (33). A similar PDK4-related mechanism on mitochondrial respiration cannot be ruled out and may be the subject of further study.

There are a few limitations to discuss. The 24-hour time frame of the vv-ECMO treatment can be considered relatively short from a clinical point of view. We chose this period as it provides a clinically relevant balance between the human situation and the material resources and technical background of *in vivo* large animal studies. The oliguric phase after the start of ECMO occurs mostly in the first 24–48 h, and recovery may start after 48 h, with the diuretic phase following (34). Therefore, we considered the 24-hour treatment suitable to examining the processes that play a role in the early development of vv-ECMO-related AKI. Another important limitation is the lack of data on RAF during vv-ECMO, which could be overcome with the application of non-invasive techniques, such as ultrasound Doppler. Nonetheless, these techniques are far less reliable than perivascular flow probes (35). Also, this might require the repositioning of the animals, which heightens the risk of accidental decannulation or of movement of the cannulas from the ideal position. Finally, it is important to note that the transpulmonary thermodilution technique may be inaccurate during ECMO due to the potential loss of the indicator. Nonetheless, recent studies have demonstrated that the method can be applied during vv-ECMO, especially when the indicator is injected *via* the jugular vein (36, 37).

CONCLUSION

We have presented a porcine model suitable for the examination of renal complications of vv-ECMO. The findings show that vv-ECMO for 24 h may induce AKI, which is more likely associated with vv-ECMO-related inflammatory signals than changes in systemic hemodynamics. Oxidative stress and mitochondrial injury are key contributors to the progression that results in structural and functional damage to the kidneys in this scenario.

DATA AVAILABILITY STATEMENT

The raw data supporting the conclusions of this article will be made available by the authors, without undue reservation.

ETHICS STATEMENT

The animal study was reviewed and approved by National Scientific Ethical Committee on Animal Experimentation (National Competent Authority of Hungary).

AUTHOR CONTRIBUTIONS

GB, GV, and DÉ designed the study. AS-B, GV, ZV, GB, GyV, ÁG, NV, ÁH, AR, MG, and DÉ performed the experiments. ZV, GyV, ÁG, NV, ÁH, and MG managed databases. AS-B, GV, and DÉ evaluated data and wrote the manuscript. GV, AN, and AR prepared figures. LJ and AN measured mitochondrial respiratory function and wrote the manuscript. ST-N performed histological evaluation. AS-B, GV, DÉ, and MB supervised and edited the manuscript. All authors contributed to the article and approved the submitted version.

FUNDING

This study was supported by Hungarian National Research, Development and Innovation Office grants NKFIH-K 116861, NKFIH-K 120232, and NKFIH-K 143534.

ACKNOWLEDGMENTS

We are grateful to Andrea Bús, Virág Molnár, Csilla Mester, Bence Győrfi, István Szabó, and Krisztián Daru for their skillful assistance.

SUPPLEMENTARY MATERIAL

The Supplementary Material for this article can be found online at: https://www.frontiersin.org/articles/10.3389/fmed.2022.866667/full#supplementary-material

REFERENCES

1. Ostermann M, Lumlertgul N. Acute kidney injury in ECMO patients. In: Vincent J-L editor. *Annual Update in Intensive Care and Emergency Medicine 2021*. Cham: Springer International Publishing (2021). p. 207–22. doi: 10.1007/978-3-030-73231-8_18
2. Zangrillo A, Landoni G, Biondi-Zoccai G, Greco M, Greco T, Frati G, et al. A meta-analysis of complications and mortality of extracorporeal membrane oxygenation. *Crit Care Resusc.* (2013) 15:172–8.
3. Askenazi DJ, Selewski DT, Paden ML, Cooper DS, Bridges BC, Zappitelli M, et al. Renal replacement therapy in critically ill patients receiving extracorporeal membrane oxygenation. *Clin J Am Soc Nephrol.* (2012) 7:1328–36. doi: 10.2215/CJN.12731211
4. Delmas C, Zapetskaia T, Conil JM, Georges B, Vardon-Bounes F, Seguin T, et al. 3-month prognostic impact of severe acute renal failure under veno-venous ECMO support: importance of time of onset. *J Crit Care.* (2018) 44:63–71. doi: 10.1016/j.jcrc.2017.10.022
5. Ostermann M, Connor MJ, Kashani K. Continuous renal replacement therapy during extracorporeal membrane oxygenation: why, when and how? *Curr Opin Crit Care.* (2018) 24:493–503. doi: 10.1097/MCC.0000000000000559
6. Thongprayoon C, Cheungpasitporn W, Lertjitbanjong P, Aeddula NR, Bathini T, Watthanasuntorn K, et al. Incidence and impact of acute kidney injury in patients receiving extracorporeal membrane oxygenation: a meta-analysis. *J Clin Med.* (2019) 8:981. doi: 10.3390/jcm8070981
7. Lin C-Y, Chen Y-C, Tsai F-C, Tian Y-C, Jenq C-C, Fang J-T, et al. RIFLE classification is predictive of short-term prognosis in critically ill patients with acute renal failure supported by extracorporeal membrane oxygenation. *Nephrol Dial Transplant.* (2006) 21:2867–73. doi: 10.1093/ndt/gfl326
8. De Corte W, Dhondt A, Vanholder R, De Waele J, Decruyenaere J, Sergoyne V, et al. Long-term outcome in ICU patients with acute kidney injury treated with renal replacement therapy: a prospective cohort study. *Crit Care.* (2016) 20:256. doi: 10.1186/s13054-016-1409-z
9. Husain-Syed F, Ricci Z, Brodie D, Vincent J-L, Ranieri VM, Slutsky AS, et al. Extracorporeal organ support (ECOS) in critical illness and acute kidney injury: from native to artificial organ crosstalk. *Intensive Care Med.* (2018) 44:1447–59. doi: 10.1007/s00134-018-5329-z
10. Beckman JS, Parks DA, Pearson JD, Marshall PA, Freeman BA. A sensitive fluorometric assay for measuring xanthine dehydrogenase and oxidase in tissues. *Free Radic Biol Med.* (1989) 6:607–15. doi: 10.1016/0891-5849(89)90068-3
11. Kuebler WM, Abels C, Schuerer L, Goetz AE. Measurement of neutrophil content in brain and lung tissue by a modified myeloperoxidase assay. *Int J Microcirc Clin Exp Spons Eur Soc Microcirc.* (1996) 16:89–97. doi: 10.1159/000179155
12. Dupont WD, Plummer WD. Power and sample size calculations: a review and computer program. *Control Clin Trials.* (1990) 11:116–28. doi: 10.1016/0197-2456(90)90005-m
13. Kim JH, Pieri M, Landoni G, Scandroglio AM, Calabrò MG, Fominskiy E, et al. Venovenous ECMO treatment, outcomes, and complications in adults according to large case series: a systematic review. *Int J Artif Organs.* (2021) 44:481–8. doi: 10.1177/0391398820975408
14. Mou Z, He J, Guan T, Chen L. Acute kidney injury during extracorporeal membrane oxygenation: VA ECMO versus VV ECMO. *J Intensive Care Med.* (2021). [Online ahead of print]. doi: 10.1177/08850666211035323
15. Adrian K, Mellgren K, Skogby M, Friberg LG, Mellgren G, Wadenvik H. Cytokine release during long-term extracorporeal circulation in an experimental model. *Artif Organs.* (1998) 22:859–63. doi: 10.1046/j.1525-1594.1998.06121.x
16. Stein B, Frank P, Schmitz W, Scholz H, Thoenes M. Endotoxin and cytokines induce direct cardiodepressive effects in mammalian cardiomyocytes via induction of nitric oxide synthase. *J Mol Cell Cardiol.* (1996) 28:1631–9. doi: 10.1006/jmcc.1996.0153
17. El Khoury N, Mathieu S, Fiset C. Interleukin-1β reduces L-type Ca^{2+} current through protein kinase C∈ activation in mouse heart. *J Biol Chem.* (2014) 289:21896–908. doi: 10.1074/jbc.m114.549642
18. Redfors B, Bragadottir G, Sellgren J, Swärd K, Ricksten SE. Effects of norepinephrine on renal perfusion, filtration and oxygenation in vasodilatory shock and acute kidney injury. *Intensive Care Med.* (2011) 37:60–7. doi: 10.1007/s00134-010-2057-4
19. Bulluck H, Maiti R, Chakraborty B, Candilio L, Clayton T, Evans R, et al. Neutrophil gelatinase-associated lipocalin prior to cardiac surgery predicts acute kidney injury and mortality. *Heart.* (2018) 104:313–7. doi: 10.1136/heartjnl-2017-311760
20. Lima C, de Paiva Haddad LB, de Melo PDV, Malbouisson LM, do Carmo LPF, D'Albuquerque LAC, et al. Early detection of acute kidney injury in the perioperative period of liver transplant with neutrophil gelatinase-associated lipocalin. *BMC Nephrol.* (2019) 20:367. doi: 10.1186/s12882-019-1566-9
21. Bari G, Érces D, Varga G, Szűcs S, Varga Z, Bogáts G, et al. Methane inhalation reduces the systemic inflammatory response in a large animal model of extracorporeal circulation. *Eur J Cardiothorac Surg.* (2019) 56:135–42. doi: 10.1093/ejcts/ezy453
22. Vogel PA, Yang X, Moss NG, Arendshorst WJ. Superoxide enhances Ca^{2+} entry through L-type channels in the renal afferent arteriole. *Hypertension.* (2015) 66:374–81. doi: 10.1161/HYPERTENSIONAHA.115.05274
23. van Smaalen TC, Ellis SR, Mascini NE, Siegel TP, Cillero-Pastor B, Hillen LM, et al. Rapid identification of ischemic injury in renal tissue by mass-spectrometry imaging. *Anal Chem.* (2019) 91:3575–81. doi: 10.1021/acs.analchem.8b05521
24. Bhatia D, Capili A, Choi ME. Mitochondrial dysfunction in kidney injury, inflammation, and disease: potential therapeutic approaches. *Kidney Res Clin Pract.* (2020) 39:244–58. doi: 10.23876/j.krcp.20.082
25. Ishimoto Y, Inagi R. Mitochondria: a therapeutic target in acute kidney injury. *Nephrol Dial Transplant.* (2016) 31:1062–9. doi: 10.1093/ndt/gfv317
26. Shen J, Yu W, Shi J, Chen Q, Hu Y, Zhang J, et al. Effect of venovenous extracorporeal membrane oxygenation on the heart in a healthy piglet model. *J Cardiothorac Surg.* (2013) 8:163. doi: 10.1186/1749-8090-8-163
27. Shen J, Yu W, Chen Q, Shi J, Hu Y, Zhang J, et al. Continuous renal replacement therapy (CRRT) attenuates myocardial inflammation and mitochondrial injury induced by venovenous extracorporeal membrane oxygenation (VV ECMO) in a healthy piglet model. *Inflammation.* (2013) 36:1186–93. doi: 10.1007/s10753-013-9654-7
28. Kastl L, Sauer SW, Ruppert T, Beissbarth T, Becker MS, Süss D, et al. TNF-α mediates mitochondrial uncoupling and enhances ROS-dependent cell migration via NF-κB activation in liver cells. *FEBS Lett.* (2014) 588:175–83. doi: 10.1016/j.febslet.2013.11.033
29. Samavati L, Lee I, Mathes I, Lottspeich F, Hüttemann M. Tumor necrosis factor α inhibits oxidative phosphorylation through tyrosine phosphorylation at subunit I of cytochrome c oxidase. *J Biol Chem.* (2008) 283:21134–44. doi: 10.1074/jbc.M801954200
30. Thurairajah K, Briggs GD, Balogh ZJ. The source of cell-free mitochondrial DNA in trauma and potential therapeutic strategies. *Eur J Trauma Emerg Surg.* (2018) 44:325–34. doi: 10.1007/s00068-018-0954-3
31. Kajimoto M, O'Kelly Priddy CM, Ledee DR, Xu C, Isern N, Olson AK, et al. Extracorporeal membrane oxygenation promotes long chain fatty acid oxidation in the immature swine heart in vivo. *J Mol Cell Cardiol.* (2013) 62:144–52. doi: 10.1016/j.yjmcc.2013.05.014
32. Zhang S, Hulver MW, McMillan RP, Cline MA, Gilbert ER. The pivotal role of pyruvate dehydrogenase kinases in metabolic flexibility. *Nutr Metab.* (2014) 11:10. doi: 10.1186/1743-7075-11-10
33. Liu X, Zuo R, Bao Y, Qu X, Sun K, Ying H. Down-regulation of PDK4 is critical for the switch of carbohydrate catabolism during syncytialization of human placental trophoblasts. *Sci Rep.* (2017) 7:8474. doi: 10.1038/s41598-017-09163-8
34. Vyas A, Bishop MA. *Extracorporeal Membrane Oxygenation in Adults*. Treasure Island, FL: StatPearls Publishing (2022).
35. Wan L, Yang N, Hiew C-Y, Schelleman A, Johnson L, May C, et al. An assessment of the accuracy of renal blood flow estimation by Doppler ultrasound. *Intensive Care Med.* (2008) 34:1503–10. doi: 10.1007/s00134-008-1106-8

36. Herner A, Lahmer T, Mayr U, Rasch S, Schneider J, Schmid RM, et al. Transpulmonary thermodilution before and during veno-venous extra-corporeal membrane oxygenation ECMO: an observational study on a potential loss of indicator into the extra-corporeal circuit. *J Clin Monit Comput.* (2020) 34:923–36. doi: 10.1007/s10877-019-00398-6
37. Lahmer T, Mayr U, Rasch S, Batres Baires G, Schmid RM, Huber W. In-parallel connected intermittent hemodialysis through ECMO does not affect hemodynamic parameters derived from transpulmonary thermodilution. *Perfusion.* (2017) 32:702–5. doi: 10.1177/0267659117707816

Conflict of Interest: The authors declare that the research was conducted in the absence of any commercial or financial relationships that could be construed as a potential conflict of interest.

Publisher's Note: All claims expressed in this article are solely those of the authors and do not necessarily represent those of their affiliated organizations, or those of the publisher, the editors and the reviewers. Any product that may be evaluated in this article, or claim that may be made by its manufacturer, is not guaranteed or endorsed by the publisher.

frontiers | Frontiers in Medicine

ORIGINAL RESEARCH
published: 28 April 2022
doi: 10.3389/fmed.2022.867298

Local Mucosal CO_2 but Not O_2 Insufflation Improves Gastric and Oral Microcirculatory Oxygenation in a Canine Model of Mild Hemorrhagic Shock

Stefan Hof[1†], Richard Truse[1], Lea Weber[1†], Anna Herminghaus[1], Jan Schulz[1], Andreas P. M. Weber[2], Eva Maleckova[2], Inge Bauer[1], Olaf Picker[1] and Christian Vollmer[1]*

[1] Department of Anesthesiology, Duesseldorf University Hospital, Duesseldorf, Germany, [2] Institute of Plant Biochemistry, Cluster of Excellence on Plant Sciences (CEPLAS), Heinrich-Heine-University Duesseldorf, Duesseldorf, Germany

OPEN ACCESS

Edited by:
Wolfgang Weihs,
Medical University of Vienna, Austria

Reviewed by:
Manabu Kinoshita,
National Defense Medical College, Japan
Sabine Beate Rita Kästner,
University of Veterinary Medicine Hannover, Germany

***Correspondence:**
Richard Truse
Richard.Truse@med.uni-duesseldorf.de

†In partial fulfillment of the requirements of the MD thesis of S. Hof and L. Weber

Specialty section:
This article was submitted to Intensive Care Medicine and Anesthesiology, a section of the journal Frontiers in Medicine

Received: 31 January 2022
Accepted: 07 April 2022
Published: 28 April 2022

Citation:
Hof S, Truse R, Weber L, Herminghaus A, Schulz J, Weber APM, Maleckova E, Bauer I, Picker O and Vollmer C (2022) Local Mucosal CO_2 but Not O_2 Insufflation Improves Gastric and Oral Microcirculatory Oxygenation in a Canine Model of Mild Hemorrhagic Shock. Front. Med. 9:867298. doi: 10.3389/fmed.2022.867298

Introduction: Acute hemorrhage results in perfusion deficit and regional hypoxia. Since failure of intestinal integrity seem to be the linking element between hemorrhage, delayed multi organ failure, and mortality, it is crucial to maintain intestinal microcirculation in acute hemorrhage. During critical bleeding physicians increase FiO_2 to raise total blood oxygen content. Likewise, a systemic hypercapnia was reported to maintain microvascular oxygenation (μHbO_2). Both, O_2 and CO_2, may have adverse effects when applied systemically that might be prevented by local application. Therefore, we investigated the effects of local hyperoxia and hypercapnia on the gastric and oral microcirculation.

Methods: Six female foxhounds were anaesthetized, randomized into eight groups and tested in a cross-over design. The dogs received a local CO_2-, O_2-, or N_2-administration to their oral and gastric mucosa. Hemorrhagic shock was induced through a withdrawal of 20% of estimated blood volume followed by retransfusion 60 min later. In control groups no shock was induced. Reflectance spectrophotometry and laser Doppler were performed at the gastric and oral surface. Oral microcirculation was visualized by incident dark field imaging. Systemic hemodynamic parameters were recorded continuously. Statistics were performed using a two-way-ANOVA for repeated measurements and *post hoc* analysis was conducted by Bonferroni testing ($p < 0.05$).

Results: The gastric μHbO_2 decreased from 76 ± 3% to 38 ± 4% during hemorrhage in normocapnic animals. Local hypercapnia ameliorated the decrease of μHbO_2 from 78 ± 4% to 51 ± 8%. Similarly, the oral μHbO_2 decreased from 81 ± 1% to 36 ± 4% under hemorrhagic conditions and was diminished by local hypercapnia (54 ± 4%). The oral microvascular flow quality but not the total microvascular blood flow was significantly improved by local hypercapnia. Local O_2-application failed to change microvascular oxygenation, perfusion or flow quality. Neither CO_2 nor

O_2 changed microcirculatory parameters and macrocirculatory hemodynamics under physiological conditions.

Discussion: Local hypercapnia improved microvascular oxygenation and was associated with a continuous blood flow in hypercapnic individuals undergoing hemorrhagic shock. Local O_2 application did not change microvascular oxygenation, perfusion and blood flow profiles in hemorrhage. Local gas application and change of microcirculation has no side effects on macrocirculatory parameters.

Keywords: gastric microcirculation, μHbO_2, hypercapnia, hyperoxia, hemorrhagic shock, mucosal barrier integrity

INTRODUCTION

The potential for hemorrhage in trauma and surgical patients represents an ongoing concern for management (1) with an estimated 1.9 million deaths per year worldwide (2). With the exception of the traumatic event itself, exsanguination is the most frequent cause of immediate death (3) later on followed by multi organ dysfunction syndrome (MODS) as the leading cause of death among patients who die in intensive care units (4). In hemorrhagic shock severe blood loss causes an inadequate oxygen delivery to meet oxygen demand on a cellular level. Early recognition of hemorrhagic shock and immediate action to stop further bleeding are crucial, since the median time from onset of shock to death is 2 h (5). However, ischemia-reperfusion injury by restoration of blood flow may further aggravate tissue damage (6).

Therefore, as adjuncts to volume resuscitation, tissue hypoxia can be attenuated amongst others by increasing arterial oxygen content, restoration of organ perfusion, and reduction in local oxygen demand. Hyperoxia by increasing the fraction of inspired oxygen is effective to increase arterial oxygen content. However, excessive normobaric oxygen supplementation may have detrimental systemic effects because of enhanced oxidative stress and inflammation and hyperoxia-derived vasoconstriction resulting in reduced microvascular perfusion (7, 8). Permissive hypercapnia is common in critically ill patients and has been associated with augmented cardiac output and tissue oxygenation in experimental models of sepsis (9, 10) and hemorrhagic shock (11). On the other hand, hypercapnic acidosis exerts potent anti-inflammatory effects (12) and may even promote microbial growth (13), which could be detrimental in the context of sepsis. To limit systemic side effects local therapy regimes have been established in various organs and diseases, like inhaled nitric oxide in pulmonary hypertension (14).

The ischemic gut seems to be an important factor in the pathogenesis of MODS after traumatic hemorrhagic shock. In pathological conditions with reduced splanchnic perfusion, such as hemorrhagic shock, bacteria and gut ischemia provoke an intestinal inflammatory response, which leads to dysfunction of additional organs (15). Therefore, maintaining adequate gastrointestinal microcirculation is of utmost importance. Current strategies to prevent or reverse gut dysfunction focus on early enteral nutrition, which has been shown to improve intestinal barrier function, gastrointestinal immunity and resorptive function and to preserve gastrointestinal mucosal architecture (16). Moreover, because of its non-invasive accessibility, particularly the gastrointestinal tract is suitable for topical therapeutic interventions. For example, topical applied nitroglycerin and iloprost improved gastric oxygenation in a hemorrhagic shock model. In the same trial nitroglycerin improved intestinal barrier function (17). Likewise, local application of melatonin (18) and losartan (19) were able to ameliorate the decrease of gastric mucosal oxygenation in a state of acute hemorrhage. Systemic hypercapnia and hyperoxia proved to exert favorable effects in the context of hemorrhagic shock (11, 20). However, to date no data are available on the effects of local mucosal hyperoxia and hypercapnia on gastrointestinal microcirculatory oxygenation and perfusion in the presence of hemorrhage.

We hypothesized that local oxygen and carbon dioxide application modulates oral and gastric microcirculation and oxygenation in a mild model of hemorrhagic shock without adverse side effects on systemic variables.

Taken together, this study was designed to address the following questions:

(i) Does local CO_2 or O_2 increase gastric and oral oxygenation in a model of mild hemorrhagic shock?
(ii) Which impact has a local CO_2- or O_2-application on oral microcirculatory variables?
(iii) Are there any systemic side effects of local gas application expected, which could limit the use of local CO_2 or O_2 in critically ill patients?

MATERIALS AND METHODS

Animals

The data were derived in a crossover design from repetitive experiments on six dogs (female foxhounds, weighing 28–36 kg) treated in accordance with the NIH guidelines for animal care. Experiments were performed with approval of the Local Animal Care and Use Committee (North Rhine-Westphalia State Agency for Nature, Environment, and Consumer Protection, Recklinghausen, Germany; ref. 84-02.04.2012.A152).

A slightly modified, well-established canine model of hemorrhagic shock was used as published previously (11). All animals were bred for experimental purposes and obtained from the animal research facility (ZETT, Zentrale Einrichtung

für Tierforschung und wissenschaftliche Tierschutzaufgaben) of the Heinrich-Heine-University Duesseldorf. The animal husbandry took place in accordance with the European Directive 2010/63/EU and the National Animal Welfare Act. All animals were kept in kennel maintenance under the care of a keeper and with access to an outdoor area. The dogs were fed daily with dry food (Deukadog nature food lamb and rice, Deutsche Tiernahrung Cremer, Duesseldorf, Germany) and wet food (Rinti Gourmet Beef, Finnern, Verden, Germany). Prior to the experiments, access to food was withheld for 12 h with water *ad libitum* to ensure complete gastric depletion and to avoid changes in mucosal perfusion and oxygenation due to digestive activity. Each dog underwent every experimental protocol in a randomized order and served as its own control. The experiments were performed at least 3 weeks apart to prevent carryover effects. The experiments were performed under general anesthesia [induction of anesthesia with 4 mg·kg-1 propofol, maintenance with sevoflurane, end-tidal concentration of 3.0% (1.5 minimum alveolar concentration (MAC) for dogs)]. Following endotracheal intubation the dogs were mechanically ventilated [FiO_2 = 0.3, VT = 12.5 ml·kg^{-1}, a physiological tidal volume for dogs (21)], and the respiratory frequency adjusted to achieve normocapnia [end-expiratory carbon dioxide ($etCO_2$) = 35 mmHg], verified by continuous capnography (Capnomac Ultima, Datex Instrumentarium, Helsinki, Finland). After taking each blood sample for blood gas analysis and determination of sucrose plasma levels, normal saline was infused three times the sampling volume to maintain blood volume. Throughout the experiments, the animals received less than 250 ml additional fluid replacement to avoid volume effects that could influence tissue perfusion and oxygenation. Following the intervention, the dogs were extubated as soon as they showed sufficient spontaneous breathing and protective reflexes. The animals remained under direct supervision of the laboratory personnel until complete recovery from anesthesia and first intake of wet food and water. After examination of all puncture sites and a detailed handover, the dogs were given back to their keepers in the animal research facility. No animal was sacrificed during or after the experiments.

Measurements

Systemic Hemodynamic and Oxygenation Variables

The aorta was catheterized via the left carotid artery for continuous measurement of mean arterial pressure (MAP, Gould-Statham pressure transducers P23ID, Elk Grove, IL) and intermittent arterial blood gas analysis (Rapidlab 860, Bayer AG, Germany). Before participation in the study, both carotid arteries were externalized in all animals (22) to enable landmark guided arterial catheterization with low complication rates. Cardiac output (CO) was determined via transpulmonary thermodilution (PiCCO 4.2 non US, PULSION Medical Systems, Munich, Germany) at the end of each intervention. Systemic oxygen delivery (DO_2) was calculated as the total oxygen content multiplied by cardiac output. Cardiac output and systemic oxygen delivery are related to the total body weight of each dog to ensure comparability between individuals. Heart rate (HR) was continuously measured by electrocardiography (Powerlab, ADInstruments, Castle Hill, Australia).

Mucosal Oxygenation and Perfusion

Microvascular oxygenation (μHbO_2) and microvascular blood flow (μflow) of the gastric and oral mucosa were continuously assessed by tissue reflectance spectrophotometry and laser Doppler flowmetry (O_2C, LEA Medizintechnik, Gießen, Germany), respectively, as detailed previously (23). White light (450–1,000 nm) and laser light (820 nm, 30 mW) were transmitted to the tissue of interest via a microlightguide and the reflected light was analyzed. The wavelength-dependent absorption and overall absorption of the applied white light can be used to calculate the percentage of oxygenated hemoglobin (μHbO_2) and the relative amount of hemoglobin (rHb). Due to the Doppler effect, magnitude and frequency distribution of changes in wavelength are proportional to the number of blood cells multiplied by the measured mean velocity (μvelo) of these cells. This product is proportional to flow and expressed in arbitrary perfusion units (aU). Hence, this method allows assessment and comparison of oxygenation and perfusion of the same region at the same time. Since light is fully absorbed in vessels with a diameter $>$ 100 μm (24) only the microvascular oxygenation of nutritive vessels of the mucosa is measured. The biggest fraction of total blood volume is stored in venous vessels; therefore, mainly postcapillary oxygenation is measured which represents the critical partial pressure of oxygen (pO_2) for ischemia (23). Two probes were used to meet the individual needs of the oral and gastric mucosal surface. According to the manufacturer's recommendation reading were obtained by placing one flat lightguide probe in the mouth facing the buccal side of the oral mucosa (LF-2, 12 × 5.5 × 44.5 mm, LEA Medizintechnik GmbH, Gießen) and a second flexible lightguide probe into the stomach (LM-10, outer diameter 2.6 mm, LEA Medizintechnik GmbH, Gießen) via an orogastric silicone tube facing the gastric mucosa. Continuous evaluation of the signal quality throughout the experiments and the immediate comparison between oral and gastric spectroscopy allows verification of the correct probe position during the experiments. The μHbO_2 and μflow values reported are 5 min means (150 spectra, 2 s each) of the respective intervention under steady state conditions. The non-traumatic access to the gastric mucosa allows the determination of mucosal microcirculation without the need of surgical stress. This is particularly desirable regarding the marked alterations that surgical stress exerts on splanchnic circulation. Under these circumstances reflectance spectrophotometry reliably detects even clinically asymptomatic reductions in μHbO_2 and highly correlates with the morphologic severity and extent of gastric mucosal tissue injury (25).

Mucosal Microcirculation—Videomicroscopy

Microcirculatory perfusion of the oral mucosa was assessed intermittently by incident dark field (IDF) -imaging (CytoCam, Braedius Medical, Huizen, Netherlands) as described elsewhere (26). Illumination was provided by light emitting diodes (LED) at a wavelength of 530 nm, the isosbestic point for deoxy- and oxyhemoglobin, and directed toward the

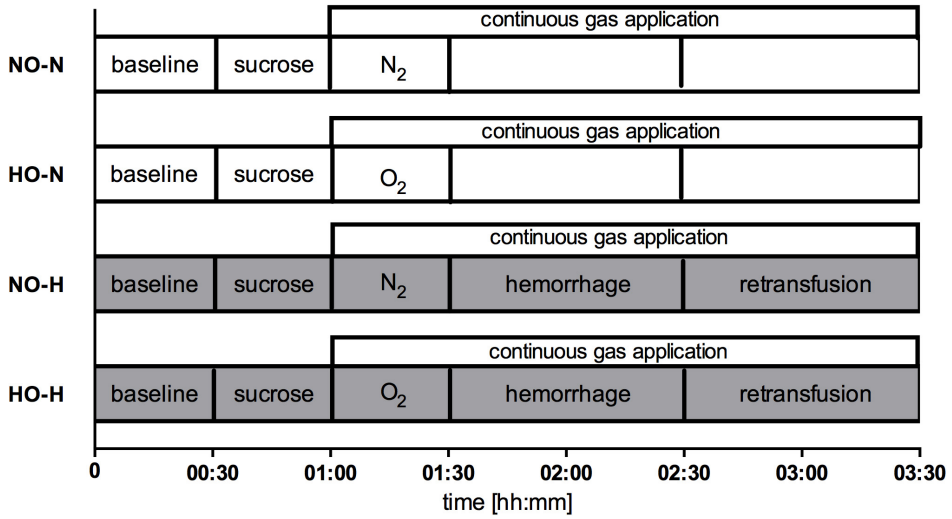

FIGURE 1 | Experimental protocol set 1: Continuous application of N_2 under normoxia (NO) or hyperoxia with application of O_2 (HO) before and during physiological (-N) or hemorrhagic (-H) condition. In shock groups 1 h of hemorrhage was followed by retransfusion, while gas application was conducted until the termination of the experimental protocol in all groups.

oral mucosa. The reflected and scattered light is filtered and visualizes red blood cells in capillaries. All videos were obtained by the same investigator. Videos were saved anonymized for blinded analysis. To assess the predominant blood flow characteristics, a well-established semiquantitative scoring method, the microcirculatory flow index (MFI), was used to characterize microcirculatory flow as "no flow," "intermittent flow," "sluggish flow," and "continuous flow" (27). Many clinical trials reported critical illness to be associated with heterogeneous blood flow patterns, which may assume microvascular shunting to be responsible for an impaired oxygen delivery in this collective (28, 29). Therefore, we calculated the heterogeneity index (HGI) as the difference between the highest and the lowest value achieved in the semiquantitative scoring system and divided it through the averaged microvascular flow index to determine spatial flow heterogeneity. To assess vessel density, the total vessel density (TVD), including perfused and non-perfused microvessels, and perfused vessel density (PVD), including perfused microvessels only, were analyzed using the appropriate software (MicroCirculation Analysis software, Braedius Medical, Huizen Netherlands) (30). The PVD/TVD ratio is used to express the proportion of perfused vessels (PPV). Only vessels with a diameter smaller than 20 μm are included in the analysis. Thus, the PVD represents the functional capillary density (FCD), which is considered to be the main determinant of microcirculatory blood supply and oxygen diffusion distance (31).

Intestinal Barrier Function

The disaccharide sucrose (D-Sucrose, Carl Roth, Karlsruhe, Germany) was infused into the stomach (1.66 $g{\cdot}kg^{-1}$ body weight) via an orogastric tube prior to the induction of hemorrhagic shock. Under physiological conditions, sucrose does not pass intact gastric mucosa. After being transported from the gastric region into the small intestine, ingested sucrose is rapidly degraded by sucrose-isomaltase into monosaccharides. Therefore, intact sucrose cannot be found in blood plasma under physiological conditions. However, under compromising conditions such as shock, barrier function is impaired, and sucrose can pass the gastric mucosal barrier into the plasma, where it does not undergo any enzymatic reaction. Sucrose plasma levels can therefore be used to assess gastric mucosal barrier function (32). Blood samples were collected under baseline conditions and during hemorrhagic shock. The collected samples were prepared as previously described (17). Briefly, blood plasma was separated via centrifugation (Rotina 420R, Hettich Zentrifugen, Mülheim a. d. R., Germany). Cold extraction mixture containing 10 μM ribitol, aceton and isopropanol (all from Carl Roth) was freshly prepared at a ratio of 2:1 and added to each probe. The supernatant was taken after the total probe was mixed and centrifugated again, denitrogenized and stored at −80°C. After completion of the experiments, extracts were dried using a speed vacuum concentrator (RVC 2-25 CDplus, Christ) for 3.5 h and obtained pellets were resuspended in 50 μl water (HPLC grade, Fisher Chemical). Subsequently, samples were purified using activated charcoal followed by filtration. After addition of a pinch of activated charcoal (Carl Roth; Karlsruhe, Germany), samples were vortexed briefly and incubated for a few minutes before centrifugation at 16,000 g and 8°C for 7 min. Collected supernatants were transferred to nylon-membrane centrifugal filters with pore size of 0.2 μm (VWR, 516-0233). Follow-throughs recovered after the centrifugation at room temperature at maximal speed for 2 min were stored at −80°C until analysis. Concentration of glucose-6-phosphate, glucose, fructose and saccharose was determined enzymatically using a modification of protocol by Stitt (33). Aliquots of 15 μl sample or 10 μl standard (ranging from 0 to 25 nM) were added to 100 mM HEPES-NaOH (pH 7.5) with 10 mM MgCl2, 3 mM

NADP + (disodium salt, Carl Roth, Karlsruhe, Germany) and 6 mM ATP (disodium salt hydrate, Sigma-Aldrich, St. Louis, MO, United States). After reading absorbance at 340 nm for 15 min, 2.1 U glucose-phosphate dehydrogenase (10127671001, Roche, Basel, Switzerland), 13.5 U hexokinase (11426362001, Roche, Basel, Switzerland), 1.5 U glucose-6-phosphate isomerase (10127396001) and approximately 7 U invertase (I4504-1G, Sigma-Aldrich. St. Louis, MO, United States) were added subsequently, with absorbance of individual reactions being read until stability using microplate reader (Synergy H1, BioTek, Winooski, VT, United States).

Experimental Protocol

The six dogs passed through two sets of experiments, each consisting of a normovolemic and a hypovolemic interventional group with their respective normoxic or normocapnic control groups. In the first set, effects of local oxygen insufflation were analyzed with and without hemorrhagic shock (**Figure 1**). In the second set, carbon dioxide was insufflated during both conditions (**Figure 2**). In both experimental setup's nitrogen (N_2) was insufflated during physiologic and hemorrhagic conditions as control. After instrumentation, 30 min were allowed to establish steady state conditions and baseline values were recorded before the animals were randomized to the respective protocol. Steady state conditions were defined as stability of hemodynamic variables (heart rate, mean arterial pressure) as well as ventilation parameters (end-tidal CO_2, end-tidal sevoflurane concentration, inspiratory oxygen fraction).

First set of experiments:

- NO-N: Normoxia during normovolemia
- HO-N: Local gastric and oral hyperoxia during normovolemia
- NO-H: Normoxia during mild hemorrhagic shock
- HO-H: Local gastric and oral hyperoxia during mild hemorrhagic shock

Second set of experiments:

- NC-N: Normocapnia during normovolemia
- HC-N: Local gastric and oral hypercapnia during normovolemia
- NC-H: Normocapnia during mild hemorrhagic shock
- HO-H: Local gastric and oral hypercapnia during mild hemorrhagic shock

Local Oxygen and Carbon Dioxide Application

To study the effects of local oxygen and carbon dioxide insufflation, 30 min after application of the sugar solution, 15 ml/min of 100% oxygen in hyperoxic groups or 100% carbon dioxide in hypercapnic groups was directed to the gastric mucosal via a multi-lumen orogastric tube and to the oral mucosa via a custom-made retainer. Both devices were manufactured in our institute. The multi-lumen orogastric tube, with its three distal orifices on the same level (consisting of three suction catheters, 80 cm, CH18, Dahlhausen, Cologne, Germany) as well as the custom-made retainer were placed without further trauma on the mucosal surfaces. The distal orifice of the tube as well as the gas-leading catheters of the retainer were in close proximity to the O_2C measuring probes (**Supplementary Figure 1**). The abdominal circumference was measured intermittently to exclude overinflation. All variables were recorded for the next 2.5 h. As time control experiments, 15 ml/min of pure nitrogen (groups NO-N and NO-H/groups NC-N and NC-H) was directed to the gastric and oral mucosa for 2.5 h.

Induction of Hemorrhagic Shock

Hemorrhagic shock was induced by removing 20% of the estimated total blood volume via a large bore intravenous cannula in a peripheral vein and the arterial catheter (i.e., 16 ml·kg^{-1} of whole blood) over 5 min. According to Advanced Trauma Life Support this model represents a class II shock (blood loss 15–30%) (34). The extracted blood was heparinized, stored and 60 min later retransfused using an infusion set with a 200 μm filter. Protamine was injected i.v. in a ratio of protamine to heparin as 1:2.

Statistical Analysis

Data for analysis were obtained during the last 5 min of baseline and intervention periods under steady-state conditions. All data are presented as absolute values of mean ± standard error (mean ± SEM) for six dogs. Normal data distribution was assessed in Q-Q-plots (IBM SPSS Statistics, International Business Machine Corp., United States). Differences within the groups and between the groups were tested using a two-way analysis of variance for repeated measurements (ANOVA) and a Bonferroni test as *post-hoc* test (GraphPad Prism version 6.05 for Windows, GraphPad Software, La Jolla California United States). Microvascular flow index and heterogeneity index as semiquantitative scores generally require non-parametric analysis. Multiple measurements with five videos à four squares per measurement approximate a normal data distribution and enable metric statistical testing. Therefore, we used Q-Q-plots, two-way ANOVA and Bonferroni *post-hoc* test for statistical analysis, too. An à priori power analysis (G*Power Version 3.1.9.2) (35) revealed a power of 0.85 for detection of differences between the different groups with $n = 6$ in 4 groups, repeated measurements, $\alpha < 0.05$ and η^2 of 0.5 (calculated from previous experiments).

RESULTS

Effect of Local Hypercapnia and Hyperoxia During Physiological Conditions

In anesthetized, ventilated dogs during otherwise physiological conditions, neither local O_2- nor CO_2-insufflation modified gastric or oral microcirculatory oxygenation and perfusion compared to the control groups (**Table 1** and **Supplementary Table 1**). Further, local CO_2-insufflation did not modify p_aCO_2 and systemic pH-values. In detail, p_aCO_2 increased from 35.5 ± 0.6 mmHg to a maximum of 37.1 ± 0.8 mmHg in the CO_2 treated group, which was not different from the normocapnic control group, where p_aCO_2 increased during the experiment

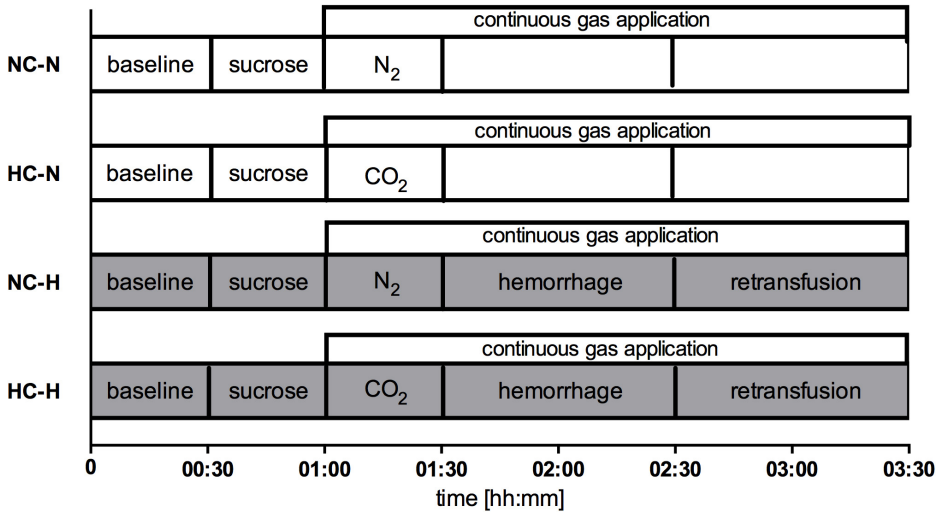

FIGURE 2 | Experimental protocol set 2: Continuous application of N_2 under normocapnia (NC) or hypercapnia with application of CO_2 (HC) before and during physiological (-N) or hemorrhagic (-H) condition. In shock groups 1 h of hemorrhage was followed by retransfusion, while gas application was conducted until the termination of the experimental protocol in all groups.

from 34.4 ± 0.3 mmHg to a maximum of 36.6 ± 0.9 mmHg. There was no difference between the respiratory rate in hypercapnic and normocapnic animals. Cardiac output and DO_2 were significantly lower in the hypercapnic group compared to the control group. However, this effect already exists during baseline conditions, remained throughout the experiment independent of the intervention and could be followed back to one individual (**Table 2**). The presentation of CO and DO_2 as the difference of baseline values demonstrates no effect in both parameters after CO_2 -insufflation. No differences between the CO_2 treated group and the control group were detected in MAP, HR and SVR.

Under physiological conditions neither macrocirculatory parameters nor blood gases were affected by local oxygen application compared to their control group. Further, animals did not show any differences in hemodynamics and systemic oxygen delivery linked to local hyperoxia (**Supplementary Table 2**).

Effect of Local Hypercapnia and Hyperoxia During Hemorrhagic Conditions

Gastric Microcirculation

Hemorrhagic shock led to a pronounced decrease in gastric μHbO_2 in the normocapnic control group from 77 ± 2 to 38 ± 4% (**Figure 3A**) and in the normoxic control group from 77 ± 2 to 45 ± 7% (**Figure 4A**). Local hypercapnia, but not hyperoxia ameliorated the shock-induced decrease in gastric μHbO_2 and led to a reduction from 83 ± 3 to 52 ± 8% in the early course of shock. Gastric insufflation of oxygen did not affect regional microcirculatory oxygenation under hypovolemic conditions. Microvascular perfusion was not altered in animals receiving hyperoxia or hypercapnia compared to their respective control group during hemorrhage (**Table 1** and **Supplementary Table 1**). After resuscitation, μHbO_2 baseline values were reached in all groups.

Oral Microcirculation

Similar to the gastric microcirculation, the induction of a hemorrhagic shock led to a significant reduction in oral μHbO_2 in the normocapnic control group from 82 ± 2 to 36 ± 4% (**Figure 3B**) and in the normoxic control group from 86 ± 2 to 46 ± 6% (**Figure 4B**). The decrease in oral μHbO_2 was diminished to 54 ± 4% in the hypercapnic group. This effect continued over the 60 min shock period. Mucosal hyperoxia had no effect on oral microcirculatory oxygenation.

Absolute μflow measured by laser Doppler and the perfused vessel density evaluated by videomicroscopy did not differ between the interventional and the control groups, there was a profound difference in the predominant microvascular flow profiles in hemorrhagic animals under hypercapnic conditions (**Figure 5**): The microvascular flow index decreased in the normocapnic control group from 2.8 ± 0.1 to 0.8 ± 0.2. Local hypercapnia ameliorated the decrease from 2.9 ± 0.1 to 1.3 ± 0. Due to reasons of imaging quality, IDF-recording of one dog receiving hypercapnia under otherwise physiological conditions had to be excluded from the analysis in accordance with common recommendations on the assessment of sublingual microcirculation (36). Therefore, microvascular flow index is reported for $n = 5$ in the experimental setup investigating effects of local CO_2. Animals that received oxygen supply did not show comparable changes in a hemorrhagic state.

Heterogeneity index increased from 0.3 ± 0.1 to 2.8 ± 0.5 in normocapnic individuals and from 0.4 ± 0 to 1.6 ± 0.3 in normoxic animals when hemorrhage was induced. Neither CO_2- (2.5 ± 0.7) nor O_2-application (1.1 ± 0.3) could significantly diminish spatial flow heterogeneity during early hemorrhage. Despite, in the late course of shock heterogeneity index was

TABLE 1 | Microcirculatory variables in normo- (NC) and hypercapnic (HC) animals during physiological (-N) or hemorrhagic (-H) conditions.

Variables	Group	00:30 h				01:00 h				01.30 h				02:00 h				02:30 h				03:00 h				03:30 h			
Gastric μHbO_2 (%)	NC-N	83	±	4		84	±	3		79	±	3		76	±	3		73	±	3		79	±	5		78	±	6	
	HC-N	77	±	2		77	±	1		80	±	4		78	±	4		76	±	3		77	±	3		79	±	2	
	NC-H	77	±	2		79	±	2		79	±	3		38	±	4	#	52	±	6	#	75	±	6		80	±	3	
	HC-H	83	±	3		83	±	2		85	±	2		52	±	8	#,*	57	±	8	#	81	±	4		82	±	3	
Gastric μflow (aU)	NC-N	153	±	10		268	±	38	#	260	±	26	#	245	±	31	#	266	±	42	#	264	±	22	#	237	±	35	
	HC-N	198	±	31		176	±	29	*	223	±	32		233	±	33		204	±	25		239	±	18		250	±	38	
	NC-H	145	±	17		172	±	19		177	±	24		171	±	19		160	±	22		185	±	30		212	±	31	
	HC-H	177	±	22		180	±	27		252	±	38		229	±	40		262	±	74	*	239	±	46		216	±	35	
Oral μHbO_2 (%)	NC-N	85	±	3		83	±	3		84	±	2		81	±	1		83	±	2		83	±	2		83	±	2	
	HC-N	82	±	2		82	±	2		83	±	2		84	±	2		81	±	1		79	±	2		86	±	2	
	NC-H	82	±	2		79	±	2		82	±	1		36	±	4	#	45	±	5	#	78	±	6		93	±	2	#
	HC-H	83	±	2		81	±	3		86	±	3		54	±	4	#,*	63	±	5	#,*	79	±	4		90	±	2	
Oral μflow (aU)	NC-N	143	±	24		163	±	35		117	±	9		144	±	34		131	±	15		137	±	20		129	±	27	
	HC-N	128	±	14		121	±	13		168	±	31		185	±	27		146	±	35		162	±	31		143	±	21	#
	NC-H	94	±	18		121	±	36		110	±	26	*	50	±	17		38	±	9		109	±	18		191	±	29	
	HC-H	126	±	21		132	±	31		195	±	38		58	±	16		80	±	18		163	±	41		179	±	28	
MFI	NC-N	3	±	0		2.8	±	0.1		2.9	±	0.1		2.9	±	0		2.9	±	0.1		2.9	±	0.1		2.9	±	0.1	
	HC-N	3	±	0.7		2.9	±	1.1		2.9	±	1.4		2.9	±	1.4		2.9	±	1.5		2.7	±	2		2.8	±	1.9	
	NC-H	2.8	±	0.1		2.9	±	0		2.9	±	0.1		0.8	±	0.2	#,*	1.4	±	0.2	#,*	2.8	±	0.2		3	±	0	
	HC-H	2.9	±	0.1		2.9	±	0.1		2.9	±	0.1		1.3	±	0	#	2	±	0.3	#	2.7	±	0.1		2.9	±	0.1	
HGI	NC-N	0.7	±	0.1		1.6	±	0.1		1.1	±	0.1		1.4	±	0.1	#	1.1	±	0.1		1.1	±	0.1		0.4	±	0.1	
	HC-N	0.7	±	0.1		1.1	±	0.1		1.4	±	0.1		1.4	±	0.1		1.5	±	0.2		2	±	0.2		1.9	±	0.2	
	NC-H	1.5	±	0.1		1.4	±	0.1		1.4	±	0.1		16.7	±	0.5	#	11.6	±	0.3	#	3.1	±	0.3		0.4	±	0.1	
	HC-H	1.1	±	0.1		1.4	±	0.1		1.4	±	0.1		14.1	±	0.3	#	6.7	±	0.2	#,*	2.3	±	0.1		1.1	±	0.1	
TVD (mm/mm^2)	NC-N	19	±	0		19	±	1		19	±	1		19	±	1		20	±	1		19	±	0		19	±	1	
	HC-N	19	±	1		19	±	0.5		19	±	1		19	±	1		18	±	1		18	±	0		18	±	0	
	NC-H	18	±	0		19	±	0.9		19	±	1		14	±	2	#	15	±	1	#	19	±	1		21	±	1	#
	HC-H	19	±	0		18	±	0.7		19	±	1		14	±	1	#	16	±	1	#	18	±	1		19	±	1	
PVD (mm/mm^2)	NC-N	11	±	1		10	±	1.8		11	±	1		11	±	1		11	±	1		10	±	2		9	±	2	
	HC-N	13	±	1		12	±	1.1		12	±	1		12	±	1		11	±	1		9	±	1	#	10	±	0	
	NC-H	10	±	1		11	±	1.4		11	±	1		3	±	1	#	4	±	1	#	11	±	1		13	±	1	#
	HC-H	12	±	1		9	±	0.9		12	±	1		5	±	1	#	6	±	1	#	9	±	1		11	±	1	

*Microvascular oxygenation (μHbO_2) in percentage (%) and microvascular flow (μflow) in arbitrary units (aU) were measured at the gastric and oral surface using reflectance spectrophotometry and laser Doppler flowmetry. Microvascular flow index (MFI), heterogeneity index (HGI), total vessel density (TVD) in (mm/mm^2) and PVD in (mm/mm^2) were evaluated by incident dark field imagine. One hour of acute hemorrhage is marked gray. Data are presented as mean ± SEM for n = 6 dogs (MFI and HGI n = 5). #p < 0.05 vs. baseline, *p < 0.05 vs. normoxic control group. 2-way ANOVA for repeated measurements followed by Bonferroni post-hoc test.*

higher in the normocapnic animals (1.9 ± 0.3) than in the hypercapnic animals (1.1 ± 0.2). In normocapnic animals total vessel density and perfused vessel density decreased when hemorrhage was induced (**Table 1**). Local hyperoxia had no effect on the changes of the structural microcirculation during hemorrhagic shock (**Supplementary Table 1**).

Intestinal Barrier Function

Plasma levels of sucrose increased in normocapnic animals from 1 ± 0.4 pmol/μl to 1.8 ± 1.3 pmol/μl and in hypercapnic animals from 0.2 ± 0.1 pmol/μl to 1.8 ± 1.1 pmol/μl during hemorrhage without any statistically significant difference between the two interventional groups. Moreover, sucrose concentration increased in normoxic and hyperoxic experiments independent of hemodynamic conditions. All experimental groups showed a wide range of inter-individual variability (**Supplementary Table 3**).

Global Hemodynamics and Ventilation

DO_2 decreased during hemorrhage in all groups irrespective of the intervention (**Table 2** and **Supplementary Table 2**). The decrease of DO_2 was based on a similar decrease in cardiac output. After retransfusion of shed blood, DO_2 was restored to baseline values in all experimental groups. Similar changes occurred in cardiac output and mean arterial blood pressure. Neither local CO_2- nor O_2-insufflation affected systemic hemodynamic parameters and did not modulate oxygen delivery or oxygen content of arterial blood (P_aO_2).

The arterial carbon dioxide concentration increased during shock paralleled by decreased pH-values without any effect of local gas application. The respiratory frequency was adjusted to maintain an endtidal carbon dioxide concentration of 35 mmHg. Local gas application had no effect on respiratory rate. Further, mucosal application of CO_2 and O_2 had no effect on systemic metabolic variables during hemorrhage. Base excess

TABLE 2 | Macrocirculatory variables and blood gas analysis in normo- (NC) and hypercapnic (HC) animals during physiological (-N) or hemorrhagic (-H) conditions.

Variables	Group	00:30 h			01:00 h				01.30 h				02:00 h				02:30 h				03:00 h				03:30 h			
DO_2 (ml/kg/min)	NC-N	16	±	1	16	±	1		16	±	1		16	±	1		16	±	1		16	±	1		16	±	1	
	HC-N	15	±	1	14	±	0	*	14	±	0	*	14	±	0	*	14	±	0	*	14	±	1	*	14	±	1	*
	NC-H	14	±	1	14	±	1		14	±	1		7	±	1	#	8	±	1	#	14	±	1		15	±	1	
	HC-H	15	±	0	14	±	0		14	±	1		7	±	1	#	8	±	1	#	14	±	1		15	±	1	
CO (ml/kg/min)	NC-N	99	±	7	95	±	8		94	±	7		95	±	6		95	±	7		96	±	5		94	±	6	
	HC-N	88	±	2	85	±	2	*	85	±	2	*	82	±	2	*	84	±	2	*	8	±	3	*	82	±	2	*
	NC-H	87	±	4	83	±	4		82	±	4		45	±	3	#	51	±	3	#	87	±	4		92	±	5	
	HC-H	87	±	1	85	±	2		81	±	2		43	±	4	#	51	±	5	#	86	±	3		89	±	5	
MAP (mmHg)	NC-N	64	±	2	67	±	3		69	±	3		69	±	3		69	±	3		69	±	3		69	±	3	
	HC-N	61	±	2	66	±	3		68	±	3		67	±	3	#	70	±	4	#	70	±	4	#	70	±	3	#
	NC-H	65	±	2	69	±	4		68	±	3	#	50	±	3		56	±	2	#	87	±	3	#	76	±	5	#
	HC-H	65	±	1	66	±	2		69	±	2		50	±	2	#	57	±	1	#	85	±	4	#	72	±	6	#
pH	NC-N	7.39	±	0.01	7.38	±	0.01		7.37	±	0.01	#	7.36	±	0.01	#	7.36	±	0.01	#	7.36	±	0.01	#	7.35	±	0.0	#
	HC-N	7.39	±	0.01	7.38	±	0.01		7.38	±	0.01		7.38	±	0.01	*	7.37	±	0.01	#	7.37	±	0.01	#	7.38	±	0.0	*
	NC-H	7.4	±	0.01	7.39	±	0.01		7.39	±	0.01		7.32	±	0.01	#	7.33	±	0.01	#	7.37	±	0.01	#	7.37	±	0.0	#
	HC-H	7.4	±	0.01	7.39	±	0.01		7.39	±	0.01	#	7.33	±	0.01	#	7.32	±	0.01	#	7.37	±	0.01	#	7.37	±	0.0	#
p_aCO_2 (mmHg)	NC-N	34	±	0	35	±	0		35	±	1		36	±	0	#	36	±	1	#	37	±	1	#	36	±	1	#
	HC-N	36	±	1	36	±	0		36	±	0		37	±	0		37	±	1	#	37	±	1	#	36	±	1	
	NC-H	35	±	1	36	±	1		36	±	1		40	±	1	#	40	±	1	#	36	±	1		37	±	1	
	HC-H	35	±	1	36	±	1		36	±	1		40	±	1	#	41	±	1	#	37	±	1	#	36	±	1	#
BE (mmol/l)	NC-N	−3.7	±	0.34	−3.9	±	0.26		−4.1	±	0.3		-4.6	±	0.37	#	-4.8	±	0.51	#	−4.6	±	0.52	#	−4.8	±	0.45	#
	HC-N	−3.1	±	0.23	−3.2	±	0.17		−3.2	±	0.2	*	-3.2	±	0.32	*	-3.4	±	0.34	*	−3.5	±	0.39	*	−3.6	±	0.44	*
	NC-H	−2.8	±	0.14	−3	±	0.12		−3.2	±	0.12		-4.7	±	0.24	#	-4.6	±	0.25	#	−3.7	±	0.22	#	−3.6	±	0.25	#
	HC-H	−2.7	±	0.33	−2.9	±	0.22		−3.3	±	0.21		-4.9	±	0.19	#	-4.7	±	0.17	#	−3.9	±	0.21	#	−4	±	0.12	#
Lactate (mmol/l)	NC-N	1.1	±	0.2	1.3	±	0.2		1.6	±	0.2		2	±	0.3	#	2.3	±	0.4	#	2.2	±	0.4	#	2.3	±	0.4	#
	HC-N	1.1	±	0.1	1.2	±	0.2		1.2	±	0.1		1.2	±	0.1		1.3	±	0.1		1.3	±	0.1		1.4	±	0.1	
	NC-H	0.9	±	0.1	1.1	±	0.1		1.2	±	0.1		1.3	±	0.1		1.3	±	0.1		1.2	±	0.1		1.2	±	0.1	
	HC-H	0.9	±	0.2	1.1	±	0.2		1.4	±	0.2		1.6	±	0.2	#	1.5	±	0.2	#	1.5	±	0.3		1.6	±	0.3	#
Resp. rate (1/min)	NC-N	15	±	2	15	±	2		15	±	2		16	±	2		17	±	2		17	±	2	#	17	±	2	
	HC-N	14	±	1	14	±	1		15	±	1		15	±	1	*	16	±	1	*	16	±	2	#,*	16	±	1	#,*
	NC-H	14	±	1	14	±	1		15	±	1		13	±	1		15	±	1		17	±	1	#	18	±	2	#
	HC-H	15	±	1	14	±	1		16	±	1		14	±	1		15	±	1		18	±	2	#	18	±	1	#
p_aO_2 (mmHg)	NC-N	153	±	2	152	±	2		155	±	4		155	±	4		155	±	3		153	±	3		161	±	4	
	HC-N	151	±	5	152	±	2		153	±	1		156	±	2		156	±	2		154	±	3		160	±	2	#
	NC-H	149	±	3	156	±	5		162	±	3	#	142	±	2		150	±	4		164	±	2	#	156	±	44	*
	HC-H	153	±	5	154	±	4		159	±	3		147	±	3		149	±	2		167	±	3	#	166	±	2	#

Systemic oxygen delivery (DO_2) in (ml/kg/min), cardiac output (CO) in (ml/kg/min), mean arterial pressure (MAP) in (mmHg), ph-values, arterial carbon dioxide pressure (p_aCO_2) in (mmHg), base excess (BE) in (mmol/l), lactate concentration in (mmol/l) and arterial oxygen pressure (p_aO_2) in (mmHg). One hour of acute hemorrhage is marked gray. Data are presented as mean ± SEM for n = 6 dogs. $^{\#}p < 0.05$ vs. baseline, $^{*}p < 0.05$ vs. normocapnic control group. 2-way ANOVA for repeated measurements followed by Bonferroni post-hoc test.

and pH were equally reduced and p_aCO_2 was increased in all groups. During hemorrhagic shock, no clinically relevant alterations in lactate plasma levels were observed (**Table 1** and **Supplementary Table 1**).

DISCUSSION

The aim of our study was to analyze the effect of a local O_2- and CO_2-application on regional microcirculation and systemic hemodynamic variables during physiologic conditions and during a mild hemorrhagic shock. Whether our results can be transferred to more severe shock conditions remains unclear and has to be addressed in further studies due to the minimal invasive experimental setting. Likewise, additional invasive measurements were prohibited in this reversible shock model. However, the shock was able to induce micro- and macrocirculatory impairment and can be declared to be reversible since retransfusion of the shed blood was able to re-establish baseline values in the course of experiments. The main findings are:

1) Local CO_2 but not O_2 increases oral and gastric microvascular oxygenation during a mild hemorrhagic shock.

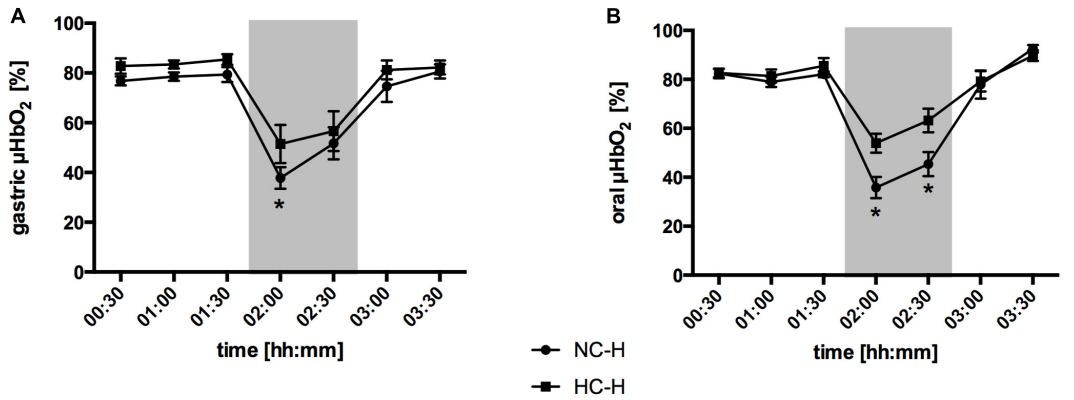

FIGURE 3 | Effect of local carbon dioxide application on microvascular oxygenation: Microvascular oxygenation (μHbO_2) in percentage (%) at the gastric **(A)** and oral **(B)** mucosa under hemorrhagic conditions. The animals received a continuous gas application with either N_2 to maintain local normocapnia (NC-H) or CO_2 for local hypercapnia (HC-H) followed by hemorrhage and retransfusion. One hour of acute hemorrhage is marked gray. Data are presented as mean ± SEM for $n = 6$ dogs; $^*p < 0.05$ vs. control group (NC-H), 2-way ANOVA for repeated measurements followed by the Bonferroni *post-hoc* test.

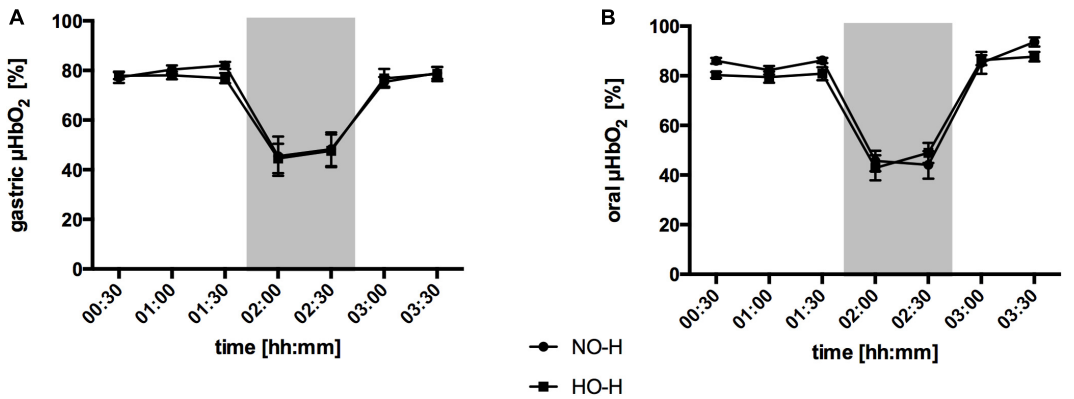

FIGURE 4 | Effect of local oxygen application on microvascular oxygenation: Microvascular oxygenation (μHbO_2) in percentage (%) at the gastric **(A)** and oral **(B)** mucosa. The animals received a continuous gas application with either N_2 to maintain local normoxia (NO-H) or O_2 for local hyperoxia (HO-H) followed by hemorrhage and retransfusion. One hour of acute hemorrhage is marked grey. Data are presented as mean SEM for $n = 6$ dogs.

2) Increases of oral microvascular oxygenation in hypercapnic individuals are associated with changes in microcirculatory flow characteristics without changing total microvascular blood flow.
3) Local O_2- and CO_2-application do not exert effects on micro- and macrocirculatory parameters under physiological conditions.

Molecular oxygen and carbon dioxide dominate the two different sites of cellular respiration and energy metabolism. O_2 is crucial to enable aerobic phosphorylation, whereas CO_2 is one main product after energy generation in the mitochondria. CO_2 needs an adequate tissue perfusion to be eliminated from the microcirculation, therefore local carbon dioxide pressure and pCO_2-gap are able to detect states of severe tissue hypoperfusion. Since a sufficient tissue oxygenation depends on an adequate tissue perfusion, local carbon dioxide pressure and pCO_2-gap may be indirect parameters of tissue oxygenation as well (37). Consequently, the ratio of veno-arterial pCO_2-gradient to the difference in arterio-venous O_2-content is reported to detect hypoxic states in critically ill patients (38, 39).

The intent to examine both gases as potential therapeutic options in experimental hemorrhagic shock is based on distinct observations. On the one hand, identifying severe hemorrhage as a state of compromised oxygen delivery leads physicians to perform a bundle of therapeutic interventions including blood and fluid replacement, vasopressor application, and an increase of inspiratory oxygen fraction to obtain total oxygen content. On the other hand, the generation of reactive oxygen species may further harm the injured tissue (40). In our experiments the additional application of local oxygen was not able to improve microvascular oxygenation. Since hyperoxia is reported to induce precapillary vasoconstriction (7), one may conclude that hyperoxic vasoconstriction might counteract the improvement of microvascular oxygenation through an increase of arterial oxygen concentration. Nevertheless, neither total microvascular flow assessed by laser flowmetry, nor microvascular flow characteristics were altered by local oxygen

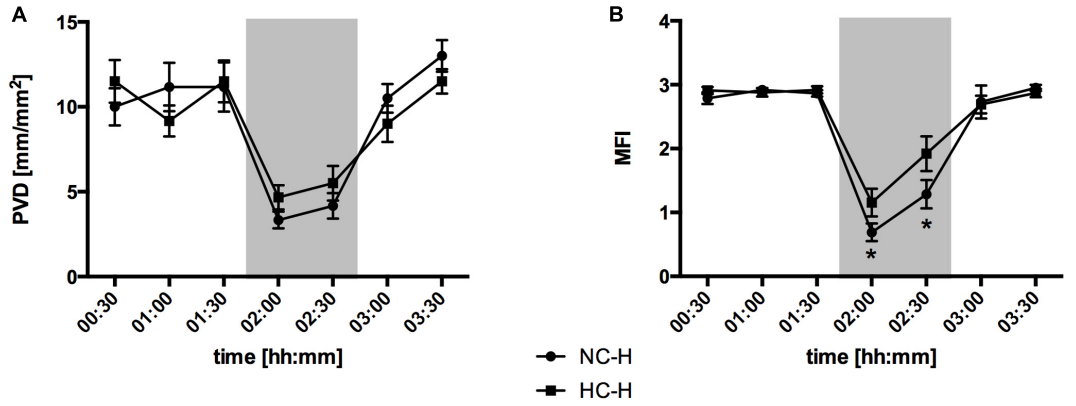

FIGURE 5 | Effect of local carbon dioxide application on microvascular perfusion variables: Perfused vessel density (PVD) in (mm/mm^2) **(A)** and Microvascular flow index (MFI) **(B)** at oral mucosa under hemorrhagic conditions. The animals received a continuous gas application with either N_2 to maintain local normocapnia (NC-H) or CO_2 for local hypercapnia (HC-H) followed by hemorrhage and retransfusion. One hour of acute hemorrhage is marked gray. Data are presented as mean SEM for $n = 6$ dogs; $^*p < 0.05$ vs. control group (NC-H), 2-way ANOVA for repeated measurements followed by the Bonferroni *post-hoc* test.

application. Further, structural microcirculation evaluated by IDF-imaging did not differ between hyperoxic and normoxic individuals. With no changes in total blood flow and structural microcirculation the question arises why hyperoxia does not lead to an increase of microcirculatory oxygenation. One aspect we cannot derive from microcirculatory measurements is the mitochondrial oxygen utilization. Oxygen utilization and mitochondrial efficiency are of large interest since oxidative respiration is acknowledged as the final goal of therapeutic interventions to optimize oxygen delivery in critical illness (41). In pulmonary endothelial cells hyperoxia reduces respiratory capacity at 12 h and basal respiration after 48 h (42). Moreover, the metabolic profile is changed with alternative energy sources and an inhibition of the tricarboxylic acid cycle under hyperoxia (43). Finally, hyperoxia is associated with morphological damage and promotes mitochondrial fragmentation (44). In conclusion, there is strong evidence, that hyperoxia exerts direct effects on cell metabolism, energy generation, and structural integrity. However, we focused on microcirculatory changes in hemorrhagic shock states and could not show any beneficial or detrimental effect of local hyperoxia on microvascular parameters. Due to the minimal-invasive setup and the intent to avoid surgical trauma to preserve a mostly physiological microcirculation we were not able to measure local oxygen partial pressure for example by Clark like electrodes. While oxygen is able to cross epithelial borders, the gastric mucus layer may be an obstacle that could hamper gastric tissue protection by local oxygen application. In our experiments neither the gastric nor the oral oxygenation, where no mucus exists to impair transepithelial oxygen transport, improved after oxygen application. We conclude that local oxygen application fails to improve gastrointestinal oxygenation independently of any limitation by biological borders like gastric mucus.

In the second set of experiments, we investigated the impact of local CO_2-application on gastrointestinal microcirculation and oxygenation. According to our previous results with systemic hypercapnia (11, 45) we could show that also locally applied CO_2 significantly improves microvascular oxygenation at the oral and the gastric surface. Since microvascular oxygenation represents predominantly postcapillary oxygen saturation, an increase in microvascular oxygenation may be paralleled by a higher local oxygen reserve (23). Avoiding hypoxic states in the course of hemorrhage could preserve intestinal integrity and impede the development of multi organ failure and systemic inflammatory states. We were not able to show that an increase of microvascular oxygenation preserves intestinal barrier function assessed by plasmatic sucrose concentration after gastric application. During the experiments we could observe a gastroesophageal reflux that led to a wide range of inter-individual variability. Additionally, sucrose itself may contribute to an increase of intestinal permeability due to its high osmolarity (46). Therefore, results from our measurements of intestinal permeability have to be considered with care.

Higher values of postcapillary oxygen saturation can be a result of an increase in local oxygen supply due to precapillary vasodilatation, lower oxygen liberalization from hemoglobin molecules, an increase of oxygen diffusion distance as a result of microvascular shunting and finally differences of mitochondrial energy metabolism.

CO_2 is reported to have vasodilatory properties through K^+_{ATP}-channels in coronary vessels (47), which might improve microvascular oxygen delivery through an increase in microvascular perfusion. However, Beck et al. could show that beneficial effects of acute hypercapnia on microcirculatory oxygenation are independent of K^+_{ATP}-channels in sepsis. Further, total microvascular blood flow did not change in our experiments when local hypercapnia was applied (10). The second crucial step of microvascular oxygen delivery is oxygen liberalization from hemoglobin molecules and the diffusion toward mitochondria. Hypercapnia and hypercapnic acidosis led to a right-shift of hemoglobin dissociation curve and a simplified oxygen liberalization. Therefore, oxygen liberalization is not expected to be hampered by local CO_2-application. We did not observe a reduction of functional capillary density in hypercapnic animals as a sign of microvascular shunting and

an increase in microvascular diffusion distance. Hampered oxygen liberalization as well as microvascular shunting led to an increased postcapillary oxygenation accompanied by cellular hypoxia and lactate generation. In the same manner, dysfunctional oxygen utilization in the mitochondria with an anaerobic energy metabolism is associated with a corresponding increase in lactate levels (48). Finally, there were no difference in lactate plasma levels between hypercapnic and normocapnic individuals undergoing hemorrhage. If cell metabolism is altered, especially a reduction of basal energy metabolism or an increase in mitochondrial effectivity without cellular hypoxia and mitochondrial failure would be compatible with our results. Direct effects of carbon dioxide on cell respiration and integrity were described in an experimental setting before (49, 50).

Like mentioned above, this study was not designed to describe mitochondrial function but functional and structural microcirculation. Microvascular oxygenation was paralleled by changes in microvascular flow characteristics at the oral surface. We could observe a more continuous microvascular blood flow under hypercapnia in hemorrhagic shock states represented by higher values of microvascular flow index (MFI). In a septic patient collective microcirculatory alterations were associated with high mortality (51–54), with the proportion of perfused vessel and microvascular flow index being the strongest predictors for a worse outcome (53, 54). Especially a compromised MFI was identified to be an independent predictor of mortality in a general ICU population (28, 29). Our results may implicate, that local hypercapnia is able to ameliorate microvascular oxygenation through a continuous blood flow within the microcirculation without any impact on total microvascular blood flow.

Hypercapnia is known to increase plasmatic vasopressin levels (55, 56). Further, hypercapnia as well as low-doses vasopressin are able to improve microvascular oxygenation under physiological conditions (45, 57). Those findings can be transferred into animals undergoing sepsis (58, 59). Whereas systemic hypercapnia is known to improve tissue oxygenation under adverse conditions like hemorrhage (11) and sepsis (9), the role of vasopressin in resuscitation bundles remain unclear. This study is pointing toward the participation of carbon dioxide in regional blood flow distribution. If this effect depends on local vasopressin release and signal transmission via vasopressin receptors has to be clarified. The V_{1A}-receptor is reported to mediate a dose-dependent effect on gastric microcirculation under physiological conditions (57) and stabilizes intestinal oxygenation during hypercapnia in septic (60) and hemorrhagic (61) animals. If the protection of gastric and oral oxygenation by local hypercapnia is mediated by a V_{1A}-receptor dependent increase in flow homogeneity and related to and improved mitochondrial respiration has to be evaluated in further studies.

Systemic side effects occur under systemic hypercapnia and could limit therapeutic approaches (62). For example, acute hemorrhage occurs in patients undergoing polytrauma, a collective that frequently suffers traumatic head injury (63). A hypercapnic precapillary vasodilation could increase intracerebral pressure (64) and proceed further neurological injury. Besides, low pH-values are leading to an insufficient hemostasis (65), which could be detrimental in the context of acute hemorrhage and major surgery with a high need for sufficient bleeding control. Beneficial effects of local hypercapnia were independent from systemic oxygen delivery, blood gases and pH-value in our experiments. Thus, local gas applications might provide safe options in the treatment of critically ill patients without any impact on systemic parameters.

One may assume, that local gas insufflation is an unsuitable therapeutic approach, due to the large intestinal surface and the corresponding gas volume needed to establish a gaseous atmosphere for all over intestinal protection. Therefore, the investigation of receptor related CO_2-effects could be the next step and a cornerstone in the development of pharmacological tissue protection during acute hemorrhage. A direct interaction of carbon dioxide and vasopressin is described in different shock models and has to be further investigated (60, 61). Beyond the treatment of injured patients, small intestinal anastomosis dehiscence is a frequent complication after abdominal surgery (66) with the need for consecutive operations. Local CO_2, when applicated endoscopically, could improve regional microcirculation, and oxygenation in intention to avoid anastomosis dehiscence. A beneficial effect of local carbon dioxide on wound healing is described in a wide context (67).

Microcirculatory alterations in critical illness are described to correlate within the vascular beds of the gastrointestinal tract when tonometry (68) or videomicroscopy (69) is used. However, our experiments showed a prolonged protective effect of local CO_2-application on oral oxygenation compared to gastric measurements, which might be an effect of a variable density of receptors providing vasoconstriction. Schwartges et al. reported a concentration-dependent increase in gastric μHbO_2 under systemic hypercapnia in normovolemic dogs (45). Despite, μHbO_2 was not altered by local CO_2-supply under physiological conditions, whereas the same amount CO_2 was able to improve μHbO_2 under hemorrhagic conditions in our experiments. Probably, the effect of local hypercapnia on mucosal microcirculation depends on the hemodynamic conditions.

CONCLUSION

Hypercapnia is reported to exert beneficial effects on intestinal microcirculation. Since systemic side effects may limit therapeutic approaches in patients with multiple comorbidities, local therapeutic regimes could be used to enable the clinical transfer of therapeutic hypercapnia into a critically ill patient collective. We could demonstrate that local carbon dioxide application is able to improve gastric and oral postcapillary oxygen saturation during a mild hemorrhagic shock. This effect might be mediated by improved microvascular flow under local carbon dioxide application. This may implicate an increase of local oxygen reserve. The redistribution of available oxygen carriers leading to continuous blood flow profiles at the mucosal surfaces seems to be more important than total blood flow within the microcirculation. While local carbon dioxide application

improved parameters of microcirculatory oxygen delivery without any effect on systemic hemodynamic variables and blood acidity, local oxygen supply did not influence postcapillary oxygen saturation, flow heterogeneity and systemic parameters. From these results we can conclude that local gas application is feasible without any systemic side effects in the chosen experimental model and might probably be applied safely, even when adverse conditions occur in critically ill patients.

DATA AVAILABILITY STATEMENT

The datasets presented in this study can be found in online repositories. The names of the repository/repositories and accession number(s) can be found in the article/ **Supplementary Material**.

ETHICS STATEMENT

The animal study was reviewed and approved by the local Animal Care and Use Committee (North Rhine-Westphalia State Agency for Nature, Environment and Consumer Protection, Recklinghausen, Germany).

AUTHOR CONTRIBUTIONS

SH: acquisition of data, analysis and interpretation of data, and drafting the article. RT: conception and design, acquisition of data, analysis and interpretation of data, and drafting the article. LW: acquisition of data, analysis and interpretation of data, and revising the article. AH and JS: analysis and interpretation of data, and revising the article. AW, IB, OP, and CV: conception and design, analysis and interpretation of data, and revising the article. EM: conception and design, acquisition of data, analysis and interpretation of data, and revising the article. All authors read and approved the final manuscript.

FUNDING

This work was supported by the departmental funds and by a grant of the Strategic Research Fund, Heinrich-Heine-University (No. 1,229) to CV.

SUPPLEMENTARY MATERIAL

The Supplementary Material for this article can be found online at: https://www.frontiersin.org/articles/10.3389/fmed.2022.867298/full#supplementary-material

REFERENCES

1. Ghadimi K, Levy JH, Welsby IJ. Perioperative management of the bleeding patient. *BJA Br J Anaesthesia.* (2016) 117(Suppl. 3):iii18–30. doi: 10.1093/bja/aew358
2. Cannon JW. Hemorrhagic shock. *New Engl J Med.* (2018) 378:370–9.
3. Lansink KWW, Gunning AC, Leenen LPH. Cause of death and time of death distribution of trauma patients in a Level I trauma centre in the Netherlands. *Eur J Trauma Emerg Surg.* (2013) 39:375–83. doi: 10.1007/s00068-013-0278-2
4. Brattström O, Granath F, Rossi P, Oldner A. Early predictors of morbidity and mortality in trauma patients treated in the intensive care unit. *Acta Anaesthesiol Scand.* (2010) 54:1007–17. doi: 10.1111/j.1399-6576.2010.02266.x
5. Tisherman SA, Schmicker RH, Brasel KJ, Bulger EM, Kerby JD, Minei JP, et al. Detailed description of all deaths in both the shock and traumatic brain injury hypertonic saline trials of the resuscitation outcomes consortium. *Ann Surg.* (2015) 261:586–90. doi: 10.1097/SLA.0000000000000837
6. Eltzschig HK, Eckle T. Ischemia and reperfusion–from mechanism to translation. *Nat Med.* (2011) 17:1391–401. doi: 10.1038/nm.2507
7. Damiani E, Donati A, Girardis M. Oxygen in the critically ill: friend or foe? *Curr Opin Anaesthesiol.* (2018) 31:129–35. doi: 10.1097/ACO.0000000000000559
8. Brugniaux JV, Coombs GB, Barak OF, Dujic Z, Sekhon MS, Ainslie PN. Highs and lows of hyperoxia: physiological, performance, and clinical aspects. *Am J Physiol Regul Integr Comp Physiol.* (2018) 315:R1–27. doi: 10.1152/ajpregu.00165.2017
9. Wang Z, Su F, Bruhn A, Yang X, Vincent J-L. Acute hypercapnia improves indices of tissue oxygenation more than dobutamine in septic shock. *Am J Respir Crit Care Med.* (2008) 177:178–83. doi: 10.1164/rccm.200706-906OC
10. Beck C, Barthel F, Hahn A-M, Vollmer C, Herminghaus A, Schäfer S, et al. The beneficial effects of acute hypercapnia on microcirculatory oxygenation in an animal model of sepsis are independent of K+ATP channels. *Microvasc Res.* (2015) 99:78–85. doi: 10.1016/j.mvr.2015.02.009
11. Schwartges I, Picker O, Beck C, Scheeren TWL, Schwarte LA. Hypercapnic acidosis preserves gastric mucosal microvascular oxygen saturation in a canine model of hemorrhage. *Shock.* (2010) 34:636–42. doi: 10.1097/SHK.0b013e3181e68422
12. Coakley RJ, Taggart C, Greene C, McElvaney NG, O'Neill SJ. Ambient pCO2 modulates intracellular pH, intracellular oxidant generation, and interleukin-8 secretion in human neutrophils. *J Leukoc Biol.* (2002) 71:603–10.
13. Curley G, Laffey JG, Kavanagh BP. Bench-to-bedside review: carbon dioxide. *Crit Care.* (2010) 14:220. doi: 10.1186/cc8926
14. Olschewski H, Simonneau G, Galiè N, Higenbottam T, Naeije R, Rubin LJ, et al. Inhaled iloprost for severe pulmonary hypertension. *N Engl J Med.* (2002) 347:322–9.
15. Deitch EA. Gut-origin sepsis: evolution of a concept. *Surgeon.* (2012) 10:350–6. doi: 10.1016/j.surge.2012.03.003
16. Schörghuber M, Fruhwald S. Effects of enteral nutrition on gastrointestinal function in patients who are critically ill. *Lancet Gastroenterol Hepatol.* (2018) 3:281–7. doi: 10.1016/S2468-1253(18)30036-0
17. Truse R, Hinterberg J, Schulz J, Herminghaus A, Weber A, Mettler-Altmann T, et al. Effect of topical iloprost and nitroglycerin on gastric microcirculation and barrier function during hemorrhagic shock in dogs. *J Vasc Res.* (2017) 54:109–21. doi: 10.1159/000464262
18. Truse R, Nolten I, Schulz J, Herminghaus A, Holtmanns T, Gördes L, et al. Topical melatonin improves gastric microcirculatory oxygenation during hemorrhagic shock in dogs but does not alter barrier integrity of Caco-2 monolayers. *Front Med (Lausanne).* (2020) 7:510. doi: 10.3389/fmed.2020.00510
19. Truse R, Voß F, Herminghaus A, Schulz J, Weber APM, Mettler-Altmann T, et al. Local gastric RAAS inhibition improves gastric microvascular perfusion in dogs. *J Endocrinol.* (2019) 241:235–47. doi: 10.1530/JOE-19-0030
20. Knöller E, Stenzel T, Broeskamp F, Hornung R, Scheuerle A, McCook O, et al. Effects of hyperoxia and mild therapeutic hypothermia during resuscitation from porcine hemorrhagic shock. *Crit Care Med.* (2016) 44:e264–77. doi: 10.1097/CCM.0000000000001412
21. Dyson DH. Positive pressure ventilation during anesthesia in dogs: assessment of surface area derived tidal volume. *Can Vet J.* (2012) 53:63–6.

22. van Leersum EC. Eine Methode zur Erleichterung der Blutdruckmessung bei Tieren. *Pflüger's Arch.* (1911) 142:377–95. doi: 10.1007/bf01849124
23. Krug A. Mikrozirkulation und Sauerstoff-versorgung des Gewebes, Methode des so genannten O2C (oxygen to see). *Phlebologie.* (2007) 36:300–12. doi: 10.1055/s-0037-1622158
24. Gandjbakhche AH, Bonner RF, Arai AE, Balaban RS. Visible-light photon migration through myocardium in vivo. *Am J Physiol-Heart Circulatory Physiol.* (1999) 277:H698–704. doi: 10.1152/ajpheart.1999.277.2.H698
25. Sato N, Kawano S, Kamada T, Takeda M. Hemodynamics of the gastric mucosa and gastric ulceration in rats and in patients with gastric ulcer. *Dig Dis Sci.* (1986) 31(Suppl. 2):35S–41S. doi: 10.1007/BF01309321
26. Aykut G, Veenstra G, Scorcella C, Ince C, Boerma C. Cytocam-IDF (incident dark field illumination) imaging for bedside monitoring of the microcirculation. *Intensive Care Med Exp.* (2015) 3:4. doi: 10.1186/s40635-015-0040-7
27. De Backer D, Hollenberg S, Boerma C, Goedhart P, Büchele G, Ospina-Tascon G, et al. How to evaluate the microcirculation: report of a round table conference. *Crit Care.* (2007) 11:R101. doi: 10.1186/cc6118
28. Vellinga NAR, Boerma EC, Koopmans M, Donati A, Dubin A, Shapiro NI, et al. International study on microcirculatory shock occurrence in acutely ill patients. *Crit Care Med.* (2015) 43:48–56.
29. Scorcella C, Damiani E, Domizi R, Pierantozzi S, Tondi S, Carsetti A, et al. MicroDAIMON study: microcirculatory DAIly MONitoring in critically ill patients: a prospective observational study. *Ann Intens Care.* (2018) 8:64. doi: 10.1186/s13613-018-0411-9
30. Guay CS, Khebir M, Shiva Shahiri T, Szilagyi A, Cole EE, Simoneau G, et al. Evaluation of automated microvascular flow analysis software AVA 4: a validation study. *Intensive Care Med Exp.* (2021) 9:15. doi: 10.1186/s40635-021-00380-0
31. Bezemer R, Bartels SA, Bakker J, Ince C. Clinical review: clinical imaging of the sublingual microcirculation in the critically ill–where do we stand? *Crit Care.* (2012) 16:224. doi: 10.1186/cc11236
32. Meddings JB, Sutherland LR, Byles NI, Wallace JL. Sucrose: a novel permeability marker for gastroduodenal disease. *Gastroenterology.* (1993) 104:1619–26. doi: 10.1016/0016-5085(93)90637-r
33. Stitt M. Product inhibition of potato tuber Pyrophosphate:Fructose-6-Phosphate phosphotransferase by phosphate and pyrophosphate 1. *Plant Physiol.* (1989) 89:628–33. doi: 10.1104/pp.89.2.628
34. Kortbeek JB, Al Turki SA, Ali J, Antoine JA, Bouillon B, Brasel K, et al. Advanced trauma life support, 8th edition, the evidence for change. *J Trauma Acute Care Surg.* (2008) 64:1638–50. doi: 10.1097/TA.0b013e3181744b03
35. Faul F, Erdfelder E, Lang A-G, Buchner A. G*Power 3: a flexible statistical power analysis program for the social, behavioral, and biomedical sciences. *Behav Res Methods.* (2007) 39:175–91. doi: 10.3758/bf03193146
36. Ince C, Boerma EC, Cecconi M, De Backer D, Shapiro NI, Duranteau J, et al. Second consensus on the assessment of sublingual microcirculation in critically ill patients: results from a task force of the European Society of Intensive Care Medicine. *Intensive Care Med.* (2018) 44:281–99. doi: 10.1007/s00134-018-5070-7
37. Mallat J, Lemyze M, Meddour M, Pepy F, Gasan G, Barrailler S, et al. Ratios of central venous-to-arterial carbon dioxide content or tension to arteriovenous oxygen content are better markers of global anaerobic metabolism than lactate in septic shock patients. *Ann Intensive Care.* (2016) 6:10. doi: 10.1186/s13613-016-0110-3
38. Mekontso-Dessap A, Castelain V, Anguel N, Bahloul M, Schauvliege F, Richard C, et al. Combination of venoarterial PCO2 difference with arteriovenous O2 content difference to detect anaerobic metabolism in patients. *Intensive Care Med.* (2002) 28:272–7. doi: 10.1007/s00134-002-1215-8
39. Ospina-Tascón GA, Umaña M, Bermúdez W, Bautista-Rincón DF, Hernandez G, Bruhn A, et al. Combination of arterial lactate levels and venous-arterial CO2 to arterial-venous O 2 content difference ratio as markers of resuscitation in patients with septic shock. *Intensive Care Med.* (2015) 41:796–805. doi: 10.1007/s00134-015-3720-6
40. Ray PD, Huang B-W, Tsuji Y. Reactive oxygen species (ROS) homeostasis and redox regulation in cellular signaling. *Cell Signal.* (2012) 24:981–90. doi: 10.1016/j.cellsig.2012.01.008
41. Merz T, Denoix N, Huber-Lang M, Singer M, Radermacher P, McCook O. Microcirculation vs. Mitochondria—What to target? *Front Med.* (2020) 7:416. doi: 10.3389/fmed.2020.00416
42. Tetri LH, Diffee GM, Barton GP, Braun RK, Yoder HE, Haraldsdottir K, et al. Sex-Specific skeletal muscle fatigability and decreased mitochondrial oxidative capacity in adult rats exposed to postnatal hyperoxia. *Front Physiol.* (2018) 9:326. doi: 10.3389/fphys.2018.00326
43. Gardner PR, Nguyen DD, White CW. Aconitase is a sensitive and critical target of oxygen poisoning in cultured mammalian cells and in rat lungs. *Proc Natl Acad Sci U S A.* (1994) 91:12248–52. doi: 10.1073/pnas.91.25.12248
44. Ma C, Beyer AM, Durand M, Clough AV, Zhu D, Norwood Toro L, et al. Hyperoxia causes mitochondrial fragmentation in pulmonary endothelial cells by increasing expression of pro-fission proteins. *Arterioscler Thromb Vasc Biol.* (2018) 38:622–35. doi: 10.1161/ATVBAHA.117.310605
45. Schwartges I, Schwarte LA, Fournell A, Scheeren TWL, Picker O. Hypercapnia induces a concentration-dependent increase in gastric mucosal oxygenation in dogs. *Intensive Care Med.* (2008) 34:1898–906. doi: 10.1007/s00134-008-1183-8
46. Pappenheimer JR, Reiss KZ. Contribution of solvent drag through intercellular junctions to absorption of nutrients by the small intestine of the rat. *J Membr Biol.* (1987) 100:123–36. doi: 10.1007/BF02209145
47. Berwick Z, Payne G, Lynch B, Dick G, Sturek M, Tune JD. Contribution Of adenosine A2A And A2B receptors to ischemic coronary dilation: role of KV and KATP channels. *Microcirculation.* (2010) 17:600–7. doi: 10.1111/j.1549-8719.2010.00054.x
48. Rivers E, Nguyen B, Havstad S, Ressler J, Muzzin A, Knoblich B, et al. Early Goal-directed therapy in the treatment of severe sepsis and septic shock. *N Engl J Med.* (2001) 345:1368–77.
49. Tao T, Liu Y, Zhang J, Xu Y, Li W, Zhao M. Therapeutic hypercapnia improves functional recovery and attenuates injury via antiapoptotic mechanisms in a rat focal cerebral ischemia/reperfusion model. *Brain Res.* (2013) 1533:52–62. doi: 10.1016/j.brainres.2013.08.014
50. Chi L, Wang N, Yang W, Wang Q, Zhao D, Sun T, et al. Protection of myocardial ischemia-reperfusion by therapeutic Hypercapnia: a mechanism involving improvements in mitochondrial biogenesis and function. *J Cardiovasc Transl Res.* (2019) 12:467–77. doi: 10.1007/s12265-019-09886-1
51. Sakr Y, Dubois M-J, De Backer D, Creteur J, Vincent J-L. Persistent microcirculatory alterations are associated with organ failure and death in patients with septic shock. *Crit Care Med.* (2004) 32:1825–31. doi: 10.1097/01.ccm.0000138558.16257.3f
52. Trzeciak S, Dellinger RP, Parrillo JE, Guglielmi M, Bajaj J, Abate NL, et al. Early microcirculatory perfusion derangements in patients with severe sepsis and septic shock: relationship to hemodynamics, oxygen transport, and survival. *Ann Emerg Med.* (2007) 49:88–98; 98.e1-2. doi: 10.1016/j.annemergmed.2006.08.021
53. Trzeciak S, McCoy JV, Phillip Dellinger R, Arnold RC, Rizzuto M, Abate NL, et al. Early increases in microcirculatory perfusion during protocol-directed resuscitation are associated with reduced multi-organ failure at 24 h in patients with sepsis. *Intensive Care Med.* (2008) 34:2210–7. doi: 10.1007/s00134-008-1193-6
54. De Backer D, Donadello K, Sakr Y, Ospina-Tascon G, Salgado D, Scolletta S, et al. Microcirculatory alterations in patients with severe sepsis: impact of time of assessment and relationship with outcome. *Crit Care Med.* (2013) 41:791–9. doi: 10.1097/CCM.0b013e3182742e8b
55. Philbin DM, Baratz RA, Patterson RW. The effect of carbon dioxide on plasma antidiuretic hormone levels during intermittent positive-pressure breathing. *Anesthesiology.* (1970) 33:345–9. doi: 10.1097/00000542-197009000-00016
56. Rose CE, Anderson RJ, Carey RM. Antidiuresis and vasopressin release with hypoxemia and hypercapnia in conscious dogs. *Am J Physiol.* (1984) 247(Pt 2):R127–34. doi: 10.1152/ajpregu.1984.247.1.R127
57. Truse R, Grewe S, Herminghaus A, Schulz J, Weber APM, Mettler-Altmann T, et al. Exogenous vasopressin dose-dependently modulates gastric microcirculatory oxygenation in dogs via V1A receptor. *Crit Care.* (2019) 23:353. doi: 10.1186/s13054-019-2643-y
58. Stübs CCM, Picker O, Schulz J, Obermiller K, Barthel F, Hahn A-M, et al. Acute, short-term hypercapnia improves microvascular oxygenation of the

colon in an animal model of sepsis. *Microvasc Res.* (2013) 90:180–6. doi: 10.1016/j.mvr.2013.07.008
59. Schulz J, Bauer I, Herminghaus A, Picker O, Truse R, Vollmer C. Sub-therapeutic vasopressin but not therapeutic vasopressin improves gastrointestinal microcirculation in septic rats: a randomized, placebo-controlled, blinded trial. *PLoS One.* (2021) 16:e0257034. doi: 10.1371/journal.pone.0257034
60. Schöneborn S, Vollmer C, Barthel F, Herminghaus A, Schulz J, Bauer I, et al. Vasopressin V1A receptors mediate the stabilization of intestinal mucosal oxygenation during hypercapnia in septic rats. *Microvasc Res.* (2016) 106:24–30. doi: 10.1016/j.mvr.2016.03.002
61. Vollmer C, Schwartges I, Naber S, Beck C, Bauer I, Picker O. Vasopressin V1A receptors mediate the increase in gastric mucosal oxygenation during hypercapnia. *J Endocrinol.* (2013) 217:59–67. doi: 10.1530/JOE-12-0526
62. Marhong J, Fan E. Carbon dioxide in the critically ill: too much or too little of a good thing? *Respir Care.* (2014) 59:1597–605. doi: 10.4187/respcare.03405
63. da Costa LGV, Carmona MJC, Malbouisson LM, Rizoli S, Rocha-Filho JA, Cardoso RG, et al. Independent early predictors of mortality in polytrauma patients: a prospective, observational, longitudinal study. *Clinics (Sao Paulo).* (2017) 72:461–8. doi: 10.6061/clinics/2017(08)02
64. Hoiland RL, Fisher JA, Ainslie PN. Regulation of the cerebral circulation by arterial carbon dioxide. *Compr Physiol.* (2019) 9:1101–54. doi: 10.1002/cphy.c180021
65. Spahn DR, Bouillon B, Cerny V, Duranteau J, Filipescu D, Hunt BJ, et al. The European guideline on management of major bleeding and coagulopathy following trauma: fifth edition. *Crit Care.* (2019) 23:98. doi: 10.1186/s13054-019-2347-3
66. Bruce J, Krukowski ZH, Al-Khairy G, Russell EM, Park KG. Systematic review of the definition and measurement of anastomotic leak after gastrointestinal surgery. *Br J Surg.* (2001) 88:1157–68. doi: 10.1046/j.0007-1323.2001.01829.x
67. Tsuji T, Aoshiba K, Itoh M, Nakamura H, Yamaguchi K. Hypercapnia accelerates wound healing in endothelial cell monolayers exposed to hypoxia. *Open Respir Med J.* (2013) 7:6–12. doi: 10.2174/1874306401307010006
68. Povoas HP, Weil MH, Tang W, Moran B, Kamohara T, Bisera J. Comparisons between sublingual and gastric tonometry during hemorrhagic shock. *Chest.* (2000) 118:1127–32. doi: 10.1378/chest.118.4.1127
69. Verdant CL, De Backer D, Bruhn A, Clausi CM, Su F, Wang Z, et al. Evaluation of sublingual and gut mucosal microcirculation in sepsis: a quantitative analysis. *Crit Care Med.* (2009) 37:2875–81. doi: 10.1097/CCM.0b013e3181b029c1

Conflict of Interest: The authors declare that the research was conducted in the absence of any commercial or financial relationships that could be construed as a potential conflict of interest.

Publisher's Note: All claims expressed in this article are solely those of the authors and do not necessarily represent those of their affiliated organizations, or those of the publisher, the editors and the reviewers. Any product that may be evaluated in this article, or claim that may be made by its manufacturer, is not guaranteed or endorsed by the publisher.

frontiers | Frontiers in Medicine

ORIGINAL RESEARCH
published: 29 April 2022
doi: 10.3389/fmed.2022.878823

Effects of Sodium Thiosulfate During Resuscitation From Trauma-and-Hemorrhage in Cystathionine-γ-Lyase Knockout Mice With Diabetes Type 1

*Michael Gröger[1†], Melanie Hogg[1†], Essam Abdelsalam[1†], Sandra Kress[1], Andrea Hoffmann[1], Bettina Stahl[1], Enrico Calzia[1], Ulrich Wachter[1], Josef A. Vogt[1], Rui Wang[2], Tamara Merz[1,3], Peter Radermacher[1] and Oscar McCook[1]**

[1] Institut für Anästhesiologische Pathophysiologie und Verfahrensentwicklung, Universitätsklinikum Ulm, Ulm, Germany, [2] Faculty of Science, York University, Toronto, ON, Canada, [3] Klinik für Anästhesiologie und Intensivmedizin, Universitätsklinikum Ulm, Ulm, Germany

OPEN ACCESS

Edited by:
Wolfgang Weihs,
Medical University of Vienna, Austria

Reviewed by:
Guangdong Yang,
Laurentian University, Canada
Risheng Xu,
The Johns Hopkins Hospital, Johns Hopkins Medicine, United States

***Correspondence:**
Oscar McCook
Oscar.McCook@uni-ulm.de

† These authors have contributed equally to this work and share first authorship

Specialty section:
This article was submitted to Intensive Care Medicine and Anesthesiology, a section of the journal Frontiers in Medicine

Received: 18 February 2022
Accepted: 06 April 2022
Published: 29 April 2022

Citation:
Gröger M, Hogg M, Abdelsalam E, Kress S, Hoffmann A, Stahl B, Calzia E, Wachter U, Vogt JA, Wang R, Merz T, Radermacher P and McCook O (2022) Effects of Sodium Thiosulfate During Resuscitation From Trauma-and-Hemorrhage in Cystathionine-γ-Lyase Knockout Mice With Diabetes Type 1. Front. Med. 9:878823. doi: 10.3389/fmed.2022.878823

Background: Sodium thiosulfate (STS) is a recognized drug with antioxidant and H_2S releasing properties. We recently showed that STS attenuated organ dysfunction and injury during resuscitation from trauma-and-hemorrhage in CSE-ko mice, confirming its previously described organ-protective and anti-inflammatory properties. The role of H_2S in diabetes mellitus type 1 (DMT1) is controversial: genetic DMT1 impairs H_2S biosynthesis, which has been referred to contribute to endothelial dysfunction and cardiomyopathy. In contrast, development and severity of hyperglycemia in streptozotocin(STZ)-induced DMT1 was attenuated in CSE-ko mice. Therefore, we tested the hypothesis whether STS would also exert organ-protective effects in CSE-ko mice with STZ-induced DMT1, similar to our findings in animals without underlying co-morbidity.

Methods: Under short-term anesthesia with sevoflurane and analgesia with buprenorphine CSE-ko mice underwent DMT1-induction by single STZ injection (100 $\mu g \cdot g^{-1}$). Seven days later, animals underwent blast wave-induced blunt chest trauma and surgical instrumentation followed by 1 h of hemorrhagic shock (MAP 35 $\pm$ 5 mmHg). Resuscitation comprised re-transfusion of shed blood, lung-protective mechanical ventilation, fluid resuscitation and continuous i.v. norepinephrine together with either i.v. STS (0.45 $mg \cdot g^{-1}$) or vehicle (n = 9 in each group). Lung mechanics, hemodynamics, gas exchange, acid–base status, stable isotope-based metabolism, and visceral organ function were assessed. Blood and organs were collected for analysis of cytokines, chemokines, and immunoblotting.

Results: Diabetes mellitus type 1 was associated with more severe circulatory shock when compared to our previous study using the same experimental design in CSE-ko mice without co-morbidity. STS did not exert any beneficial therapeutic effect. Most of

the parameters measured of the inflammatory response nor the tissue expression of marker proteins of the stress response were affected either.

Conclusion: In contrast to our previous findings in CSE-ko mice without underlying co-morbidity, STS did not exert any beneficial therapeutic effect in mice with STZ-induced DMT1, possibly due to DMT1-related more severe circulatory shock. This result highlights the translational importance of both integrating standard ICU procedures and investigating underlying co-morbidity in animal models of shock research.

Keywords: gluconeogenesis, ureagenesis, hydrogen sulfide, cystathionine-β-synthase, heme oxygenase-1, IκBα, glucocorticoid receptor, lipolysis

INTRODUCTION

Sodium thiosulfate, $Na_2S_2O_3$, (STS) is an H_2S donor with minimal side effects and clinically approved for decades for the treatment of calciphylaxis, *cis*-Pt toxicity and cyanide poisoning (1). Along with its sulfide releasing properties it is a known antioxidant, and in various rodent models was shown to be organ-protective after ischemia reperfusion injury (2, 3), acute liver injury (4), endotoxemia (5, 6), and bacterial sepsis (7). However, none of these models integrated standard intensive care measures into the experimental design, and STS was mostly administered either before or simultaneously with the systemic challenge. Using a post-treatment approach in a long-term, large animal model of hemorrhage-and-resuscitation, we recently showed lung-protective properties (8) in "human-sized" swine with ubiquitous atherosclerosis and, hence, decreased expression of the H_2S-producing enzyme cystathionine-γ-lyase (CSE) (9). We confirmed these beneficial effects of post-treatment STS administration under conditions of impaired endogenous H_2S availability by attenuation of lung, liver and kidney injury in mice with genetic CSE deletion (CSE-ko) undergoing trauma-and-hemorrhage and subsequent intensive care-based resuscitation (10, 11).

Diabetes mellitus type 1 and 2 are disorders of glucose metabolism where the evidence points to the involvement of H_2S and/or its endogenous producing enzymes (12, 13). In type 2 diabetes mellitus (i.e., diabetes due to insulin resistance), the endogenous availability of H_2S or the exogenous administration play a special role with regard to the prevention and/or treatment of vascular complications of diabetes (14, 15). Type 2 diabetes mellitus *per se* significantly reduced CSE expression in the kidneys (16), while exogenous H_2S improved insulin receptor sensitivity (17), reduced the hyperglycemia-induced oxidative stress and, subsequently, the activation of renin angiotensin system in the kidney (18). In addition, H_2S administration prevented the progression of diabetic nephropathy (19, 20) and improved wound healing impaired by type 2 diabetes mellitus (21, 22). Inhibiting CSE, on the other hand, further worsened wound healing (21).

Limited data is only available regarding the importance of the H_2S system in diabetes mellitus type 1 (DMT1), i.e., diabetes due to absolute insulin deficiency, and the little there is contradictory: While in CSE ko mice the development of diabetes mellitus type 1 induced by injection of streptozotocin (STZ) was both delayed (23) and attenuated, therapy with exogenous H_2S prevented the development of diabetic nephropathy in a rat model of diabetes mellitus type 1 (24). Moreover, H_2S treatment also attenuated STZ-induced diabetic retinopathy in rats (25).

Given the limited experimental evidence in diabetes mellitus type 1 (DMT1) and the fact that it may be an independent risk factor for mortality in critically ill surgical and trauma patients (26, 27), we therefore tested the hypothesis whether STS would also exert organ-protective effects in CSE-ko mice with STZ induced DMT1, similar to our recent findings in CSE-ko mice without underlying co-morbidity (10).

MATERIALS AND METHODS

The study was approved by the University of Ulm Animal Care Committee and the Federal Authorities for Animal Research (Regierungspräsidium Tübingen, Baden-Württemberg, Germany, Reg.-Nr. 1387), and all experiments were performed in adherence with the National Institutes of Health Guidelines on the Use of Laboratory Animals and the European Union "Directive 2010/63 EU on the protection of animals used for scientific purposes." The present experiments were part of a larger protocol including also wild type and diabetes type 2 animals. The federal authorities for animal protection, however, had only approved experiments in CSE-ko mice where the strongest effect of STS was expected. Thus, we were not allowed to include WT control mice in the present study as originally planned.

At the time of the experiment, a total of 23 homozygous (CSE-ko) deficient mice (C57BL/6J.129SvEv) (10) bred in house had been injected with STZ. Mice were 12–16 weeks old and weighed between 30 and 40 g. Five animals had to be excluded from the final data analysis due to hemothorax and pericardial tamponade subsequent to blunt chest trauma or uncontrollable bleeding during surgery. Thus, the subsequent data refer to 18 mice analyzed (vehicle group: $n = 9$; STS group: $n = 9$). This drop-out rate of 6/31 is similar to the previous study using the same model in CSE-ko mice without comorbidity (10) and is due to the extensive surgical instrumentation as well as the severe combined trauma injury mechanism of blunt chest trauma and hemorrhagic shock.

Figure 1 shows a flow chart of the experimental procedure. The procedures for anesthesia, blast wave-induced blunt chest trauma, surgical instrumentation, induction of hemorrhagic

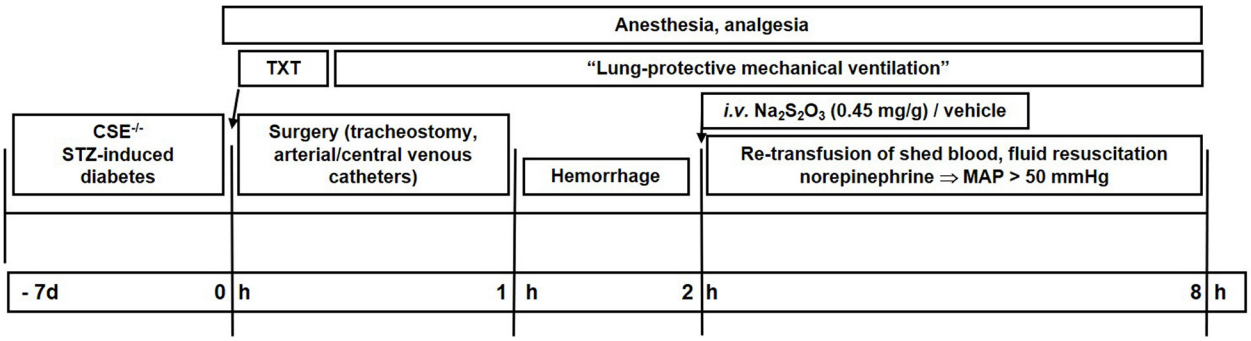

FIGURE 1 | Flow chart of the experimental procedure. Txt, thoraxtrauma; MAP, mean arterial pressure; HR, heart rate, STZ, streptozotocin.

shock and subsequent resuscitation as well as the methods for immunoblotting, assessment of metabolism *via* stable isotope approach are only briefly outlined as they are identical to that in CSE-ko mice without comorbidity (10).

Induction of Diabetes Type1

To develop a DMT1 state, streptozotocin (STZ) administration was used, as it is a common method to induce DMT1 in mice (28–30). STZ is an antimicrobial and a chemotherapeutic alkylating agent that causes specific necrosis of the pancreatic β-cells. Female mice show a significantly lower sensitivity against STZ induced diabetes than male mice (30), so only male CSE-ko mice received a single intraperitoneal (IP) injection of 100 $\mu g \cdot g^{-1}$ streptozotocin 7 days before the experiment under short term inhalational anesthesia with sevoflurane and subcutaneous (s.c.) injection of 1.5 $\mu g \cdot g^{-1}$ buprenorphine as analgesia. This "*single moderate-dose injection*" model was used, because according to the literature it is associated with the least mortality and at the same time progressive hyperglycemia within a week post-STZ injection (30, 31).

Anesthesia, Blunt Chest Trauma, Surgical Instrumentation, and Hemorrhagic Shock

Briefly, mice were anesthetized, received a single blast wave-generated blunt chest trauma and subsequently underwent surgical instrumentation comprising tracheostomy, and placement of catheters in the jugular vein, in the carotid and the femoral artery and in the urinary bladder. After completion of surgical instrumentation, mice underwent 1 h of hemorrhagic shock by removal of 30 $\mu L \cdot g^{-1}$ of blood and titration of mean arterial pressure (MAP) to 35 ± 5 mmHg. After 1 h, resuscitation was started with the re-transfusion of shed blood, administration of hydroxyethyl starch and – if necessary – norepinephrine to maintain a MAP of 50 mmHg. Immediately upon initiation of resuscitation mice randomly received either a bolus injection of 0.45 $mg \cdot g^{-1}$ sodium thiosulfate [$Na_2S_2O_3$, STS (Dr. Franz Köhler Chemie GmbH, Bensheim, Germany)] or the same amount of vehicle solution (NaCl 0.9%). After 6 h of lung-protective mechanical ventilation and intensive care (or if MAP could no longer be maintained >50 mmHg despite maximum norepinephrine infusion rates (i.e., ≤ 1 $\mu g \cdot g^{-1} \cdot min^{-1}$), mice were exsanguinated and blood and tissue samples were collected for further analysis (10).

Parameters of Lung Mechanics, Hemodynamics, Gas Exchange, and Acid-Base Status

Core temperature, hemodynamics and lung mechanics (10) were recorded hourly. Arterial blood samples were taken at baseline (i.e., immediately after insertion of the arterial catheter), at 3 h of resuscitation, and at the end of the experiment.

Metabolism and Organ Function

Arterial lactate and glucose levels were measured at baseline (i.e., immediately after insertion of the arterial catheter) and at the end of the experiment. Together with urine output, gas chromatography/mass spectrometry (GC/MS) measurement of plasma und urinary creatinine concentrations using $^2H_3$-creatinine as internal standard allowed for calculation of creatinine clearance (10, 32). Endogenous glucose production and direct, aerobic glucose oxidation as well as the production rates of urea, glycerol, and leucine as markers of hepatic metabolic capacity, lipolysis, and protein degradation (10, 32), were derived from the measurement of the respective plasma isotope enrichment during continuous intravenous isotope infusion as described in detail previously (10, 32).

Cytokines and Chemokines

As described previously (10) cytokine and chemokine levels in lung and kidney tissue as well as plasma were determined by using a mouse multiplex cytokine kit (Bio-Plex Pro Cytokine Assay, Bio-Rad, Hercules, CA, United States) according to the manufacturers' instructions.

Immunoblots

As described previously (10), expression of lung and kidney heme oxygenase-1 (HO-1; Abcam, Cambridge, United Kingdom), the inducible isoform of the nitric oxide synthase (iNOS; Thermo Fisher Scientific, Rockford, IL, United States), the endogenous inhibitor of the nuclear transcription factor NF-kB alpha

(IκBα; Cell Signaling, Danvers, MA, United States), the second major H_2S-producing enzyme cystathionine-β-synthase (CBS) (Signaling, Danvers, MA, United States caspase-3 (Signaling, Danvers, MA, United States), and the glucocorticoid receptor (GR; Cell Signaling, Danvers, MA, United States) were assessed by immunoblotting.

Statistical Analysis

All data are presented as medians and quartiles unless otherwise stated. Intergroup differences were analyzed using the Mann-Whitney rank sum test. A p-value of <0.05 was considered statistically significant. Survival curves were compared using the log-rank (Mantel Cox) test. Sample sizes were based on our previous experiments. A statistical power analysis using creatinine clearance (as the marker of acute kidney injury) and the norepinephrine infusion rate (as the marker of the severity of circulatory shock) as main criteria yielded a minimum number of 11 – 14 animals for two experimental groups based on two-sided testing, $\alpha = 0.05$, power of 80%, and non-parametric analysis of variance. Since an interim analysis at $n = 9$ had not yielded any significant intergroup difference for the main criteria, the experiment was terminated due to a futile result and in order to comply with the "3R principle". GraphPad Prism 9 software was used for statistical evaluation and graphical display.

RESULTS

Table 1 summarizes the parameters recorded of systemic hemodynamic, lung mechanics, gas exchange, acid-base status and metabolic parameters at the end of the experiment. In this murine model of STZ-induced DMT1, which tested the drug effects using a post-treatment approach together with standard ICU measures, STS had no significant effect on any of these parameters. Furthermore, as shown in **Table 2**, the stable isotope-based quantification of assessment of whole-body and organ-specific metabolic pathways and kidney function confirmed the lacking effect of STS under these conditions: neither the parameters measured of hepatic metabolic capacity (i.e., urea production), lipolysis (i.e., glycerol production), and protein degradation (i.e., leucine rate of appearance), nor kidney function (i.e., creatinine clearance) showed any significant difference when compared to the vehicle group. Finally, as shown in **Figure 2** and **Table 3**, STS did not affect inflammatory markers measured systemically nor in the organ tissue with the exception of limited anti-inflammatory properties in the lungs, where STS treatment significantly reduced interleukin-6 and monocyte-chemoattractant-protein-1 expression. In contrast, in the kidney, the STS group presented with increased interleukin-18 expression, again, with no apparent clinical impact. The overall unchanged organ cytokine and chemokine concentrations were supported by the results of the immunoblotting: neither lung nor kidney expression of HO-1, IκBα, CBS, caspase 3, or the GR, showed any significant intergroup difference (see **Figure 2**). Ultimately, all these findings coincided with similar survival times in the two experimental groups (see **Figure 3**).

TABLE 1 | Systemic hemodynamic, lung mechanics, gas exchange, acid-base status, and metabolic parameters at the end of the experiment.

	Vehicle	Sodium thiosulfate	*p*-value
Heart rate [min^{-1}]	580 (360;595)	500 (435;600)	0.7126
Mean arterial pressure [mmHg]	44 (31;61)	48 (32;63)	0.6287
Norepinephrine infusion rate [$\mu g \cdot kg^{-1} \cdot min^{-1}$]	0.58 (0.12;0.89)	0.24 (0.00;0.63)	0.5759
Compliance [$\mu L \cdot cmH_2O^{-1}$]	98 (88;107)	93 (82;118)	0.9962
Respiratory minute volume [$\mu L \cdot g^{-1} \cdot min^{-1}$]	750 (625;875)	850 (760;965)	0.2686
Arterial PCO_2 [mmHg]	36 (22;50)	31 (28;35)	0.7465
Arterial PO_2 [mmHg]	73 (59;93)	86 (70;95)	0.4672
Hemoglobin [$g \cdot dL^{-1}$]	6.1 (4.5;7.6)	6.2 (5.4;7.4)	0.9088
Arterial pH	7.22 (7.00;7.31)	7.25 (7.17;7.30)	0.6165
Arterial base excess [$mmol \cdot L^{-1}$]	−13.8 (−18.9; −8.4)	−11.4 (−14.6; −10.3)	0.4406
Arterial lactate [$mmol \cdot L^{-1}$]	3.6 (1.8;5.7)	3.6 (1.1;7.4)	0.9559
Urine output [mL]	0.9 (0.6;2.1)	2.0 (1.6;2.9)	0.2370

All data are median (interquartile range), n = 9 in both groups.

TABLE 2 | Terminal stable isotope-based metabolic flux and organ function parameters.

	Vehicle	Sodium thiosulfate	*p*-value
CO_2 release [$\mu L \cdot g^{-1} \cdot min^{-1}$]	23 (13; 26)	21 (15;25)	0.6943
Ra glucose [$\mu mol \cdot g^{-1} \cdot h^{-1}$]	2.7 (1.9;3.5)	2.4 (2.3;2.7)	0.7308
Arterial glucose baseline [$mg \cdot dL^{-1}$]	255 (230;309)	268 (212;283)	>0.9999
Arterial glucose end [$mg \cdot dL^{-1}$]	80 (49;82)	79 (66;91)	0.6823
Glucose oxidation rate [%]	51 (43;54)	47 (39;52)	0.7789
Ra glycerol [$\mu mol \cdot g^{-1} \cdot h^{-1}$]	2.1 (1.6;3.1)	2.5 (1.7;3.0)	0.8357
Urea [$\mu g \cdot mL^{-1}$]	477 (384; 557)	402 (218;525)	0.4452
Ra urea [$\mu mol \cdot g^{-1} \cdot h^{-1}$]	2 (1.5;2.5)	1.6 (1.3;1.9)	0.4452
Ra leucine [$\mu mol \cdot g^{-1} \cdot h^{-1}$]	0.45 (0.30;0.55)	0.34 (0.26;0.41)	0.1789
Arterial creatinine [$\mu g \cdot mL^{-1}$]	1.28 (1.17;1.52)	1.31 (1.10;1.62)	0.8703
Creatinine-clearance [$\mu L \cdot min^{-1}$]	411 (234; 478)	367 (290; 537)	>0.9999

All data are median (interquartile range), n = 9 in both groups; Ra, rate of appearance.

DISCUSSION

In this study, we tested the hypothesis whether STS would exert organ-protective effects in CSE-ko mice with STZ-induced DMT1. The main findings were that (i) in contrast to our previous findings in CSE-ko mice without underlying co-morbidity (10), STS did not exert any beneficial therapeutic effect under these conditions, (ii) possibly at least in part due to more severe circulatory shock. In addition, (iii) we confirmed previous findings (23) that metabolic derangements associated with STZ-induced DMT1 are less severe in CSE-ko mice, (iv) apparently in as a result of lower rates of endogenous glucose release (33).

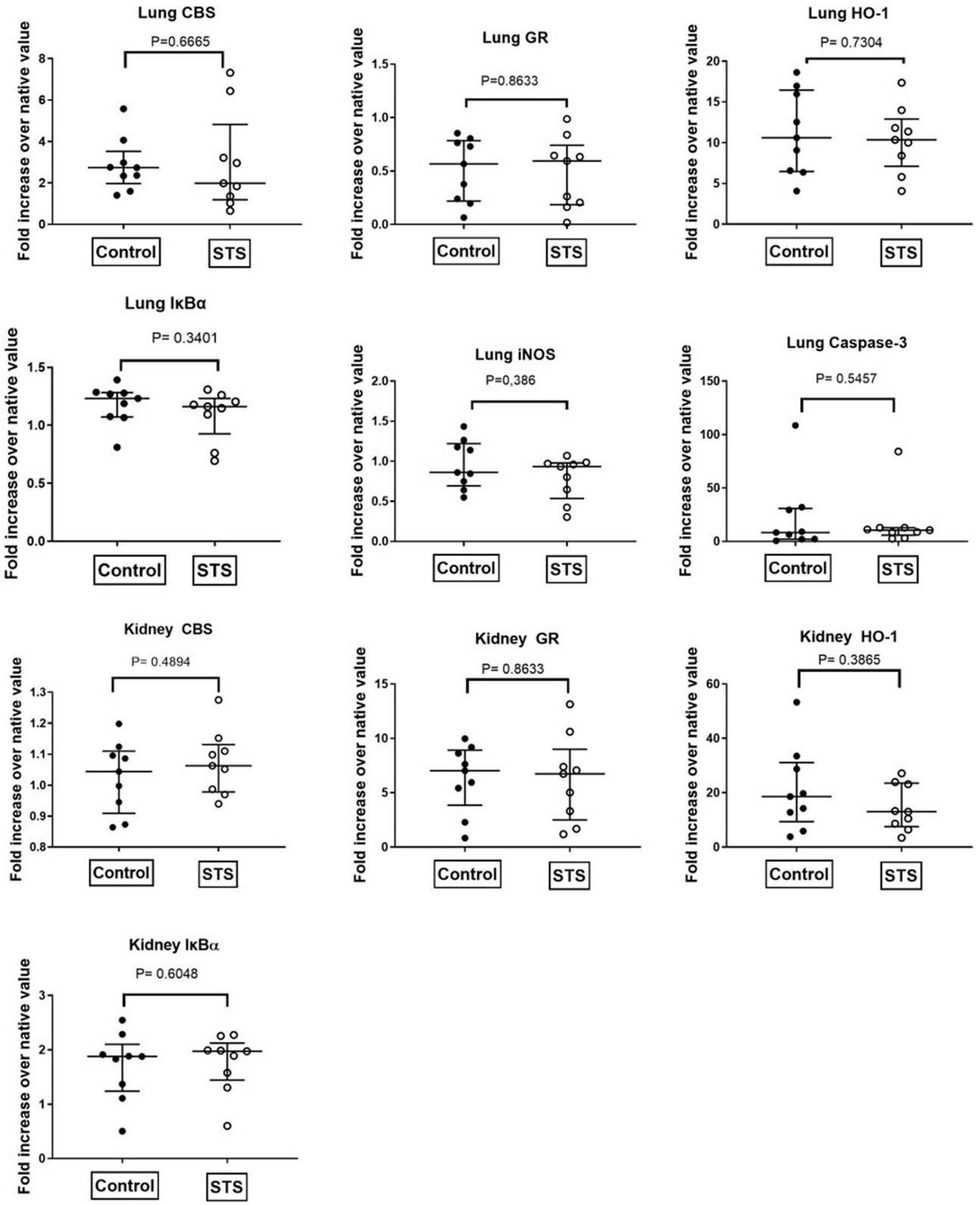

FIGURE 2 | Quantitative analysis of immunoblots of lung and kidney tissue. CBS, Cystathionine-β-synthase; GR, glucocorticoid receptor; HO-1, heme-oxygenase 1; IκBα, nuclear factor of kappa light polypeptide gene enhancer in B-cells inhibitor, alpha; iNOS, inducible nitric oxide synthase.

TABLE 3 | Terminal plasma (in [pg·mL) and tissue (kidney and lung, [pg·mg$_{protein}^{-1}$]) cytokine and chemokine concentrations.

		Vehicle	Sodium thiosulfate	*P*-value
Tumor necrosis factor	Lung	40 (33;49)	38 (27;45)	0.6048
	Kidney	138 (116;163)	130 (111;159)	0.6048
	Plasma	45 (39;84)	43 (39;105)	0.8633
Interleukin-18	Lung	2445 (1590;4090)	4164 (3219;5570)	0.1049
	Kidney	2884 (2771;3458)	3861 (3671;4080)	0.0002
	Plasma	497 (294;767)	913 (293;2250)	0.3865
Interleukin-6	Lung	259 (198;349)	52 (27;201)	0.0152
	Kidney	104 (83;467)	222 (59;441)	0.7756
	Plasma	4150 (2062;17663)	3525 (1605;34089)	>0.999
Interleukin-1β	Lung	55 (37;159)	37 (24;94)	0.2973
	Kidney	26 (17;46)	9 (3;24)	0.0712
	Plasma	2 (1;8)	5 (1;12)	0.9999
Interleukin-10	Lung	43 (34;46)	40 (35;52)	0.6048
	Kidney	183 (170;265)	174 (172;202)	0.6214
	Plasma	39 (15; 309)	38 (10; 77)	0.8884
Keratinocyte-derived	Lung	1798 (1211;4272)	1446 (924;2162)	0.3401
chemokine	Kidney	1222 (831;3495)	650.1 (355;2051)	0.0939
	Plasma	132 (85;178)	82 (31;320)	0.6665
Monocyte-	Lung	3941 (3002;6448)	677 (374;721)	<0.0001
chemoattractant-	Kidney	n.d.	n.d.	
protein-1	Plasma	2781 (904;11175)	1195 (678;16830)	0.6665

All data are median (interquartile range), n = 9 in both groups, n.d. not determined.

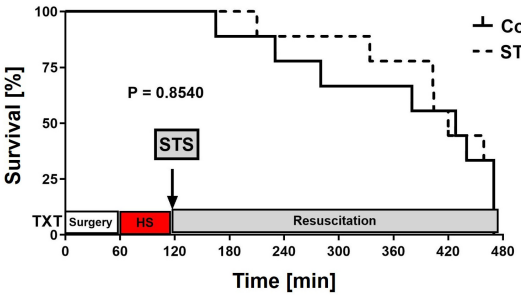

FIGURE 3 | Survival curves. Survival curves were compared using the Log-rank (Mantel–Cox) test.

Despite promising reports (34, 35) exogenous H_2S administration produced equivocal results in murine models of hemorrhage-and-resuscitation, inasmuch undesired side effects were due to potentially high H_2S peak concentrations (36) when the H_2S-releasing salts NaSH and/or Na_2S were used, or aggravation of shock due to the vasodilatory properties of so-called "*slow-releasing H_2S donors*" (37). Therefore, STS was used, an H_2S donor devoid of major undesired side effects and recognized for cyanide intoxication, *cis*-Pt-overdosing in oncology, as well as calciphylaxis in end stage kidney disease (1). STS has been shown to be beneficial in LPS- and polymicrobial sepsis-induced ALI (5), acute liver failure (4) and I/R injury (3), *Pseudomonas aeruginosa*-bacteremia (7) and colon ascendens stent peritonitis-induced sepsis (38) as well as both LPS- (6) and I/R-induced (2) brain injury. Moreover, STS also protected against arterial hypertension-induced congestive heart failure (39, 40) and kidney disease (41, 42). Finally, we have recently shown that post-treatment STS administration attenuated of lung, liver and kidney injury in non-comorbid CSE-ko mice undergoing trauma-and-hemorrhage and subsequent intensive care-based resuscitation (10).

We chose a single intraperitoneal STZ injection to induce DMT1 in in order to minimize any stress on the test animals from repeated i.p. administration. Moreover, this "*single moderate-dose injection*" has been referred to be associated with the least mortality, decreased renal toxicity, reduced "off target effects" and at the same time progressive hyperglycemia within a week post-STZ injection (30, 31, 43). Genetic CSE deletion attenuated this hyperglycemic response to the STZ injection: before the start of the actual trauma or MICU phase, all test animals showed hyperglycemia ≈260 mg·dL^{-1}, in contrast to the blood glucose levels of approx. 100 mg·dL^{-1} reported in naïve CSE-ko mice (23). Hence, the degree of hyperglycemia was less than described in the literature for murine STZ-induced DMT1, i.e., in general ≥400 mg·dL^{-1} (30, 31) and e.g., at day 30 after five daily injections of 40 μg·g^{-1} STZ (508 ± 47 mg·dL^{-1} (23). Nevertheless, these values are in accordance with what is reported for STZ-DMT1 in CSE-ko mice, i.e., 259 ± 70 mg·dL^{-1} at the same time point (23). Strikingly, in both groups glycemia values returned to normal levels by the end of the experiment. Since glucose oxidation accounted for approx. 50% of the infused isotope-labeled substrate, i.e., was similar as previously shown in CSE-ko mice without DMT1 (10), this finding suggests a reduced rate of endogenous glucose release. Gluconeogenesis is a highly oxygen-dependent metabolic pathway, and both we and others previously showed that a lacking rise of glucose formation upon catecholamine stimulation and/or a fall in gluconeogenesis reflects impaired renal (44) and/or hepatic (45, 46) metabolic capacity. Moreover, even short-term (2 h only) (47) elevation of norepinephrine concentrations can compromise hepatocellular function. In addition, naïve CSE-ko mice *per se* have a reduced rate of gluconeogenesis, which was reversed by i.p. administration of the H_2S releasing salt NaHS (33). In good agreement with these findings, we showed in CSE-ko mice undergoing trauma, hemorrhage and resuscitation that the "*slow-releasing H_2S donor*" GYY4137 restored reduced blood glucose levels to the values found in wild type animals (48). Additionally, wild type mice undergoing a similar hemorrhage-and-resuscitation protocol showed a 20% higher stable isotope infusion-derived rate of gluconeogenesis (32) than both the non-diabetic CSE-ko mice in the previous (10) as well as the DMT1 animals in the present study (median 3.6 *vs.* 3.2 and 2.7 μmol·g^{-1}·h^{-1}, respectively). A limitation of this study was imposed by the Federal Authorities for Animal

Research (Regierungspräsidium Tübingen Baden-Württemberg, Germany, Reg.-Nr. 1387, approval January 31, 2018), which only approved experiments for CSE-ko mice where the strongest effect of STS was expected. Thus, we would only be able to speculate on the results of STS treatment in DMT1 in WT mice when exposed to resuscitation from trauma-and-hemorrhage as in the current protocol, but the effects of hyperglycemia *per se* would imply more severe disturbance of mitochondrial respiration, possibly more profound oxidative stress and concomitant depressed liver metabolic capacity (49, 50). Furthermore, though we used single injection of a low dose of STZ known for its minimal collateral effects, Nørgaard et al. (43) found that all STZ doses they investigated, including ours, led to significant enlargement of the stomach with no pathological changes and not caused by food intake. Hence, albeit, they studied short-term effects (1 day post injection) while our animals had a "recovery" period of 7 days, nevertheless, we cannot rule out that these non-specific effects of STZ, a fundamental issue of the model *per se*, may have masked any beneficial STS effects. Although in rat STZ models of DMT1, with an intact endogenous H_2S enzymes system, chronic administration of H_2S prevented the development of diabetic nephropathy (24) and attenuated diabetic retinopathy (25). A very important piece of the puzzle was denied us by the authorities limiting our original experimental design (which included WT mice) to only CSEko mice. Thus we are unable to conclude if the lack of CSE or non-specific effects of STZ interfered with the potential benefits of acute administration of STS in our resuscitated circulatory shock model, as observed in our previous experiment without the DMT1 comorbidity (10).

The limited data available in CSE-ko mice in resuscitative circulatory shock models show increased local and systemic pro-inflammatory chemokine and cytokine concentrations, higher heart rate and MAP as well as lower glucose levels in comparison to WT. The administration of GYY4137, a slow releasing H2S donor, restored glucose levels to normal and slightly reduced MAP but had no effect on heart rate (48, 51).

In the present study compared to vehicle-treated animals, STS treatment affected neither systemic hemodynamics, lung mechanics, gas exchange, metabolism nor organ (dys)function. Most of the parameters measured of the systemic and organ inflammatory response nor the tissue expression of marker proteins of the stress response were affected either. These findings are in contrast to our previous study in CSE-ko mice without underlying co-morbidity (10). In fact, the role of H_2S in DMT1 is controversial: on the one hand, DMT1 in patients has been reported to be associated with reduced H_2S production as a result of decreased CSE activity (52), even suggesting a window for potential exogenous H_2S therapy (53, 54). "*Non-obese*", genetic DMT1 mice showed impaired H_2S biosynthesis, the degree of which was directly related to the severity of glucosuria (55). In addition, reduced H_2S availability has been referred to contribute to both diabetes-induced endothelial dysfunction (56) and cardiomyopathy (57). In contrast, increased H_2S levels and/or CSE overexpression have been shown to at least partially inhibit high glucose-induced insulin secretion (58) due to activation of K_{ATP} channels in islet cells (59). Moreover, as mentioned-above, development and severity of hyperglycemia after STZ injection was attenuated in CSE-ko mice when compared to wild type littermates (23).

Irrespective of the lacking organ-protective effect of STS, DMT1 in CSE-ko mice was associated with aggravated severity of shock when compared to non-diabetic animals in our previous investigation (10): norepinephrine requirements to achieve hemodynamic targets were higher (median 0.58 *vs.* 0.27 $\mu g \cdot kg^{-1} \cdot min^{-1}$) and lactic acidosis more severe (arterial lactate and base excess median 3.6 *vs.* 2.5 and −13.8 *vs.* −10.3 $mmol \cdot L^{-1}$, respectively; arterial pH median 7.22 *vs.* 7.30). It is tempting to speculate that hyperglycemia *per se* plays a central role in this context: hyperglycemia >250 $mg \cdot dL^{-1}$ in mice with STZ-induced DMT1 was associated with aggravation of ventilator-induced acute lung injury (60), and blood glucose levels as high as 755 $mg \cdot dL^{-1}$ caused marked aggravation of acute kidney injury after hemorrhagic shock in 20-weeks old *db/db* mice, i.e., with diabetes type 2 (61). Finally, we had shown that mice with septic shock rendered hyperglycemic by i.v. glucose required the highest norepinephrine infusion rates in order to achieve pre-defined hemodynamic target values, which despite comparable parameters of microcirculatory perfusion and oxygen supply was associated with the most pronounced decrease in mitochondrial respiration and severity of lactic acidosis (49).

The above findings underscore the need to further investigate the treatment of the metabolic imbalance in DMT1 patients admitted to the ICU. In contrast to the general population adults with DMT1 have a higher admission and increased mortality in the ICU (62). Furthermore, the unexpected findings by Liou et al. (63) that a higher mortality rate after moderate to serious trauma is associated with DMT1 but not with DMT2 suggests a need to taper patient care specifically to the DMT1 trauma patients: early ICU admission, rapid hyperglycemia and related insulin therapy especially after moderate to severe trauma in an effort to increase survival (63). It is also noteworthy that in the current COVID-19 pandemic, caused by SARS-CoV-2, DMT1 patients are at higher risk for severe outcomes and ICU admission than those without diabetes and those with DMT2 (64). These results were echoed in a pediatric study where the strongest risk factors for hospitalization and severe COVID-19 was DMT1 (65). Interestingly, "a hallmark of COVID-19" are significantly reduced H_2S levels in non-survivors. Therefore, the therapeutic potential for H_2S donors in their ability to maintain physiological homeostasis attenuating endothelial dysfunction and kidney injury (common disorders in DMT1) in COVID-19 patients, especially STS, may assume particular importance under this condition. A separate discussion is beyond the scope of this paper (66–71).

CONCLUSION

In the present study and in contrast to our previous findings in CSE-ko mice without underlying co-morbidity (10) STS did not exert any beneficial therapeutic effect in mice with STZ-induced DMT1 under these conditions, possibly due to DMT1-related more severe circulatory shock and/or unspecific STZ-related effects. This result highlights the translational importance

not only of integrating standard ICU procedures into the design of experimental models for shock research, but also the investigation of underlying co-morbidity, even when rodents are used because of the availability of genetically modified strains.

DATA AVAILABILITY STATEMENT

All data is contained within the article and **Supplementary Material**.

ETHICS STATEMENT

The animal study was reviewed and approved by the University of Ulm Animal Care Committee and the Federal Authorities for Animal Research (Regierungspräsidium Tübingen, Baden-Württemberg, Germany, Reg. No. 1387, approval January 31, 2018).

AUTHOR CONTRIBUTIONS

PR: conceptualization, funding, project administration, and supervision. MG, SK, EA, AH, and UW: surgical instrumentation and methodology. EA, EC, MG, AH, MH, TM, BS, JV, and UW: investigation. EA, MH, OM, BS, and JV: data curation. TM and OM: figures and visualization. OM and PR: writing – original draft preparation. PR, OM, RW, and TM: writing – review and editing. All authors have read and agreed to the published version of the manuscript.

FUNDING

PR and TM are supported by the Deutsche Forschungsgemeinschaft (CRC 1149, project no. 251293561). RW was supported by a Discovery Grant from Natural Science and Engineering Research Council of Canada.

ACKNOWLEDGMENTS

We are indebted to Rosemarie Mayer and Marina Fink for skillful technical assistance.

SUPPLEMENTARY MATERIAL

The Supplementary Material for this article can be found online at: https://www.frontiersin.org/articles/10.3389/fmed.2022.878823/full#supplementary-material

REFERENCES

1. McGeer PL, McGeer EG, Lee M. Medical uses of sodium thiosulfate. *J Neurol Neuromed.* (2016) 1:28–30. doi: 10.1016/j.ekir.2018.10.002
2. Marutani E, Yamada M, Ida T, Tokuda K, Ikeda K, Kai S, et al. Thiosulfate mediates cytoprotective effects of hydrogen sulfide against neuronal ischemia. *J Am Heart Assoc.* (2015) 4:e002125. doi: 10.1161/JAHA.115.002125
3. Bauer M, Radermacher P, Wepler M. Sodium thiosulfate: a new player for circulatory shock and ischemia/reperfusion injury? In: Vincent JL editor. *Annual Update in Intensive Care and Emergency Medicine*. (Cham: Springer) (2019). p. 167–78.
4. Shirozu K, Tokuda K, Marutani E, Lefer D, Wang R, Ichinose F. Cystathionine γ-lyase deficiency protects mice from galactosamine/lipopolysaccharide-induced acute liver failure. *Antioxid Red Signal.* (2014) 20:204–16. doi: 10.1089/ars.2013.5354
5. Sakaguchi M, Marutani E, Shin HS, Chen W, Hanaoka K, Xian M, et al. Sodium thiosulfate attenuates acute lung injury in mice. *Anesthesiology.* (2014) 121:1248–57. doi: 10.1097/ALN.0000000000000456
6. Acero G, Nava Catorce M, González-Mendoza R, Meraz-Rodríguez MA, Hernández-Zimbron LF, González-Salinas R, et al. Sodium thiosulphate attenuates brain inflammation induced by systemic lipopolysaccharide administration in C57BL/6J mice. *Inflammopharmacology.* (2017) 25:585–596. doi: 10.1007/s10787-017-0355-y
7. Renieris G, Droggiti DE, Katrini K, Koufargyris P, Gkavogianni T, Karakike E, et al. Host cystathionine-γ lyase derived hydrogen sulfide protects against *Pseudomonas aeruginosa* sepsis. *PLoS Pathog.* (2021) 17:e1009473. doi: 10.1371/journal.ppat.1009473
8. Datzmann T, Hoffmann A, McCook O, Merz T, Wachter U, Preuss J, et al. Effects of sodium thiosulfate (Na2S2O3) during resuscitation from hemorrhagic shock in swine with preexisting atherosclerosis. *Pharmacol Res.* (2020) 151:104536. doi: 10.1016/j.phrs.2019.104536
9. Merz T, Stenzel T, Nußbaum B, Wepler M, Szabo C, Wang R, et al. Cardiovascular disease and resuscitated septic shock lead to the downregulation of the H_2S-producing enzyme cystathionine-γ-lyase in the porcine coronary artery. *Intensive Care Med Exp.* (2017) 1:17. doi: 10.1186/s40635-017-0131-8
10. Gröger M, Hogg M, Abdelsalam E, Kress S, Hoffmann A, Stahl B, et al. Effects of sodium thiosulfate during resuscitation from trauma-and-hemorrhage in cystathionine gamma lyase (CSE) knockout mice. *Shock.* (2022) 57:131–9. doi: 10.1097/SHK.0000000000001828
11. Yang G, Wu L, Jiang B, Yang W, Qi J, Cao K, et al. H_2S as a physiologic vasorelaxant: hypertension in mice with deletion of cystathionine gamma-lyase. *Science.* (2008) 322:587–90. doi: 10.1126/science.1162667
12. Wu L, Yang W, Jia X, Yang G, Duridanova D, Cao K, et al. Pancreatic islet overproduction of H_2S and suppressed insulin release in zucker diabetic rats. *Lab Invest.* (2009) 89:59–67. doi: 10.1038/labinvest.2008.109
13. Zhang H, Huang Y, Chen S, Tang C, Wang G, Du J, et al. Hydrogen sulfide regulates insulin secretion and insulin resistance in diabetes mellitus, a new promising target for diabetes mellitus treatment? A review. *J Adv Res.* (2020) 27:19–30. doi: 10.1016/j.jare.2020.02.013
14. Feliers D, Lee HJ, Kasinath BS. Hydrogen sulfide in renal physiology and disease. *Antioxid Redox Signal.* (2016) 25:720–31. doi: 10.1089/ars.2015.6596
15. Sen U, Pushpakumar S. Mini-review: diabetic renal complications, a potential stinky remedy. *Am J Physiol Renal Physiol.* (2016) 310:F119–22. doi: 10.1152/ajprenal.00299.2015
16. Yamamoto J, Sato W, Kosugi T, Yamamoto T, Kimura T, Taniguchi S. Distribution of hydrogen sulfide (H2S)-producing enzymes and the roles of the H2S donor sodium hydrosulfide in diabetic nephropathy. *Clin Exp Nephrol.* (2013) 1:32–40. doi: 10.1007/s10157-012-0670-y
17. Xue R, Hao DD, Sun JP, Li WW, Zhao MM, Li XH, et al. Hydrogen sulfide treatment promotes glucose uptake by increasing insulin receptor sensitivity and ameliorates kidney lesions in type 2 diabetes. *Antioxid Redox Signal.* (2013) 19:5–23. doi: 10.1089/ars.2012.5024
18. Xue H, Yuan P, Ni J, Li C, Shao D, Liu J, et al. HS inhibits hyperglycemia-induced intrarenal renin-angiotensin system activation *via* attenuation of reactive oxygen species generation. *PLoS One.* (2013) 8:e74366. doi: 10.1371/journal.pone.0074366
19. Ahmad FU, Sattar MA, Rathore HA, Abdullah MH, Tan S, Abdullah NA, et al. Exogenous hydrogen sulfide (H_2S) reduces blood pressure and prevents the

progression of diabetic nephropathy in spontaneously hypertensive rats. *Ren Fail.* (2012) 34:203–10. doi: 10.3109/0886022X.2011.643365
20. Ng HH, Yildiz GS, Ku JM, Miller AA, Woodman OL, Hart JL. Chronic NaHS treatment decreases oxidative stress and improves endothelial function in diabetic mice. *Diab Vasc Dis Res.* (2017) 14:246–53. doi: 10.1177/1479164117692766
21. Liu F, Chen DD, Sun X, Xie HH, Yuan H, Jia W, et al. Hydrogen sulfide improves wound healing *via* restoration of endothelial progenitor cell functions and activation of angiopoietin-1 in type 2 diabetes. *Diabetes.* (2014) 63:1763–78. doi: 10.2337/db13-0483
22. Wang G, Li W, Chen Q, Jiang Y, Lu X, Zhao X. Hydrogen sulfide accelerates wound healing in diabetic rats. *Int J Clin Exp Pathol.* (2015) 8:5097–104.
23. Yang G, Tang G, Zhang L, Wu L, Wang R. The pathogenic role of cystathionine γ-lyase/hydrogen sulfide in streptozotocin-induced diabetes in mice. *Am J Pathol.* (2011) 179:869–79. doi: 10.1016/j.ajpath.2011.04.028
24. Zhou X, Feng Y, Zhan Z, Chen J. Hydrogen sulfide alleviates diabetic nephropathy in a streptozotocin-induced diabetic rat model. *J Biol Chem.* (2014) 289:28827–34. doi: 10.1074/jbc.M114.596593
25. Si YF, Wang J, Guan J, Zhou L, Sheng Y, Zhao J. Treatment with hydrogen sulfide alleviates streptozotocin-induced diabetic retinopathy in rats. *Br J Pharmacol.* (2013) 169:619–31. doi: 10.1111/bph.12163
26. Esper AM, Martin GS. The impact of comorbid [corrected] conditions on critical illness. *Crit Care Med.* (2011) 12:2728–35. doi: 10.1097/CCM.0b013e318236f27e
27. Chang MW, Huang CY, Liu HT, Chen YC, Hsieh CH. Stress-induced and diabetic hyperglycemia associated with higher mortality among intensive care unit trauma patients: cross-sectional analysis of the propensity score-matched population. *Int J Environ Res Public Health.* (2018) 15:992. doi: 10.3390/ijerph15050992
28. Leiter EH. Multiple low-dose streptozotocin-induced hyperglycemia and insulitis in C57BL mice: influence of inbred background, sex, and thymus. *Proc Natl Acad Sci USA.* (1982) 79:630–4. doi: 10.1073/pnas.79.2.630
29. King AJ. The use of animal models in diabetes research. *Br J Pharmacol.* (2012) 166:877–94. doi: 10.1111/j.1476-5381.2012.01911.x
30. Deeds MC, Anderson JM, Armstrong AS, Gastineau DA, Hiddinga HJ, Jahangir A, et al. Single dose streptozotocin-induced diabetes: considerations for study design in islet transplantation models. *Lab Anim.* (2011) 45:131–40. doi: 10.1258/la.2010.010090
31. Hayashi K, Kojima R, Ito M. Strain differences in the diabetogenic activity of streptozotocin in mice. *Biol Pharm Bull.* (2006) 29:1110–9. doi: 10.1248/bpb.29.1110
32. Langgartner D, Wachter U, Hartmann C, Gröger M, Vogt J, Merz T, et al. Effects of psychosocial stress on subsequent hemorrhagic shock and Resuscitation in male mice. *Shock.* (2019) 51:725–30. doi: 10.1097/SHK.0000000000001204
33. Untereiner AA, Wang R, Ju Y, Wu L. Decreased gluconeogenesis in the absence of cystathionine gamma-lyase and the underlying mechanisms. *Antioxid Redox Signal.* (2016) 24:129–40. doi: 10.1089/ars.2015.6369
34. Morrison ML, Blackwood JE, Lockett SL, Iwata A, Winn RK, Roth MB. Surviving blood loss using hydrogen sulfide. *J Trauma.* (2008) 65:183–8. doi: 10.1097/TA.0b013e3181507579
35. Dyson A, Dal-Pizzol F, Sabbatini G, Lach AB, Galfo F, Dos Santos Cardoso J, et al. Ammonium tetrathiomolybdate following ischemia/reperfusion injury: chemistry, pharmacology, and impact of a new class of sulfide donor in preclinical injury models. *PLoS Med.* (2017) 14:e1002310. doi: 10.1371/journal.pmed.1002310
36. Whiteman M, Li L, Rose P, Tan CH, Parkinson DB, Moore PK. The effect of hydrogen sulfide donors on lipopolysaccharide-induced formation of inflammatory mediators in macrophages. *Antioxid Redox Signal.* (2010) 12:1147–54. doi: 10.1089/ars.2009.2899
37. Wepler M, Merz T, Wachter U, Vogt J, Calzia E, Scheuerle A, et al. The mitochondria-targeted H_2S-donor AP39 in a murine model of combined hemorrhagic shock and blunt chest Trauma. *Shock.* (2019) 52:230–9. doi: 10.1097/SHK.0000000000001210
38. Schulz J, Kramer S, Kanatli Y, Kuebart A, Bauer I, Picker O, et al. Sodium thiosulfate improves intestinal and hepatic microcirculation without affecting mitochondrial function in experimental sepsis. *Front Immunol.* (2021) 12:671935. doi: 10.3389/fimmu.2021.671935
39. Snijder PM, Frenay AR, de Boer RA, Pasch A, Hillebrands JL, Leuvenink HG, et al. Exogenous administration of thiosulfate, a donor of hydrogen sulfide, attenuates angiotensin II-induced hypertensive heart disease in rats. *Br J Pharmacol.* (2015) 172:1494–504. doi: 10.1111/bph.12825
40. Nguyen ITN, Wiggenhauser LM, Bulthuis M, Hillebrands JL, Feelisch M, Verhaar MC, et al. Cardiac protection by oral sodium thiosulfate in a rat model of L-NNA-induced heart disease. *Front Pharmacol.* (2021) 12:650968. doi: 10.3389/fphar.2021.650968
41. Snijder PM, Frenay AR, Koning AM, Bachtler M, Pasch A, Kwakernaak AJ, et al. Sodium thiosulfate attenuates angiotensin II-induced hypertension, proteinuria and renal damage. *Nitric Oxide.* (2014) 42:87–98. doi: 10.1016/j.niox.2014.10.002
42. Nguyen ITN, Klooster A, Minnion M, Feelisch M, Verhaar MC, van Goor H, et al. Sodium thiosulfate improves renal function and oxygenation in L-NNA-induced hypertension in rats. *Kidney Int.* (2020) 98:366–77. doi: 10.1016/j.kint.2020.02.020
43. Nørgaard SA, Søndergaard H, Sørensen DB, Galsgaard ED, Hess C, Sand FW. Optimising streptozotocin dosing to minimise renal toxicity and impairment of stomach emptying in male 129/Sv mice. *Lab Anim.* (2020) 54:341–52. doi: 10.1177/0023677219872224
44. Maitra SR, Homan CS, Pan W, Geller ER, Henry MC, Thode HC Jr. Renal gluconeogenesis and blood flow during endotoxic shock. *Acad Emerg Med.* (1996) 3:1006–10. doi: 10.1111/j.1553-2712.1996.tb03343.x
45. Albuszies G, Radermacher P, Vogt J, Wachter U, Weber S, Schoaff M, et al. Effect of increased cardiac output on hepatic and intestinal microcirculatory blood flow, oxygenation, and metabolism in hyperdynamic murine septic shock. *Crit Care Med.* (2005) 33:2332–8. doi: 10.1097/01.ccm.0000182817.20977.e9
46. Albuszies G, Vogt J, Wachter U, Thiemermann C, Leverve XM, Weber S, et al. The effect of iNOS deletion on hepatic gluconeogenesis in hyperdynamic murine septic shock. *Intensive Care Med.* (2007) 33:1094–101. doi: 10.1007/s00134-007-0638-7
47. Yang S, Koo DJ, Zhou M, Chaudry IH, Wang P. Gut-derived norepinephrine plays a critical role in producing hepatocellular dysfunction during early sepsis. *Am J Physiol Gastrointest Liver Physiol.* (2000) 279:G1274–81. doi: 10.1152/ajpgi.2000.279.6.G1274
48. Merz T, Lukaschewski B, Wigger D, Rupprecht A, Wepler M, Gröger M, et al. Interaction of the hydrogen sulfide system with the oxytocin system in the injured mouse heart. *Intensive Care Med Exp.* (2018) 6:41. doi: 10.1186/s40635-018-0207-0
49. Merz T, Vogt JA, Wachter U, Calzia E, Szabo C, Wang R, et al. Impact of hyperglycemia on cystathionine-γ-lyase expression during resuscitated murine septic shock. *Intensive Care Med Exp.* (2017) 5:30. doi: 10.1186/s40635-017-0140-7
50. Vogt JA, Wachter U, Wagner K, Calzia E, Gröger M, Weber S, et al. Effects of glycemic control on glucose utilization and mitochondrial respiration during resuscitated murine septic shock. *Intensive Care Med Exp.* (2014) 2:19. doi: 10.1186/2197-425X-2-19
51. Hartmann C, Hafner S, Scheuerle A, Möller P, Huber-Lang M, Jung B, et al. The role of cystathionine-γ-lyase in blunt chest trauma in cigarette smoke exposed Mice. *Shock.* (2017) 47:491–9. doi: 10.1097/SHK.0000000000000746
52. Manna P, Gungor N, McVie R, Jain SK. Decreased cystathionine-γ-lyase (CSE) activity in livers of type 1 diabetic rats and peripheral blood mononuclear cells (PBMC) of type 1 diabetic patients. *J Biol Chem.* (2014) 289:11767–78. doi: 10.1074/jbc.M113.524645
53. Gheibi S, Samsonov AP, Gheibi S, Vazquez AB, Kashfi K. Regulation of carbohydrate metabolism by nitric oxide and hydrogen sulfide: implications in diabetes. *Biochem Pharmacol.* (2020) 176:113819. doi: 10.1016/j.bcp.2020.113819
54. Lefer DJ. Potential importance of alterations in hydrogen sulphide (H_2S) bioavailability in diabetes. *Br J Pharmacol.* (2008) 155:617–9. doi: 10.1038/bjp.2008.359
55. Brancaleone V, Roviezzo F, Vellecco V, De Gruttola L, Bucci M, Cirino G. Biosynthesis of H_2S is impaired in non-obese diabetic (n.d.) mice. *Br J Pharmacol.* (2008) 155:673–80. doi: 10.1038/bjp.2008.296
56. Sun HJ, Wu ZY, Nie XW, Bian JS. Role of endothelial dysfunction in cardiovascular diseases: the link between inflammation and hydrogen sulfide. *Front Pharmacol.* (2020) 10:1568. doi: 10.3389/fphar.2019.01568

57. Sun HJ, Wu ZY, Nie XW, Wang XY, Bian JS. An updated insight into molecular mechanism of hydrogen sulfide in cardiomyopathy and myocardial ischemia/reperfusion injury under diabetes. *Front Pharmacol.* (2021) 12:651884. doi: 10.3389/fphar.2021.651884
58. Kaneko Y, Kimura Y, Kimura H, Niki I. L-cysteine inhibits insulin release from the pancreatic beta-cell: possible involvement of metabolic production of hydrogen sulfide, a novel gasotransmitter. *Diabetes.* (2006) 55:1391–7. doi: 10.2337/db05-1082
59. Yang W, Yang G, Jia X, Wu L, Wang R. Activation of KATP channels by H_2S in rat insulin-secreting cells and the underlying mechanisms. *J Physiol.* (2005) 569:519–31. doi: 10.1113/jphysiol.2005.097642
60. Xiong XQ, Wang WT, Wang LR, Jin LD, Lin LN. Diabetes increases inflammation and lung injury associated with protective ventilation strategy in mice. *Int Immunopharmacol.* (2012) 13:280–3. doi: 10.1016/j.intimp.2012.04.020
61. Dupuy V, Mayeur N, Buléon M, Jaafar A, Al Saati T, Schaak S, et al. Type 2 diabetes mellitus in mice aggravates the renal impact of hemorrhagic shock. *Shock.* (2012) 38:351–5. doi: 10.1097/SHK.0b013e318268810f
62. Marrie RA, Sellers EAC, Chen H, Fransoo R, Bernstein CN, Hitchon CA, et al. Markedly increased incidence of critical illness in adults with Type 1 diabetes. *Diabet Med.* (2017) 34: doi: 10.1111/dme.13404
63. Liou DZ, Singer MB, Barmparas G, Harada MY, Mirocha J, Bukur M, et al. Insulin-dependent diabetes and serious trauma. *Eur J Trauma Emerg Surg.* (2016) 42:491–6. doi: 10.1007/s00068-015-0561-5
64. Barrett CE, Park J, Kompaniyets L, Baggs J, Cheng YJ, Zhang P, et al. Intensive care unit admission, mechanical ventilation, and mortality among patients with type 1 diabetes hospitalized for COVID-19 in the U.S. *Diabetes Care.* (2021) 44:1788–96. doi: 10.2337/dc21-0604
65. Kompaniyets L, Agathis NT, Nelson JM, Preston LE, Ko JY, Belay B, et al. Underlying medical conditions associated with severe COVID-19 illness among children. *JAMA Netw Open* (2021) 4:e2111182. doi: 10.1001/jamanetworkopen.2021.11182
66. Renieris G, Katrini K, Damoulari C, Akinosoglou K, Psarrakis C, Kyriakopoulou M, et al. Serum hydrogen sulfide and outcome association in pneumonia by the SARS-CoV-2 coronavirus. *Shock.* (2020) 54:633–7. doi: 10.1097/SHK.0000000000001562
67. Dominic P, Ahmad J, Bhandari R, Pardue S, Solorzano J, Jaisingh K, et al. Decreased availability of nitric oxide and hydrogen sulfide is a hallmark of COVID-19. *Redox Biol.* (2021) 43:101982. doi: 10.1016/j.redox.2021.101982
68. Gorini F, Del Turco S, Sabatino L, Gaggini M, Vassalle C. H_2S as a bridge linking inflammation, oxidative stress and endothelial biology: a possible defense in the fight against SARS-CoV-2 infection? *Biomedicines.* (2021) 9:1107. doi: 10.3390/biomedicines9091107
69. Radermacher P, Calzia E, McCook O, Wachter U, Szabo C. To the editor. *Shock.* (2021) 55:138–9. doi: 10.1097/SHK.0000000000001602
70. Datzmann T, Merz T, McCook O, Szabo C, Radermacher P. H_2S as a therapeutic adjuvant against covid-19: why and how? *Shock.* (2021) 56:865–7. doi: 10.1097/SHK.0000000000001723
71. Dugbartey GJ, Alornyo KK, Ohene BO, Boima V, Antwi S, Sener A. Renal consequences of the novel coronavirus disease 2019 (COVID-19) and hydrogen sulfide as a potential therapy. *Nitric Oxide.* (2022) 120:16–25. doi: 10.1016/j.niox.2022.01.002

Conflict of Interest: The authors declare that the research was conducted in the absence of any commercial or financial relationships that could be construed as a potential conflict of interest.

Publisher's Note: All claims expressed in this article are solely those of the authors and do not necessarily represent those of their affiliated organizations, or those of the publisher, the editors and the reviewers. Any product that may be evaluated in this article, or claim that may be made by its manufacturer, is not guaranteed or endorsed by the publisher.

frontiers | Frontiers in Medicine

ORIGINAL RESEARCH
published: 09 May 2022
doi: 10.3389/fmed.2022.867796

A Porcine Sepsis Model With Numerical Scoring for Early Prediction of Severity

Attila Rutai[1†], Bettina Zsikai[1†], Szabolcs Péter Tallósy[1], Dániel Érces[1], Lajos Bizánc[1], László Juhász[1], Marietta Zita Poles[1], József Sóki[2], Zain Baaity[2], Roland Fejes[1], Gabriella Varga[1], Imre Földesi[3], Katalin Burián[2], Andrea Szabó[1], Mihály Boros[1‡] and József Kaszaki[1‡]*

[1] Institute of Surgical Research, Albert Szent-Györgyi Medical School, University of Szeged, Szeged, Hungary, [2] Institute of Medical Microbiology, Albert Szent-Györgyi Health Center and Medical School, University of Szeged, Szeged, Hungary, [3] Department of Laboratory Medicine, Albert Szent-Györgyi Health Center, University of Szeged, Szeged, Hungary

OPEN ACCESS

Edited by:
Andrey V. Kozlov,
Institute for Experimental and Clinical Traumatology (LBG), Austria

Reviewed by:
Marcin Filip Osuchowski,
Ludwig Boltzmann Institute for Experimental and Clinical Traumatology, Austria
Inge Bauer,
University Hospital of Düsseldorf, Germany

***Correspondence:**
József Kaszaki
kaszaki.jozsef@med.u-szeged.hu

[†] These authors have contributed equally to this work and share first authorship
[‡] These authors have contributed equally to this work and share last authorship

Specialty section:
This article was submitted to Intensive Care Medicine and Anesthesiology, a section of the journal Frontiers in Medicine

Received: 01 February 2022
Accepted: 06 April 2022
Published: 09 May 2022

Citation:
Rutai A, Zsikai B, Tallósy SP, Érces D, Bizánc L, Juhász L, Poles MZ, Sóki J, Baaity Z, Fejes R, Varga G, Földesi I, Burián K, Szabó A, Boros M and Kaszaki J (2022) A Porcine Sepsis Model With Numerical Scoring for Early Prediction of Severity. Front. Med. 9:867796. doi: 10.3389/fmed.2022.867796

Introduction: Sepsis can lead to organ dysfunctions with disturbed oxygen dynamics and life-threatening consequences. Since the results of organ-protective treatments cannot always be transferred from laboratory models into human therapies, increasing the translational potential of preclinical settings is an important goal. Our aim was to develop a standardized research protocol, where the progression of sepsis-related events can be characterized reproducibly in model experiments within clinically-relevant time frames.

Methods: Peritonitis was induced in anesthetized minipigs injected intraperitoneally with autofeces inoculum ($n = 27$) or with saline (sham operation; $n = 9$). The microbial colony-forming units (CFUs) in the inoculum were retrospectively determined. After awakening, clinically relevant supportive therapies were conducted. Nineteen inoculated animals developed sepsis without a fulminant reaction. Sixteen hours later, these animals were re-anesthetized for invasive monitoring. Blood samples were taken to detect plasma TNF-α, IL-10, big endothelin (bET), high mobility group box protein1 (HMGB1) levels and blood gases, and sublingual microcirculatory measurements were conducted. Hemodynamic, respiratory, coagulation, liver and kidney dysfunctions were detected to characterize the septic status with a pig-specific Sequential Organ Failure Assessment (pSOFA) score and its simplified version (respiratory, cardiovascular and renal failure) between 16 and 24 h of the experiments.

Results: Despite the standardized sepsis induction, the animals could be clustered into two distinct levels of severity: a sepsis ($n = 10$; median pSOFA score = 2) and a septic shock ($n = 9$; median pSOFA score = 8) subgroup at 18 h of the experiments, when the decreased systemic vascular resistance, increased DO_2 and VO_2, and markedly increased ExO_2 demonstrated a compensated hyperdynamic state. Septic animals showed severity-dependent scores for organ failure with reduced microcirculation despite the adequate oxygen dynamics. Sepsis severity characterized later with pSOFA scores was in correlation with the germ count in the induction inoculum ($r = 0.664$)

and CFUs in hemocultures ($r = 0.876$). Early changes in plasma levels of TNF-α, bET and HMGB1 were all related to the late-onset organ dysfunctions characterized by pSOFA scores.

Conclusions: This microbiologically-monitored, large animal model of intraabdominal sepsis is suitable for clinically-relevant investigations. The methodology combines the advantages of conscious and anesthetized studies, and mimics human sepsis and septic shock closely with the possibility of numerical quantification of host responses.

Keywords: sepsis, septic shock, fecal peritonitis, organ dysfunction, SOFA score, pig model, inflammatory markers

INTRODUCTION

Sepsis is defined as life-threatening organ dysfunction caused by a dysregulated host response to infection (1). Clinical characteristics have repeatedly been standardized in recent decades, and today the Sequential (sepsis-related) Organ Failure Assessment (SOFA) scoring system adequately characterizes the level of dysfunction of vital organs (2). In parallel, the recently established MQTiPSS (Minimum Quality Threshold in Pre-Clinical Sepsis Studies) recommendations for study designs enables us to standardize experimental sepsis, including the assessment of organ failure/dysfunction parameters (as described in Recommendation 12), which reflect the specificities of the human disease (3).

Nevertheless, it is recognized that the development of septic signs is determined by a number of individual reactions, all of which can mask the effects of interventions (4). Porcine models of sepsis have many advantages over rodent studies because domestic pigs are more closely related to humans in terms of anatomy, genetics and physiology (5, 6). Furthermore, pigs are more suitable for clinically-relevant anesthesia, instrumentation and intensive care, including invasive hemodynamic monitoring, fluid resuscitation and repetitive blood sampling (7). These characteristics allow for a more standardized induction and individual evaluation of disease progression and severity (8–10), but the need for anesthesia and observation time are still restrictive or limiting factors (8–10).

Unlike in many other areas, basic research with laboratory animals has not resulted in major therapeutic breakthroughs in this field, with one of the possible reasons being that better models are needed to translate the experimental results into clinical practice (4, 7, 11).

Based on this background, our objective was to improve the design of swine models of sepsis, with the final goal being to reduce heterogeneity and the gap between the messages of animal and human studies. In this context, our aim was to establish a standardized protocol, where the progression of events can be characterized in sufficient detail by a pig-specific SOFA (pSOFA) scoring system without the confounding effects of continuous anesthesia (10, 12).

In this line, tracking changes in oxygen dynamics and plasma mediators may be crucial in assessing the severity of the evolving septic reaction and organ damage (13–16). We hypothesized that the dynamics of typical indicators of systemic inflammation, such as tumor necrosis factor alpha (TNF-α) and interleukin-10 (IL-10), or biomarkers of tissue hypoxia and necrosis, such as big endothelin (bET) and high-mobility group box 1 protein (HMGB1), may be associated with numerical pSOFA score changes and that this relationship can therefore be useful in recognizing the development of organ dysfunctions in experimental sepsis.

MATERIALS AND METHODS

Animals

The experiments were performed on outbred Vietnamese minipigs of both sexes ($n = 36$, 35 ± 9 kg bw) in accordance with National Institutes of Health guidelines on the handling of and care for experimental animals and EU Directive 2010/63 on the protection of animals used for scientific purposes (approval number V/175/2018). The animals were fasted for 12 h with free access to tap water before the start of the procedures.

Experimental Protocol

The study was divided into four stages: (1) baseline measurements and baseline blood sampling under temporary anesthesia; (2) induction of sepsis with intraperitoneal (ip) fecal inoculum or sham-operation with ip sterile saline at time zero of the experiment; (3) progression of sepsis in extubated, unrestrained, awake animals for 15 h; and (4) re-anesthesia, instrumentation and monitoring between 16 and 24 h with pSOFA scoring. The experimental protocol for the sham-operated animals followed the same four stages.

Sample size was estimated with a 0.33 ratio of control to experimental animals assuming ∼20% mortality after septic induction. If the presumed true hazard ratio of septic subjects relative to controls is 0.2 with a power of $1 - \beta = 0.9$ and the Type I error probability is $\alpha = 0.05$, the inclusion of nine control and 27 septic animals was recommended based on the survival estimate.

Animals were randomly assigned into sham-operated (Group 1, $n = 9$) and septic (Group 2, $n = 27$) groups. As no septic reaction was observed in five animals in the septic group during the entire study period, these non-responders were later excluded from the study. A further three animals had to be humanely euthanized before stage 4 due to the fulminant septic reaction they developed (see below). Therefore, data from $n = 19$ animals in the septic group were finally used in the subsequent evaluations.

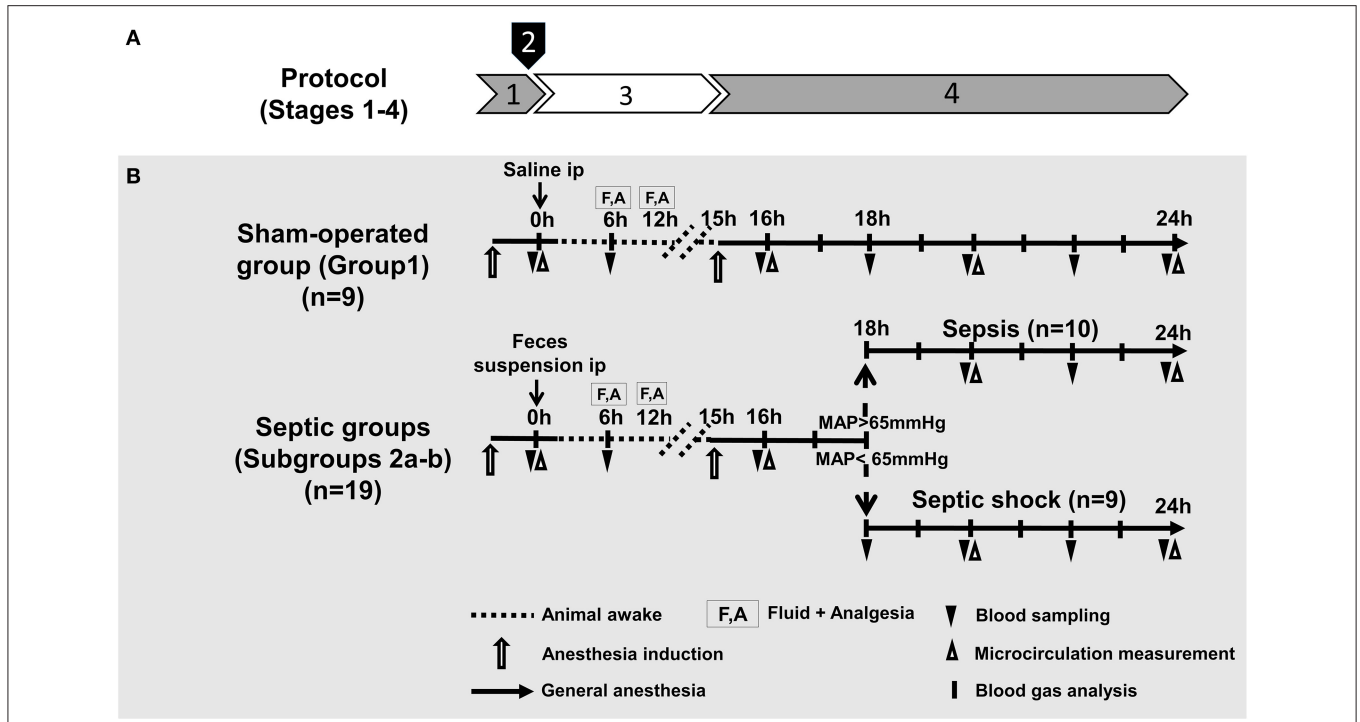

FIGURE 1 | Experimental stages **(A)**, experimental protocol, groups, interventions and assessments **(B)**. **(A)** Experimental stages: (1) baseline measurements (under temporary anesthesia); (2) sepsis induction with intraperitoneal (ip) fecal inoculum; (3) sepsis progression (in awake animals); and (4) re-anesthesia, instrumentation, monitoring and scoring **(B)**. Groups: The animals were randomly assigned into sham-operated and septic groups. Based on disease severity and vasopressor requirement (at 18 h after sepsis induction), animals in the septic group were allocated into sepsis and septic shock subgroups.

Based on disease severity and vasopressor requirement, septic animals were allocated into two subgroups, a sepsis (Subgroup 2a; $n = 10$) and a septic shock group (Subgroup 2b; $n = 9$) 18 h after induction. More specifically, the allocation was based on the consensus criteria of the 'Sepsis-3' definitions (sepsis involves proven organ damage, with a SOFA score $\geq$2; lactate level $\geq$2 mmol L^{-1}; septic shock is sepsis with persistent hypotension, requiring vasopressors to maintain mean arterial pressure (MAP) $\geq$65 mmHg despite adequate fluid resuscitation) (**Figure 1**).

Stage 1. Baseline Measurements and Baseline Blood Sampling Under Temporary Anesthesia

Anesthesia was induced with an intramuscular mixture of tiletamine-zolepam (Zoletil, Virbac, Carros, France 5 mg kg^{-1}) and xylasin (2 mg kg^{-1}) and continued with an infusion of a mixture of propofol (6 mg $kg^{-1}h^{-1}$ iv; Fresenius Kabi, Bad Homburg, Germany), fentanyl (0.02 mg $kg^{-1}h^{-1}$; Richter Gedeon, Budapest, Hungary) and midazolam (1.2 mg kg^{-1} h^{-1}; Torrex Chiesi Pharma, Vienna, Austria) through an ear vein Braun cannula. A permanent central venous catheter with three lumina (7 F; Edwards Lifesciences LLC, Irvine, U.S.A) was introduced into the jugular vein using an aseptic surgical technique for fluid therapy and blood sampling.

Endotracheal intubation was performed, and the animals were ventilated mechanically (Carescape R860, GE Healthcare, Madison, Wisconsin, U.S.A.). Basic ventilation settings [respiratory rate (RR): 10–12 min^{-1}; tidal volume (TV): 8 mL kg^{-1}; positive end-expiratory pressure (PEEP): 4–5 cmH_2O; fraction of inspired oxygen (FiO_2): 21%] were checked by pulse oximetry (OxiPen®; EnviteC, Wismar, Germany) using a sensor fitted to the tongue of the animals. The adequacy of the depth of anesthesia was assessed by monitoring the jaw tone and the pain reaction of the hind leg regularly. The central venous catheter was used for blood sampling at $t = 0$ h and for fluid administration (10 mL kg^{-1} Ringerfundin®, B. Braun, Melsungen, Germany). Heart rate (HR) and oxygen saturation were detected by pulse oximetry, and the sublingual microcirculation was monitored by intravital videomicroscopy (see below).

Stage 2. Sepsis Induction

Polymicrobial peritonitis was induced with an ip administered autologous feces suspension. Fecal induction inoculum was injected through a 1-cm incision at the umbilicus using a blunt-pointed 12G Veress needle at $t = 0$ h. The sham-operated animals received 200 mL sterile saline ip in the same manner.

Preparation of the Sepsis-Inducing Fecal Inoculum

Autologous fresh feces was collected and suspended in 200 ml saline with a 0.6 g kg^{-1} final concentration 6 h before the scheduled intra-abdominal injection. The inoculum was incubated in a water bath for 6 h at 37°C, and the suspension was filtered to remove the pellet. For microbiological analysis, 0.1 mL

samples were taken from the suspension before ip administration to determine the microbial concentration (in colony-forming units; CFU mL^{-1}) with the standard viable plate count method under aseptic conditions. Readings of CFUs were obtained retrospectively 12 h after sepsis induction and converted to the cell numbers per milliliter inoculum.

The microbial composition of the inoculum was analyzed for the most frequent species by MALDI-TOF mass spectrometry (MS; Bruker Daltonics, Germany) as described earlier (17). Briefly, parallel to the injection of the sepsis inoculum to the animals, 0.1 mL of the fecal suspension was spread on Mueller–Hinton solid media (Bio-Rad, Budapest, Hungary) to isolate the aerobic strains after a 12-h incubation period (37°C). Anaerobic strains were inoculated on a Columbia agar base (Oxoid, Budapest, Hungary) supplemented with 5% (v/v) bovine blood, hemin (1 mg/mL) and vitamin K1 (5 mg/mL) for 48 h (37°C). Fungal and yeast species were isolated on Sabouraud dextrose agar (Bio-Rad, Budapest, Hungary). The spectra from the microbiological samples were acquired using the Microflex LT system (Bruker Daltonik, Bremen, Germany) and analyzed with MALDI Biotyper 3.3 (Bruker, Daltonik) software (18).

Stage 3. Sepsis Progression

After induction, the animals were extubated and awakened with the gradual reduction of anesthesia and mechanical ventilation. The spontaneously breathing septic and sham-operated animals were placed in a test cage and observed for visible signs of sepsis progression, and a blood sample was taken 6 h after sepsis induction. The animals in both groups received 15 mL $kg^{-1}h^{-1}$ crystalloid iv at 6 h and 12 h after sepsis induction to maintain fluid balance (Ringerfundin®, B. Braun, Melsungen, Germany), while analgesia was performed with nalbuphine iv (0.2 mg kg^{-1}; Orpha-Devel Handels und Vertriebs GmbH, Austria) through the jugular vein.

Stage 4. Invasive Hemodynamic Monitoring, Sampling and Severity Scoring

The animals were re-anesthetized 15 h after sepsis induction with an iv mixture of ketamine (2.5 mg kg^{-1}) and xylazine (0.5 mg kg^{-1}), and anesthesia was maintained with a continuous infusion of propofol (6 mg $kg^{-1}h^{-1}$ iv; Fresenius Kabi, Bad Homburg, Germany), midazolam (1.2 mg $kg^{-1}h^{-1}$; Torrex Chiesi Pharma, Vienna, Austria) and fentanyl (0.02 mg $kg^{-1}h^{-1}$; Richter Gedeon, Budapest, Hungary). The adequacy of the depth of anesthesia was assessed by monitoring the jaw tone and the pain reaction of the hind leg regularly. After reintubation, mechanical ventilation was started, the settings (RR: 10–12 min^{-1}; TV: 10 mL kg^{-1}; PEEP: 4–5 cmH_2O; FiO_2: 21%) were checked and adjusted based on arterial and venous blood gas values (pH: 7.35–7.45; arterial partial carbon dioxide pressure ($PaCO_2$): 35–45 mmHg (4.6–5.9 kPa), PaO_2/FiO_2 ratio > 400) during the monitoring period. After induction of anesthesia, the right femoral artery was dissected free using an aseptic technique, and a thermistor-tip transpulmonary thermodilution catheter (PiCCO, PULSION Medical Systems SE, Munich, Germany) was placed in the right femoral artery for invasive hemodynamic monitoring and core temperature measurement. A urinary catheter was placed surgically in the bladder via an inguinal incision to measure hour diuresis (mL kg^{-1} h^{-1}).

The monitoring period for SOFA scoring started 16 h after induction on sepsis. Hemodynamic measurements, blood gas analysis and an assessment of organ failure were performed hourly between 16 and 24 h of the experiments. Cardiac output (CO) and cardiac index (CI) were measured by transpulmonary thermodilution analysis, HR and MAP were monitored with the pressure sensor of a transpulmonary thermodilution system. All hemodynamic parameters were indexed for body surface area or body weight. Central venous pressure (CVP) was measured via a central venous catheter at the same times as the other hemodynamic variables. Blood gases were analyzed with a cooximetry blood gas analyzer (Cobas b 123, Roche Ltd., Basel, Switzerland) simultaneously every hour.

Oxygen delivery (DO_2) = CO × [(1.38 × Hb × SaO_2) + (0.003 × PaO_2)], oxygen consumption (VO_2) = CO × [(1.38 × Hb × (SaO_2- SvO_2)) + (0.003 × PaO_2)] and oxygen extraction (ExO_2) = DO_2 VO_2^{-1} values were calculated. The degree of respiratory failure was determined using the PaO_2/FiO_2 ratio. The vascular resistance index (SVRI) and stroke volume index (SVI) were calculated according to standard formulas (SVRI = MAP-CVP CO^{-1}; SVI = CI HR^{-1}).

Fluid resuscitation was started during the monitoring period with combinations of balanced crystalloid solutions (Ringerfundin®, Ringer-lactate®, Sterofundin G®, B. Braun, Melsungen, Germany) of 15 mL kg^{-1}. Goal-directed fluid resuscitation was performed to achieve physiological SVI values (SVI: 35–45 mL $beat^{-1}$ m^{-2}). The volume and type of crystalloid infusion were guided by continuously monitored CVP (5–8 mmHg) pulse pressure variance (8–12%), extravascular lung water index (ELWI: 6–8 ml kg^{-1}) and venous glucose (4.1–5.6 mmol L^{-1}) values (19).

Detection of Organ Functions, and Metabolic and Inflammatory Markers

Blood samples were taken from the central venous line and placed in precooled, EDTA-containing tubes, centrifuged (1,200 g at 4°C for 10 min) and stored at −70°C until assay. Liver dysfunction was assessed by measuring plasma bilirubin, aspartate aminotransferase (AST) and alanine aminotransferase (ALT) levels, whereas the extent of kidney injury was estimated by measuring plasma creatinine and albumin levels using a Roche/Hitachi 917 analyzer (F. Hoffmann-La Roche AG, Switzerland). The lactate level as an indicator of metabolic imbalance was measured from venous blood samples (Accutrend Plus Kit, Roche Diagnostics Ltd., Rotkreuz, Switzerland). All analyses were performed on coded samples in a blinded fashion. Plasma levels of TNF-α and IL-10 as well as bET and HMGB1 were determined from these samples using commercial ELISA kits (Cusabio Biotechnology Ltd., Wuhan, China and Biomedica Ltd., Vienna, Austria, respectively) according to manufacturer's instructions.

Blood Cell Counts

Samples for platelet, white blood cell and red blood cell counts were placed in EDTA-coated tubes and analyzed within 4 h

with an automated cell counter (based on electrical impedance, Sysmex XE2100, Japan).

Blood Culture Analysis

Five mL blood samples were obtained from the right jugular vein of 14 randomly selected animals in the septic group at 18 h of the experiments with the aseptic technique and then transferred to aerobic and anaerobic media bottles. BD BACTEC Plus/Anaerobic/F bottles (Becton Dickinson, Hungary) were used in a qualitative procedure to identify microbial occurrence in the blood samples as another part of the microbial profile. Then, the pairs of blood culture bottles were immediately transferred to the microbiology laboratory for analysis. The bottles were incubated in a BD BACTEC™ FX blood-culturing instrument (Becton Dickinson, UK) until positive signaling from the system occurred. Bottles containing blood without bacteria were used and incubated for 24 h as a control measurement. Microorganisms were identified according to manufacturer's instructions in the MALDI-TOF MS (Bruker Daltonics, Germany), as described before (18).

Calculation of pSOFA Scores

Similarly to the human SOFA and quick SOFA scores, we established two scoring systems for the pigs consisting of three or five domains of organ/organ system dysfunction parameters. The 3-domain-pSOFA (3D-pSOFA) score involves respiration, MAP and hour diuresis, which can be determined based on readings of online measurements, while the 5-domain-pSOFA (5D-pSOFA) score also includes additional laboratory tests (i.e. bilirubin and platelet count) (**Table 1**).

As a respiratory parameter, the PaO_2/FiO_2 ratio was used with threshold values similar to those in humans, but, in the case of MAP (used as a cardiovascular parameter), the blood pressure-lowering effect of continuous anesthesia and analgesia (10) was also taken into consideration. Therefore, MAP values above 75 mmHg were considered normal (SOFA = 0). Due to the relatively short observation period, the common first-line vasoactive drug norepinephrine was used for vasopressor therapy due to its efficacy, potency and safer dosing compared to dopamine (19). Norepinephrine was administered if MAP decreased to 55 mmHg and if it did not respond to at least 60 min of crystalloid resuscitation.

During 3D- or 5D-pSOFA scoring, urine output (and not serum creatinine level) was used as an indicator of renal dysfunction (**Table 1**). Furosemide (10 mg; iv) administration was initiated if urine output was low (<0.25 mL kg^{-1} h^{-1}) despite the fluid administration or in the case of elevated ELWI (>10 mL kg^{-1}). Repeated furosemide was administered if urine output and/or ELWI did not respond to the previous dose.

In addition to these parameters, the 5D-pSOFA score was also included (similarly to the human SOFA score) as well as platelet counts and plasma bilirubin values. Since pigs display a broader platelet count range than humans (10), values up to 200 10^9 L^{-1} were considered normal (pSOFA scores $t = 0$ h; **Table 1**). We used the same threshold values for bilirubin as those used in human SOFA scoring. We also calculated the De Ritis ratio (AST/ALT) to detect liver damage and injury of non-liver cells (kidney, heart and muscle cells), but, ultimately, it was not used for scoring.

Before stage 4, we continuously evaluated the activity and alertness of the pigs to assess the well-being of the awake animals. We used a semi-quantitative 0–1 scoring system, but this neurological assessment was not incorporated into the pSOFA scoring system, as it was not considered to be equivalent to the human Glasgow Coma Score.

Intravital Videomicroscopy

The Incident Dark Field (IDF) imaging technique (CytoCam Video Microscope System, Braedius Medical, Huizen, the Netherlands) was used for a non-invasive, contrast agent-free examination of the sublingual microcirculation. Cytocam-IDF imaging is optimized for visualization of hemoglobin-containing structures by illuminating the tissue surface with linearly polarized light and detecting the reflected light with a computer-controlled sensor (20, 21). Microcirculatory measurements were performed at $t = 0$, 16, 20 and 24 h, and the images were captured and recorded in six, 50-frame-long, high-quality video clips (spatial resolution 14 megapixels; temporal resolution 60 fps). Each video was recorded at separate locations of the sublingual area by the same investigator and saved as digital AVI-DV files to a hard drive. Every video clip was divided into four quarters and was determined by offline software-assisted analysis (AVA 3.0; Automated Vascular Analysis, Academic Medical Center, University of Amsterdam). The proportion of perfused vessels (PPV) was calculated as the ratio of the length of vessels with measurable flow to the length of all detected vessels (%) (22, 23).

Statistical Analysis

Data analysis was performed with a statistical software package (SigmaStat for Windows, Jandel Scientific, Erkrath, Germany). Normality of data distribution was analyzed with the Shapiro–Wilk test. The Friedman analysis of variance on ranks was applied within groups. Time-dependent differences from the baseline for each group were assessed with Dunn's method. In this study, differences between groups were analyzed with the Kruskal–Wallis one-way analysis of variance on ranks, followed by Dunn's method. Median values and 75th and 25th percentiles are provided in the figures; P values <0.05 were considered significant. Correlations between two variables were examined using the Spearman Rank correlation coefficient (r); regression lines and 95% confidence intervals are given in the figures.

RESULTS

Despite the standardized sepsis induction protocol used in 27 pigs, eight experiments had to be excluded from the analysis for objective reasons. As noted before, five pigs were non-responders (non-septic) (**Supplementary Table 1**), showing higher values only in oxygen dynamic parameters and lower plasma albumin values compared to sham-operated animals between 18 and 24 h of the experiment. Another three pigs acted as over-responders with a fulminant septic reaction. These animals were humanely

TABLE 1 | The pig-specific Sequential Organ Function Assessment (pSOFA) scoring system with 3 or 5 domains (3D-pSOFA and 5D-pSOFA scores) to assess sepsis-induced organ dysfunction.

pSOFA scores		Organ dysfunction	Parameters	Score values					Need for laboratory analytics	Detection time
				0	1	2	3	4		
5D-pSOFA score	**3D-pSOFA score**	Respiration	PaO_2/FiO_2 ratio	≥400	<400	<300	<200	<100	No	Online (continuous)
		Cardiovascular	MAP (mmHg)	≥75	<75	<65	N<0.1	N>0.1	No	Online (continuous)
				(≥70)	*(<70)*	*(D < 5 or Db)*	*(D > 5.1 or E ≤ 0.1 or N ≤ 0.1)*	*(D > 15 or E > 0.1 or N > 0.1)*		
		Renal	Urine output (mL kg^{-1} h^{-1})	>0.5	<0.5	<0.25	F < 10	F > 10	No	Online (continuous)
				-	-	-	*(< ~0.25)*	*(> ~0.13)*		
		Liver	Bilirubin (μmol L^{-1})	<20	>20	>32	>101	>204	Yes	Hours
		Coagulation	Platelet Count (x10^9 L^{-1})	≥200 *(≥150)*	<200 *(<150)*	<150 *(<100)*	<100 *(<50)*	<50 *(<20)*	Yes	Hours

Arterial partial pressure of oxygen dissolved in the plasma (PaO_2); fraction of inspired oxygen (FiO_2); mean arterial pressure (MAP); N, norepinephrine; D, dopamine; Db, dobutamine; E, epinephrine; F, furosemide. Catecholamine doses are given as μg kg^{-1} min^{-1} and furosemide doses as mg.
Human reference values (if different) are also shown (in italics). The 3D-pSOFA scoring system contains parameters which do not require laboratory diagnostics and can be evaluated continuously, thus allowing for closer monitoring. The 5D-pSOFA scoring system provides more information by assessing blood coagulation and liver function at the price of time-consuming laboratory tests.

terminated (between 6 and 15 h of the study). The severity of their condition was characterized by signs of acute respiratory and/or circulatory failure, early (6 h) rise in lactate, bilirubin and hemoglobin levels, and steep decreases in venous oxygen saturation and albumin levels (**Supplementary Table 2**). Data from the non-septic and terminated animals are not included in further results.

Changes in pSOFA Scores

In the septic animals, the average 3D-pSOFA scores ranged from 1 to 3, while the score reached values between 5 and 9 in the case of septic shock (**Figure 2A**). In the septic shock subgroup, significantly higher 3D-pSOFA and 5D-pSOFA scores were detected than those in the sham-operated group and sepsis subgroup throughout the 8-h observation period (**Figures 2B,C**). A significant difference was observed between the sham-operated and septic groups at 24 h after the sepsis induction for both scores. As compared to $t = 16$ h, a temporal deterioration in the condition of the animals with septic shock was evident in the last 2–3 h of the experiments with both scores.

Changes in Different Components of pSOFA Scores and in Biomarkers of Organ Dysfunction

Significantly lower MAP, urine output and platelet count values were evidenced in animals with septic shock than those seen in sham-operated animals during the entire 8-h observation period (**Figures 3A,B,D**). A temporary hypotension also developed in the sepsis subgroup in the last two hours (**Figure 3A**). Deteriorations in urine output and in PaO_2/FiO_2 ratio reached a similar extent in the sepsis and septic shock subgroups at most examined time points (**Figures 3B,C**). A progressive decrease in platelet count was observed in all groups during the last 3 h of the study period, with the lowest values in the septic shock subgroup (**Figure 3D**). As compared to the sham-operated animals, only the septic shock subgroup showed significant elevations in plasma bilirubin concentrations and in the (hepatic and non-hepatic cell degradation marker) AST/ALT ratio (De Ritis ratio), which occurred during the last 3–4 hours of the study (**Figures 3E,F**). Plasma creatinine levels were also higher in the septic shock subgroup than in the other groups (**Figure 3G**), and we only found a negative correlation between plasma creatinine levels and the decreased urine output in the septic shock group ($r = -0.352$) (**Supplementary Figure 1**). A progressive decrease in plasma albumin levels was observed in all the groups. As compared to sham-operated animals, septic shock was always associated with significantly lower albumin values, and the animals in the sepsis subgroup also showed temporarily lower albumin values during $t = 16$–24 h of the study (**Figure 3H**).

Blood Cell Counts

White blood cell counts did not change in the sham-operated groups, while significant leucopenia developed after 16 h of sepsis induction in both sepsis-inoculated groups (**Figure 4A**). The red blood cell counts did not change in any of the groups studied (data not shown). Whole blood lactate showed some degree of elevation at 6 h after induction in both septic groups, but it only reached significantly higher values in the septic shock group, which persisted during the entire period $t = 16$–24 h (**Figure 4B**).

Hemodynamic Changes

In both sepsis-inoculated groups, a significant increase in HR and a significant decrease in stroke volume were observed during the

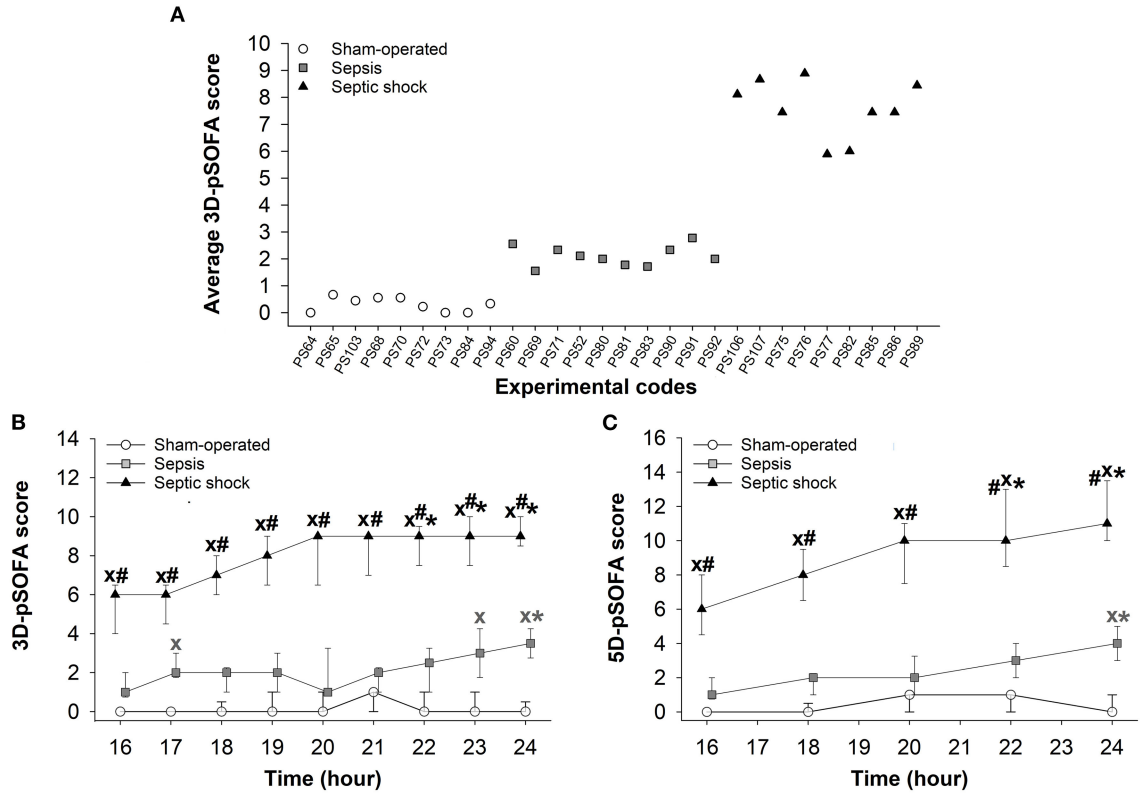

FIGURE 2 | Average values for basic pSOFA scores in individual animals during the 8-h invasive monitoring period (during $t = 16$–24 h) **(A)** in the sham-operated group (open circles) and the sepsis (gray square) and septic shock subgroups (black triangle). Changes in 3D-pSOFA **(B)** and 5D-pSOFA **(C)** values as a function of time in the sham-operated group and the sepsis and septic shock subgroups. The plots demonstrate the median values and the 25th (lower whisker) and 75th (upper whisker) percentiles. $^{X}P < 0.05$ vs. sham-operated group; $^{\#}P < 0.05$ vs. sepsis group; $^{*}P < 0.05$ vs. $t = 16$ h.

entire examination period and temporary decreases also occurred in systemic vascular resistance (**Figures 5A,C,D**). In the septic shock group, cardiac index also deteriorated during the last two hours of the experiments (**Figure 5B**).

Changes in Oxygen Dynamics and Microcirculation

The 24-h sepsis progression markedly affected the oxygen dynamic parameters. Although no differences were observed in DO_2 (**Figure 6A**), significantly increased VO_2 values were measured in septic shock subgroup at 18 and 24 h compared to the sham-operated animals (**Figure 6B**). Both sepsis-challenged groups showed a significantly elevated degree of oxygen extraction (**Figure 6C**) and septic shock was associated with significantly deteriorated microvascular perfusion (reduced PPV values) in the sublingual mucosa (**Figure 6D**).

Microbial Features of the Inducer Inoculum

Different CFU ranges in the sepsis-inducer inoculum caused a different degree of sepsis severity. The retrospective microbiological analysis demonstrated that the microbial concentration of the inoculum ranged between 6.2×10^5 and 1.6×10^{10} CFU and that concentrations under 1.34×10^7 CFU did not result in a septic reaction in the 24 h period of the experiment ($n = 5$, non-responder subgroup). Concentrations above 4×10^8 CFU increased the likelihood of sepsis and septic shock, while CFU values above 8×10^9 resulted in a devastating condition with quick deterioration in animal well-being ($n = 3$, 8×10^9-1.6×10^{10} CFU). The most common microorganisms found in the feces suspension were *Escherichia coli* and *Klebsiella pneumoniae*, which generally cause Gram-negative sepsis in humans. The occurrence of *Escherichia coli* was 100% in the fecal samples. We also found several *Lactobacilli* species, which are indicators of normal microbiota but can also cause sepsis under dysbiotic conditions or when the intestinal epithelial layer is injured (**Supplementary Table 3**).

Relationship Between Microbiological Concentrations and pSOFA Scores

The correlation between the severity of organ dysfunction and the concentration of injected microorganisms or the presence of microbes in the blood samples were analyzed further in septic animals. There was a moderate, significant positive correlation between the inoculum CFUs and the 3D-pSOFA ($r = 0.677$) and

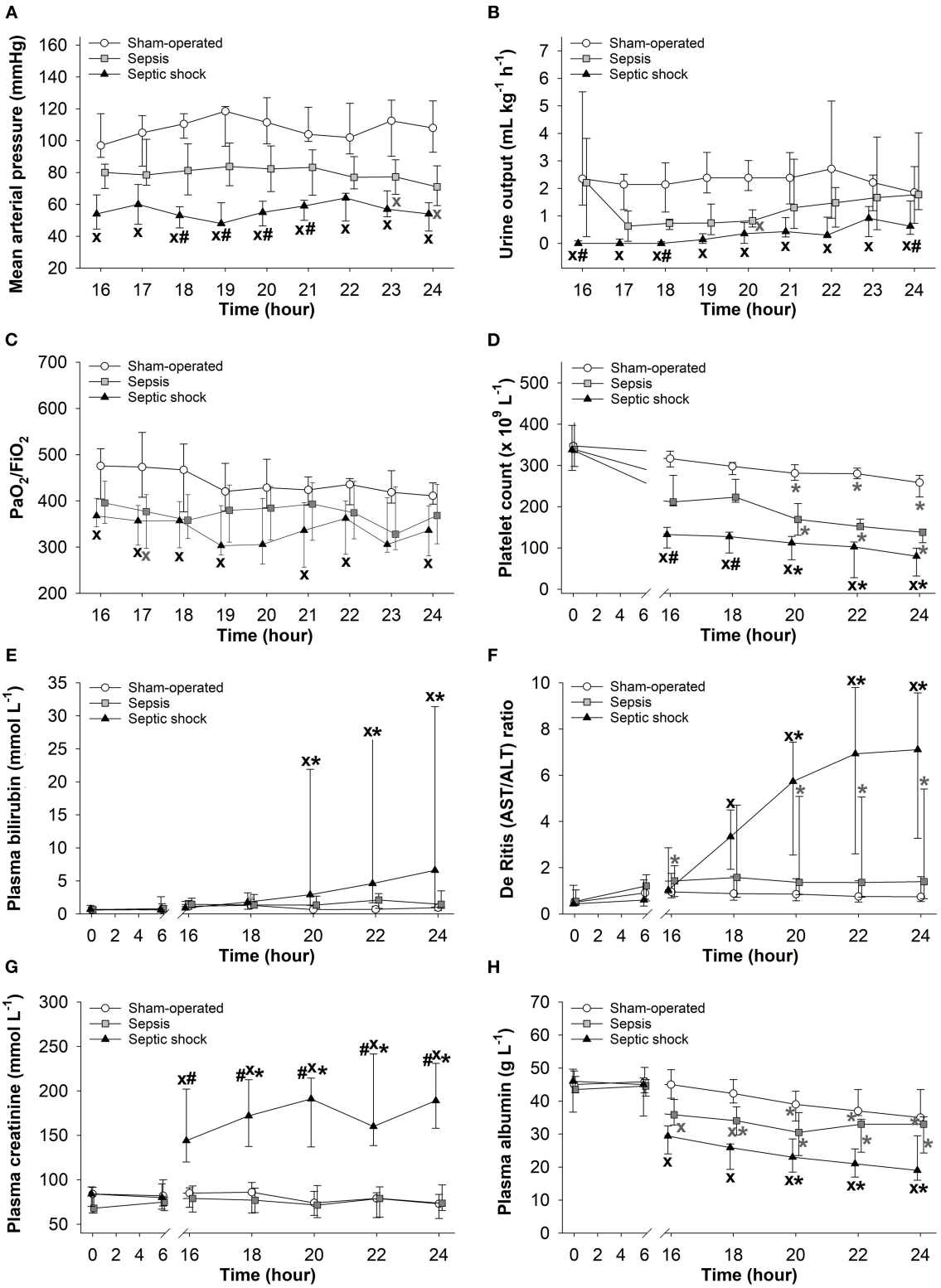

FIGURE 3 | Changes in mean arterial pressure **(A)**, urine output **(B)**, PaO_2/FiO_2 ratio **(C)**, platelet count **(D)**, plasma bilirubin **(E)**, De Ritis (AST/ALT) ratio **(F)**, plasma creatinine **(G)**, and plasma albumin levels **(H)** in the sham-operated group (open circles) and the sepsis (gray square) and septic shock subgroups (black triangle). The plots demonstrate the median values and the 25th (lower whisker) and 75th (upper whisker) percentiles. $^{X}P < 0.05$ vs. sham-operated group; $^{\#}P < 0.05$ vs. sepsis group; **(A–D)** $^{*}P < 0.05$ vs. $t = 16$ h; **(E–H)** $^{*}P < 0.05$ vs. $t = 0$ h.

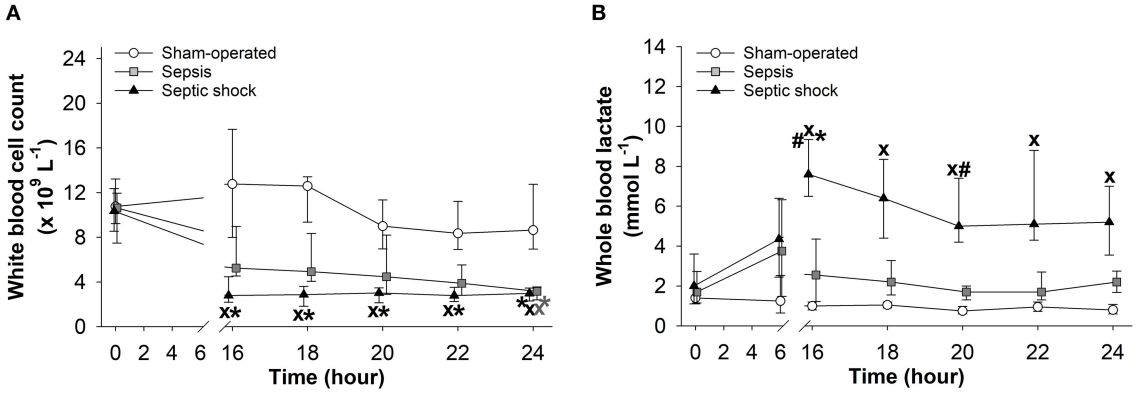

FIGURE 4 | Changes in white blood cell count **(A)** and whole blood lactate levels **(B)** in the sham-operated group (open circles) and the sepsis (gray square) and septic shock subgroups (black triangle). The plots demonstrate the median values and the 25th (lower whisker) and 75th (upper whisker) percentiles. $^{X}P < 0.05$ vs. sham-operated group; $^{\#}P < 0.05$ vs. sepsis group; $^{*}P < 0.05$ vs. $t = 0$ h.

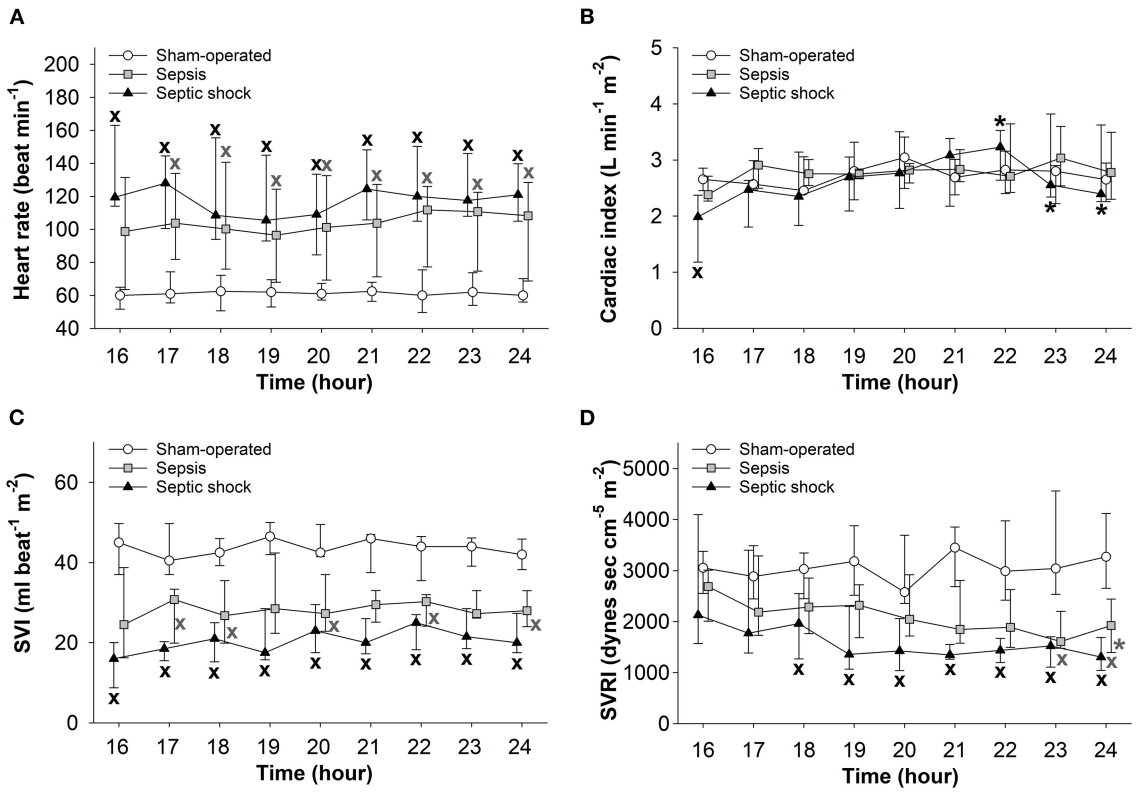

FIGURE 5 | Changes in heart rate **(A)**, cardiac index **(B)**, stroke volume index (SVI) **(C)**, and systemic vascular resistance index (SVRI) **(D)** in the sham-operated group (open circles) and the sepsis (gray square) and septic shock subgroups (black triangle). The plots demonstrate the median values and the 25th (lower whisker) and 75th (upper whisker) percentiles. $^{X}P < 0.05$ vs. sham-operated group; $^{*}P < 0.05$ vs. $t = 16$ h.

the 5D-pSOFA score values ($r = 0.664$; $n = 19$) (**Figure 7A**). The concentration of microbes in the blood culture showed a strong, significant correlation ($r = 0.866$, $P < 0.001$) with both the 3D-pSOFA and the 5D-pSOFA score values ($n = 14$) (**Figure 7B**).

Changes in Plasma Levels of Inflammatory Biomarkers

As compared to the baseline, plasma TNF-α concentration peaked at 6 h after sepsis induction, and this significant elevation persisted during the entire period of invasive hemodynamic

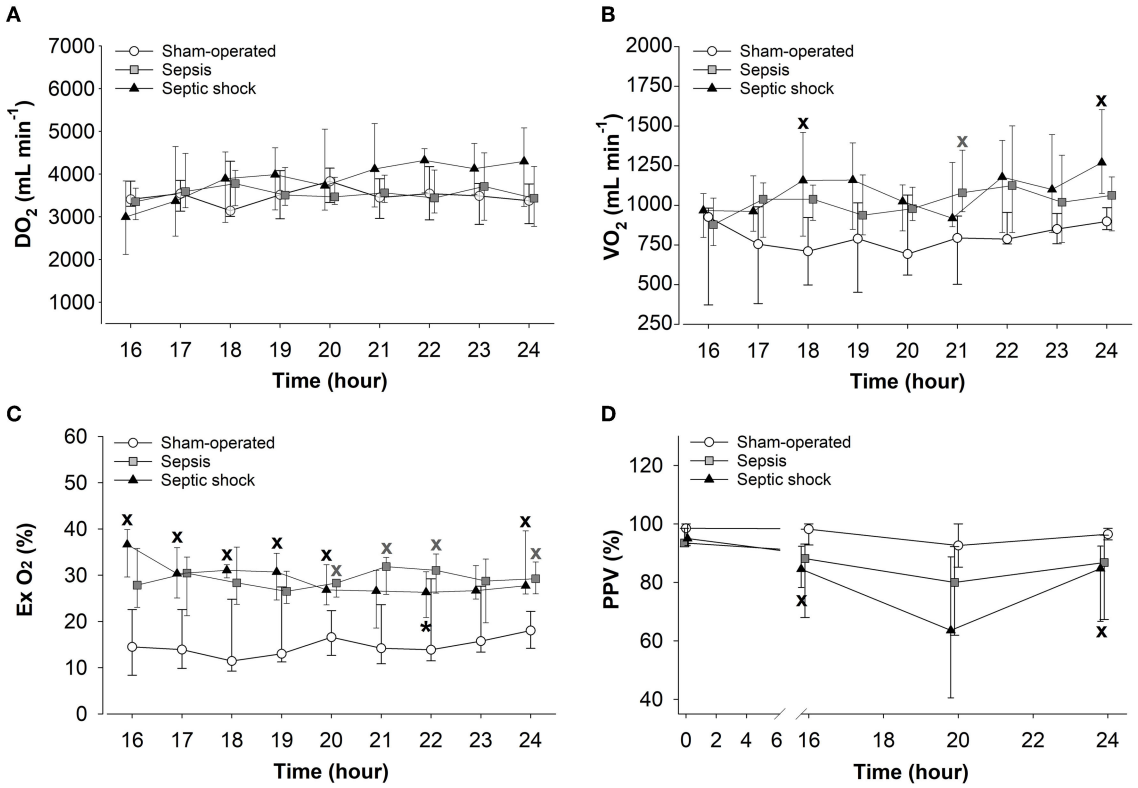

FIGURE 6 | Changes in oxygen delivery (DO_2) **(A)**, oxygen consumption (VO_2) **(B)**, oxygen extraction (Ex O_2) **(C)**, and the proportion of perfused vessels (PPV) **(D)** in the sham-operated group (open circles) and the sepsis (gray square) and septic shock subgroups (black triangle). The plots demonstrate the median values and the 25th (lower whisker) and 75th (upper whisker) percentiles. $^{X}P < 0.05$ vs. sham-operated group; $^{*}P < 0.05$ vs. $t = 16$ h.

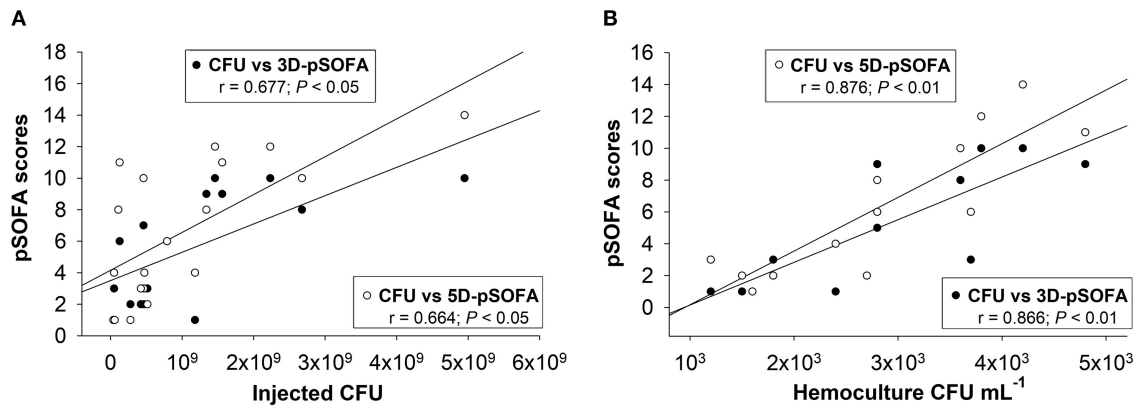

FIGURE 7 | Correlation between the concentration of injected microorganism in feces and the pSOFA score values **(A)**. Correlation between the microbial concentration in the hemoculture and the pSOFA score values **(B)**.

monitoring in the septic shock subgroup (**Figure 8A**). In this phase, similar TNF-α levels were detected in both septic groups. Plasma levels of IL-10 also showed a peak at 16 h in both septic groups (**Figure 8B**). Plasma levels of bET and HMGB1 only increased in the septic shock subgroup at 16–24 h post-inoculation (**Figures 8C,D**).

Correlation Between Plasma Biomarkers and pSOFA Scores

We found significant correlations between the 6-h TNF-α (**Figure 9A**), the 16-h bET (**Figure 9C**) and the 16-h HMGB1 levels (**Figure 9D**) as well as the 24-h 3D- and 5D-pSOFA scores. However, we did not find any correlation between the

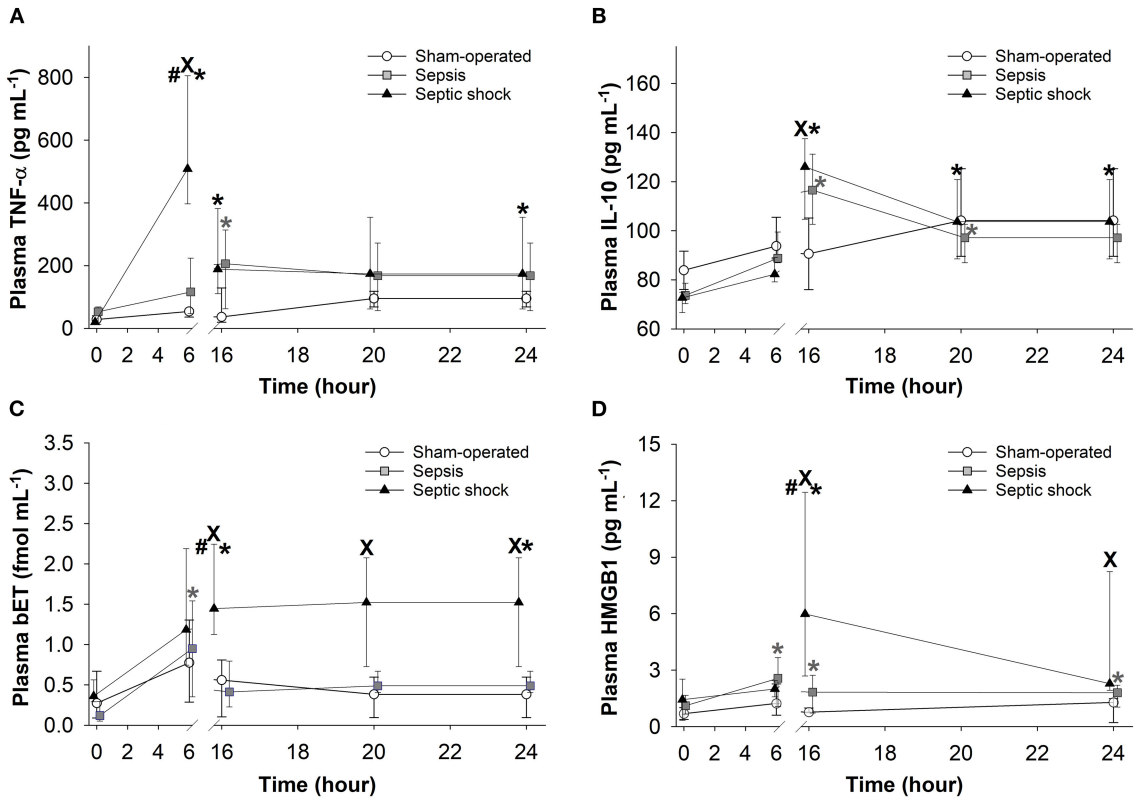

FIGURE 8 | Changes in plasma tumor necrosis factor alpha (TNF-α) **(A)**, interleukin-10 (IL-10) **(B)**, big endothelin (bET) **(C)**, and high-mobility group box 1 protein (HMGB1) **(D)** levels in the sham-operated group (open circles) and in the sepsis (gray square) and septic shock subgroups (black triangle). The plots demonstrate the median values and the 25th (lower whisker) and 75th (upper whisker) percentiles. $^{X}P < 0.05$ vs. sham-operated group; $^{\#}P < 0.05$ vs. sepsis group; $^{*}P < 0.05$ $t = 0$ h.

16-h IL-10 values and the 24-h 3D- or 5D-pSOFA scores (**Figure 9B**).

DISCUSSION

Overview of the Experimental Model

Here we present a porcine model of polymicrobial, intraabdominal sepsis with clinically relevant hemodynamic responses, a laboratory profile, inflammatory biomarkers and bacteremia. We also introduce a simple and a more complex pSOFA scoring system to assess organ dysfunction according to the Sepsis-3 criteria. Further, we have established the predictive significance of plasma biomarkers indicative of inflammation, tissue hypoxia or necrosis to diagnose late-onset organ damage. It should be added that the protocol was designed according to the recommendations of the MQTiPSS guidelines with respect to infection types, study design, assessment of organ failure, proper analgesia, fluid resuscitation and humane endpoints (3).

This setup combines the advantages of conscious, anesthetized *in vivo* models, while adhering to ethical standards on the use of animals for scientific purposes. After a relatively short (∼45 min) general anesthesia with limited instrumentation, sepsis develops in a conscious state. Non-invasive monitoring with adequate postoperative analgesia and restrictive fluid therapy is then maintained in the first 15 h of progression. After re-anesthesia, animals can safely be subjected to extensive invasive instrumentation, with complex monitoring and resuscitation for at least 8 h. A minor limitation is that a design with an observation time of this length or longer requires age- and time-matched sham-operated controls to avoid the distorting effect of self-control comparisons.

The majority of large animal models of bacterial sepsis involve administration of living bacterial monocultures (such as *E coli* and *S aureus*) or polymicrobial fecal inoculum (8–10, 24, 25). Nevertheless, in terms of clinical relevance, polymicrobial autofeces induction is probably more reliable then bacterial monocultures. Although the predominant microorganisms in feces are variable, the inflammatory host response caused by the invading pathogens might be identical to the clinical situation (9). Here we also confirmed that the standardized, autologous inoculum resulted in a predominantly *E coli*-characterized bacteremia, similarly to many clinical and preclinical observations (9, 26).

Organ supportive therapies (respiratory, fluid, diuretic and vasopressor or inotropic) are used as in the ICUs. These individualized treatments began 16 h after the insult in a goal-directed manner according to the current condition of the animals and using recommendations similar to those

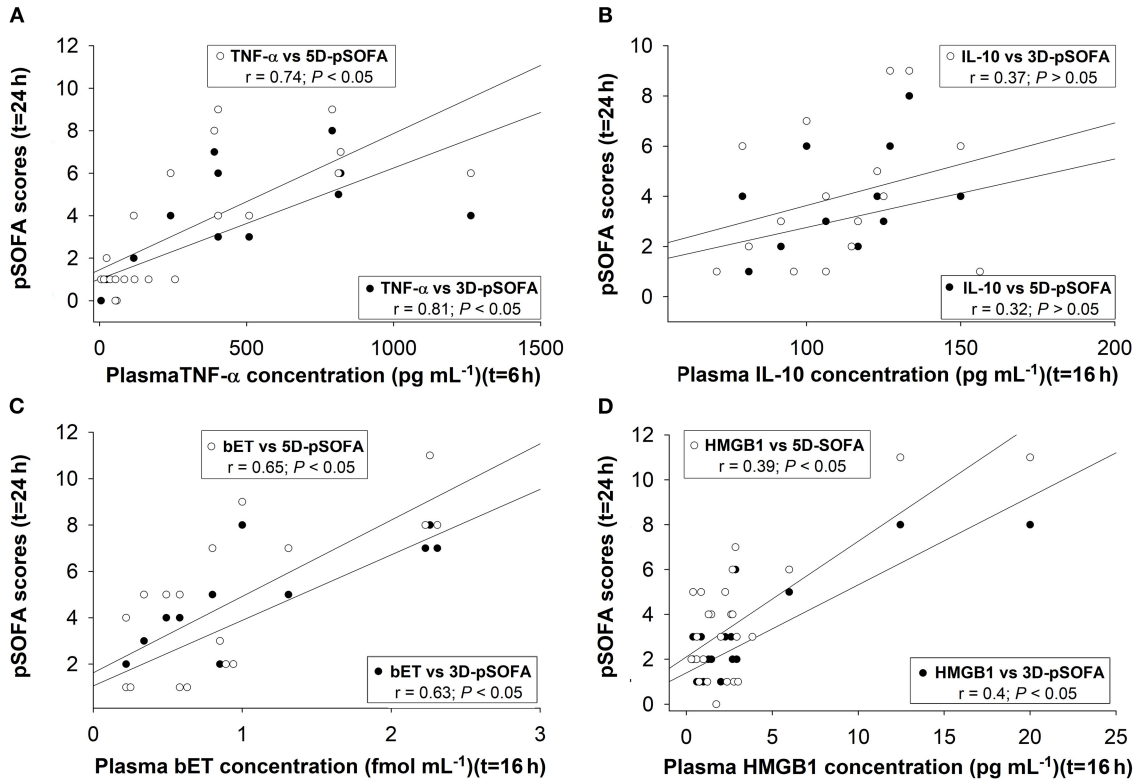

FIGURE 9 | Correlations between plasma concentrations of TNF-α at 6t = h **(A)**, interleukin-10 (IL-10) **(B)**, big endothelin (bET) **(C)**, high-mobility group box 1 protein (HMGB1) at $t = 16$ h **(D)**, and 3D-pSOFA and 5D-pSOFA scores at $t = 24$ h.

for humans (27, 28). Fluid resuscitation was performed with balanced crystalloid solutions based on the current state of the animals to avoid metabolic (hypo- and hyperglycemia) or ion imbalance (29).

The hemodynamic and biochemical changes were severity-dependent, but the oxygen dynamic parameters differed less between the animals in the sepsis and septic shock groups within the observation period. The decreased SVRI, increased DO_2 and VO_2, and markedly increased ExO_2 demonstrated a compensated hyperdynamic state in this model of progressive sepsis. In this line, sublingual microcirculation was reduced significantly in both septic groups, but an improving trend was observed in capillary perfusion rate, probably in association with the resuscitation therapies applied.

Assessing Sepsis Severity Using 3-Domain and 5-Domain-pSOFA Scoring Systems

In this model, the animals presented an almost human-like septic reaction, including elevated lactate level, hypotension, hypovolemia and multi-organ dysfunction caused by a polymicrobial infection. Furthermore, despite the highly standardized inducer conditions, each of the inoculated animals presented with various, individual reactions. Therefore, we divided the treated animals into non-septic, septic, septic shock and fulminant sepsis subgroups, but only the data from the septic and septic shock subgroups were examined in detail. The severity of organ damage ranged from less severe to septic shock, and a numerical characterization of these individual reactions was achieved using a pig-specific scoring system. It should be added that the human SOFA score has already been applied in unchanged form (8) or in a modified version (10) in preclinical porcine sepsis studies. Here we propose the use of 3- and 5-domain froms of pSOFA to quantify organ damage comprehensively. Like human quick scoring, the simplified pSOFA score is suitable for "bedside" evaluation of the severity of sepsis with basic parameters (MAP, PaO_2/FiO_2 ratio and urine output), which does not require time-consuming laboratory testing, thus allowing for a quick, online evaluation of the status of organ function. The extended scoring and measurement of the components of the 5D-pSOFA score (platelet counts and bilirubin levels) require laboratory testing and thus may not capture the dysfunction of individual organ systems promptly, but, with higher offline resolution, it provides more information on sepsis progression. This possibility is supported by the fact that it was only the 5D-pSOFA score that indicated sepsis progression in the "non-septic" group as compared to the sham-operated group (**Supplementary Table 1**).

In our protocol, the scoring systems were applied 16 h after induction. However, it has already been shown that human-like SOFA scores can be used at earlier time points in pigs

(10). Park et al. reported on changes in relevant parameters of sepsis progression (including some of the SOFA parameters) in anesthetized pigs approx. after 6–12 h after induction (9). Similar changes were observed in conscious pigs with a longer follow-up (8, 10). Based on these references, we hypothesized that the earliest signs of multi-organ failure could be detected by our pSOFA scoring system between 6 and 12 h.

Calculating the Components of pSOFA Scoring System

Among the elements of the human SOFA score, the PaO_2/FiO_2 ratio was used in its original form (30). Other elements, such as the cardiovascular score, can be affected by iatrogenic interventions or anesthesia. Since general anesthetics can be cardiodepressive and decrease systemic blood pressure due to reduced sensitivity of the baroreflex (12, 31, 32), a higher threshold value for the MAP (75 mmHg) was defined to indicate the beginning of cardiovascular dysfunction.

In the case of the renal system, plasma creatinine levels increased significantly and only showed a correlation with urine output in the septic shock group. The increase of the creatinine plasma level was insufficient to demonstrate renal dysfunction in the sepsis group, while a decreased tendency in urine output was evident here. This suggests that urine output is a more sensitive indicator of early renal injury after the septic insult in this experimental setup. Since creatinine is a measure of renal perfusion/filtration, a large percentage of the kidney mass has to be dysfunctional before a rise in creatinine concentration is seen (8). Therefore, we recommend monitoring urine output to assess renal damage in relevant preclinical studies. The additional decrease in albumin level can also provide useful information on renal and liver function (33).

In addition, according to the latest literature data, novel cell cycle arrest biomarkers and neutrophil gelatinase-associated lipocalin can indicate kidney dysfunction even earlier than urine output and creatinine (34).

Plasma bilirubin is an accepted biomarker for assessment of liver dysfunction in large animal studies. Nevertheless, significant changes occurred in later phases, between 20 and 24 h, and only in a few animals with septic shock. This suggests that liver damage develops relatively late and depends on the severity of insult. In septic human patients, significantly increased bilirubin levels within 72 h indicate severe hepatic insufficiency and a high risk of mortality (35). In previous reports, the human range of plasma bilirubin was used in pigs with minor modifications (10). In addition, AST, ALT and creatine kinase data are often used to diagnose hepatic dysfunction in preclinical sepsis models. The De Ritis ratio (as AST/ALT ratio) is another commonly used marker of hepatic cell degradation. Increasing ALT level is a relatively specific sign of hepatocellular damage, while separated elevation of AST is usually due to injury of liver and non-liver cells (kidney, heart and muscle cells) as well (36). Therefore, we propose the use of the De Ritis ratio for the assessment of sepsis-related liver damage in short-term experimental designs.

A decreased platelet count is a measure of the activation of the coagulation system in human SOFA scoring; it has previously been used in other porcine sepsis studies (8–10, 37). However, pigs are normally hypercoagulable as compared to other species, including humans, and the normal platelet counts in pigs fall on a much broader range as compared to humans (38). Therefore, we defined higher platelet count categories for the 5D-pSOFA scoring to assess the presence of coagulation dysfunction (see **Table 1**). In our model, platelet number change seems to be a sensitive and early marker of severity of the septic process. It should be noted, however, that platelet activation easily occurs in pigs, especially when blood samples are collected through catheters, and the mechanical contact increases the chances of aggregation (38).

Examining the Relationship Between Microbiology and Sepsis Severity

Quantitative microbiological analysis of the fecal inoculum showed that the onset and progression of sepsis–septic shock requires a critical number of germs in the induction suspension. We also examined the relationship between the degree of microbiological invasion and the host response leading to organ dysfunctions characterized by 3D- or 5D-pSOFA scoring. The initial microbial concentration of the inducer inoculum was moderately associated with the severity of organ dysfunction, while the concentration of microbes in the blood showed a much stronger correlation. Although the predominant microorganism in a fecal sample is variable, the inflammatory response of the host to the invading pathogens might be consistent, which is identical to the clinical situation (9). Nevertheless, it is important to note that individual microbiological diversity can contribute to the severity statuses observed in our experimental animals, which can complicate standardization. Therefore, frequent preliminary microflora testing may also facilitate the standardization of an autologous fecal inoculum-induced sepsis model.

Assessing the Prognostic Value of Plasma Biomarkers in Sepsis

The pathogenesis of sepsis involves the release and activation of hundreds of mediator molecules, cytokines, acute phase proteins and stress hormones, which can be considered prognostic biomarkers (39) in animal models and human clinical studies as well (14). In our study, an early release of TNF-α at 6 h was noted, while the time-dependent kinetics of other detected biomarkers (IL-10, bET and HMGB1) were consistent with sepsis progression. Moreover, the dynamics of all the inflammatory mediators under examination showed significant differences between the sepsis and septic shock groups. Therefore, early (6 h) detection of plasma TNF-α and a somewhat late elevation of bET and HMGB1 levels may indicate the probability of septic shock-linked organ dysfunction quantified by the 3D- and 5D-pSOFA scores as well. Hence, we suggest that these biomarkers may have a potentially predictive importance in experimental sepsis.

Study Limitations

This study has certain limitations. First, we used healthy young adult pigs which lacked comorbidities commonly associated with human sepsis. Second, the Glasgow Coma Scale used to quantify the damage to the central nervous system cannot be employed.

Third, antibiotic treatment was not applied, since there was not enough monitoring time to evaluate the effect of the antibiotics on the blood culture results (which are available after 24–48 h, while a non-specific antibiotic treatment can be ineffective in 30% of cases), and knowledge of the untreated microbiological profile was an important point to consider in these experiments (40). Controlling the efficacy of antibiotic therapy by detecting the plasma procalcitonin level would be an alternative option, but this approach also requires a longer experimental protocol (41).

CONCLUSION

We have described a porcine model of polymicrobial, intraabdominal sepsis in detail. The methodology combines the advantages of conscious and anesthetized studies, and mimics human sepsis and multi-organ failure very closely. The host responses were quantified with modified human SOFA-like 3D- and 5D-pSOFA scoring systems. 3D-pSOFA scoring is suitable for evaluation of the cardiovascular, pulmonary and renal dysfunctions online without laboratory biochemical testing, while the use of the 5D-pSOFA score improves reproducibility (with the extended assessment of coagulation and hepatic dysfunction parameters) and provides an alternative endpoint instead of mortality. In this context, sepsis and septic shock can also be well-distinguished. We thus propose that the standardization of large animal studies with the pSOFA scoring systems will make different models comparable, thus reducing the gap between preclinical and clinical outcomes.

DATA AVAILABILITY STATEMENT

The raw data supporting the conclusions of this article will be made available by the authors, without undue reservation.

ETHICS STATEMENT

The animal study was reviewed and approved by National Scientific Ethical Committee on Animal Experimentation (National Competent Authority of Hungary; approval number: V/175/2018).

AUTHOR CONTRIBUTIONS

AR, BZ, ST, DÉ, LB, LJ, RF, GV, LB, and JK performed experiments and wrote the manuscript. ST, ZB, and JS performed microbiological examinations. MP and AS prepared figures. KB, AS, MB, and JK supervised and edited the manuscript. All authors read and approved the manuscript.

FUNDING

Research grant from the National Research Development and Innovation Office, NKFI K120232.

SUPPLEMENTARY MATERIAL

The Supplementary Material for this article can be found online at: https://www.frontiersin.org/articles/10.3389/fmed.2022.867796/full#supplementary-material

Supplementary Figure 1 | Correlation between plasma creatinine concentration and urine output in the sepsis **(A)** and septic shock **(B)** subgroups.

Supplementary Table 1A | Changes in the components and score values of the 3D-pSOFA and 5D-pSOFA scoring systems in the sham-operated ($n = 9$) and non-septic animals ($n = 5$) during 16 and 24 h of the monitoring period.

Supplementary Table 1B | Changes in the hemodynamics in the sham-operated ($n = 9$) and non-septic animals ($n = 5$) during 16 and 24 h of the monitoring period.

Supplementary Table 1C | Changes in the oxygen dynamics, microcirculation and white blood cell count in the sham-operated ($n = 9$) and non-septic animals ($n = 5$) during the monitoring period.

Supplementary Table 1D | Changes in markers of organ dysfunction in the sham-operated ($n = 9$) and non-septic animals ($n = 5$) during the monitoring period.

Supplementary Table 2 | Changes in the parameters of terminated animals (with fulminant septic reaction) at $t = 0$ and 6 h.

Supplementary Table 3 | Microbial composition of the sepsis-inducing inoculum expressed as the incidence of the current strain per total number of samples (%).

REFERENCES

1. Singer M, Deutschman CS, Seymour CW, Shankar-Hari M, Annane D, Bauer M, et al. The Third International Consensus definitions for sepsis and septic shock (Sepsis-3). *JAMA*. (2016) 315:801. doi: 10.1001/jama.2016.0287
2. Vincent JL, de Mendonça A, Cantraine F, Moreno R, Takala J, Suter PM, et al. Use of the SOFA score to assess the incidence of organ dysfunction/failure in intensive care units: results of a multicenter, prospective study. Working group on "sepsis-related problems" of the European Society of Intensive Care Medicine. *Crit Care Med.* (1998) 26:1793–800. doi: 10.1097/00003246-199811000-00016
3. Osuchowski MF, Ayala A, Bahrami S, Bauer M, Boros M, Cavaillon J-M, et al. Minimum quality threshold in pre-clinical sepsis studies (MQTiPSS). *SHOCK.* (2018) 50:377–80. doi: 10.1097/SHK.0000000000001212
4. Dyson A, Singer M. Animal models of sepsis: why does preclinical efficacy fail to translate to the clinical setting? *Crit Care Med.* (2009) 37:S30-7. doi: 10.1097/CCM.0b013e3181922bd3
5. Swindle MM, Makin A, Herron AJ, Clubb FJ, Frazier KS. Swine as models in biomedical research and toxicology testing. *Vet Pathol.* (2012) 49:344–56. doi: 10.1177/0300985811402846
6. Meurens F, Summerfield A, Nauwynck H, Saif L, Gerdts V. The pig: a model for human infectious diseases. *Trends Microbiol.* (2012) 20:50–7. doi: 10.1016/j.tim.2011.11.002
7. Guillon A, Preau S, Aboab J, Azabou E, Jung B, Silva S, et al. Preclinical septic shock research: why we need an animal ICU. *Ann Intensive Care.* (2019) 9:66. doi: 10.1186/s13613-019-0543-6
8. Soerensen KE, Nielsen OL, Birck MM, Soerensen DB, Leifsson PS, Jensen HE, et al. The use of sequential organ failure assessment parameters in an awake porcine model of severe Staphylococcus aureus sepsis. *APMIS.* (2012) 120:909–21. doi: 10.1111/j.1600-0463.2012.02917.x
9. Park I, Lee JH, Jang D-H, Kim D, Chang H, Kwon H, et al. Characterization of fecal peritonitis–induced sepsis in a porcine model. *J Surg Res.* (2019) 244:492–501. doi: 10.1016/j.jss.2019.06.094
10. Waterhouse A, Leslie DC, Bolgen DE, Lightbown S, Dimitrakakis N, Cartwright MJ, et al. Modified clinical monitoring assessment criteria

for multiorgan failure during bacteremia and sepsis progression in a pig model. *Adv Crit Care Med.* (2018) 1:002. Available online at: http://www.scientificoajournals.org/pdf/ccm.1002.pdf
11. Remick DG, Ayala A, Chaudry IH, Coopersmith CM, Deutschman C, Hellman J, et al. Premise for standardized sepsis models. *Shock.* (2019) 51:4–9. doi: 10.1097/SHK.0000000000001164
12. Cruz FF, Rocco PRM, Pelosi P. Anti-inflammatory properties of anesthetic agents. *Crit Care.* (2017) 21:67. doi: 10.1186/s13054-017-1645-x
13. Li X, Xu Z, Pang X, Huang Y, Yang B, Yang Y, et al. Interleukin-10/lymphocyte ratio predicts mortality in severe septic patients. *PLoS ONE.* (2017) 12:e0179050. doi: 10.1371/journal.pone.0179050
14. Rivers EP, Jaehne AK, Nguyen HB, Papamatheakis DG, Singer D, Yang JJ, et al. Early biomarker activity in severe sepsis and septic shock and a contemporary review of immunotherapy trials. *Shock.* (2013) 39:127–37. doi: 10.1097/SHK.0b013e31827dafa7
15. Tschaikowsky K, Sägner S, Lehnert N, Kaul M, Ritter J. Endothelin in septic patients: effects on cardiovascular and renal function and its relationship to proinflammatory cytokines. *Crit Care Med.* (2000) 28:1854–60. doi: 10.1097/00003246-200006000-00028
16. Yagmur E, Buendgens L, Herbers U, Beeretz A, Weiskirchen R, Koek GH, et al. High mobility group box 1 as a biomarker in critically ill patients. *J Clin Lab Anal.* (2018) 32:e22584. doi: 10.1002/jcla.22584
17. Tallósy SP, Poles MZ, Rutai A, Fejes R, Juhász L, Burián K, et al. The microbial composition of the initial insult can predict the prognosis of experimental sepsis. *Sci Rep.* (2021) 11:22772. doi: 10.1038/s41598-021-02129-x
18. Nagy E, Becker S, Kostrzewa M, Barta N, Urbán E. The value of MALDI-TOF MS for the identification of clinically relevant anaerobic bacteria in routine laboratories. *J Med Microbiol.* (2012) 61:1393–400. doi: 10.1099/jmm.0.043927-0
19. Rhodes A, Evans LE, Alhazzani W, Levy MM, Antonelli M, Ferrer R, et al. Surviving sepsis campaign: international guidelines for management of sepsis and septic shock: 2016. *Intensive Care Med.* (2017) 43:304–77. doi: 10.1007/s00134-017-4683-6
20. Aykut G, Veenstra G, Scorcella C, Ince C, Boerma C. Cytocam-IDF (incident dark field illumination) imaging for bedside monitoring of the microcirculation. *Intensive Care Med Exp.* (2015) 3:40. doi: 10.1186/s40635-015-0040-7
21. Sherman H, Klausner S, Cook WA. Incident dark-field illumination: a new method for microcirculatory study. *Angiology.* (1971) 22:295–303. doi: 10.1177/000331977102200507
22. Massey MJ, Shapiro NI. A guide to human *in vivo* microcirculatory flow image analysis. *Crit Care.* (2016) 20:35. doi: 10.1186/s13054-016-1213-9
23. Dobbe JGG, Streekstra GJ, Atasever B, van Zijderveld R, Ince C. Measurement of functional microcirculatory geometry and velocity distributions using automated image analysis. *Med Biol Eng Comput.* (2008) 46:659–70. doi: 10.1007/s11517-008-0349-4
24. Wolfárd A, Kaszaki J, Szabó C, Szalay L, Nagy S, Boros M. Prevention of early myocardial depression in hyperdynamic endotoxemia in dogs. *Shock.* (2000) 13:46–51. doi: 10.1097/00024382-200013010-00009
25. Kutzsche S, Schlichting E, Aspelin T, Lyberg T. Hemodynamic changes and systemic activation of coagulation and fibrinolysis during controlled endotoxemia in pigs. *Thromb Res.* (2000) 98:517–29. doi: 10.1016/S0049-3848(00)00189-4
26. Vincent JL, Sakr Y, Sprung CL, Ranieri VM, Reinhart K, Gerlach H, et al. Sepsis in European intensive care units: results of the SOAP study. *Crit Care Med.* (2006) 34:344–53. doi: 10.1097/01.CCM.0000194725.48928.3A
27. Corrêa TD, Vuda M, Blaser AR, Takala J, Djafarzadeh S, Dünser MW, et al. Effect of treatment delay on disease severity and need for resuscitation in porcine fecal peritonitis. *Crit Care Med.* (2012) 40:2841–9. doi: 10.1097/CCM.0b013e31825b916b
28. Head LW, Coopersmith CM. Evolution of sepsis management: from early goal-directed therapy to personalized care. *Adv Surg.* (2016) 50:221–34. doi: 10.1016/j.yasu.2016.04.002
29. Kang D, Yoo KY. Fluid management in perioperative and critically ill patients. *Acute Crit Care.* (2019) 34:235–45. doi: 10.4266/acc.2019.00717
30. Matute-Bello G, Frevert CW, Martin TR. Animal models of acute lung injury. *Am J Physiol Lung Cell Mol Physiol.* (2008) 295:L379–99. doi: 10.1152/ajplung.00010.2008
31. Muzi M, Ebert TJ. A comparison of baroreflex sensitivity during isoflurane and desflurane anesthesia in humans. *Anesthesiology.* (1995) 82:919–25. doi: 10.1097/00000542-199504000-00015
32. Lee HT, Emala CW, Joo JD, Kim M. Isoflurane improves survival and protects against renal and hepatic injury in murine septic. peritonitis. *Shock.* (2007) 27:373–9. doi: 10.1097/01.shk.0000248595.17130.24
33. Yin M, Si L, Qin W, Li C, Zhang J, Yang H, et al. Predictive value of serum albumin level for the prognosis of severe sepsis without exogenous human albumin administration: a prospective cohort study. *J Intensive Care Med.* (2018) 33:687–94. doi: 10.1177/0885066616685300
34. Bellomo R, See EJ. Novel renal biomarkers of acute kidney injury and their implications. *Intern Med J.* (2021) 51:316–8. doi: 10.1111/imj.15229
35. Yao Y, Wang D, Yin Y. Advances in sepsis-associated liver dysfunction. *Burn Trauma.* (2014) 2:97. doi: 10.4103/2321-3868.132689
36. Botros M, Sikaris KA. The de ritis ratio: the test of time. *Clin Biochem Rev.* (2013) 34:117–30.
37. Leifsson PS, Iburg T, Jensen HE, Agerholm JS, Kjelgaard-Hansen M, Wiinberg B, et al. Intravenous inoculation of *Staphylococcus aureus* in pigs induces severe sepsis as indicated by increased hypercoagulability and hepatic dysfunction. *FEMS Microbiol Lett.* (2010) 309:208–16. doi: 10.1111/j.1574-6968.2010.02042.x
38. Velik-Salchner C, Schnürer C, Fries D, Müssigang PR, Moser PL, Streif W, et al. Normal values for thrombelastography (ROTEM®) and selected coagulation parameters in porcine blood. *Thromb Res.* (2006) 117:597–602. doi: 10.1016/j.thromres.2005.05.015
39. László I, Trásy D, Molnár Z, Fazakas J. Sepsis: from pathophysiology to individualized patient care. *J Immunol Res.* (2015) 2015:510436. doi: 10.1155/2015/510436
40. Mettler J, Simcock M, Sendi P, Widmer AF, Bingisser R, Battegay M, et al. Empirical use of antibiotics and adjustment of empirical antibiotic therapies in a University hospital: a prospective observational study. *BMC Infect Dis.* (2007) 7:21. doi: 10.1186/1471-2334-7-21
41. Trásy D, Tánczos K, Németh M, Hankovszky P, Lovas A, Mikor A, et al. Early procalcitonin kinetics and appropriateness of empirical antimicrobial therapy in critically ill patients. A prospective observational study. *J Crit Care.* (2016) 34:50–5. doi: 10.1016/j.jcrc.2016.04.007

Conflict of Interest: The authors declare that the research was conducted in the absence of any commercial or financial relationships that could be construed as a potential conflict of interest.

frontiers | Frontiers in Medicine

REVIEW
published: 16 May 2022
doi: 10.3389/fmed.2022.869372

A Toolbox to Investigate the Impact of Impaired Oxygen Delivery in Experimental Disease Models

Stefan Hof[1], Carsten Marcus[1], Anne Kuebart[1], Jan Schulz[1], Richard Truse[1], Annika Raupach[1], Inge Bauer[1], Ulrich Flögel[2], Olaf Picker[1], Anna Herminghaus[1†] and Sebastian Temme[1*†]*

[1] Department of Anaesthesiology, Medical Faculty and University Hospital Düsseldorf, Heinrich-Heine-University Düsseldorf, Düsseldorf, Germany, [2] Experimental Cardiovascular Imaging, Department of Molecular Cardiology, Medical Faculty and University Hospital Düsseldorf, Heinrich-Heine-University Düsseldorf, Düsseldorf, Germany

OPEN ACCESS

Edited by:
Wolfgang Weihs, Medical University of Vienna, Austria

Reviewed by:
Yun Long, Peking Union Medical College Hospital (CAMS), China
Tomasz Skirecki, Medical Centre for Postgraduate Education, Poland

***Correspondence:**
Anna Herminghaus
Anna.Herminghaus@med.uni-duesseldorf.de
Sebastian Temme
sebastian.temme@med.uni-duesseldorf.de

† These authors share last authorship

Specialty section:
This article was submitted to Intensive Care Medicine and Anesthesiology, a section of the journal Frontiers in Medicine

Received: *04 February 2022*
Accepted: *25 April 2022*
Published: *16 May 2022*

Citation:
Hof S, Marcus C, Kuebart A, Schulz J, Truse R, Raupach A, Bauer I, Flögel U, Picker O, Herminghaus A and Temme S (2022) A Toolbox to Investigate the Impact of Impaired Oxygen Delivery in Experimental Disease Models. Front. Med. 9:869372. doi: 10.3389/fmed.2022.869372

Impaired oxygen utilization is the underlying pathophysiological process in different shock states. Clinically most important are septic and hemorrhagic shock, which comprise more than 75% of all clinical cases of shock. Both forms lead to severe dysfunction of the microcirculation and the mitochondria that can cause or further aggravate tissue damage and inflammation. However, the detailed mechanisms of acute and long-term effects of impaired oxygen utilization are still elusive. Importantly, a defective oxygen exploitation can impact multiple organs simultaneously and organ damage can be aggravated due to intense organ cross-talk or the presence of a systemic inflammatory response. Complexity is further increased through a large heterogeneity in the human population, differences in genetics, age and gender, comorbidities or disease history. To gain a deeper understanding of the principles, mechanisms, interconnections and consequences of impaired oxygen delivery and utilization, interdisciplinary preclinical as well as clinical research is required. In this review, we provide a "tool-box" that covers widely used animal disease models for septic and hemorrhagic shock and methods to determine the structure and function of the microcirculation as well as mitochondrial function. Furthermore, we suggest magnetic resonance imaging as a multimodal imaging platform to noninvasively assess the consequences of impaired oxygen delivery on organ function, cell metabolism, alterations in tissue textures or inflammation. Combining structural and functional analyses of oxygen delivery and utilization in animal models with additional data obtained by multiparametric MRI-based techniques can help to unravel mechanisms underlying immediate effects as well as long-term consequences of impaired oxygen delivery on multiple organs and may narrow the gap between experimental preclinical research and the human patient.

Keywords: microcirculation, sepsis, hemorrhagic shock, mitochondria, MRI, ^{19}F MRI

INTRODUCTION

Impaired oxygen delivery and utilization are caused by various diseases with high morbidity and mortality. Many of the mechanisms leading to dysfunctional oxygen exploitation are known, but the acute effects and long-term consequences, as well as their underlying mechanisms, are only poorly understood. Impaired oxygen delivery can impact multiple organs simultaneously, and

organ damage can be aggravated by an intense organ cross-talk or the presence of a systemic inflammatory response. In addition to immediate effects, oxygen deprivation might also lead to long-term alterations due to the reprogramming of cells and tissue.

An imbalance between cellular oxygen demand and oxygen supply induces complex adaptive mechanisms in tissues and cells (1, 2). If those mechanisms fail to maintain oxygen delivery and utilization, a shock state establishes. The most frequent forms of shock are acute hemorrhagic and septic shock that are related to high mortality and comprise more than 75% of all clinical cases of shock (3). Importantly, shock-induced impaired oxygen exploitation can occur at multiple sites like the macrocirculation and the local tissue-microcirculation. Of note, local microcirculation does not always correlate with systemic hemodynamics and tissue hypoperfusion can occur despite normal systemic and regional blood flow (4). This indicates the crucial importance to monitor microcirculatory parameters like the structure of the microvasculature, tissue perfusion and oxygen levels or local hemoglobin concentrations. Oxygen utilization is closely connected to mitochondrial function. Mitochondria are the crucial organelles for cellular energy generation, being responsible for about 90% of total oxygen consumption in mammalian cells, 80% of which is coupled to ATP synthesis.

Experimental preclinical animal models in combination with technologies to determine macro- and microvascular structure and function, energy metabolism, tissue damage and subsequent inflammation and organ function can help to gain important novel mechanistic insights into short- and long-term consequences of impaired oxygen delivery and utilization. In this review, we provide an overview about the advantages and limitations of the most widely used animal models for sepsis/septic shock and hemorrhagic shock (Section "Animal Disease Models to Study Hemorrhagic and Septic Shock") and we describe technologies to measure a broad spectrum of microcirculatory characteristics like the structure of the microvasculature, perfusion, local oxygen levels or mitochondrial function (Section "Technical Devices to Determine Structure and Function of Tissue Microcirculation"). In the Section "Imaging the Consequences of Impaired Oxygen Delivery by MRI" we discuss possible applications of magnetic resonance imaging (MRI) which is a whole-body multimodal imaging technology that can complement and extend the information obtained by techniques described in the Section "Technical Devices to Determine Structure and Function of Tissue Microcirculation". Moreover, we provide a supplementary overview of at least some preclinical animal studied, where structural or functional aspects of the microcirculation have been determined by imaging technologies (**Supplementary Table S1**). In the last part of the manuscript (Section "From Bench to Bedside"), we display a brief outlook of how the information obtained by preclinical animal models and technologies to determine microcirculation, mitochondrial function and MRI can be used to obtain complementary information that could be integrated to gain a data-set that might help the clinician for an individual decision making.

ANIMAL DISEASE MODELS TO STUDY HEMORRHAGIC AND SEPTIC SHOCK

In general, animal models should be characterized by a high grade of reproducibility and a realistic depiction of pathophysiological changes that are also found in the corresponding human shock states. The most common small animal models are based on rodents (5), because they are widely available, experiments with these animals cause relatively low costs and there is a large amount of experimental evidence available that can be used for the design of the study and also for comparison of the results. Mice and to a lesser extent rats, allow for a detailed analysis of the impact of certain genes, or even point mutation for a specific disease state under *in vivo* conditions (6). However, their small size hampers surgical interventions and instrumentation (7), and the small total blood volume prohibits intermittent blood gas analysis from determining base excess (8, 9) and lactate levels (10) as metabolic surrogates for adequate tissue perfusion. Due to their larger size, rats offer the opportunity to perform more laborious surgical interventions, invasive monitoring (11) and also intermittent blood gas analysis. Disease models based on mice and rats allow for a high degree of standardization and a detailed analysis of the pathophysiological mechanism. However, one has to keep in mind that the physiological and immunological response to blood loss or sepsis may differ from humans (12, 13). Shock models in pigs or sheep are more similar to human disease under physiological and hemodynamic aspects and do also enable more clinically relevant surgical interventions. However, the requirements for surgical interventions and for animal care are very high, which renders experiments with these animals rather expensive. They are only available in specialized facilities and therefore will not be covered in this review. Taken together, there is no optimal animal model for modeling hemorrhagic or septic shock which perfectly mimics the human situation. Therefore, the specific research questions, individual experience as well as financial and practical aspects should be carefully considered before planning an animal study.

Hemorrhagic Shock

The state of hemorrhagic shock is defined as a mismatch of oxygen delivery and cellular oxygen demand due to a loss of cellular and noncellular blood components during critical bleeding (3). Hemorrhage leads to tissue hypoperfusion and to a shift to anaerobic cell metabolism (14, 15). During the last years, the pathophysiological understanding of hemorrhagic shock states developed from a hemodynamic and mechanistic point of view to a more complex process including a differentiated neuronal (16), humoral, (17), microcirculatory and immunological response (18). To gain deeper insights into the mechanisms associated with hemorrhagic shock, multiple small animal models were developed which can be roughly subdivided into (i) controlled hemorrhage, (ii) uncontrolled hemorrhage or (iii) hemorrhagic shock combined with traumatic injury (see below and **Table 1** for an overview).

TABLE 1 | Experimental models of hemorrhage and their advantages / disadvantages and the specific areas which they are used for.

	Advantages	Disadvantages	Utilization
Fixed-volume hemorrhage (FVH)	Reproducible; Standardized; Easy to perform; Linked to ATLS shock-classification	Individual compensatory capacity Differences in shock depth in the late course of shock Differences between the estimated and the actual total blood volume	Investigation of cardiovascular compensatory mechanisms (e.g., adrenergic activation, RAAS)
Fixed-pressure hemorrhage (FPH)	Reproducible; Standardized; Easy to perform; Stable shock depth without individual compensation; A clinical and macro-hemodynamic point of view on shock processes	No standardized registration of lost blood volume Focus on hemodynamic changes only	Investigation of hemodynamic coherence and microcirculatory alterations
Oxygen debt directed hemorrhage (ODH)	Unique model focusing on oxygen demand as the primary target Reproducible; Standardized	Imprecision in the case of microvascular shunting Not related to tissue-specific oxygen metabolism	To investigate metabolic changes during general hypoxia
Uncontrolled hemorrhage	Mimics the clinical situation of uncontrolled and isolated hemorrhage	Limited to a few clinical situations like esophageal- or cancer-bleeding No quantification of total blood volume loss and macrocirculatory hemodynamics High inter-experimental variability	Investigation of physiological cardiovascular changes and internal compensatory mechanisms especially coagulation
Hemorrhage with traumatic injury	Close to the clinical situation of severe trauma and surgical bleeding Comprises immunological, metabolic and neurohumoral responses to tissue injury	Very complex and barely comparable due to many different experimental protocols A high number of confounders that impact the results (cytokine release, neuroendocrine activation)	Investigation of immunological, metabolic and neurohumoral changes

Controlled Hemorrhage

Fixed-Volume Hemorrhage (FVH)

FVH models are characterized by an acute withdrawal of a predetermined blood volume within a short period of time to induce hemorrhage (19). After withdrawal of the defined blood volume, no further interventions, like fluid replacement, are performed. Models differ in the relative amount of the removed final blood volume, the severity of hemorrhage and the duration of hemorrhage. Commonly, the shed blood volume is calculated as the percentage of the estimated total blood volume (20, 21). According to Advanced Trauma Life Support (ATLS), a class IV hemorrhagic shock is apparent when bleeding exceeds 40% of the estimated circulating blood volume which leads to a mortality of more than 30% in humans (22). Therefore, many investigators choose a corresponding shock model to test if a therapeutic intervention results in a survival advantage (23, 24). More moderate shock states are used when the focus is not on survival rates, but, e.g., on repetitive measurements in individual animals (25–27). As stated above, also the shock duration can be adjusted (28). Therefore, investigators should justify shock duration and depth, for example by the individual hypoxia tolerance of the investigated tissues and species. Importantly, the obtained results are not always comparable between species since blood volume is not consistently associated with the total body weight. Of note, even in the same species an increase in body weight does not always result in a linear increase in total blood volume possibly due to a higher percentage of barely perfused adipose tissue (29).

Fixed-Pressure Hemorrhage (FPH)

To integrate hemodynamic considerations into the experimental protocol of hemorrhagic shock Wiggers (30) and Penfield (31) were the first to use a fixed-pressure hemorrhage model. In this model, blood is constantly removed until a defined mean arterial blood pressure is reached. To account for compensation or further disarrangements, intermittent bleeding or volume substitution is used to maintain blood pressure.

An FPH model gives the opportunity to investigate microcirculatory alterations independent of macrocirculatory parameters. Especially when changes in the macrocirculation are not paralleled by changes in microcirculatory variables, a FPH model could illuminate new aspects of microcirculatory failure. In this case, the dissociation of micro- and macrocirculatory variables is called hemodynamic incoherence, a field of growing interest in critical care medicine (32). In FPH models, changes in microcirculatory variables after pharmacological interventions may not be reflected in macrocirculatory alterations and probably are a result of adaptive processes within the microcirculation itself. Of note, the FPH model mirrors the clinical point of view, because during the onset of acute hemorrhage physicians first evaluate the macrocirculation to determine hemodynamic stability. Moreover, the total blood loss and especially the relative amount of total circulating blood volume is often difficult to determine in the clinical setting.

Oxygen Debt Directed Hemorrhage (ODH)

In the experimental hemorrhage models mentioned above, total blood volume loss or mean arterial pressure is modified, because they impact the maximal blood oxygen content and also tissue perfusion. In ODH, blood loss is controlled by oxygen debt, which is defined as the difference between prehemorrhage oxygen consumption and oxygen consumption during hemorrhage. Oxygen debt is calculated from macrocirculatory variables and

blood gas analysis. During hemorrhage, oxygen-carrying capacity decreases due to a reduction of circulating erythrocytes and blood convection within the microcirculation (9). Here it is important to note that systemic oxygen debt often coincides with local tissue hypoperfusion, probably to a varying degree in individual organs, but that these terms are not fully interchangeable.

Oxygen debt is measured for 30 years as a secondary parameter, but Dunham et al. were the first who used this as a target measurement to guide hemorrhage in dogs (33). Furthermore, in follow-up studies they could show, that oxygen debt in hemorrhage is an independent predictor of death and organ failure (34). Crowell and Smith figured out that an oxygen debt of 100 ml/kg or less was not associated with death, whereas an increase of up to 120 ml/kg led to a mortality of 50% (14). Interestingly, this specific correlation seems to be species-dependent (35).

Microcirculatory disarrangements may limit the use of oxygen debt directed hemorrhage models in microvascular research, since blood shunted within the microcirculation is not deoxygenated (36). The resulting increase in postcapillary oxygen content and central venous oxygen saturation may assume a decreased oxygen demand while mortality can be even increased (37). Oxygen debt is calculated from macrocirculatory parameters and represents the systemic oxygen deficit. Those hemorrhage models do not account for the tissue-specific oxygen demand (38). For example, adipose individuals need a lower oxygen amount per total body weight to maintain their basic metabolism (39).

Uncontrolled Hemorrhage

In uncontrolled hemorrhage models, animals undergo an open vascular trauma without further bleeding control. This procedure reflects the clinical setting of uncontrolled traumatic bleeding. Thus, the rate of blood loss and hypoperfusion underlies a wide range of variations between individuals and can be barely quantified. Studies using uncontrolled hemorrhage are suitable to investigate internal compensatory mechanisms like coagulation (40). In the past, uncontrolled hemorrhage models were utilized to investigate therapeutical interventions and resuscitation protocols in uncontrolled surgical bleeding (41, 42), that resulted in a paradigm change in fluid resuscitation, pointing toward permissive hypotension in uncontrolled bleeding (43).

Hemorrhagic Shock Combined With Traumatic Injury

Isolated hemorrhage barely reflects clinical situations, because hemorrhage usually occurs in combination with tissue injury as a result of surgical interventions or trauma. Tissue injury itself can then cause additional damage through immunological (44) or neurohumoral responses (45). For example, Chaudry et al. observed an increased mortality when laparotomy was performed in addition to hemorrhage (46).

Generally, fixed-pressure models or uncontrolled hemorrhage are combined with additional tissue damage (16). Those models pay attention to neurohumoral, endocrinological and immunological changes during hemorrhage. However, the high complexity of the experimental protocols and the physiological cross-talk of hemorrhage and trauma renders the interpretation and comparison with other studies difficult. Indeed, not only the diversity of possible trauma categories, but different experimental protocols to achieve a certain trauma category are manifold. For example, long bone fractures can be performed as open or close fracture models. Bone fragment implantation and bone marrow injection are called pseudo-fractures and are expected to imitate the immunological effect of long bone fractures without a soft tissue damage through open fracture types (16).

Brief Summary of Experimental Hemorrhagic Shock Models

All controlled hemorrhage models enable a high grade of standardization and reproducibility and are therefore suitable for experimental protocols in life science (47) (see **Table 1**). Of note, all hemorrhage models are defined by the initiation of shock, whereas the posthemorrhagic period underlies a high grade of variation. For example, resuscitation in a FVH model can be achieved by retransfusion of blood, by an increase of mean arterial pressure to a predetermined threshold, or a normalization of base deficit and lactate acidemia through blood, fluid and/or vasopressor substitution and some investigators do not perform resuscitation at all. Reperfusion and resuscitation have a large impact on tissue damage (48, 49), interventions undertaken post hemorrhage have to be reported in detail to allow for a valid interpretation of findings. Importantly, our pathophysiological understanding of hemorrhagic shock states has changed during the last years from a hemodynamic point of view to a more complex process including neuronal, humoral, microcirculatory and immunological aspects. This huge complexity is covered by uncontrolled and combined hemorrhage models that are associated with experimental trauma and tissue injury. However, the large variability within the models makes a standardized application of those shock models in life science challenging.

Sepsis and Septic Shock

Sepsis is defined as a "life-threatening organ dysfunction caused by a dysregulated host response to infection". If the severity of these dysregulations is associated with additional hypotension and increased serum lactate >2 mmol/l (18 mg/dl), which substantially increases the mortality, the condition is referred to as septic shock (50). Sepsis remains one of the main problems in healthcare, especially in the ICU (intensive care unit), as sepsis and septic shock are associated with a mortality of about 40% (51). However, the availability of effective supportive therapies that can complement, replace or even prevent treatment with antibiotics and surgical source control are very limited (52). Therefore, basic research is urgently needed to gain a better understanding of the underlying mechanisms that may improve the transfer from preclinical research to clinical usability. In the last century, many different animal sepsis models have been developed that aim to closely mimic human sepsis. In the following paragraph, we provide an overview of the most frequently used sepsis models in rodents.

Lipopolysaccharide (LPS) or Bacterial Injection Models

One of the first models was based on an intraperitoneal or intravenous injection of lipopolysaccharide (LPS, also referred to as endotoxin). LPS is a purified part of the wall of gram-negative bacteria (53) and injection of LPS into animals results in similarities to septic shock in humans, like elevated cytokine levels. However, there are fundamental differences in the cytokine dynamics, as cytokine levels rise and fall much faster than in humans (54). This might explain why clinical studies showed no beneficial effect of cytokine inhibiting agents blocking tumor necrosis factor-α or interleukin-1 (55). Many authors consent, that using LPS is not useful for finding an adequate sepsis therapy, as it is absent in gram-positive pathogens, but can be of use to understand the pathophysiology of single aspects of sepsis (53–57).

To more closely mimic human sepsis, but maintaining the easy handling and good reproducibility, different research groups have developed models based on intravenous or intraperitoneal injection of viable bacteria like *Escherichia coli (E. coli)*, *Pseudomonas aeruginosa* or *Bacteroides fragilis* (58–60). Intravenous bolus administration of *E. coli* leads to similar cytokine dynamics like the LPS models. Therefore, injection of bacteria leads to an endotoxin intoxication rather than induction of a true sepsis (61). This is the reason why several authors criticized the bacterial inoculation model and recommended a continuous bacterial infusion to simulate continuous bacterial release as it is present in human abdominal sepsis (61, 62). The combination of different aerobic and anaerobic pathogens covers a broader range of pathomechanisms than the LPS models. In addition to the choice of pathogens, the severity of the induced sepsis can be modified by the amount of colony-forming units and the specific strain (63).

A large proportion of septic patients suffer from respiratory infections, that are the original cause of sepsis (64). To mimic the human situation in experimental disease models, several investigators induce respiratory infection by administration of bacteria either directly into the lungs, or infuse them intratracheally or intranasally (65). These models helped to better understand the pathophysiology of bacterial, but also of viral pneumonia (66). However, investigators should take into account that besides systemic effects of generalized infections, the local tissue damage at the primary source of infection can impact the course of sepsis.

Fibrin or Fecal Clot Implantation and Cecal Slurry Injection

In 1980, Ahrenholz and Simmons presented a bacterial inoculum model based on a clot composed of fibrin and viable bacteria. The aim was to generate a slow and continuous bacterial release to gain a more realistic simulation of human sepsis compared to previous models (67). Technically, the clot is implanted into the peritoneal cavity *via* a midline laparotomy and can contain single or multiple strains of bacteria, or alternatively feces (63, 68, 69) and the severity of the disease can be adjusted by the choice and proportion of bacteria. Of note, the cardiovascular response that occurred after implantation of the bacterial fibrin clot showed similarities to human septic shock such as a decrease in peripheral vascular resistance and an increase in stroke volume index (70, 71). One disadvantage of this model is that that it mimics an abscess with peritonitis rather than abdominal sepsis (72).

Starr et al. developed a new protocol for cecal slurry (CS) injection that can be used in neonatal and adult mice (73). The aim was to generate a model that mimics neonatal diseases like necrotizing enterocolitis. To this end, cecal components of adult mice were mixed and resuspended with sterile water to generate the CS. Subsequently, the CS was filtered and mixed with phosphate-buffered saline (PBS) and injected intraperitoneally in mice of different age which resulted in sepsis with a severity that correlated with the dose of the CS. This method is particularly useful, as the small size of the neonatal cecum makes the use of a more complex sepsis model like the cecal ligation and puncture (CLP) or colon ascendence stent peritonitis (CASP) (see below) very difficult (74).

Cecal Ligation and Puncture and Colon Ascendens Stent Peritonitis

The surgical sepsis model "cecal ligation and puncture" (CLP) is considered to be the "gold standard" for polymicrobial sepsis (52). A median laparotomy is performed under general anesthesia, subsequently a section of the cecum is ligated on its oral part and then perforated by a needle (most commonly 18–25 Gauge) (75). CLP is characterized by a continuous bacterial release, which results in a more realistic simulation of an abdominal sepsis than bacterial injections. Size and number of the perforations, as well as the size of the ligation and the resulting cecal volume have a direct impact on the severity of sepsis in the CLP model (53). Moreover, this model shows an early hyperdynamic and a late hypodynamic phase, that is also present in human sepsis (76). To verify patency of the lesions, it is essential to slightly compress the cecum to push a small amount of feces through the perforations (75). Importantly, preclinical results of CLP models led to improved diagnostics and therapy. For example, interleukin-6 was found to be useful as a biomarker to assess the probability for sepsis mortality or the improved treatment of septic shock patients with low-dose glucocorticoids (77).

A variant of the CLP model, the so-called colon ascendens stent peritonitis (CASP) technique, was initially described in 1998 by Zantl et al. in mice and later on transferred to rats (78, 79). Similar to CLP, a median laparotomy is performed under general anesthesia. Subsequently, a stent is placed in the ascending colon and fixed with a surgical suture to induce a colon perforation or anastomotic insufficiency, leading to polymicrobial sepsis. As control, sham-operation is performed where stents are sewed to the cecal wall without inducing a perforation. The severity of the sepsis can be adjusted by removing the stents after a certain period of time (CASPi) (78) or by changing the size of the stents, allowing to study mild sepsis as well as septic shock (80). Moreover, removing the stents after 3 h has been used to simulate infectious source control and completely abolished mortality (78). The major difference between CLP and CASP is the resulting disease. CLP shows a more localized inflammation,

TABLE 2 | Experimental sepsis models and their specific advantages and disadvantages and the research areas where these models are useful for.

	Advantages	Disadvantages	Utilization
LPS / Bacterial Inoculation	Easy handling; No surgical trauma; Dose of LPS or bacteria can be standardized and used to adjust severity of disease	Leads to endotoxemia and septic shock Does not reflect the complexity of polymicrobial human sepsis	Insights into specific mechanisms or pathways associated with sepsis
Fibrin Clot	Low mortality and slow septic progress Continuous bacterial release	Surgical trauma Less bacterial variation if used with single bacterial strains	Useful to investigate abdominal peritonitis
Cecal slurry	No surgical trauma; Sepsis severity can be adjusted; Polymicrobial	Lethality varies between different donors	Sepsis especially in neonatal mice
CLP	Similar to human sepsis; Severity of disease can be adjusted; Polymicrobial	Variability depending on the size of the cecal ligation/perforation	Abscess formation with sepsis
CASP	Similar to human sepsis; Sepsis severity can be adjusted; Polymicrobial; Lower variability than CLP	Surgical trauma Time-consuming	Abdominal sepsis Investigation of surgical intervention (CASPi)

similar to an intraabdominal abscess, while CASP leads to diffuse, generalized peritonitis mostly seen in patients with anastomotic insufficiency (81).

Brief Summary of Experimental Sepsis and Septic Shock Models

The ideal sepsis model should "accurately reproduce the human disease" (82), which implies, that—in terms of abdominal sepsis—it should be polymicrobial, associated with similar pathophysiological changes and with a comparable rate of mortality. The main advantage of the LPS models is that they are highly standardized and easier to perform than surgical procedures like CASP or CLP. However, the most important limitation is that it does not adequately represent the complexity of the human pathology. Therefore, LPS- or bacterial injection models can be used to investigate the relevance of specific questions like the impact of certain cytokine pathways in sepsis (52). Application of pellets that contain bacteria or feces is very suitable to depict peritonitis, but has limited value for abdominal sepsis (57). Utilization of defined bacterial strains strongly reduces complexity, but does not display the polymicrobial character of human sepsis. However, a compromise could be to use defined mixed bacterial cultures (63). Those models that display the highest similarity to human abdominal sepsis like perforated diverticulosis, cholecystitis, bowel ischemia or anastomotic insufficiency are CLP and CASP. In both models, there is a high interindividual variability in the amount of feces that is released into the abdominal cavity (74). However, it should be kept in mind that CASP leads to abdominal sepsis, whereas CLP induces an abdominal abscess. Taken together, every model has its advantages and disadvantages (**Table 2**), and it should be carefully evaluated which model is suitable to provide the insights that are necessary to answer a specific research question.

TECHNICAL DEVICES TO DETERMINE STRUCTURE AND FUNCTION OF TISSUE MICROCIRCULATION

In the previous section, we described animal models that can be used to investigate certain aspects of hemorrhagic and septic shock. All shock-forms severely affect the local microcirculation that subsequently leads to impaired oxygen delivery and/or utilization. This has profound impact on organ function and can also lead to tissue damage. To gain a better understanding of how shock forms affect the local oxygen exploitation, it is important to investigate how microcirculatory parameters are altered in certain animal disease models. In the following paragraphs, we provide an overview about methods to assess the structure (Section "Evaluating the Structure of the Microcirculation"), and functional aspects of the microcirculation such as perfusion (Section "Microvascular Perfusion: Laser Doppler Flowmetry or Regional Capnometry"), oxygen levels (Section "Oxygen Levels and Hemoglobin") and mitochondrial function (Section "Mitochondrial Function").

Evaluating the Structure of the Microcirculation

The term "structural microcirculation" takes into account that a heterogeneous tissue perfusion can result in hypoxic areas while the total microcirculatory perfusion is maintained (83). Landmark papers from De Backer (84), Ince (85) and Trzeciak (86) found a discrepancy between macro- and microcirculatory variables in septic patients and suspected microcirculatory parameters to be more sensitive to predict multiorgan failure and mortality. This has led to the development of guidelines for the evaluation of microcirculatory alterations in critically ill patients (87, 88). Thus, assessment of microcirculatory status is still a serious clinical challenge, especially under pathological circumstances, like shock. Tissue perfusion is a very dynamic process that can be visualized by videomicroscopic techniques like nailfold videocapillaroscopy or hand-held vital microscopy (HVM).

Nailfold videocapillaroscopy has been used at the bedside to evaluate structural abnormalities in chronic diseases such as vasculitis (89) and diabetes (90). To this end, fingers are placed on the stage of an ordinary microscope, covered with oil and then the capillary density, microvascular blood flow and the averaged vessel thickness can be evaluated and results are interpolated to the general microvascular status. Unfortunately, nailfold videocapillaroscopy is not suitable to

evaluate structural microcirculation in shock states due to the high responsiveness of the nailfold arterioles to vasoconstrictor effects of catecholamines, which are standard therapeutics for any kind of shock. Furthermore, this technique can also barely utilized for other parts of the human body.

HVM-devices were developed to visualize the structural microcirculation and were primarily used for imaging sublingual vessels. First-generation HVM-devices were based on orthogonally polarized spectrum (OPS-) imaging (91), but are no longer available. The second generation utilizes sidestream (SDF-) dark-field imaging. Green-light electrodes surrounding the detector field are emitting pulsed light with a wavelength of 530 nm, which is the isobestic point for hemoglobin. This means that the obtained image is composed of the amount of absorbed light, which is independent of hemoglobin's oxygenation state and the light reflected by deep layers of the investigated tissue. Erythrocytes appear as dark spots and generate the vessel images *via* their axial migration (92). The variable focus of a complex lens system determines the penetration depth and enables the assignment to a specific tissue layer. The third generation HVM is characterized by a very high grade of optical resolution and image quality (for an example image, see **Figure 1**). The underlying principle is called incident dark-field (IDF-) imaging and it employs a high-resolution imaging chip and short pulsed illumination source that are synchronized to control illumination and image acquisition (93). Aykut et al. performed a prospective, observational study to compare SDF- and IDF-imaging devices and came to the conclusion, that IDF showed increased contrast, sharpness, and image quality for venules and capillaries and therefore gained an improved imaging modality for clinical assessment of microcirculatory alterations (94). Many research groups used HVM to evaluate the microcirculation, particularly in the sublingual area, of critically ill patients.

The main advantage of HVM is the simultaneous evaluation of tissue perfusion and oxygen diffusion distance. To measure tissue perfusion, the main flow characteristics of erythrocytes are scored from 0 (no flow) to 3 (continuous red blood cell flow) and merged to the averaged value "microvascular flow index" (MFI). More important than the absolute velocity of erythrocytes is the predominant type of vascular flow (stopped-flow vs. high velocity capillaries) and flow continuity (pulsatile, intermittent or continuous). Furthermore, spatial heterogeneity in capillary density can also be estimated by HVM. In this context, De Backer et al. introduced a method to evaluate the functional capillary density (FCD) as a marker of oxygen diffusion distance (87). For a quantitative estimation of microcirculatory parameters, they combined total vessel density (TVD) with flow categories (existent, intermittent or absent) to determine the perfused vessel density (PVD) and to calculate the proportion of perfused vessels (PPV). Finally, depiction of flow characteristics in space-time-diagrams can offer further information on the geometrical and functional structure of microvascular beds, flow profiles and the rolling and adhesion of leukocytes (95). Even, if IDF-imaging is a method to visualize the structure of the microcirculation, it can provide multiple additional functional parameters like blood convection, flow characteristics and inflammatory response. In summary, each individual technique has a focus on different aspects of the complex microcirculatory network and the combination of different methods can lead to a more precise picture of the microvascular oxygen delivery and exploitation.

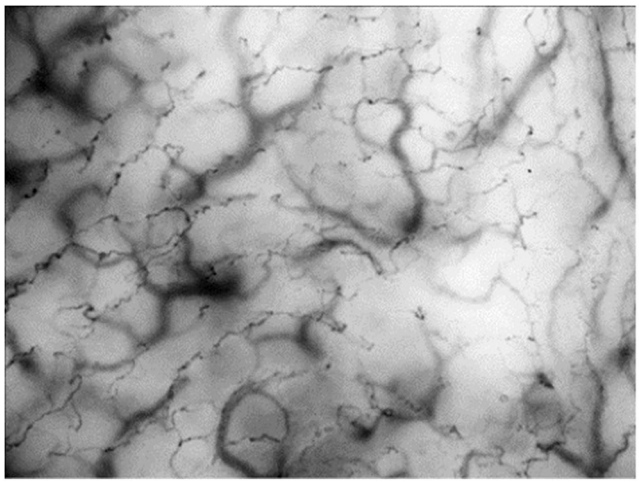

FIGURE 1 | Incident dark-field (IDF-) imaging of oral microcirculation in dogs using hand-held vital microscopy (HVM). Red blood cells are visualized as dark spots forming vessels through their axial migration. According to manufactures IDF-devices are able to register a field of view with 1.55 × 1.16 mm. Oral microcirculation is shown with an additional magnification factor of 4.

Microvascular Perfusion: Laser Doppler Flowmetry or Regional Capnometry

Laser doppler flowmetry (LDF) utilizes the doppler shift that is a frequency shift when laser of a specific wavelength is reflected by moving particles or cells (96). The surrounding tissue does also reflect the light, but does not induce a frequency shift and therefore the obtained datasets are composed of shifted and unshifted laser light. LDF provides information about the average blood flow in a variable sample volume that depends on the individual vascularization of the examined tissue, but it is not possible to get information of single microvessels. This means that results obtained with LSF are provided as relative units that pays attention to a variable number of vessels, differences in sampling volume and various directions of blood flow (97).

Adequate tissue perfusion is not only needed for sufficient oxygen delivery, but also crucial for the removal of metabolic products. Thirty years ago, Tang et al. suggested tissue carbon dioxide concentration (p_tCO_2) as a marker of adequate tissue perfusion (98). Post resuscitation, an increase in end-expiratory CO_2 indicates circulatory restoration, which is able to perfuse microvascular beds to wash out carbon dioxide. Moreover, an increasing arteriovenous CO_2-gap in controlled ventilated patients can indicate a perfusion deficit in high-risk surgery (99). In conclusion, p_tCO_2 and especially p_tCO_2-p_aCO_2-gradients (regional tissue vs arterial CO_2 partial pressure) may be valuable indicators of tissue perfusion (100). Regional CO_2-tension can be measured by tonometry or a CO_2-sensing fluorescence dye (e.g., l-hydroxy-pyrene-3,6,8-trisulfonate (pyranine), shortly

HPTS) (101) and can be performed sublingual, endogastral, transcutaneous or in the bladder (102). Technically, saline or air is enclosed by a membrane that is semi-permeable for CO_2 (103) and after equilibration of the CO_2-partial pressure between both compartments, the content is aspired and analyzed by infrared spectrometry or conventional gas analysis methods (102).

Oxygen Levels and Hemoglobin

Oxygen—once released from hemoglobin—follows the gradient of its partial pressure from the vascular space to the intracellular mitochondria. In conclusion, pO_2-distribution is inhomogeneous within tissues and therefore experimentally determine pO_2-values are the mean of a local oxygen gradient. The most widely used techniques to determine pO_2-values are *via* electrodes or phosphorescent probes.

Due to alterations of the structural microcirculation and regional perfusion heterogeneity hemoglobin levels determined from arterial blood gas analysis cannot be transferred directly to the calculation of microvascular variables. Technically, regional hemoglobin levels can be evaluated non-invasively by reflectance spectroscopy (104). In short, white light is emitted into the investigated tissue and scattered at cellular components or absorbed by hemoglobin molecules. The proportion of absorbed light correlates with the total amount of hemoglobin and the difference between emitted and reflected light can be used to calculate the regional hemoglobin concentrations (97). In this case, the hemoglobin content refers to the examined tissue volume instead of the intravascular volume and therefore is named regional hemoglobin concentration (rHb) (104).

Besides the measurement of rHb, light-spectrophotometry can also determine the microvascular hemoglobin oxygen saturation (μHbO_2). Whereas oxygenated hemoglobin mainly absorbs light with wavelengths about 900 nm at the near infrared spectrum, deoxygenated hemoglobin dominantly absorbs red light with wavelengths about 680 nm. The analysis of the reflected light-spectra allows for calculation of the proportion of oxygenated hemoglobin. Fortunately, this technique is limited to small capillaries since vessels with diameters larger than 100 μm lead to total absorption, due to the high amount of hemoglobin (105). Therefore, light-spectrophotometry is suitable to evaluate microcirculatory variables without any impact of macrocirculatory vessels. Technically, spectrophotometry cannot distinguish between arterial and venous vessels, because the regional volume of the venous system exceeds that of the arteria and therefore μHbO_2 mainly indicates postcapillary oxygen saturation. Thus, μHbO_2 does not represent microvascular oxygen delivery, but microvascular oxygen content. However, the correlation of μHbO_2 and cellular oxygen reserve is only valid if the tissue-perfusion is homogeneous. Shunting within the microcirculation leads to an inhomogeneous tissue-perfusion and an increase in μHbO_2, which was shown to be related increased mortality (37). Increased μHbO_2 can falsely suggest a sufficient oxygen delivery, but rather reflects an impaired oxygen utilization due to inhomogeneous microcirculation.

Clark electrodes usually consist of serial platinum wires acting as proton donators. Oxygen diffusion through a semipermeable membrane leads to proton transfer and the formation of OH^-, which reacts with a corresponding anode (106) and the current is proportional to the oxygen tension (107). Thereby, pO_2 is measured in a defined volume independent of the grade of vascularization. Results have to be interpreted carefully, because Clark electrodes are typically used in homogeneous samples with a constant oxygen tension. In heterogeneous samples, measurements are more sensitive to the highest values in the sampling volume that leads to an overestimation of the local pO_2 (108). Measurement of oxygen tension in epithelial cell layers (109) or deeper target tissues can be done with surface- and needle-electrodes that do not affect microcirculatory parameters (110). However, correct placement of the electrodes leads to tissue trauma, which may influence regional metabolism and thus oxygen balance (104).

Palladium-containing porphyrine compounds show an oxygen tension dependent phosphorescence quenching after a pulsed light stimulation (111). To address the fact, that oxygen diffusion through tissues mainly depends on the magnitude of intravascular oxygen tension, palladium porphyrine is conjugated to human albumin to verify that the probe is maintained within the vascular system and does not diffuse into tissue (104). Therefore, palladium porphyrine based methods focus on intravascular oxygen tension. Limitations of this method are the time-dependent decrease in palladium porphyrine concentration and its potential to provoke allergic reactions. Furthermore, palladium-dyes are toxic for humans, which prohibits the use in patients (112).

Mitochondrial Function

Regarding a very complex cascade of impaired processes by oxygen delivery and utilization in a shock state, it is pivotal to assess also the final step of oxygen consumption taking place in the respiratory chain in the inner mitochondrial membrane. Unfortunately, there are no clinically established methods for bedside measurement of all aspects of the mitochondrial respiration. The assessment of the functionality and efficacy of the respiratory chain can only be performed *in vitro* or *ex vivo* as described in the following chapter. A short insight into the novel but very promising devices for mapping the mitochondrial oxygen consumption in a clinical setting can be found in the last chapter "From bench to bedside" (see section From Bench to Bedside).

States of Mitochondrial Respiration

Mitochondria are those intracellular organelles that are responsible for about 90% of total oxygen consumption in mammalian cells, 80% of which is coupled to ATP synthesis. Present in nearly all types of human cells, mitochondria are vital to our survival. Besides their main task the energy production, they are also involved in many other cellular processes, including calcium homeostasis, and regulation of cell death (113).

Mitochondrial respiration takes places in the inner mitochondrial membrane through four large protein complexes (I–IV) as well as the adenosine triphosphate (ATP) synthase (AS) (also called complex V). Coenzyme Q (Q) and cytochrome C (C)

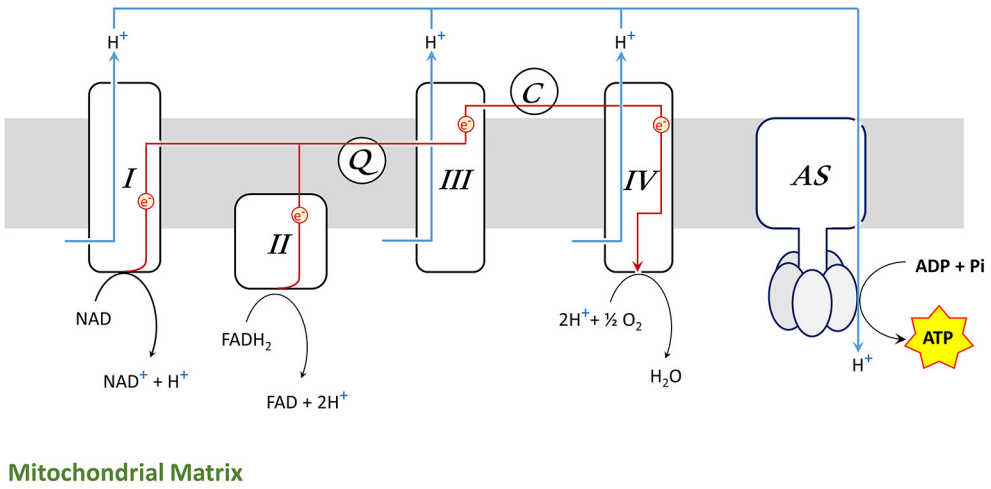

FIGURE 2 | Electron transport chain (ETS) in the inner mitochondrial membrane [complexes I–IV, ATP synthase (AS), coenzyme Q (Q), cytochrome C (C)].

are diffusible electron carriers between complex II and III (Q) and between complex III and IV (C), respectively (**Figure 2**).

Complex I oxidizes NADH to NAD^+ and complex II reduces $FADH_2$ to FAD, donating electrons, which are transported along the complexes to generate H_2O in a reaction involving molecular oxygen and hydrogen protons (H^+) at complex IV. Simultaneously, complex I, III, and IV are pumping H^+ across the inner membrane, creating a gradient which drives hydrogen back through AS and provides energy for phosphorylation of adenosine diphosphate (ADP) into ATP. The synthesis of ATP by mitochondria is called oxidative phosphorylation (OXPHOS).

The mechanism that underlies the energy-generating capacity of mitochondria was described by Mitchell in 1961 (114) and awarded with the 1978 Nobel Prize in chemistry. He described four states of mitochondrial respiration, which occur under physiological circumstances and can be simulated by the selective use of different stimulators and inhibitors to gain a detailed insight into the mitochondrial respiration (**Figure 3**).

Mitochondrial state 1 respiration is a basal form of oxygen consumption that occurs in an environment which is poor in substrates for the electron transport chain and ADP. Mitochondrial state 2 respiration represents a situation with an abundance of substrates for the electron transport chain. Complex I is triggered by glutamate and malate, which both provide NADH as substrate for complex I. Glutamate is oxidized by the enzyme glutamate dehydrogenase to α-ketoglutarate and the malate dehydrogenase oxidizes malate to oxaloacetate. Both reactions are driven by the reduction of NAD^+ to NADH. In parallel, complex II is fueled by electrons derived from $FADH_2$ which is generated *via* the succinate dehydrogenase that converts succinate to fumarate.

To differentiate between the function of complex I and II, complex I can be blocked by adding rotenone prior to the addition of succinate. Rotenone prevents the back-flow

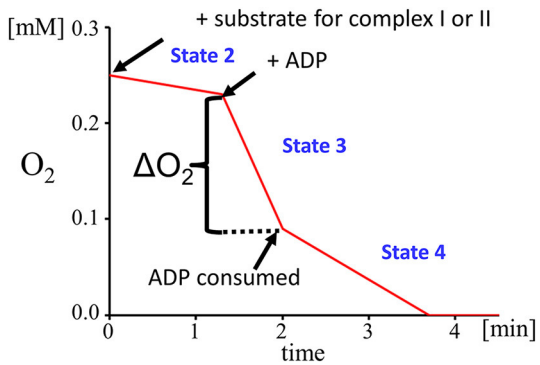

FIGURE 3 | Respiratory states: state 2 (substrate dependent respiration), state 3 (ADP dependent respiration), state 4 (steady state respiration after ADP depletion).

of electrons from complex II to complex I. The low level of mitochondrial respiration (state 2) can be altered experimentally by the addition of ADP, which initiates a flow of protons from the intermembrane space to the mitochondrial matrix. This proton gradient provides the energy that is required by the ATP synthase to phosphorylate the added ADP into ATP. This is the so-called state 3 mitochondrial respiration. A limiting factor for state 3 respiration is the concentration of ADP. To define a measure of the coupling between the electron transport chain and the OXPHOS the respiratory control index (RCI) is calculated by dividing state 3 by state 2. Another parameter reflecting the efficiency of OXPHOS is the ADP/O ratio that is calculated from the amount of ADP added and the O_2-consumption measured during state 3. When ADP is consumed, a steady state of respiration is reached which is called state 4 respiration.

It should be noted that, even though there is only one outcome parameter (oxygen consumption), the conditions of the experiment can be chosen very specifically to link effects to a particular part of the respiratory chain or to a specific enzymatic reaction. Using combinations of different mitochondrial substrates, inhibitors, and stimulating agents, mitochondrial capacity can be characterized extensively and very precisely, just by measuring oxygen consumption under these experimental conditions.

Measurement of Mitochondrial Respiration

Measurement of mitochondrial respiration can be performed in either isolated mitochondria, or tissue- and cell-preparations, in which the barrier function of the plasma membrane is either mechanically disrupted or dissolved by application of mild detergents.

Assessment of mitochondrial respiration on isolated mitochondria obtained by differential centrifugation was considered as the gold standard for decades. But there are severe limitations and drawbacks of this isolation technique, as it is impossible to obtain the whole population of the tissue mitochondria. For example, only 40% of cerebral and about 10% of hepatic mitochondria can be retrieved by this procedure (115). Furthermore, the mitochondrial fraction obtained by this isolation technique is not pure but is contaminated with microsomes. Further purification steps are laborious and require time, money, and resources.

As an alternative, tissue homogenates are also routinely used for assessment of mitochondrial oxygen consumption, enzyme activities (116), membrane potential, or protein content (117). The main advantages of using tissue homogenates are: limited workload, stability of the tissue samples, small tissue sample required for measurement (a fivefold of tissue is needed for analogous measurement with isolated mitochondria) (115). This method has also drawbacks like the heterogeneity of the cells (especially in tissues consisting of different cell types like gut or lung) and a large amount of biological active substances such as enzymes, substrates or inhibitors of the respiratory chain which can possibly affect the results. The measured parameters of mitochondrial functions are similar in both tissue homogenates and isolated mitochondria and they are both widely used dependent on research questions, tissue, and study design. It is also possible to measure mitochondrial respiration in cell culture. Of note, assessment of mitochondrial respiration is hampered by the cellular plasma membrane. The plasma membrane consists of a lipid bilayer, proteins, and further organic molecules that prevent the passage of many water-soluble mitochondrial substrates, such as succinate or ADP, that are required for the analysis of mitochondrial respiration. To overcome this difficulty, mild detergents such as digitonin and saponin can be applied to selectively permeabilize the plasma membrane but not the mitochondrial membranes, since the cholesterol content of the plasma membrane is higher compared to mitochondrial membranes.

Different devices based either on polarographic principle (Clark electrode) or on fluorophore's technique are available for the assessment of mitochondrial oxygen consumption. Both methods are suitable for isolated mitochondria, tissue homogenates or cells (see below).

Available Devices for Respirometry

Polarographic Respirometry for Measurement of Oxygen Consumptions in Isolated Mitochondria, Cells or Tissue Homogenates in a Closed Chamber

The main principle of polarographic respirometry is that oxygen diffuses through a teflon/polypropylene membrane, which is permeable to uncharged gases but not to water. A platinum/silver/KCl coupled electrode reduces oxygen and oxidizes silver, producing a current which is proportional to the oxygen concentration (118). This method can be used for measurements in intact cells, tissue homogenates and isolated mitochondria.

Optical Sensor Probes to Determine O_2 Consumption in Multiwell Plates

Oxygen consumption can also be determined using an optical probe. Changes in oxygen concentration and pH are detected by two fluorophores and automatically calculated and reported as Oxygen Consumption Rate (OCR) and ExtraCellular Acidification Rate (ECAR). The measurements are performed in real time, which enables collecting kinetic data of cell metabolism.

The probes are inserted into the culture medium within a small chamber and placed in close vicinity to the cells. Another possibility to monitor oxygen consumption is using plates coated with porphyrine. Porphyrine molecules are characterized by fluorescence signals in the near-infrared range that are quenched in the presence of oxygen. This technology is mainly used for cytotoxicity measurement, because O_2 consumption is one of the most sensitive parameters for cell toxicity (119).

IMAGING THE CONSEQUENCES OF IMPAIRED OXYGEN DELIVERY BY MRI

In the previous chapters, we describe technologies that allow for measurement of structural and functional microcirculation, oxygen levels and mitochondrial activity—processes that are strongly impaired in the acute phase of septic and hermorrhagic shock. These technologies allow for a detailed characterization of the structure and function of the local microcirculation, but they are invasive or only applicable to the surface of specific tissues. Here we present magnetic resonance imaging as a versatile imaging technology that is not limited by penetration depth and which can be utilized for animal models described in section "Animal Disease Models to Study Hemorrhagic and Septic Shock" and can complement the technologies described in the third part of this review. Sepsis and hemorrhagic shock are very complex diseases and MRI as multimodal whole-body imaging technology can acquire parallel information about anatomy, organ function, metabolism, inflammation and thrombotic processes. In the clinical context, MRI is not the optimal technology for the acute phase of critically ill patients, but it can be used to monitor the short- and long-term effects and consequences of impaired oxygen delivery over time in multiple inner organs.

^{1}H MRI to Determine Anatomy and Function of Organs

The most widely used biomedical application of magnetic resonance imaging is the visualization of the anatomy of inner organs that can be used to detect tumors, abnormalities in the brain tissue or the spinal cord, or to diagnose cardiovascular diseases such as atherosclerotic plaques, the formation of aneurysms or heart disease. MRI can acquire three-dimensional datasets, therefore it does not only determine regional alterations in cross-section images, but can also provide volumetric data of whole organs.

In addition, it is possible to derive multiple types of functional information. Cardiovascular MRI of the heart is used to determine endsystolic-, enddiastolic volumes, stroke volume, ejection fraction and multiple other parameters (120). Brain activity is associated with changes in blood flow and the amount of oxy- and desoxyhemoglobin and these parameters are used by functional MRI (fMRI) to gain information about brain activity (121). One crucial aspect of proper organ functionality is the integrity of the vascular system. MR-angiography (MRA) enables the visualization of the flowing blood, that is used to assess vessel geometry or to calculate pulse-wave velocities to identify stenosis or aneurysms (122). More recently, sophisticated four-dimensional angiographic imaging techniques have been developed that enable a quantitative assessment of time-resolved flow profiles of larger vessels (123). Due to limitations in sensitivity, MRI of small capillaries (microcirculation) is more difficult. To gain information about the functionality of the microcirculatory system, perfusion-imaging techniques have been developed, which are conducted by the application of gadolinium-based contrast agents, the utilization of oxy- and deoxyhemoglobin or arterial spin labeling (124, 125).

Another interesting feature of MRI is that it has the capability to quantitatively characterize alterations in tissue properties. Parametric MR-mapping techniques to determine T1- and T2-relaxation values (T1-, T2-mapping), proton density or CEST (chemical exchange saturation transfer) effects. These mapping techniques provide a quantitative pixel-by-pixel representation of the obtained values for a certain organ (126). T1- or T2-mapping has been used to gain information about the presence of tissue edema or fibrosis (127–129), whereas proton density mapping has been utilized to determine tissue water content (130), hepatic fat (131) or for tissue-texture analysis (132). An important feature of the tissue-texture is the extracellular matrix that contains numerous exchangeable protons—in particular in the hydroxylated sugar moieties of hyaluronic acid and glycosaminoglycans—that can be visualized by CEST (133). CEST-mapping has for example been performed in mice after myocardial infarction or in graves orbitopathy to monitor remodeling of the extracellular matrix (127, 134).

Magnetic Resonance Spectroscopic Imaging and MRI of X-Nuclei

It is important to note that the magnetic properties of ^{1}H-protons are not all identical, but the resonance frequency depends on the chemical structure of the molecule. For example, the ^{1}H-protons of water and fat show a chemical shift of 3.4 ppm and therefore, fat and water can be measured separately which has been used to determine alterations in the fat content (135). However, other hydrogen atoms in a certain chemical environment possess distinct chemical shift properties that can be identified *in vivo* by single voxel magnetic resonance spectroscopy (MRS) or multi-voxel MR-spectroscopic imaging [also called chemical shift imaging (CSI)]. These techniques allow for a non-invasive detection and quantification of a number of metabolites from localized volumes within living organisms (136). This has been used to detect N-acetyl aspartate acid, choline, creatine, lactate, myo-inositol and glutamate as well as glutamine in the brain (136). Of note, chemical shift imaging is not limited to ^{1}H, but can also be applied to other MR-active nuclei like ^{13}C, ^{31}P that have been utilized in the past for visualization of metabolites in the heart or the liver (137, 138).

TABLE 3 | NMR-relevant properties of some nuclei. Data is adapted from references (139, 142, 143).

Element	Isotope	Nuclear spin	Gyromagnetic Ratio (γ) [10^7 × rad × s^{-1} × T^{-1}]	Natural abundance [%]	NMR frequency (MHz) at 9.4T
Hydrogen	**^{1}H**	1/2	26.75	99.98	400,2
Carbon	**^{13}C**	1/2	6.73	1.07	100.7
Oxygen	**^{17}O**	5/2	−3.63	0.04	54.3
Sodium	**^{23}Na**	3/2	7.08	100.00	105.9
Phosphorous	**^{31}P**	1/2	10.84	100.00	162.2
Chlorine	**^{35}Cl**	3/2	2.62	75.77	39.3
Potassium	**^{39}K**	3/2	1.25	93.10	18.7
Rubidium	**^{87}Rb**	3/2	8.79	27.83	131.4
Fluorine	**^{19}F**	1/2	25.16	100.00	376.7

Apart from ^{1}H-protons, MRI can detect a number of other nuclei with a nonzero spin quantum number like ^{35}Cl, ^{31}P, ^{39}K, ^{17}O, ^{13}C, ^{23}Na or ^{19}F (139, 140) (see **Table 3**). Detection of these X-nuclei is not used for anatomical purposes, but can provide insights into physiological processes (139, 141). Na^+, K^+ and Cl^- regulate cell membrane potential and impact the cell volume, whereas ^{17}O can provide insights into oxygen consumption. ATP and phosphocreatine are important products of the cellular energy metabolism that can be detected by ^{31}P MRI and has been used to get insights into the metabolism of murine hearts (137). Organic molecules contain a backbone of carbon atoms and ^{13}C-spectroscopy has been widely used to track organic metabolites (139). However, most of the X-nuclei display a quite low sensitivity compared to the ^{1}H nucleus, which makes the detection and imaging quite challenging. One interesting exception is fluorine 19 (^{19}F) that has a gyromagnetic ratio close to ^{1}H, a natural abundance of 100% and is nearly absent from biological tissues. As a consequence, detection of ^{19}F tracer molecules by ^{19}F MRI within living organisms can be conducted with high sensitivity and specific and makes this very attractive for a variety of MRI approaches (Section "Tracking of Immune Cell Trafficking by ^{1}H/^{19}F MRI").

Septic and hemorrhagic shock states both coincide with alterations in tissue metabolisms partly due to limited oxygen supply or the action of proinflammatory cytokines. Noninvasive MR-imaging of metabolites like lactate, or the assessment of energy levels (ATP or PCr) could help to identify severely affected organs and to localize and characterize those regions within organs that are suffering from impaired oxygen delivery and exploitation.

Imaging of Inflammatory Processes by MRI

Both hemorrhagic as well as septic shock are associated with inflammatory processes that contribute to tissue injury and in severe cases can lead to multi organ failure (144, 145). Noninvasive imaging of the associated inflammatory reaction by MRI can help to assess the overall magnitude of the systemic inflammatory response, can identify affected organs or help to unravel novel mechanisms. Direct visualization of inflammatory processes or inflammatory cells by classical MRI is difficult, because particularly in the early phase the affected tissue with infiltrated cells does not cause physical alterations that can be converted into MR-contrast. To overcome this limitation, contrast agents or tracers have been developed that highlight certain aspects of the inflammatory reaction (146).

One of the most important hallmarks of an immune response is the infiltration and accumulation of different kinds of inflammatory cells like neutrophils, monocytes and macrophages or T-cells. One of the most popular MR contrast agents that are used for the visualization of monocytes and macrophages are SPIOs or USPIOs (small/ultra-small paramagnetic iron oxide nanoparticles). SPIOs have a size of 50–100 nm, are strongly internalized by monocytes and macrophages and therefore utilized for detection of tumors (liver) and inflammatory processes (147, 148). USPIOs have a diameter of <50 nm, possess a longer blood retention time and can also be used as contrast agents for MR angiography (149). The major advantage of this approach is a very high sensitivity, but there are also drawbacks. The local accumulation of iron oxide particles leads to the disruption of the ^{1}H signal (negative contrast) in this area that can make the identification of correct anatomical localization difficult and there is no linear correlation between signal decay and iron oxide concentration that complicates absolute quantification.

Tracking of Immune Cell Trafficking by ^{1}H/^{19}F MRI

An alternative approach to visualize inflammatory immune cells is based on perfluorocarbon nanoemulsions (PFCs) or nanoparticles that are visualized by ^{19}F MRI. The accumulation of ^{19}F atoms within organisms can be detected with high sensitivity and specificity and as opposed to iron oxide nanoparticles generates a true positive contrast that does not interfere with the anatomical ^{1}H images. Perfluorocarbons are fluorinated organic molecules with a high ^{19}F-content that have to be emulsified or encapsulated for biomedical applications (150). High pressure homogenization or microfluidization with lipids as emulsifier leads to the generation of PFC-droplets with a hydrodynamic diameter of 100–200 nm (**Figure 4**) (150). Alternative methods to generate biocompatible perflurorocarbon ^{19}F-tracers are the emulsification with poloxamers or encapsulation into PLGA (Polylactid-co-Glycolid) nanoparticles (151, 152).

Accumulation of PFCs in inflammatory lesions has already been observed in the 1980s (153), but the first systematic investigation that verified the internalization of intravenously administered PFCs by monocytes and macrophages after myocardial infarction and stroke has been published in 2008 (154). Density separation of the blood, flow cytometry and histochemistry verified that PFCs can be internalized by monocytes and that PFCs colocalized with monocytes and macrophages within the infarct area. These findings were confirmed in follow-up studies of this group (155–159) and independent studies from other groups (160–167), which has manifested the concept that intravenously injected PFCs are internalized by phagocytic immune cells that accumulate at inflammatory lesions and can be detected by combined ^{1}H/^{19}F MRI (**Figure 4**). However, cellular uptake of PFCs is not purely specific for monocytes/macrophages and under certain circumstances other cells like neutrophils (156, 168) or even specific progenitor cells within the heart (169) can contribute to the local ^{19}F signal.

An alternative strategy to visualize immune cell trafficking is the *ex vivo* labeling of cells with PFCs followed by reimplantation and subsequent ^{1}H/^{19}F MR imaging. This approach is of particular interest for specific cell types that cannot be selectively labeled by intravenous injection of PFCs or for cell-therapeutic approaches like dendritic cells (DC) or T-cells. A pioneering study by Ahrens et al. (170) utilized PFCs to label dendritic cells *ex vivo* and monitored DC migration into the popliteal lymph nodes by ^{19}F MRI. In principle, *ex vivo* labeling requires strong phagocytic properties which are absent in T-cells. However, the addition of transfection reagents or the development of specialized PFCs enabled an efficient labeling of T-cells that made it possible to track their migration into lymph nodes or the pancreas (171, 172). *Ex vivo* labeling is an interesting strategy to load isolated cell types, but the isolation and incubation can change the functionality of the cell types and the cell population has to be purified from PFCs that were not internalized during the loading process.

Visualization of Thromboinflammatory Processes by Multiplex ^{1}H/^{19}F MRI

The chemical shift range for ^{19}F atoms spans over 400 ppm (173) and some of the perfluorocarbons display individual spectral signatures. Utilizing PFCs with distinct spectral properties enables the detection of several target structures or cell types. The first report for such a multispectral ^{19}F MRI was published in 2007 and showed the labeling of human progenitor cells with PFOB- or PFCE-PFCs (174). With raising interest in ^{19}F MRI, several recent publications addressed multispectral or multicolor ^{19}F MRI for *in vivo* imaging of distinct ^{19}F-nanotracers such as nanoemulsions, nanoparticles or even nanocrystals (175–179). These approaches nicely show the feasibility of multispectral ^{19}F MRI, but do not combine multispectral ^{19}F-MRI with the targeting and visualization of several structures *in vivo*.

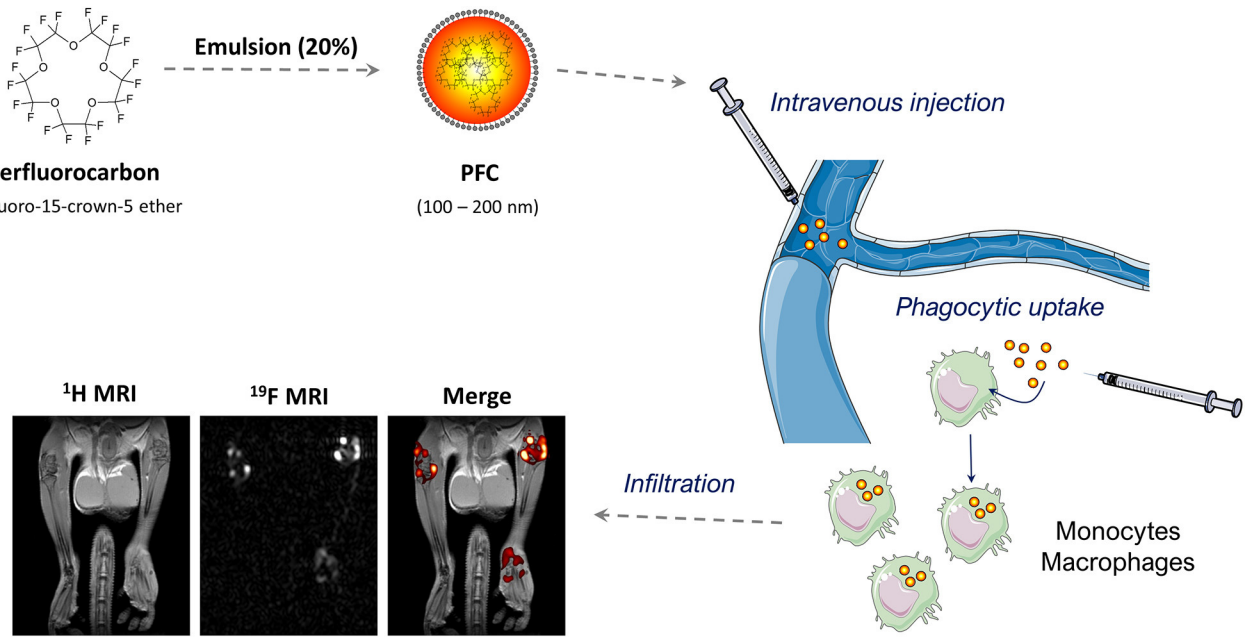

FIGURE 4 | ^{19}F MRI-based inflammation imaging: Perfluorocarbons are emulsified by high-pressure homogenization to generate perfluorocarbon nanoemulsions (PFCs) with a size between 100 and 200 nm. Intravenous injection of PFCs leads to cellular uptake by circulating or local phagocytic immune cells—particularly monocytes and macrophages. The accumulation of these cells is detected by combined ^{1}H/^{19}F MRI. The MRI images show the anatomy of legs and hips of a male mouse with collagen-induced arthritis (left), the corresponding ^{19}F dataset (middle) and a merging of both (right). Note that the merged image reveals the anatomical localization of the phagocytic immune cells. ^{1}H/^{19}F MRI images were adapted from Flögel et al. (156), and elements of the schematic figures were derived from: https://smart.servier.com/.

Over the past years, our group has established a platform for the active targeting of PFCs and we were able to functionalize PFCs with specific targeting ligands and to use this technology to visualize thrombi (180–182), activated platelets (183), cells expressing synthetic receptors (184) or specific progenitor cells of the heart (185). Moreover, we recently implemented a ^{19}F-imaging technology, which enables the simultaneous detection of PFCs with distinct ^{19}F spectra and combined this with the simultaneous visualization of factor XIIIa-activity, fibrin and monocytes/macrophages (186). We exposed mice that express a hypomorphic mutant form of apolipoprotein E and also lack the scavenger receptor class B type I to a high fat/high cholesterol diet that leads to a thromboinflammatory phenotype with plaque ruptures and subsequent myocardial infarction (187). Using this multitargeted approach, it was possible to identify high-risk areas at very early time points and importantly the ^{19}F signal was predictive for consecutive development of myocardial infarction (186).

Preclinical MRI of Hemorrhagic and Septic Shock

Although shock states are of high clinical relevance and MRI systems provide a versatile multimodal whole body platform, the number of preclinical studies that utilize MRI to analyze the short- and long term-effects and consequences of hemorrhagic and septic shock is relatively limited. Animal studies have utilized classical ^{1}H-based anatomical, functional or parametric MRI mapping techniques to investigate alterations in tissue structure or perfusion in different organs. Below, the reader finds some examples for research studies including MRI measurements that have been conducted in different models of septic and hemorrhagic shock.

Septic Shock

Cerebral edema is a frequent finding in sepsis and is caused by breakdown of the blood brain barrier and by energy depletion of neutrons due to microcirculatory failure. Rosengarten et al. addressed the question whether early microcirculatory failure leads to brain edema (188). To this end, the authors utilized a rat model of LPS-induced endotoxemic shock, followed by sequential MRI investigations over several hours. Brain edema was monitored by diffusion weighted MRI and T2-mapping in several regions of the brain. However, the authors did not find alterations in diffusion coefficient or T2-values indicating that at least in this system, microcirculatory failure is not associated with the occurrence of brain edema (188).

Another organ-system that is severely affected by septic shock are the kidneys (189). To gain information about kidney function in polymicrobial cecal ligation and puncture (CLP), a gadolinium-based G4 dendrimer was administered and the accumulation of this agent was observed in the kidneys (190). The authors found that this technique can distinguish between different forms of renal failure but more importantly, that it has the capability to detect renal dysfunction earlier than an

increase in serum creatinine. An effect of septic shock on kidney function has also been found by Weidensteiner et al. (191) using dynamic contrast enhanced MRI after CLP. Gadolinium-DTPA (DTPA = diethylenetriaminepentacetate) was used to monitor the accumulation of the contrast agent in the kidneys and in the bladder. Interestingly, CLP led to a delayed washout of the contrast agent from the kidneys into the bladder that indicates impaired glomerular filtration.

It is known that shock can lead to the generation of reactive oxygen species, which can aggravate tissue damage. Visualizing reactive oxygen species by MRI is difficult, because of their very short half-life. To overcome this limitation, spin-trapping has been developed which is a technique that can be used to scavenge reactive oxygen species followed by visualization of the reaction products. Towner et al. investigated the possibility to visualize shock-induced free radicals by combined immuno-spin trapping and molecular MRI after CLP (192). The authors used DMPO (5,5-dimethyl pyrroline N-oxide) to trap reactive oxygen species 6 h after CLP and then administered a gadolinium-labeled anti-DMPO probe for MRI-detection. The authors found increased amounts of DMPO-adducts and elevated oxidative products in septic brains compared to sham controls. Another free radical that is produced by the vascular system under inflammatory conditions is nitrogen oxide (NO). To investigate the generation of NO during LPS-induced sepsis in mice and rats, Fuji et al. also utilized an iron-dithiocarbamate complex ($(MGD)_2$-Fe(II) = N-methyl-D-glucamine dithiocarbamate) which leads to the generation of $(MGD)_2$-Fe(II)-NO. This reaction product strongly decreases T1- and T2-relaxation of the surrounding water which was exploited to visualize the generation of NO under *in vivo* conditions in the liver tissue and vasculature of rats and mice under septic shock (193).

Hemorrhagic Shock

The liver is an important organ that responds to low flow states that are associated with trauma and hemorrhage. Experimental studies have demonstrated that these conditions lead to adhesion of leukocytes to the liver endothelium (194), changes in hepatic macrophages (195) and tissue damage (196). In this context, Matot et al. (197) utilized MRI of the liver in a rat model of hemorrhagic shock to evaluate tissue injury caused by reduced perfusion. Acute hemorrhage led to significantly reduced relative MRI signal changes, reflecting lower liver perfusion. Signal intensity also correlated with the percentage of blood loss. In another experimental study in rats, Maier et al. (198) investigated the impact of hemorrhagic shock on liver function and the activation of hepatic macrophages by MRI. The authors used a liver-specific contrast agent (Gd-EOB-DTPA) that is absorbed by hepatocytes and secreted into the bile fluid as well as SPIOs to label liver macrophages. Application of Gd-EOB-DTPA revealed a reduced secretory function of hepatocytes 24 h after shock, no difference was found after administration of SPIOs. However, the authors observed an activation of liver macrophages by fluorescently labeled latex beads, which could suggest that this MRI-approach is not sensitive enough to visualize the activation of liver macrophages under these conditions.

FROM BENCH TO BEDSIDE

Shock states are commonly characterized by regional hypoxia, anaerobic metabolism and cell damage. Consequently, the optimization of microcirculatory oxygen delivery as well as the maintenance of physiological cell metabolism should be the therapeutic goal to obtain tissue integrity and avoid cell damage. Nowadays, physicians still rely on surrogate markers to guide therapeutic interventions in critical care medicine. Integrating information about novel mechanisms, microcirculation, mitochondrial function and tissue damage with subsequent inflammatory reaction could strongly improve individual therapy decisions.

Patients under severe shock states are barely compensated and suffer from additional comorbidities and confounders that make the situation even more complex. Unfortunately, only a few microvascular beds are accessible that can be used to assess microcirculatory structure and function like the sublingual surface. HVM of sublingual vessels can provide a visual impression of microcirculatory alteration in shock states, but the application of HVM to other sides of the gastrointestinal tract is challenging and restricted to special situations like ICU patients with enterostoma (199) or open abdominal surgery (200, 201). However, imaging of the microcirculation can not only be used for diagnosis but also to monitor therapeutic approaches like the application of vasoactive substances to optimize blood flow kinetics and to prevent total vessel occlusion by pharmacological vasoconstriction (202, 203). Septic patients often receive excessive fluid substitution to maintain normal blood pressure which does not necessarily lead to increased cellular oxygen delivery (204), but results in tissue edema that enlarges the oxygen diffusion distance and may even impair tissue oxygenation.

Monitoring mitochondrial function in real-time *in vivo* is still not employed in clinical settings, but could complement the information obtained from microcirculation measurements, because it provides insights into O_2 utilization and energy production. One possibility to evaluate the activity of the respiratory chain *in vivo* is to measure the mitochondrial NADH redox state by monitoring UV absorbance or blue fluorescence of NADH (205). This technology still has some limitation like a need for better correction for hemodynamic artifacts and for quantification of the signals (205). Measurement of mitochondrial function in skeletal muscle is based on the recovery of muscle homeostasis after exercise by near-infrared spectroscopy (NIRS) and determines the return of muscle oxygen consumption to basal levels (206). Based on the protoporphyrine IX-triplet state lifetime technique (PpIX-TSLT) (207), Neu et al. established a new measurement protocol for the "Cellular Oxygen Metabolism" (COMET) allowing assessment of mitochondrial oxygen tension, consumption and delivery (208). The first results with septic patients were promising, but further studies in greater cohorts are required to establish potential diagnostic and therapeutic benefit of this method.

One of the disadvantages of the methods described above is that these techniques are mainly limited to superficial tissues. In contrast, MRI is not limited by penetration depth, but on the

other hand, it is not portable, expensive and has limited spatial resolution compared to HVM. In addition, MRI examinations are not suitable for critically ill patients in the emergency situation, but in the post-emergency situation, MRI can enable the assessment of organ anatomy, function, perfusion, oxygenation, alterations in the tissue texture and also metabolism. In this context, even mitochondrial function has been monitored by ^{31}P NMR-spectroscopy in skeletal muscle mostly in sports-medicine (209). Moreover, the technical capabilities of MRI systems are rapidly expanding with higher field strength, the development and implementation of multichannel array coils, novel imaging techniques and innovative data acquisition schemes like compressed sensing that shorten imaging times and increase sensitivity. Another field with high developmental potential is MR-based molecular imaging. Detection of macrophages in liver tumors has been conducted in the past with paramagnetic iron oxide nanoparticles (210). The translational potential of ^{19}F MRI is shown by the fact that PFCs have already been used in clinical trials as blood substitutes, that conventional ^{19}F-based inflammation imaging is feasible with clinical MRI systems at 3T in large animals (211, 212) and also a cell tracking study using autologous DCs in human patients with colorectal cancer has been performed (213). ^{19}F MRI is of particular interest, because there is negligible endogenous ^{19}F background (214), the accumulation of ^{19}F-atoms results in a true positive contrast that can be quantified and does not impair anatomical, functional and parametric ^{1}H MRI. Additionally, ^{19}F MRI is very versatile and multiple interesting approaches just recently emerged in the preclinical field like multispectral ^{19}F MRI, environmental responsive smart probes or active targeting of ^{19}F tracers (215, 216).

Finally, combining the information obtained by multiple types of devices for local microcirculation, oxygenation, function of mitochondria and organs with mechanistic insights derived from animal models could strongly support clinical decision-making and revolutionize therapy control in critical care medicine. Microcirculatory and mitochondrial monitoring could adjust global therapeutic approaches to the individual metabolic needs enabling differentiated vasopressor, fluid and transfusion regimes in the early course of disease. Later on, MR could identify tissues at risk as a consequence of temporary hypoxia, anaerobic metabolism and systemic and local inflammation. Paying attention to those critically compensated tissues and initiating organ-specific protective measures could avoid the entry in destructive cascades through an intensive organ cross talk and impede the development of multi organ failure.

AUTHOR CONTRIBUTIONS

SH, CM, AH, JS, RT, UF, and ST wrote individual chapters of the manuscript. IB, AR, OP, AK, SH, CM, JS, RT, UF, AH, and ST critically revised the whole manuscript. All authors contributed to the article and approved the submitted version.

FUNDING

This work was supported by the Deutsche Forschungsgemeinschaft (UF: SFB 1116, TRR 259, FL303/6-1/2, INST 208/764-1 FUGG and ST: TE1209/1-1/2) and the European Commission (MSCA-ITN-2019 NOVA-MRI, MSCA-RISE-2019 PRISAR2 to UF).

SUPPLEMENTARY MATERIAL

The Supplementary Material for this article can be found online at: https://www.frontiersin.org/articles/10.3389/fmed.2022.869372/full#supplementary-material

REFERENCES

1. Davis MJ. Perspective: physiological role(s) of the vascular myogenic response. *Microcirc N Y N 1994*. (2012) 19:99–114. doi: 10.1111/j.1549-8719.2011.00131.x
2. Granger HJ, Goodman AH, Cook BH. Metabolic models of microcirculatory regulation. *Fed Proc.* (1975) 34:2025–30.
3. Standl T, Annecke T, Cascorbi I, Heller AR, Sabashnikov A, Teske W. The nomenclature, definition and distinction of types of shock. *Dtsch Arzteblatt Int.* (2018) 115:757–68. doi: 10.3238/arztebl.2018.0757
4. Kanoore Edul VS, Ince C, Dubin A. What is microcirculatory shock? *Curr Opin Crit Care.* (2015) 21:245–52. doi: 10.1097/MCC.0000000000000196
5. Perlman RL. Mouse models of human disease: an evolutionary perspective. *Evol Med Public Health.* (2016) 2016:170–6. doi: 10.1093/emph/eow014
6. Council (US) NR. *Genetically Altered Mice: A Revolutionary Research Resource [Internet]. Sharing Laboratory Resources: Genetically Altered Mice: Summary of a Workshop Held at the National Academy of Sciences, 1993*. US: National Academies Press (1994). Available at: https://www.ncbi.nlm.nih.gov/books/NBK231336/
7. Frink M, Andruszkow H, Zeckey C, Krettek C, Hildebrand F. Experimental trauma models: an update. *J Biomed Biotechnol.* (2011) 2011:797383. doi: 10.1155/2011/797383
8. Rixen D, Raum M, Bouillon B, Lefering R, Neugebauer E. Arbeitsgemeinschaft "Polytrauma" of the Deutsche Gesellschaft fur Unfallchirurgie. Base deficit development and its prognostic significance in posttrauma critical illness: an analysis by the trauma registry of the Deutsche Gesellschaft für Unfallchirurgie. *Shock.* (2001) 15:83–9. doi: 10.1097/00024382-200115020-00001
9. Rixen D, Siegel JH. Bench-to-bedside review: oxygen debt and its metabolic correlates as quantifiers of the severity of hemorrhagic and post-traumatic shock. *Crit Care Lond Engl.* (2005) 9:441–53. doi: 10.1186/cc3526
10. Bakker J, Coffernils M, Leon M, Gris P, Vincent JL. Blood lactate levels are superior to oxygen-derived variables in predicting outcome in human septic shock. *Chest.* (1991) 99:956–62. doi: 10.1378/chest.99.4.956
11. Herminghaus A, Barthel F, Heinen A, Beck C, Vollmer C, Bauer I, et al. Severity of polymicrobial sepsis modulates mitochondrial function in rat liver. *Mitochondrion.* (2015) 24:122–8. doi: 10.1016/j.mito.2015.08.001
12. Skelton JK, Purcell R. Preclinical models for studying immune responses to traumatic injury. *Immunology.* (2021) 162:377–88. doi: 10.1111/imm.13272
13. Tremoleda JL, Watts SA, Reynolds PS, Thiemermann C, Brohi K. Modeling acute traumatic hemorrhagic shock injury: challenges and guidelines for preclinical studies. *Shock.* (2017) 48:610–23. doi: 10.1097/SHK.0000000000000901
14. Crowell JW, Smith EE. Oxygen deficit and irreversible hemorrhagic shock. *Am J Physiol.* (1964) 206:313–6. doi: 10.1152/ajplegacy.1964.206.2.313
15. Reynolds PS, Barbee RW, Ward KR. Low volume resuscitation with hbocs in hemorrhagic shock. In: Kim HW. *Hemoglobin-Based Oxygen Carriers as Red Cell Substitutes and Oxygen Therapeutics*. (2013). p. 411–33. doi: 10.1007/978-3-642-40717-8_24

16. Marques SM, Naves LM, Silva T de M. e, Cavalcante KVN, Alves JM, Ferreira-Neto ML, et al. Medullary noradrenergic neurons mediate hemodynamic responses to osmotic and volume challenges. *Front Physiol.* (2021) 12:381. doi: 10.3389/fphys.2021.649535
17. Loegering DJ. Humoral factor depletion and reticuloendothelial depression during hemorrhagic shock. *Am J Physiol März.* (1977) 232:H283–7. doi: 10.1152/ajpheart.1977.232.3.H283
18. Catania RA, Chaudry IH. Immunological consequences of trauma and shock. *Ann Acad Med Singapore.* (1999) 28:120–32.
19. Deitch EA. Animal models of sepsis and shock: a review and lessons learned. *Shock.* (1998) 9:1–11. doi: 10.1097/00024382-199801000-00001
20. Cabrales P, Tsai AG, Intaglietta M. Is resuscitation from hemorrhagic shock limited by blood oxygen-carrying capacity or blood viscosity? *Shock.* (2007) 27:380–9. doi: 10.1097/01.shk.0000239782.71516.ba
21. Kauvar DS, Baer DG, Dubick MA, Walters TJ. Effect of fluid resuscitation on acute skeletal muscle ischemia-reperfusion injury after hemorrhagic shock in rats. *J Am Coll Surg.* (2006) 202:888–96. doi: 10.1016/j.jamcollsurg.2006.03.003
22. Frankel DAZ, Acosta JA, Anjaria DJ, Porcides RD, Wolf PL, Coimbra R, et al. Physiologic response to hemorrhagic shock depends on rate and means of hemorrhage. *J Surg Res.* (2007) 143:276–80. doi: 10.1016/j.jss.2007.01.031
23. Kaplan LJ, Philbin N, Arnaud F, Rice J, Dong F, Freilich D. Resuscitation from hemorrhagic shock: fluid selection and infusion strategy drives unmeasured ion genesis. *J Trauma.* (2006) 61:90–8. doi: 10.1097/01.ta.0000222578.85413.4e
24. Awasthi V, Yee S-H, Jerabek P, Goins B, Phillips WT. Cerebral oxygen delivery by liposome-encapsulated hemoglobin: a positron-emission tomographic evaluation in a rat model of hemorrhagic shock. *J Appl Physiol Bethesda Md 1985.* (2007) 103:28–38. doi: 10.1152/japplphysiol.00136.2006
25. Truse R, Nolten I, Schulz J, Herminghaus A, Holtmanns T, Gördes L, et al. Topical melatonin improves gastric microcirculatory oxygenation during hemorrhagic shock in dogs but does not alter barrier integrity of Caco-2 monolayers. *Front Med.* (2020) 7:510. doi: 10.3389/fmed.2020.00510
26. Truse R, Smyk M, Schulz J, Herminghaus A, Weber APM, Mettler-Altmann T, et al. Regional hypothermia improves gastric microcirculatory oxygenation during hemorrhage in dogs. *PLoS ONE.* (2019) 14:e0226146. doi: 10.1371/journal.pone.0226146
27. Vollmer C, Weber APM, Wallenfang M, Hoffmann T, Mettler-Altmann T, Truse R, et al. Melatonin pretreatment improves gastric mucosal blood flow and maintains intestinal barrier function during hemorrhagic shock in dogs. *Microcirc.* (2017) 24:e12345. doi: 10.1111/micc.12345
28. Moochhala S, Wu J, Lu J. Hemorrhagic shock: an overview of animal models. *Front Biosci.* (2009) 14:4631–9. doi: 10.2741/3555
29. Gainer JL, Lipa MJ, Ficenec MC. Hemorrhagic shock in rats. *Lab Anim Sci.* (1995) 45:169–72.
30. Wiggers CJ. The present status of the shock problem. *Physiol Rev.* (1942) 22:74–123. doi: 10.1152/physrev.1942.22.1.74
31. Penfield WG. The treatment of severe and progressive hemorrhage by intravenous injections. *Am J Physiol.* (1919) 48:121–32. doi: 10.1152/ajplegacy.1919.48.1.121
32. De Santis P, De Fazio C, Franchi F, Bond O, Vincent J-L, Creteur J, et al. Incoherence between systemic hemodynamic and microcirculatory response to fluid challenge in critically Ill patients. *J Clin Med.* (2021) 10:507. doi: 10.3390/jcm10030507
33. Dunham CM, Siegel JH, Weireter L, Fabian M, Goodarzi S, Guadalupi P, et al. Oxygen debt and metabolic acidemia as quantitative predictors of mortality and the severity of the ischemic insult in hemorrhagic shock. *Crit Care Med.* (1991) 19:231–43. doi: 10.1097/00003246-199102000-00020
34. Rixen D, Raum M, Holzgraefe B, Sauerland S, Nagelschmidt M, Neugebauer EA, et al. A pig hemorrhagic shock model: oxygen debt and metabolic acidemia as indicators of severity. *Shock.* (2001) 16:239–44. doi: 10.1097/00024382-200116030-00012
35. Hannon JP, Wade CE, Bossone CA, Hunt MM, Loveday JA. Oxygen delivery and demand in conscious pigs subjected to fixed-volume hemorrhage and resuscitated with 75% NaCl in 6% Dextran. *Circ Shock.* (1989) 29:205–17.
36. Haase N, Perner A. Central venous oxygen saturation in septic shock - a marker of cardiac output, microvascular shunting and/or dysoxia? *Crit Care.* (2011) 15:184. doi: 10.1186/cc10314
37. Textoris J, Fouché L, Wiramus S, Antonini F, Tho S, Martin C, et al. High central venous oxygen saturation in the latter stages of septic shock is associated with increased mortality. *Crit Care.* (2011) 15:R176. doi: 10.1186/cc10325
38. Ortiz-Prado E, Dunn JF, Vasconez J, Castillo D, Viscor G. Partial pressure of oxygen in the human body: a general review. *Am J Blood Res.* (2019) 9:1–14.
39. Lempesis IG, van Meijel RLJ, Manolopoulos KN, Goossens GH. Oxygenation of adipose tissue: a human perspective. *Acta Physiol.* (2020) 228:e13298. doi: 10.1111/apha.13298
40. Soller B, Zou F, Prince M, Dubick M, Sondeen J. Comparison of noninvasive pH and blood lactate as predictors of mortality in a swine hemorrhagic shock with restricted volume resuscitation model. *Shock.* (2015) 44:90–5. doi: 10.1097/SHK.0000000000000307
41. Burris D, Rhee P, Kaufmann C, Pikoulis E, Austin B, Eror A, et al. Controlled resuscitation for uncontrolled hemorrhagic shock. *J Trauma.* (1999) 46:216–23. doi: 10.1097/00005373-199902000-00003
42. Stern S, Jwayyed S, Dronen S. Wang X. Resuscitation of severe uncontrolled hemorrhage: 75% sodium chloride/6% dextran 70 vs 09% sodium chloride. *Acad Emerg Med.* (2000) 7:847–56. doi: 10.1111/j.1553-2712.2000.tb02060.x
43. Tran A, Yates J, Lau A, Lampron J, Matar M. Permissive hypotension versus conventional resuscitation strategies in adult trauma patients with hemorrhagic shock: a systematic review and meta-analysis of randomized controlled trials. *J Trauma Acute Care Surg.* (2018) 84:802–8. doi: 10.1097/TA.0000000000001816
44. Mackway-Jones K, Foëx BA, Kirkman E, Little RA. Modification of the cardiovascular response to hemorrhage by somatic afferent nerve stimulation with special reference to gut and skeletal muscle blood flow. *J Trauma Acute Care Surg.* (1999) 47:481–5. doi: 10.1097/00005373-199909000-00008
45. Pierce A, Pittet J-F. Inflammatory response to trauma: implications for coagulation and resuscitation. *Curr Opin Anaesthesiol.* (2014) 27:246–52. doi: 10.1097/ACO.0000000000000047
46. Chaudry I, Wang P, Singh G, Hauptman J, Ayala A. Rat and mouse models of hypovolemic-traumatic shock (1993). In: Schlag G, Redl H, editors. *Pathophysiology of Shock, Sepsis, and Organ Failure*. Berlin, Heidelberg: Springer. doi: 10.1007/978-3-642-76736-4_28
47. Fülöp A, Turóczi Z, Garbaisz D, Harsányi L, Szijártó A. Experimental models of hemorrhagic shock: a review. *Eur Surg Res.* (2013) 50:57–70. doi: 10.1159/000348808
48. Eltzschig HK, Eckle T. Ischemia and reperfusion—from mechanism to translation. *Nat Med.* (2011) 17:1391–401. doi: 10.1038/nm.2507
49. Heusch G. Myocardial ischaemia–reperfusion injury and cardioprotection in perspective. *Nat Rev Cardiol.* (2020) 17:773–89. doi: 10.1038/s41569-020-0403-y
50. Singer M, Deutschman CS, Seymour CW, Shankar-Hari M, Annane D, Bauer M, et al. The third international consensus definitions for sepsis and septic shock (sepsis-3). *JAMA.* (2016) 315:801. doi: 10.1001/jama.2016.0287
51. SepNet Critical Care Trials Group. Incidence of severe sepsis and septic shock in German intensive care units: the prospective, multicentre INSEP study. *Intensive Care Med.* (2016) 42:1980–9. doi: 10.1007/s00134-016-4504-3
52. Dejager L, Pinheiro I, Dejonckheere E, Libert C. Cecal ligation and puncture: the gold standard model for polymicrobial sepsis? *Trends Microbiol.* (2011) 19:198–208. doi: 10.1016/j.tim.2011.01.001
53. Lewis AJ, Seymour CW, Rosengart MR. Current murine models of sepsis. *Surg Infect.* (2016) 17:385–93. doi: 10.1089/sur.2016.021
54. Chen P, Stanojcic M, Jeschke MG. Differences between murine and human sepsis. *Surg Clin North Am.* (2014) 94:1135–49. doi: 10.1016/j.suc.2014.08.001
55. Fisher CJ, Agosti JM, Opal SM, Lowry SF, Balk RA, Sadoff JC, et al. Treatment of septic shock with the tumor necrosis factor receptor: Fc fusion protein. *N Engl J Med.* (1996) 334:1697–702. doi: 10.1056/NEJM199606273342603
56. Remick DG, Ward PA. Evaluation of endotoxin models for the study of sepsis. *Shock.* (2005) 24:7–11. doi: 10.1097/01.shk.0000191384.34066.85
57. Rittirsch D, Hoesel LM, Ward PA. The disconnect between animal models of sepsis and human sepsis. *J Leukoc Biol.* (2007) 81:137–43. doi: 10.1189/jlb.0806542

58. Nakatani T, Sato T, Trump BF, Siegel JH, Kobayashi K. Manipulation of the size and clone of an intra-abdominal abscess in rats. *Res Exp Med.* (1996) 196:117–26. doi: 10.1007/BF02576833
59. Bosscha K, Nieuwenhuijs VB, Gooszen AW, van Duijvenbode-Beumer H, Visser MR, Verweij WR, et al. A standardised and reproducible model of intraabdominal infection and abscess formation in rats. *Eur J Surg Acta Chir.* (2000) 166:963–7. doi: 10.1080/110241500447146
60. Wegiel B, Larsen R, Gallo D, Chin BY, Harris C, Mannam P, et al. Macrophages sense and kill bacteria through carbon monoxide-dependent inflammasome activation. *J Clin Invest.* (2014) 124:4926–40. doi: 10.1172/JCI72853
61. Poli-de-Figueiredo LF, Garrido AG, Nakagawa N, Sannomiya P. Experimental models of sepsis and their clinical relevance. Shock. (2008) 30:53–9. doi: 10.1097/SHK.0b013e318181a343
62. Fink MP, Heard SO. Laboratory models of sepsis and septic shock. *J Surg Res.* (1990) 49:186–96. doi: 10.1016/0022-4804(90)90260-9
63. Ghanta S, Kwon M-Y, Perrella MA. Induction of sepsis *via* fibrin clot implantation. *Methods Mol Biol Clifton NJ.* (2021) 2321:17–25. doi: 10.1007/978-1-0716-1488-4_3
64. Vincent J-L, Rello J, Marshall J, Silva E, Anzueto A, Martin CD, et al. International study of the prevalence and outcomes of infection in intensive care units. *JAMA.* (2009) 302:2323–9. doi: 10.1001/jama.2009.1754
65. Dietert K, Gutbier B, Wienhold SM, Reppe K, Jiang X, Yao L, et al. Spectrum of pathogen- and model-specific histopathologies in mouse models of acute pneumonia. *PLoS ONE.* (2017) 12:e0188251. doi: 10.1371/journal.pone.0188251
66. Muñoz-Fontela C, Dowling WE, Funnell SGP, Gsell PS, Riveros-Balta AX, Albrecht RA, et al. Animal models for COVID-19. *Nature.* (2020) 586:509–15. doi: 10.1038/s41586-020-2787-6
67. Ahrenholz DH, Simmons RL. Fibrin in peritonitis. I Beneficial and adverse effects of fibrin in experimental E coli peritonitis. *Surgery.* (1980) 88:41–7.
68. Nichols RL, Smith JW, Balthazar ER. Peritonitis and intraabdominal abscess: an experimental model for the evaluation of human disease. *J Surg Res.* (1978) 25:129–34. doi: 10.1016/0022-4804(78)90066-5
69. Weinstein WM, Onderdonk AB, Bartlett JG, Gorbach SL. Experimental intra-abdominal abscesses in rats: development of an experimental model. *Infect Immun.* (1974) 10:1250–5. doi: 10.1128/iai.10.6.1250-1255.1974
70. Mathiak G, Szewczyk D, Abdullah F, Ovadia P, Feuerstein G, Rabinovici R. An improved clinically relevant sepsis model in the conscious rat. *Crit Care Med.* (2000) 28:1947–52. doi: 10.1097/00003246-200006000-00043
71. Natanson C, Fink MP, Ballantyne HK, MacVittie TJ, Conklin JJ, Parrillo JE. Gram-negative bacteremia produces both severe systolic and diastolic cardiac dysfunction in a canine model that simulates human septic shock. *J Clin Invest.* (1986) 78:259–70. doi: 10.1172/JCI112559
72. Volk HW, Schneider J, Dämmrich J, Döll W, Hörl M, Bruch HP. Animal model for chronic-abscess-forming peritonitis: histology and microbiology. *Eur Surg Res.* (1990) 22:347–55. doi: 10.1159/000129121
73. Starr ME, Steele AM, Saito M, Hacker BJ, Evers BM, Saito H, et al. New cecal slurry preparation protocol with improved long-term reproducibility for animal models of sepsis. Raju R, Herausgeber. *PLoS ONE.* (2014) 9:e115705. doi: 10.1371/journal.pone.0115705
74. Rincon JC, Efron PA, Moldawer LL, Larson SD. Cecal slurry injection in neonatal and adult mice. *Methods Mol Biol Clifton NJ.* (2021) 2321:27–41. doi: 10.1007/978-1-0716-1488-4_4
75. Drechsler S, Osuchowski M. Cecal ligation and puncture. *Methods Mol Biol Clifton NJ.* (2021) 2321:1–8. doi: 10.1007/978-1-0716-1488-4_1
76. Deitch EA. Rodent models of intra-abdominal infection. *Shock.* (2005) 24:19–23. doi: 10.1097/01.shk.0000191386.18818.0a
77. Osuchowski MF, Remick DG, Lederer JA, Lang CH, Aasen AO, Aibiki M, et al. Abandon the mouse research ship? Not just yet! *Shock.* (2014) 41:463–75. doi: 10.1097/SHK.0000000000000153
78. Zantl N, Uebe A, Neumann B, Wagner H, Siewert JR, Holzmann B, et al. Essential role of gamma interferon in survival of colon ascendens stent peritonitis, a novel murine model of abdominal sepsis. *Infect Immun.* (1998) 66:2300–9. doi: 10.1128/IAI.66.5.2300-2309.1998
79. Lustig MK, Bac VH, Pavlovic D, Maier S, Gründling M, Grisk O, et al. Colon ascendens stent peritonitis–a model of sepsis adopted to the rat: physiological, microcirculatory and laboratory changes. *Shock.* (2007) 28:59–64. doi: 10.1097/SHK.0b013e31802e454f
80. Herminghaus A, Picker O. Colon Ascendens Stent Peritonitis (CASP). *Methods Mol Biol Clifton NJ.* (2021) 2321:9–15. doi: 10.1007/978-1-0716-1488-4_2
81. Maier S, Traeger T, Entleutner M, Westerholt A, Kleist B, Hüser N, et al. Cecal ligation and puncture versus colon ascendens stent peritonitis: two distinct animal models for polymicrobial sepsis. *Shock.* (2004) 21:505–11. doi: 10.1097/01.shk.0000126906.52367.dd
82. Zingarelli B, Coopersmith CM, Drechsler S, Efron P, Marshall JC, Moldawer L, et al. Part I: Minimum Quality Threshold in Preclinical Sepsis Studies (MQTiPSS) for study design and humane modeling endpoints. *Shock.* (2019) 51:10–22. doi: 10.1097/SHK.0000000000001243
83. Ince C. Hemodynamic coherence and the rationale for monitoring the microcirculation. *Crit Care.* (2015) 19:S8. doi: 10.1186/cc14726
84. De Backer D, Creteur J, Preiser J-C, Dubois M-J, Vincent J-L. Microvascular blood flow is altered in patients with sepsis. *Am J Respir Crit Care Med.* (2002) 166:98–104. doi: 10.1164/rccm.200109-016OC
85. Sakr Y, Dubois M-J, De Backer D, Creteur J, Vincent J-L. Persistent microcirculatory alterations are associated with organ failure and death in patients with septic shock. *Crit Care Med.* (2004) 32:1825–31. doi: 10.1097/01.CCM.0000138558.16257.3F
86. Trzeciak S, McCoy JV, Phillip Dellinger R, Arnold RC, Rizzuto M, Abate NL, et al. Early increases in microcirculatory perfusion during protocol-directed resuscitation are associated with reduced multi-organ failure at 24 h in patients with sepsis. *Intensive Care Med.* (2008) 34:2210–7. doi: 10.1007/s00134-008-1193-6
87. De Backer D, Hollenberg S, Boerma C, Goedhart P, Büchele G, Ospina-Tascon G, et al. How to evaluate the microcirculation: report of a round table conference. *Crit Care.* (2007) 11:R101. doi: 10.1186/cc6118
88. Ince C, Boerma EC, Cecconi M, De Backer D, Shapiro NI, Duranteau J, et al. Second consensus on the assessment of sublingual microcirculation in critically ill patients: results from a task force of the European Society of Intensive Care Medicine. *Intensive Care Med.* (2018) 44:281–99. doi: 10.1007/s00134-018-5070-7
89. Anders HJ, Haedecke C, Sigl T, Krüger K. Avascular areas on nailfold capillary microscopy of patients with Wegener's granulomatosis. *Clin Rheumatol.* (2000) 19:86–8. doi: 10.1007/s100670050022
90. Tubiana-Rufi N, Priollet P, Lévy-Marchal C, Czernichow P. Detection by nailfold capillary microscopy of early morphologic capillary changes in children with insulin dependent diabetes mellitus. *Diabete Metab.* (1989) 15:118–22.
91. Groner W, Winkelman JW, Harris AG, Ince C, Bouma GJ, Messmer K, et al. Orthogonal polarization spectral imaging: a new method for study of the microcirculation. *Nat Med.* (1999) 5:1209–12. doi: 10.1038/13529
92. Goedhart PT, Khalilzada M, Bezemer R, Merza J, Ince C. Sidestream Dark Field (SDF) imaging: a novel stroboscopic LED ring-based imaging modality for clinical assessment of the microcirculation. *Opt Express.* (2007) 15:15101–14. doi: 10.1364/OE.15.015101
93. Sherman H, Klausner S, Cook WA. Incident dark-field illumination: a new method for microcirculatory study. *Angiology.* (1971) 22:295–303. doi: 10.1177/000331977102200507
94. Aykut G, Veenstra G, Scorcella C, Ince C, Boerma C. Cytocam-IDF (incident dark field illumination) imaging for bedside monitoring of the microcirculation. *Intensive Care Med Exp.* (2015) 3:4. doi: 10.1186/s40635-015-0040-7
95. Uz Z, van Gulik TM, Aydemirli MD, Guerci P, Ince Y, Cuppen D, et al. Identification and quantification of human microcirculatory leukocytes using handheld video microscopes at the bedside. *J Appl Physiol.* (2018) 124:1550–7. doi: 10.1152/japplphysiol.00962.2017
96. Bonner RF, Nossal R. Principles of laser-doppler flowmetry. In: Shepherd AP, Öberg PÅ, editors. *Laser-Doppler Blood Flowmetry. Developments in Cardiovascular Medicine*, vol 107. Boston, MA: Springer.
97. Krug A. Mikrozirkulation und Sauerstoffversorgung des Gewebes, Methode des so genannten O2C (oxygen to see). *Phlebologie.* (2007) 36:300–12. doi: 10.1055/s-0037-1622158

98. Tang W, Weil MH, Sun S, Noc M, Gazmuri RJ, Bisera J. Gastric intramural PCO2 as monitor of perfusion failure during hemorrhagic and anaphylactic shock. *J Appl Physiol.* (1994) 76:572–7. doi: 10.1152/jappl.1994.76.2.572
99. Futier E, Robin E, Jabaudon M, Guerin R, Petit A, Bazin J-E, et al. Central venous O_2 saturation and venous-to-arterial CO_2 difference as complementary tools for goal-directed therapy during high-risk surgery. *Crit Care.* (2010) 14:R193. doi: 10.1186/cc9310
100. Levy B, Gawalkiewicz P, Vallet B, Briancon S, Nace L, Bollaert P-E. Gastric capnometry with air-automated tonometry predicts outcome in critically ill patients. *Crit Care Med.* (2003) 31:474–80. doi: 10.1097/01.CCM.0000050445.48656.28
101. Mills A, Hodgen S. Fluorescent carbon dioxide indicators. In: Geddes CD, Lakowicz JR, editors. *Topics in Fluorescence Spectroscopy. Topics in Fluorescence Spectroscopy*, vol 9. Boston, MA: Springer.
102. Bar S, Fischer M-O. Regional capnometry to evaluate the adequacy of tissue perfusion. *J Thorac Dis.* (2019) 11:S1568–73. doi: 10.21037/jtd.2019.01.80
103. Severinghaus JW, Astrup P, Murray JF. Blood gas analysis and critical care medicine. *Am J Respir Crit Care Med.* (1998) 157:S114–122. doi: 10.1164/ajrccm.157.4.nhlb1-9
104. Schober P, Schwarte LA. From system to organ to cell: oxygenation and perfusion measurement in anesthesia and critical care. *J Clin Monit Comput.* (2012) 26:255–65. doi: 10.1007/s10877-012-9350-4
105. Gandjbakhche AH, Bonner RF, Arai AE, Balaban RS. Visible-light photon migration through myocardium in vivo. *Am J Physiol-Heart Circ Physiol.* (1999) 277:H698–704. doi: 10.1152/ajpheart.1999.277.2.H698
106. Clark LC. Measurement of oxygen tension: a historical perspective. *Crit Care Med.* (1981) 9:690–2. doi: 10.1097/00003246-198110000-00002
107. Clark LC, Wolf R, Granger D, Taylor Z. Continuous recording of blood oxygen tensions by polarography. *J Appl Physiol.* (1953) 6:189–93. doi: 10.1152/jappl.1953.6.3.189
108. De Backer D, Ospina-Tascon G, Salgado D, Favory R, Creteur J, Vincent J-L. Monitoring the microcirculation in the critically ill patient: current methods and future approaches. *Intensive Care Med.* (2010) 36:1813–25. doi: 10.1007/s00134-010-2005-3
109. Maier S, Hasibeder W, Pajk W, Hengl C, Ulmer H, Hausdorfer H, et al. Arginine-vasopressin attenuates beneficial norepinephrine effect on jejunal mucosal tissue oxygenation during endotoxinaemia. *BJA Br J Anaesth.* (2009) 103:691–700. doi: 10.1093/bja/aep239
110. Armbruster K, Nöldge-Schomburg GF, Dressler IM, Fittkau AJ, Haberstroh J, Geiger K. The effects of desflurane on splanchnic hemodynamics and oxygenation in the anesthetized pig. *Anesth Analg.* (1997) 84:271–7. doi: 10.1213/00000539-199702000-00007
111. Borisov SM, Zenkl G, Klimant I. Phosphorescent Platinum (II) and Palladium (II) Complexes with Azatetrabenzoporphyrins—new red laser diode-compatible indicators for optical oxygen sensing. *ACS Appl Mater Interfaces.* (2010) 2:366–74. doi: 10.1021/am900932z
112. Yan L, Wang X, Wang Y, Zhang Y, Li Y, Guo Z. Cytotoxic palladium (II) complexes of 8-aminoquinoline derivatives and the interaction with human serum albumin. *J Inorg Biochem.* 106:46–51 (2012). doi: 10.1016/j.jinorgbio.2011.09.032
113. Osellame LD, Blacker TS, Duchen MR. Cellular and molecular mechanisms of mitochondrial function. *Best Pract Res Clin Endocrinol Metab.* (2012) 26:711–23. doi: 10.1016/j.beem.2012.05.003
114. Mitchell P. Coupling of phosphorylation to electron and hydrogen transfer by a chemi-osmotic type of mechanism. *Nature.* (1961) 191:144–8. doi: 10.1038/191144a0
115. Pecinová A, Drahota Z, Nusková H, Pecina P, Houštěk J. Evaluation of basic mitochondrial functions using rat tissue homogenates. *Mitochondrion.* (2011) 11:722–8. doi: 10.1016/j.mito.2011.05.006
116. Benard G, Faustin B, Passerieux E, Galinier A, Rocher C, Bellance N, et al. Physiological diversity of mitochondrial oxidative phosphorylation. *Am J Physiol Cell Physiol.* (2006) 291:C1172–1182. doi: 10.1152/ajpcell.00195.2006
117. Gnaiger E, Aasander Frostner E, Abdul Karim N, Abumrad NA, Acuna-Castroviejo D, Adiele RC, et al. *Mitochondrial Respiratory States and Rates.* (2019). Available at: https://www.mitoeagle.org/index.php/Gnaiger_2019_MitoFit_Preprint_Arch
118. Li Z, Graham BH. Measurement of mitochondrial oxygen consumption using a clark electrode. In: Wong LJ, editors. *Mitochondrial Disorders. Methods in Molecular Biology (Methods and Protocols)*, vol 837 (2012). Totowa: Humana Press.
119. Simonnet H, Vigneron A, Pouysségur J. Chapter eight—conventional techniques to monitor mitochondrial oxygen consumption. *Meth Enzymol.* (2014) 542:151–61. doi: 10.1016/B978-0-12-416618-9.00008-X
120. Lahoti N, Jabbour RJ, Ariff B, Wang BX. Cardiac MRI in cardiomyopathies. *Future Cardiol.* (2021) 18:51–65. doi: 10.2217/fca-2020-0233
121. Pekar JJ, A. brief introduction to functional MRI. *IEEE Eng Med Biol Mag.* (2006) 25:24–6. doi: 10.1109/MEMB.2006.1607665
122. Miyazaki M, Akahane M. Non-contrast enhanced MR angiography: established techniques. *J Magn Reson Imaging.* (2012) 35:1–19. doi: 10.1002/jmri.22789
123. Bovenkamp PR, Brix T, Lindemann F, Holtmeier R, Abdurrachim D, Kuhlmann MT, et al. Velocity mapping of the aortic flow at 94 T in healthy mice and mice with induced heart failure using time-resolved three-dimensional phase-contrast. *MRI (4D PC MRI) Magma N Y N.* (2015) 28:315–27. doi: 10.1007/s10334-014-0466-z
124. Zhang JL, Lee VS. Renal perfusion imaging by MRI. *J Magn Reson Imaging JMRI.* (2020) 52:369–79. doi: 10.1002/jmri.26911
125. Hernandez-Garcia L, Lahiri A, Schollenberger J. Recent progress in ASL. *NeuroImage 15.* (2019) 187:3–16. doi: 10.1016/j.neuroimage.2017.12.095
126. Ferreira VM, Piechnik SK, CMR. Parametric mapping as a tool for myocardial tissue characterization. *Korean Circ J.* (2020) 50:658. doi: 10.4070/kcj.2020.0157
127. Flögel U, Schlüter A, Jacoby C, Temme S, Banga JP, Eckstein A, et al. Multimodal assessment of orbital immune cell infiltration and tissue remodeling during development of graves disease by 1H19F MRI. *Magn Reson Med.* (2018) 80:711–8. doi: 10.1002/mrm.27064
128. Haberkorn SM, Jacoby C, Ding Z, Keul P, Bönner F, Polzin A, et al. Cardiovascular magnetic resonance relaxometry predicts regional functional outcome after experimental myocardial infarction. *Circ Cardiovasc Imaging.* (2017) 10:e006025. doi: 10.1161/CIRCIMAGING.116.006025
129. Montant P, Sigovan M, Revel D, Douek P, MR. imaging assessment of myocardial edema with T2 mapping. *Diagn Interv Imaging.* (2015) 96:885–90. doi: 10.1016/j.diii.2014.07.008
130. Abbas Z, Gras V, Möllenhoff K, Oros-Peusquens A-M, Shah NJ. Quantitative water content mapping at clinically relevant field strengths: a comparative study at 15T and 3T. *NeuroImage.* (2015) 106:404–13. doi: 10.1016/j.neuroimage.2014.11.017
131. Noureddin M, Lam J, Peterson MR, Middleton M, Hamilton G, Le T-A, et al. Utility of magnetic resonance imaging versus histology for quantifying changes in liver fat in nonalcoholic fatty liver disease trials. *Hepatology.* (2013) 58:1930–40. doi: 10.1002/hep.26455
132. Yu H, Buch K, Li B, O'Brien M, Soto J, Jara H, et al. Utility of texture analysis for quantifying hepatic fibrosis on proton density MRI. *J Magn Reson Imaging.* (2015) 42:1259–65. doi: 10.1002/jmri.24898
133. Ling W, Regatte RR, Navon G, Jerschow A. Assessment of glycosaminoglycan concentration in vivo by chemical exchange-dependent saturation transfer (gagCEST). *Proc Natl Acad Sci 19.* (2008) 105:2266–70. doi: 10.1073/pnas.0707666105
134. Petz A, Grandoch M, Gorski DJ, Abrams M, Piroth M, Schneckmann R, et al. Cardiac hyaluronan synthesis is critically involved in the cardiac macrophage response and promotes healing after ischemia reperfusion injury. *Circ Res.* (2019) 124:1433–47. doi: 10.1161/CIRCRESAHA.118.313285
135. Tucci S, Flögel U, Sturm M, Borsch E, Spiekerkoetter U. Disrupted fat distribution and composition due to medium-chain triglycerides in mice with a β-oxidation defect. *Am J Clin Nutr.* (2011) 94:439–49. doi: 10.3945/ajcn.111.012948
136. Muñoz-Hernández MC, García-Martín ML. In Vivo 1H magnetic resonance spectroscopy (2018). In: García Martín M, López Larrubia P, editors. *Preclinical MRI. Methods in Molecular Biology*, vol 1718. New York, NY: Humana Press. doi: 10.1007/978-1-4939-7531-0_10
137. Flögel U, Jacoby C, Gödecke A, Schrader J. In vivo 2D mapping of impaired murine cardiac energetics in NO-induced heart failure. *Magn Reson Med.* (2007) 57:50–8. doi: 10.1002/mrm.21101
138. Thiaudière E, Biran M, Delalande C, Bouligand B, Canioni P. In vivo13C chemical shift imaging of the human liver. *Magn Reson Mater Phys Biol Med.* (1994) 2:425–8. doi: 10.1007/BF01705289

139. Gottwald E, Neubauer A, Schad LR. Tracking cellular functions by exploiting the paramagnetic properties of X-nuclei. assessment of cellular and organ function and dysfunction using direct and derived MRI methodologies. *IntechOpen*. (2016). Available online at: https://www.intechopen.com/chapters/52210
140. Konstandin S, Schad LR. 30 years of sodium/X-nuclei magnetic resonance imaging. *Magn Reson Mater Phys Biol Med.* (2014) 27:1–4. doi: 10.1007/s10334-013-0426-z
141. Hu R, Kleimaier D, Malzacher M, Hoesl MAU, Paschke NK, Schad LR. X-nuclei imaging: current state, technical challenges, and future directions. *J Magn Reson Imaging.* (2020) 51:355–76. doi: 10.1002/jmri.26780
142. Flögel U. *Moderne Magnetresonanzmethoden zur kardiovaskulären Phänotypisierung von Mäusen*. (2012). Available online at: https://docserv.uni-duesseldorf.de/servlets/DocumentServlet?id=23022 (accessed November 7, 2021).
143. NMR. *Periodic Table*. (2008-2013). Available online at: https://web.archive.org/web/20210507044647/http://triton.iqfr.csic.es/guide/eNMR/chem/NMRnuclei.html (accessed November 26, 2021).
144. Annane D, Bellissant E, Cavaillon J-M. Septic shock. *The Lancet*. (2005) 365:63–78. doi: 10.1016/S0140-6736(04)17667-8
145. Hierholzer C, Billiar TR. Molecular mechanisms in the early phase of hemorrhagic shock. *Langenbeck's Arch Surg.* (2001) 386:302–8. doi: 10.1007/s004230100242
146. Ahrens ET, Bulte JWM. Tracking immune cells in vivo using magnetic resonance imaging. *Nat Rev Immunol.* (2013) 13:755–63. doi: 10.1038/nri3531
147. Bulte JWM, Kraitchman DL. Iron oxide MR contrast agents for molecular and cellular imaging. *NMR Biomed.* (2004) 17:484–99. doi: 10.1002/nbm.924
148. Corot C, Robert P, Idée J-M, Port M. Recent advances in iron oxide nanocrystal technology for medical imaging. *Adv Drug Deliv Rev.* (2006) 58:1471–504. doi: 10.1016/j.addr.2006.09.013
149. Anzai Y, Prince MR, Chenevert TL, Maki JH, Londy F, London M, et al. MR angiography with an ultrasmall superparamagnetic iron oxide blood pool agent. *J Magn Reson Imaging.* (2005) 7:209–14. doi: 10.1002/jmri.1880070132
150. Grapentin C, Mayenfels F, Barnert S, Süss R, Schubert R, Temme S, et al. Optimization of perfluorocarbon nanoemulsions for molecular imaging by 19F MRI. In: *Nanomedicine*. Machester, UK: One Central Press (2014). p. 268–86.
151. Janjic JM, Ahrens ET. Fluorine-containing nanoemulsions for MRI cell tracking. *Wiley Interdiscip Rev Nanomed Nanobiotechnol.* (2009) 1:492–501. doi: 10.1002/wnan.35
152. Srinivas M, Boehm-Sturm P, Figdor CG, de Vries IJ, Hoehn M. Labeling cells for in vivo tracking using 19F MRI. *Biomaterials.* (2012) 33:8830–40. doi: 10.1016/j.biomaterials.2012.08.048
153. Longmaid HE. 3rd, Adams DF, Neirinckx RD, Harrison CG, Brunner P, Seltzer SE, et al. In vivo 19F NMR imaging of liver, tumor, and abscess in rats preliminary results. *Invest Radiol.* (1985) 20:141–5. doi: 10.1097/00004424-198503000-00009
154. Flögel U, Ding Z, Hardung H, Jander S, Reichmann G, Jacoby C, et al. In vivo monitoring of inflammation after cardiac and cerebral ischemia by fluorine magnetic resonance imaging. *Circulation.* (2008) 118:140–8. doi: 10.1161/CIRCULATIONAHA.107.737890
155. Ebner B, Behm P, Jacoby C, Burghoff S, French BA, Schrader J, et al. Early assessment of pulmonary inflammation by 19F MRI in vivo. *Circ Cardiovasc Imaging.* (2010) 3:202–10. doi: 10.1161/CIRCIMAGING.109.902312
156. Flögel U, Burghoff S, van Lent PLEM, Temme S, Galbarz L, Ding Z, et al. Selective activation of adenosine A2A receptors on immune cells by a CD73-dependent prodrug suppresses joint inflammation in experimental rheumatoid arthritis. *Sci Transl Med.* (2012) 4:146ra108. doi: 10.1126/scitranslmed.3003717
157. Flögel U, Su S, Kreideweiss I, Ding Z, Galbarz L, Fu J, et al. Noninvasive detection of graft rejection by in vivo (19) F MRI in the early stage. *Am J Transplant.* (2011) 11:235–44. doi: 10.1111/j.1600-6143.2010.03372.x
158. Jacoby C, Borg N, Heusch P, Sauter M, Bönner F, Kandolf R, et al. Visualization of immune cell infiltration in experimental viral myocarditis by 19F MRI in vivo. *Magn Reson Mater Phys Biol Med.* (2014) 27:101–6. doi: 10.1007/s10334-013-0391-6
159. Temme S, Yakoub M, Bouvain P, Yang G, Schrader J, Stegbauer J, et al. Beyond vessel diameters: non-invasive monitoring of flow patterns and immune cell recruitment in murine abdominal aortic disorders by multiparametric MRI. *Front Cardiovasc Med.* (2021) 8:1421. doi: 10.3389/fcvm.2021.750251
160. Balducci A, Helfer BM, Ahrens ET, O'Hanlon CF. 3rd, Wesa AK. Visualizing arthritic inflammation and therapeutic response by fluorine-19 magnetic resonance imaging (19F MRI). *J Inflamm.* (2012) 9:24. doi: 10.1186/1476-9255-9-24
161. Gaudet JM, Hamilton AM, Chen Y, Fox MS, Foster PJ. Application of dual (19) F and iron cellular MRI agents to track the infiltration of immune cells to the site of a rejected stem cell transplant. *Magn Reson Med.* (2017) 78:713–20. doi: 10.1002/mrm.26400
162. Hertlein T, Sturm V, Kircher S, Basse-Lusebrink T, Haddad D, Ohlsen K, et al. Visualization of abscess formation in a murine thigh infection model of Staphylococcus aureus by 19F-magnetic resonance imaging (MRI). *PLoS ONE.* (2011) 6:e18246. doi: 10.1371/journal.pone.0018246
163. Hitchens TK, Ye Q, Eytan DF, Janjic JM, Ahrens ET, Ho C. (19F MRI detection of acute allograft rejection with in vivo perfluorocarbon labeling of immune cells. *Magn Reson Med.* (2011) 65:1144–53. doi: 10.1002/mrm.22702
164. Shin SH, Kadayakkara DK, Bulte JWM. In Vivo 19F MR imaging cell tracking of inflammatory macrophages and site-specific development of colitis-associated dysplasia. *Radiology.* (2017) 282:194–201. doi: 10.1148/radiol.2016152387
165. Waiczies H, Lepore S, Drechsler S, Qadri F, Purfurst B, Sydow K, et al. Visualizing brain inflammation with a shingled-leg radio-frequency head probe for 19F/1H MRI. *Sci Rep.* (2013) 3:1280. doi: 10.1038/srep01280
166. Weise G, Basse-Lusebrink TC, Kleinschnitz C, Kampf T, Jakob PM, Stoll G. In vivo imaging of stepwise vessel occlusion in cerebral photothrombosis of mice by 19F MRI. *PLoS ONE.* (2011) 6:e28143. doi: 10.1371/journal.pone.0028143
167. Zhong J, Narsinh K, Morel PA, Xu H, Ahrens ET. In vivo quantification of inflammation in experimental autoimmune encephalomyelitis rats using fluorine-19 magnetic resonance imaging reveals immune cell recruitment outside the nervous system. *PLoS ONE.* (2015) 10:e0140238. doi: 10.1371/journal.pone.0140238
168. Temme S, Jacoby C, Ding Z, Bönner F, Borg N, Schrader J, et al. Technical advance: monitoring the trafficking of neutrophil granulocytes and monocytes during the course of tissue inflammation by noninvasive 19F MRI. *J Leukoc Biol.* (2014) 95:689–97. doi: 10.1189/jlb.0113032
169. Ding Z, Temme S, Quast C, Friebe D, Jacoby C, Zanger K, et al. Epicardium-derived cells formed after myocardial injury display phagocytic activity permitting in vivo labeling and tracking. *Stem Cells Transl Med.* (2016) 5:639–50. doi: 10.5966/sctm.2015-0159
170. Ahrens ET, Flores R, Xu H, Morel PA. In vivo imaging platform for tracking immunotherapeutic cells. *Nat Biotechnol.* (2005) 23:983–7. doi: 10.1038/nbt1121
171. Janjic JM, Srinivas M, Kadayakkara DKK, Ahrens ET. Self-delivering nanoemulsions for dual fluorine-19 MRI and fluorescence detection. *J Am Chem Soc 1.* (2008) 130:2832–41. doi: 10.1021/ja077388j
172. Srinivas M, Morel PA, Ernst LA, Laidlaw DH, Ahrens ET. Fluorine-19 MRI for visualization and quantification of cell migration in a diabetes model. *Magn Reson Med.* (2007) 58:725–34. doi: 10.1002/mrm.21352
173. NMR Periodic *Table: Fluorine NMR*. (2008-2013). Available online at: https://web.archive.org/web/20200214134947/http://triton.iqfr.csic.es/guide/eNMR/chem/F.html (accessed November 26, 2021).
174. Partlow KC, Chen J, Brant JA, Neubauer AM, Meyerrose TE, Creer MH, et al. (19F magnetic resonance imaging for stem/progenitor cell tracking with multiple unique perfluorocarbon nanobeacons. *FASEB J.* (2007) 21:1647–54. doi: 10.1096/fj.06-6505com
175. Koshkina O, White PB, Staal AHJ, Schweins R, Swider E, Tirotta I, et al. Nanoparticles for "two color" 19F magnetic resonance imaging: Towards combined imaging of biodistribution and degradation. *J Colloid Interface Sci.* (2020) 565:278–87. doi: 10.1016/j.jcis.2019.12.083
176. Ashur I, Allouche-Arnon H, Bar-Shir A. Calcium fluoride nanocrystals: tracers for in vivo 19 F magnetic resonance imaging. *Angew Chem.* (2018) 57:7478–82. doi: 10.1002/anie.201800838

177. Schoormans J, Calcagno C, Daal MRR, Wüst RCI, Faries C, Maier A, et al. An iterative sparse deconvolution method for simultaneous multicolor 19 F-MRI of multiple contrast agents. *Magn Reson Med.* (2020) 83:228–39. doi: 10.1002/mrm.27926
178. Chirizzi C, Morasso C, Caldarone AA, Tommasini M, Corsi F, Chaabane L, et al. A bioorthogonal probe for multiscale imaging by 19F-MRI and raman microscopy: from whole body to single cells. *J Am Chem Soc.* (2021) 143:12253–60. doi: 10.1021/jacs.1c05250
179. Shusterman-Krush R, Tirukoti ND, Bandela AK, Avram L, Allouche-Arnon H, Cai X, et al. Single fluorinated agent for multiplexed 19 F-MRI with micromolar detectability based on dynamic exchange. *Angew Chem.* (2021) 60:15405–11. doi: 10.1002/anie.202100427
180. Temme S, Grapentin C, Quast C, Jacoby C, Grandoch M, Ding Z, et al. Noninvasive imaging of early venous thrombosis by 19F magnetic resonance imaging with targeted perfluorocarbon nanoemulsions. *Circulation*. (2015) 131:1405–14. doi: 10.1161/CIRCULATIONAHA.114.010962
181. Güden-Silber T, Temme S, Jacoby C, Flogel U. Biomedical (19)F MRI Using Perfluorocarbons. *Methods Mol Biol Clifton NJ.* (2018) 1718:235–57. doi: 10.1007/978-1-4939-7531-0_14
182. Krämer W, Grapentin C, Bouvain P, Temme S, Flögel U, Schubert R. Rational manufacturing of functionalized, long-term stable perfluorocarbon-nanoemulsions for site-specific 19F magnetic resonance imaging. *Eur J Pharm Biopharm.* (2019) 142:114–22. doi: 10.1016/j.ejpb.2019.06.014
183. Wang X, Temme S, Grapentin C, Palasubramaniam J, Walsh A, Krämer W, et al. Fluorine-19 magnetic resonance imaging of activated platelets. *J Am Heart Assoc.* (2020) 9:e016971. doi: 10.1161/JAHA.120.016971
184. Temme S, Baran P, Bouvain P, Grapentin C, Krämer W, Knebel B, et al. Synthetic cargo internalization receptor system for nanoparticle tracking of individual cell populations by fluorine magnetic resonance imaging. *ACS Nano*. (2018) 12:11178–92. doi: 10.1021/acsnano.8b05698
185. Straub T, Nave J, Bouvain P, Akbarzadeh M, Dasa SSK, Kistner J, et al. MRI-based molecular imaging of epicardium-derived stromal cells (EpiSC) by peptide-mediated active targeting. *Sci Rep.* (2020) 10:21669. doi: 10.1038/s41598-020-78600-y
186. Flögel U, Temme S, Jacoby C, Oerther T, Keul P, Flocke V, et al. Multi-targeted 1H/19F MRI unmasks specific danger patterns for emerging cardiovascular disorders. *Nat Commun.* (2021) 12:5847. doi: 10.1038/s41467-021-26146-6
187. Hermann S, Kuhlmann MT, Starsichova A, Eligehausen S, Schäfers K, Stypmann J, et al. Imaging reveals the connection between spontaneous coronary plaque ruptures, atherothrombosis, and myocardial infarctions in HypoE/SRBI–/– Mice. *J Nucl Med 1.* (2016) 57:1420–7. doi: 10.2967/jnumed.115.171132
188. Rosengarten B, Walberer M, Allendoerfer J, Mueller C, Schwarz N, Bachmann G, et al. LPS-induced endotoxic shock does not cause early brain edema formation—an MRI study in rats. *Inflamm Res.* (2008) 57:479–83. doi: 10.1007/s00011-008-8042-5
189. Petejova N, Martinek A, Zadrazil J, Kanova M, Klementa V, Sigutova R, et al. Acute kidney injury in septic patients treated by selected nephrotoxic antibiotic agents-pathophysiology and biomarkers—a review. *Int J Mol Sci.* (2020) 21:E7115. doi: 10.3390/ijms21197115
190. Dear JW, Kobayashi H, Jo S-K, Holly MK, Hu X, Yuen PST, et al. Dendrimer-enhanced MRI as a diagnostic and prognostic biomarker of sepsis-induced acute renal failure in aged mice. *Kidney Int.* (2005) 67:2159–67. doi: 10.1111/j.1523-1755.2005.00321.x
191. Weidensteiner C, Reichard W, Struck J, Kirchherr A, Wagner K, Wagner F, von Elverfeldt D. Analysis of kidney function and therapy monitoring with DCE-MRI in a murine model of septic shock. *Proc of ISMRM*. (2018). Available at: https://index.mirasmart.com/ISMRM2018/PDFfiles/4599.html
192. Towner RA, Garteiser P, Bozza F, Smith N, Saunders D. d'Avila JCP, et al. In vivo detection of free radicals in mouse septic encephalopathy using molecular MRI and immuno-spin trapping. *Free Radic Biol Med.* (2013) 65:828–37. doi: 10.1016/j.freeradbiomed.2013.08.172
193. Fujii H, Wan X, Zhong J, Berliner LJ, Yoshikawa K. In vivo imaging of spin-trapped nitric oxide in rats with septic shock: MRI spin trapping. *Magn Reson Med.* (1999) 42:235–9. 3.0. doi: 10.1002/(SICI)1522-2594(199908)42:2<235::AID-MRM4>3.0.CO;2-Y
194. Marzi I, Bauer C, Hower R, Bühren V. Leukocyte-endothelial cell interactions in the liver after hemorrhagic shock in the rat. *Circ Shock.* (1993) 40:105–14.
195. Hunt JP, Hunter CT, Brownstein MR, Ku J, Roberts L, Currin RT, et al. Alteration in Kupffer cell function after mild hemorrhagic shock. *Shock.* (2001) 15:403–7. doi: 10.1097/00024382-200115050-00012
196. Veith NT, Histing T, Menger MD, Pohlemann T, Tschernig T. Helping prometheus: liver protection in acute hemorrhagic shock. *Ann Transl Med.* (2017) 5:206. doi: 10.21037/atm.2017.03.109
197. Matot I, Cohen K, Pappo O, Barash H, Abramovitch R. Liver response to hemorrhagic shock and subsequent resuscitation: MRI analysis. *Shock.* (2008) 29:16–24. doi: 10.1097/shk.0b013e3180556964
198. Maier M, Hahn P, Schneider G, Marzi I. Magnetic resonance imaging (MRI) for non-invasive analysis of hepatic function after hemorrhagic shock in the rat. *Eur J Trauma.* (2006) 32:449–55. doi: 10.1007/s00068-006-6031-3
199. Boerma EC, van der Voort PHJ, Spronk PE, Ince C. Relationship between sublingual and intestinal microcirculatory perfusion in patients with abdominal sepsis. *Crit Care Med.* (2007) 35:1055–60. doi: 10.1097/01.CCM.0000259527.89927.F9
200. Shen L, Uz Z, Ince C, van Gulik T. Alterations in intestinal serosal microcirculation precipitated by the Pringle manoeuvre. *BMJ Case Rep.* (2019) 12:e228111. doi: 10.1136/bcr-2018-228111
201. Uz Z, Ince C, Shen L, Ergin B, van Gulik TM. Real-time observation of microcirculatory leukocytes in patients undergoing major liver resection. *Sci Rep.* (2021) 11:4563. doi: 10.1038/s41598-021-83677-0
202. Potter EK, Hodgson L, Creagh-Brown B, Forni LG. Manipulating the microcirculation in sepsis—the impact of vasoactive medications on microcirculatory blood flow: a systematic review. *Shock.* (2019) 52:5–12. doi: 10.1097/SHK.0000000000001239
203. Boerma EC, Ince C. The role of vasoactive agents in the resuscitation of microvascular perfusion and tissue oxygenation in critically ill patients. *Intensive Care Med.* (2010) 36:2004–18. doi: 10.1007/s00134-010-1970-x
204. Bennett VA, Vidouris A, Cecconi M. Effects of Fluids on the Macro- and Microcirculations. *Crit Care.* (2018) 22:74. doi: 10.1186/s13054-018-1993-1
205. Mayevsky A, Rogatsky GG. Mitochondrial function in vivo evaluated by NADH fluorescence: from animal models to human studies. *Am J Physiol Cell Physiol.* (2007) 292:C615–640. doi: 10.1152/ajpcell.00249.2006
206. Lagerwaard B, Keijer J, McCully KK, de Boer VCJ, Nieuwenhuizen AG. In vivo assessment of muscle mitochondrial function in healthy, young males in relation to parameters of aerobic fitness. *Eur J Appl Physiol.* (2019) 119:1799–808. doi: 10.1007/s00421-019-04169-8
207. Mik EG, Johannes T, Zuurbier CJ, Heinen A, Houben-Weerts JHPM, Balestra GM, et al. In vivo mitochondrial oxygen tension measured by a delayed fluorescence lifetime technique. *Biophys J.* (2008) 95:3977–90. doi: 10.1529/biophysj.107.126094
208. Neu C, Baumbach P, Plooij AK, Skitek K, Götze J, von Loeffelholz C, et al. Non-invasive assessment of mitochondrial oxygen metabolism in the critically Ill patient using the protoporphyrin IX-triplet state lifetime technique—a feasibility study. *Front Immunol.* (2020) 11:757. doi: 10.3389/fimmu.2020.00757
209. Kemp GJ, Ahmad RE, Nicolay K, Prompers JJ. Quantification of skeletal muscle mitochondrial function by 31P magnetic resonance spectroscopy techniques: a quantitative review. *Acta Physiol.* (2015) 213:107–44. doi: 10.1111/apha.12307
210. Dadfar SM, Roemhild K, Drude NI, von Stillfried S, Knüchel R, Kiessling F, et al. Iron oxide nanoparticles: diagnostic, therapeutic and theranostic applications. *Adv Drug Deliv Rev.* (2019) 138:302–25. doi: 10.1016/j.addr.2019.01.005
211. Bönner F, Merx MW, Klingel K, Begovatz P, Flögel U, Sager M, et al. Monocyte imaging after myocardial infarction with 19F MRI at 3 T: a pilot

study in explanted porcine hearts. *Eur Heart J Cardiovasc Imaging.* (2015) 16:612–20. doi: 10.1093/ehjci/jev008

212. Rothe M, Jahn A, Weiss K, Hwang J-H, Szendroedi J, Kelm M, et al. In vivo 19F MR inflammation imaging after myocardial infarction in a large animal model at 3T. *Magma N Y N.* (2019) 32:5–13. doi: 10.1007/s10334-018-0714-8
213. Ahrens ET, Helfer BM, O'Hanlon CF, Schirda C. Clinical cell therapy imaging using a perfluorocarbon tracer and fluorine-19 MRI. *Magn Reson Med.* (2014) 72:1696–701. doi: 10.1002/mrm.25454
214. Castro CI, Briceno JC. Perfluorocarbon-based oxygen carriers: review of products and trials. *Artif Organs.* (2010) 34:622–34. doi: 10.1111/j.1525-1594.2009.00944.x
215. Bouvain P, Temme S, Flögel U. Hot spot 19F magnetic resonance imaging of inflammation. *Wiley Interdiscip Rev Nanomed Nanobiotechnol.* (2020) 12:e1639. doi: 10.1002/wnan.1639
216. Lin H, Tang X, Li A, Gao J. Activatable ^{19}F MRI nanoprobes for visualization of biological targets in living subjects. *Adv Mater.* (2021) 33:2005657. doi: 10.1002/adma.202005657

Conflict of Interest: The authors declare that the research was conducted in the absence of any commercial or financial relationships that could be construed as a potential conflict of interest.

Publisher's Note: All claims expressed in this article are solely those of the authors and do not necessarily represent those of their affiliated organizations, or those of the publisher, the editors and the reviewers. Any product that may be evaluated in this article, or claim that may be made by its manufacturer, is not guaranteed or endorsed by the publisher.

frontiers | Frontiers in Medicine

ORIGINAL RESEARCH
published: 30 June 2022
doi: 10.3389/fmed.2022.925433

Brain Histology and Immunohistochemistry After Resuscitation From Hemorrhagic Shock in Swine With Pre-Existing Atherosclerosis and Sodium Thiosulfate ($Na_2S_2O_3$) Treatment

*Nicole Denoix[1,2], Oscar McCook[2], Angelika Scheuerle[3], Thomas Kapapa[4], Andrea Hoffmann[2], Harald Gündel[1], Christiane Waller[5], Csaba Szabo[6], Peter Radermacher[2] and Tamara Merz[2]**

[1] Clinic for Psychosomatic Medicine and Psychotherapy, Ulm University Medical Center, Ulm, Germany, [2] Institute for Anesthesiological Pathophysiology and Process Engineering, Ulm University Medical Center, Ulm, Germany, [3] Division of Neuropathology, Institute for Pathology, Ulm University Medical Center, Ulm, Germany, [4] Clinic for Neurosurgery, Ulm University Medical Center, Ulm, Germany, [5] Department of Psychosomatic Medicine and Psychotherapy, Nuremberg General Hospital, Paracelsus Medical University, Nuremberg, Germany, [6] Department of Science and Medicine, University of Fribourg, Fribourg, Switzerland

OPEN ACCESS

Edited by:
Johanna Catharina Duvigneau,
University of Veterinary Medicine Vienna, Austria

Reviewed by:
Zhangle Hu,
Second Hospital of Anhui Medical University, China
Sandra Högler,
University of Veterinary Medicine Vienna, Austria

***Correspondence:**
Tamara Merz
tamara.merz@uni-ulm.de

Specialty section:
This article was submitted to Intensive Care Medicine and Anesthesiology, a section of the journal Frontiers in Medicine

Received: 21 April 2022
Accepted: 09 June 2022
Published: 30 June 2022

Citation:
Denoix N, McCook O, Scheuerle A, Kapapa T, Hoffmann A, Gündel H, Waller C, Szabo C, Radermacher P and Merz T (2022) Brain Histology and Immunohistochemistry After Resuscitation From Hemorrhagic Shock in Swine With Pre-Existing Atherosclerosis and Sodium Thiosulfate ($Na_2S_2O_3$) Treatment. Front. Med. 9:925433. doi: 10.3389/fmed.2022.925433

Background: The hydrogen sulfide (H_2S) and the oxytocin/oxytocin receptor (OT/OTR) systems interact in the central nervous and cardiovascular system. As a consequence of osmotic balance stress, H_2S stimulates OT release from the paraventricular nuclei (PVN) in the hypothalamic regulation of blood volume and pressure. Hemorrhagic shock (HS) represents one of the most pronounced acute changes in blood volume, which, moreover, may cause at least transient brain tissue hypoxia. Atherosclerosis is associated with reduced vascular expression of the main endogenous H_2S producing enzyme cystathionine-γ-lyase (CSE), and, hence, exogenous H_2S administration could be beneficial in these patients, in particular after HS. However, so far cerebral effects of systemic H_2S administration are poorly understood. Having previously shown lung-protective effects of therapeutic $Na_2S_2O_3$ administration in a clinically relevant, long-term, porcine model of HS and resuscitation we evaluated if these protective effects were extended to the brain.

Methods: In this study, available unanalyzed paraffin embedded brain sections ($Na_2S_2O_3$ $N = 8$ or vehicle $N = 5$) of our recently published HS study were analyzed *via* neuro-histopathology and immunohistochemistry for the endogenous H_2S producing enzymes, OT, OTR, and markers for brain injury and oxidative stress (glial fibrillary acidic protein (GFAP) and nitrotyrosine).

Results: Neuro-histopathological analysis revealed uninjured brain tissue with minor white matter edema. Protein quantification in the hypothalamic PVN showed no significant inter-group differences between vehicle or $Na_2S_2O_3$ treatment.

Conclusions: The endogenous H_2S enzymes, OT/OTR co-localized in magnocellular neurons in the hypothalamus, which may reflect their interaction in response to HS-induced hypovolemia. The preserved blood brain barrier (BBB) may have resulted in impermeability for $Na_2S_2O_3$ and no inter-group differences in the PVN. Nonetheless, our results do not preclude that $Na_2S_2O_3$ could have a therapeutic benefit in the brain in an injury that disrupts the BBB, e.g., traumatic brain injury (TBI) or acute subdural hematoma (ASDH).

Keywords: hydrogen sulfide, cystathionine-γ-lyase, cystathionine-β-synthase, oxytocin receptor, hypoxia, glial fibrillary acidic protein, nitrotyrosine, paraventricular nucleus

INTRODUCTION

Recently, we described lung-protective effects of therapeutic sodium thiosulfate ($Na_2S_2O_3$) administration in a clinically relevant, long-term, porcine model of hemorrhagic shock (HS) and resuscitation in swine with pre-existing atherosclerosis (1). The lung-protective effects comprised amelioration of shock-induced impairment of lung mechanics and gas exchange, and coincided with a significantly higher glucocorticoid receptor (GR) expression in the lung tissue of treated animals (1). It is not yet understood, to what extent relevant effects of systemic $Na_2S_2O_3$ administration reach the brain (2–4). However, exogenous hydrogen sulfide (H_2S) administration was shown to stimulate H_2S availability by upregulation of its endogenous enzymes cystathionine-γ-lyase (CSE) and cystathionine-β-synthase (CBS) (5, 6) as an adaptive stress response (7). In a previous study, we reported a significant reduction of CSE in the media of the coronary arteries in atherosclerotic pigs, which was further aggravated in circulatory shock (8). A reduction of CSE is implicated in barrier dysfunction in the kidney (9, 10) and reduced vascular H_2S availability (6). Therefore, $Na_2S_2O_3$ administration after HS may be beneficial for atherosclerotic patients since the lack of vascular H_2S production might be compensated by the exogenous administration. Moreover, H_2S and the oxytocin (OT)/ oxytocin receptor (OTR) systems interact in trauma in the heart and the brain (11–15) and are both reported to have anti-oxidative, and vasculo-protective effects (15). Hence, activation of either system could be beneficial in HS, since severe hypovolemia can induce at least transitory cerebral tissue hypoxia events (16–19), redox imbalance (20), barrier dysfunction (18, 21) and, upon resuscitation, ischemia/reperfusion (I/R) injury (22).

Interestingly, HS has been shown to induce OT release (23), and OTR upregulation was associated with protection against ischemic injury around the cerebral vasculature and was co-localized with glial fibrillary acidic protein (GFAP), an established marker of reactive astroglial cells, which are reported to be increased in regions of ischemic injury. Moreover, H_2S can stimulate hypothalamic release of OT in response to fluid deprivation in rats and osmotic challenge in uninjured rat hypothalamic explants, respectively (23, 24). Central to these observations is the paraventricular nucleus (PVN) (25) of the hypothalamus, the PVN is highly vascularized, protected by the BBB and adjacent to the third ventricle, (not to be confused with periventricular nucleus which lies below the third ventricle and does not have an effective BBB), as part of the hypothalamic-pituitary-adrenal axis (26), important interface in the regulation of fluid homeostasis (27) and site for cardiorespiratory output, blood pressure and heart rate regulation during hypoxia (23, 28). Thiosulfate can release H_2S under hypoxic conditions, thus we investigated $Na_2S_2O_3$ as a H_2S donor during resuscitated HS, since it is a clinically approved drug with a good safety profile and antioxidant properties (29–31).

Thiosulfate is proposed to be "a circulating 'carrier' molecule of beneficial effects of H_2S" (4, 30). Furthermore, $Na_2S_2O_3$ elicited neuroprotective effects in a rodent global cerebral ischemia model (4) and its therapeutic efficacy has been shown in other *in vivo* models of organ failure and cardiovascular dysfunction (31, 32). We therefore investigated the effects of $Na_2S_2O_3$ on the brain, and how the H_2S and OT/OTR systems in swine with pre-existing atherosclerosis are regulated after HS and resuscitation. The hypothalamic PVN was investigated, since H_2S and OT are known to interact in the hypothalamic regulation of fluid homeostasis and HS represents the most drastic shift in blood volume after trauma. The data presented are a post hoc analysis of material available from the above-mentioned previous study (1).

MATERIALS AND METHODS

The present study is a *post-hoc* analysis of post mortem brain tissue sections obtained from the previous study of Datzmann et al. (1). Experiments were conducted after approval by the Federal Authorities for Animal Research (Regierungspräsidium Tübingen; Reg.-Nr. 1341, date of approval May 2, 2017), and the local University of Ulm Animal Care Committee, in adherence to the National Institute of Health Guidelines on the Use of Laboratory Animals and the European Union "Directive 2010/63/EU on the protection of animals used for scientific purposes." Anesthesia, surgical instrumentation, as well as the protocol of hemorrhage and resuscitation have been described in detail previously (1). Briefly, induction of HS was performed by passive blood withdrawal of 30% of the calculated total blood volume. Hemorrhage was titrated to a targeted mean arterial pressure of 40 ± 5 mmHg for 3 h. Resuscitation of the animals included shed blood re-transfusion,

TABLE 1 | Primary antibodies (anti-human) to sus scrofa Protein BLAST search.

Primary antibody (source, catalog No., RRID)	Host species	Query cover	Homology	Immunogen sequence	Concentration used for IHC
anti-CSE (Protein Tech, 12217-1-AP, AB_2087497)	Rabbit Polyclonal	100 %	87.05 %	Gamma cystathionase fusion protein Ag2872	1:200
anti-CBS (Protein Tech, 14787-1-AP, AB_2070970)	Rabbit Polyclonal	100 %	90.46 %	CBS fusion protein Ag6437	1:100
anti-OT (Millipore, AB911, AB_2157629)	Rabbit Polyclonal	100 %	100 %	CYIQNCPLG (Synthetic oxytocin (Sigma) conjugated to thyroglobulin)	1:500
anti-OTR (Protein Tech, 23045-1-AP, AB_2827425)	Rabbit Polyclonal	92 %	83.05 %	Oxytocin Receptor fusion protein Ag19074	1:100
anti-GFAP (Abcam, ab7260, AB_305808)	Rabbit Polyclonal	100 %	92.13 %	full length GFAP sequence UniProt ID: 14136	1:2500

fluid administration (balanced electrolyte solutions), vasopressor support (norepinephrine) based on need to restore mean arterial pressure to baseline values, and lung-protective mechanical ventilation. Sodium thiosulfate ($Na_2S_2O_3$) (Dr. Franz Köhler Chemie GmbH, Bensheim, Germany, 25%, diluted in 500 mL NaCl 0.9%; infusion rate 0.1 $g{\cdot}kg^{-1} \cdot h^{-1}$) ($N = 8$) or the vehicle solution (2 $mL{\cdot}kg^{-1} \cdot h^{-1}$) ($N = 5$) was administered during the first 24 h of re-transfusion. After 72 h of intensive care treatment or premature termination of the experiment due to pre-defined termination criteria (acute respiratory distress syndrome, refractory hypotension), pigs were sacrificed under further deepened anesthesia, by injection of potassium chloride, and the brain was immediately removed (1).

Experimental Protocol

Available porcine brain tissue sections from a recently published HS study (1) were analyzed in this study. Brain sections from seven female and six castrated male "Familial Hypercholesterolemia Bretoncelles Meishan" (FBM) pigs with median (interquartile range) body weight of 58 (49, 66) kg and age of 24 (23, 28) months, were investigated. These FBM pigs are a model for "human-like coronary atherosclerosis" (8, 33, 34). Group assignment was performed randomly, irrespective of sex.

Neuro-Histophathology and Immunohistochemistry

All brains were identically fixed in 4% formalin for 6days, dissected into 4 mm thick consecutive coronal sections: frontal to occipital. If the macroscopic section was too large to fit as a whole into the embedding cassette (26 x 31 x 4 mm) they were laid flat and further dissected in up to five pieces in a manner which allows for reconstruction of the entire section. For the purpose of this study the macroscopic section, which included the hypothalamus was selected for analysis. The tissue was then dehydrated and embedded in paraffin blocks. 3–5 µm sections, were deparaffinized in xylene, and rehydrated in a graded series of ethanol and deionized water. Hematoxylin and eosin (HE) staining was performed for general neuro-histophathological evaluation, an experienced neuro-histopathologist (AS) focused on determining if hypoxic events led to brain tissue injury in cortico-subcortical brain regions. Criteria to evaluate brain tissue injury included: morphology of nerve and glia cells, white matter and perivascular edema formation, necrosis of parenchyma and appearance of eosinophilic cells. Due to minor injury, descriptive evaluation was performed without quantification.

Immunohistochemical (IHC) analysis with a colorimetric detection system, as method of choice, allowed for visualizing tissue architecture, cellular morphology and cytoplasmic or nuclear protein localization, in the general landscape of the brain. Important here, by not homogenizing the tissue spatial expression patterns remain intact, and it is possible to distinguish e.g,. between vasculature (containing blood) and brain parenchyma, which is a known confounding factor in techniques requiring tissue homogenates.

IHC was performed as previously described (15). Briefly, after deparaffinizing, heat-induced antigen retrieval in citrate buffer (pH 6) was performed, followed by blocking with normal goat serum (10%) before incubating with the following primary antibodies: endogenous H_2S producing enzymes anti-cystathionine-γ-lyase (CSE) (Protein Tech, 12217-1-AP, RRID:AB_2087497) and anti-cystathionine-β-synthase (CBS) (Protein Tech, 14787-1-AP, RRID:AB_2070970), anti-OT (Millipore, AB911, RRID:AB_2157629), anti-OTR (Protein Tech, 23045-1-AP, RRID:AB_2827425), which were verified in porcine cerebral tissue previously by Denoix et al. (22), anti-GFAP (Abcam, ab7260, RRID:AB_305808) as a marker of cerebral injury, anti-pig Albumin (Abcam, ab79960,

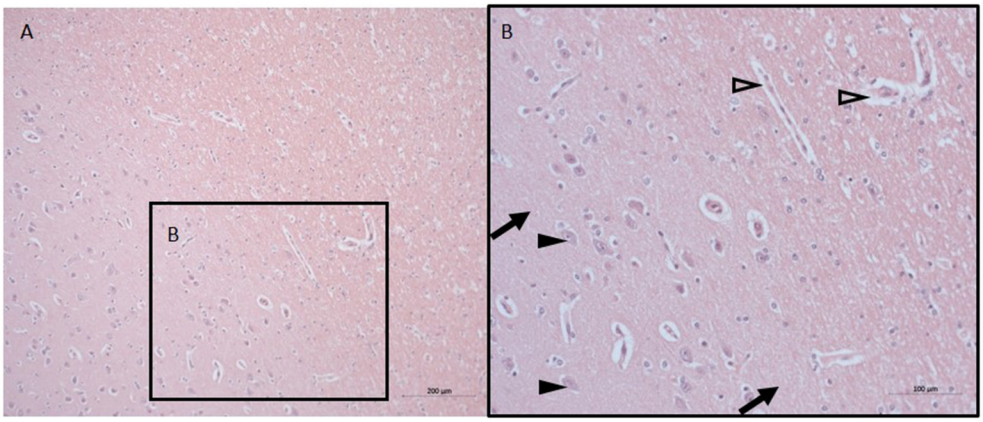

FIGURE 1 | Neuro-histopathological evaluation. Exemplary pictures of HE staining in cortico-subcortical brain tissue with signs of minor perivascular edema in sections from the same macroscopic sectional plane as the PVN at 10X **(A)** and 20X **(B)**. Black arrows point to intact parenchyma, black arrowheads depict nerve cells, open arrowheads point to minor perivascular edema. HE, Hematoxylin and eosin; PVN, paraventricular nucleus.

RRID:AB_1658916) as a marker of barrier dysfunction and anti-nitrotyrosine (Merck Millipore, ab5411, RRID:AB_177459), as a marker of oxidative and nitrosative stress, since NO can react with superoxide to peroxynitrite, leading to nitrotyrosine formation due to nitration of protein tyrosine residues (13). All primary antibodies were titrated to their optimal dilution according to the manufacturer recommendations (see **Table 1**). Negative controls were performed concurrently (15) by incubation with diluent instead of primary antibody in order to control for specificity of the secondary system, or, whenever available, we performed pre-incubation of the primary antibody with the respective immunogen peptide and incubated the brain tissue with the pre-absorbed primary antibody instead of normal primary antibody (15). Additionally, NCBI BLAST searches were performed in order to compare immunogen sequences of the used antibodies to the sus scrofa database (courtesy of the U.S. National Library of Medicine) (**Table 1**) to further confirm the specificity of the used primary antibodies.

Primary antibodies were detected via the Dako REAL detection system based on alkaline phosphatase conjugated secondary antibodies (anti-mouse; anti-rabbit) and visualized with a Fast Red-type chromogen followed by counterstaining with Mayer's hematoxylin (9, 10). A Zeiss Axio Imager A1 microscope with a 10X objective was used for visualizing the slides. Multiple 800,000-μm^2 sections were used for quantification of % positive area using the Zen Image Analysis Software (Zeiss). Data are presented as % positive area.

Statistical Analysis

Graph Pad Prism Version 8 was used for statistical analysis. Normal distribution was excluded with the Kolmogorov–Smirnov test and inter-group differences were analyzed with the Mann-Whitney rank sum test. The data are presented as median (quartiles) with interquartile ranges.

RESULTS

Minor Neuro-Histopathological Damage

The histopathological findings were minimal with signs of discrete swelling and minor perivascular edema in cortico-subcortical brain regions (in the same macroscopic sectional plane as the PVN, see **Figure 1**), otherwise the brain tissue looked histologically uninjured, presenting with normal appearing singular heterotopic ganglion cells, and intact parenchyma. There were no indications of blood brain barrier disruption.

Lack of Effect of $Na_2S_2O_3$ on CSE, CBS, OT, OTR, GFAP and Nitrotyrosine in the PVN

None of the proteins of interest showed any significant inter-group difference in the porcine hypothalamic PVN (**Figures 2–4**). The endogenous H_2S producing enzymes CSE, CBS, and OT and its receptor were present in the porcine hypothalamic PVN (**Figures 2**, **3**). CSE, CBS, OT and the OTR were found to be present in the magnocellular neurons of the PVN in consecutive sections of the porcine hypothalamus (35). GFAP was also present in the PVN of both groups (see **Figure 4**) but, again, did not show a significant inter-group difference. Nitrotyrosine showed negligible to no expression in the analyzed tissue specimens (vehicle: $n = 5$, 0.00[0.00; 0.00] %; $Na_2S_2O_3$: $n = 8$, 0.01[0.00; 0.03] %). No Albumin extravasation could be detected (data not shown).

DISCUSSION

The aim of this study was to investigate the protein levels of CSE, CBS, OT, and OTR in the PVN after HS-and resuscitation in a clinically relevant, long-term porcine model, since HS represents one of the most pronounced acute fluid shifts in blood volume. Given the fact that the H_2S and OT systems interact in trauma

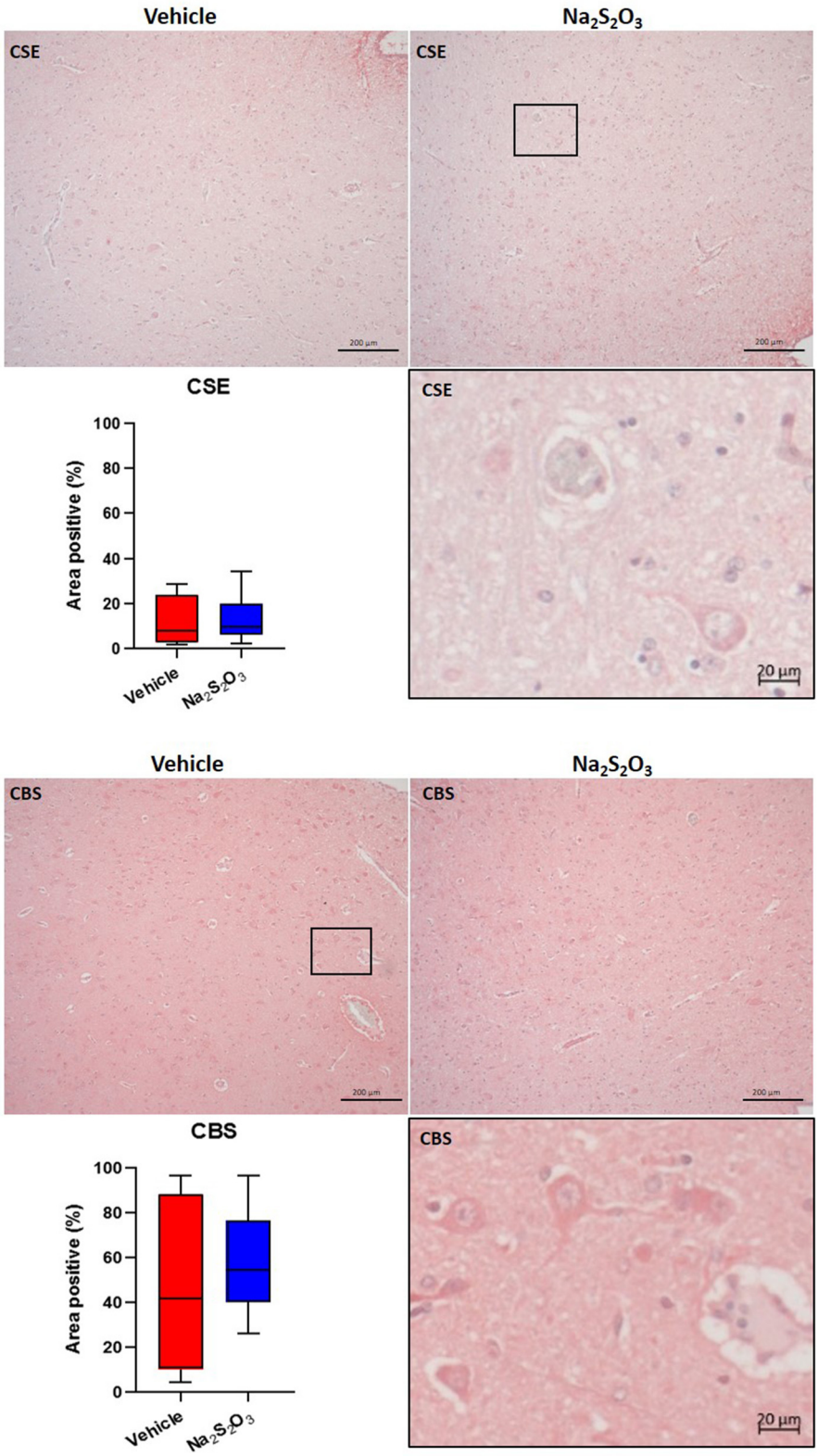

FIGURE 2 | H_2S producing enzymes in the porcine PVN. Quantification of the immunohistochemical stainings as positive percentage area in the PVN for CSE (vehicle: $n = 4$; $Na_2S_2O_3$: $n = 6$) and CBS (vehicle: $n = 5$; $Na_2S_2O_3$: $n = 7$). Boxes represent the interquartile ranges with the median (black line), whiskers represent minimum and maximum values. Exemplary immunohistochemical pictures of CSE and CBS in the PVN of vehicle and $Na_2S_2O_3$ treated animals (10X). Higher

(Continued)

FIGURE 2 | magnification pictures of CSE and CBS originate from the black box in the respective 10X picture. PVN, paraventricular nucleus; CSE, cystathionine-γ-lyase; CBS, cystathionine-β-synthase; $Na_2S_2O_3$, sodium thiosulfate.

(11–15) and in hypothalamic regulation of fluid homeostasis (23–28), we hypothesized that $Na_2S_2O_3$ would lead to changes in the expression of theses markers. The results in this porcine model of HS-and resuscitation, showed mostly uninjured brain tissue with minor perivascular edema in cortico-subcortical brain regions. Immunohistochemical data revealed that (i) the proteins of interest CSE, CBS, OT and OTR were all localized in the porcine PVN after HS, but in contrast to our underlying hypothesis, (ii) there were no significant differences in protein levels of CSE, CBS, OT, OTR, GFAP nor nitrotyrosine in the PVN of either group after HS.

Previously, we showed in atherosclerotic swine that CSE, CBS, OT and the OTR were found to be present in magnocellular neurons in consecutive sections of the porcine hypothalamus after HS, which may be indicative of their hypothalamic interaction in response to HS-induced hypovolemia (35). In rodents, there is evidence that $Na_2S_2O_3$ can reach the brain 90 min after intraperitoneal administration, as demonstrated by elevated $Na_2S_2O_3$ levels in plasma and brain tissue, mediating protective effects after neuronal I/R injury in un-resuscitated, young and otherwise healthy male mice (4). In our model of HS, we did not see the same results as in the previously mentioned I/R injury rodent model, which may be due to the fact that our large animal model included a pre-existing comorbidity and was resuscitated in an ICU, thus mimicking the human situation unlike the rodent model (4). In fact, the pig is a very relevant translational model: structurally very similar to the human brain, the presence of gyri and sulci (gyrencephalic brain), white matter to gray matter proportion and tentorium cerebelli, unlike in the rodent brain, is reflective of the human pathophysiology (36). Administration of $Na_2S_2O_3$ after brain injury in rodents stimulated H_2S availability by upregulation of CBS (5). In contrast, in this pig study, CSE, CBS and OT/OTR expression levels did not show any inter-group difference. Although the systemic blood sulfide levels were significantly higher in animals at 24 h of $Na_2S_2O_3$ administration compared to vehicle treated swine (1). Clearly, $Na_2S_2O_3$ administration had lung-protective effects and induced higher pulmonary GR expression, whereas the other visceral organs and blood cells were not affected (1). Organ specific pathophysiology has been shown in other models of circulatory shock, which led to the concept of compartmentalization, suggesting that there are differences in response patterns between single organs and systemic factors, as proposed by Cavallion et al. (37). The compartmentalization in the brain may be due in part to the blood brain barrier (BBB). The lack of effect of $Na_2S_2O_3$ on the evaluated parameters in the brain in our pig model may suggest its inability to cross the BBB, which is, in contrast to the aforementioned results in rodents, but would be, however, consistent with findings in humans that show that $Na_2S_2O_3$ does not cross the intact BBB (3, 38). In comparison to our applied dose of $Na_2S_2O_3$ (0.1 $g \cdot kg^{-1} \cdot h^{-1}$), even more than 5-fold higher doses of $Na_2S_2O_3$ did not cross the intact BBB in humans (3, 38). The lack of resuscitation in the reported rodent studies might have facilitated the breakdown of the BBB and thus allowed for $Na_2S_2O_3$ to cross the dysfunctional barrier and promote neuroprotective effects. These results, however, would not translate to the human clinical situation, which would always entail resuscitation to defined neuro-intensive care endpoints. The clinical scenario was closely replicated in the present large animal study, suggesting that the results presented here are very relevant observation for translational medicine. Based on previous data from rodent experiments, which show that exogenous H_2S administration can induce neuroprotective effects and the hypothalamic OT system and endogenous H_2S producing enzymes in response to fluid shifts (5, 23, 24, 27), we specifically looked for CSE, CBS, OT and OTR in the PVN with other markers, relevant to hypoxia, fluid shifts and injury (GFAP, Albumin and nitrotyrosine) after resuscitated HS with and without systemic $Na_2S_2O_3$ administration and could not find significant effects. Our negative findings, though disappointing, assume significance in the light of the many successful unresuscitated rodent pre-clinical trials that ultimately failed to translate to the clinic in neurotrauma research (15, 36).

It remains to be elucidated whether the $Na_2S_2O_3$-mediated neuroprotective effects (observed *in vitro* and in *in vivo* experiments in young and otherwise healthy male mice) as well as the stimulating effect of H_2S on OT release within the hypothalamus during osmotic balance stress (observed in healthy, fluid deprived rats or uninjured, brain explants osmotically challenged), are translatable into large animals or humans (4, 23, 24). Long-term studies in large animals, which focus on the brain after HS, are scarce and report impaired cerebral microcirculation and perfusion pressure, increase in cerebrovascular resistance, altered energy metabolism and BBB dysfunction due to damaged astroglial cells immediately after blood loss (18, 39). GFAP expression is reported to increase in ischemic events, but there was no difference in GFAP expression between vehicle and $Na_2S_2O_3$ treated animals after HS in the current study. To the best of our knowledge, reports on HS-induced histopathological changes or protein expression variations after profound tissue hypoxia in adult porcine brain tissue are lacking. Most large animal studies, either perform a combination of HS and acute brain injury or cardiac arrest, which indicates a "no-flow" instead of a "low-flow" state and are therefore not comparable to our results (40, 41). Large animal studies that specifically investigate cerebral effects of HS often lack post HS intensive care (42). Although it has been shown for both pigs and rodents that implementation of resuscitative measures effectively preserves the BBB (43), which was also the case in our study, as indicated by the lack of albumin extravasation. The existing literature about HS alone without brain injury does not seem to result in major morphological damage (42), which is in agreement with our findings. Histopathological examination of brain sections in

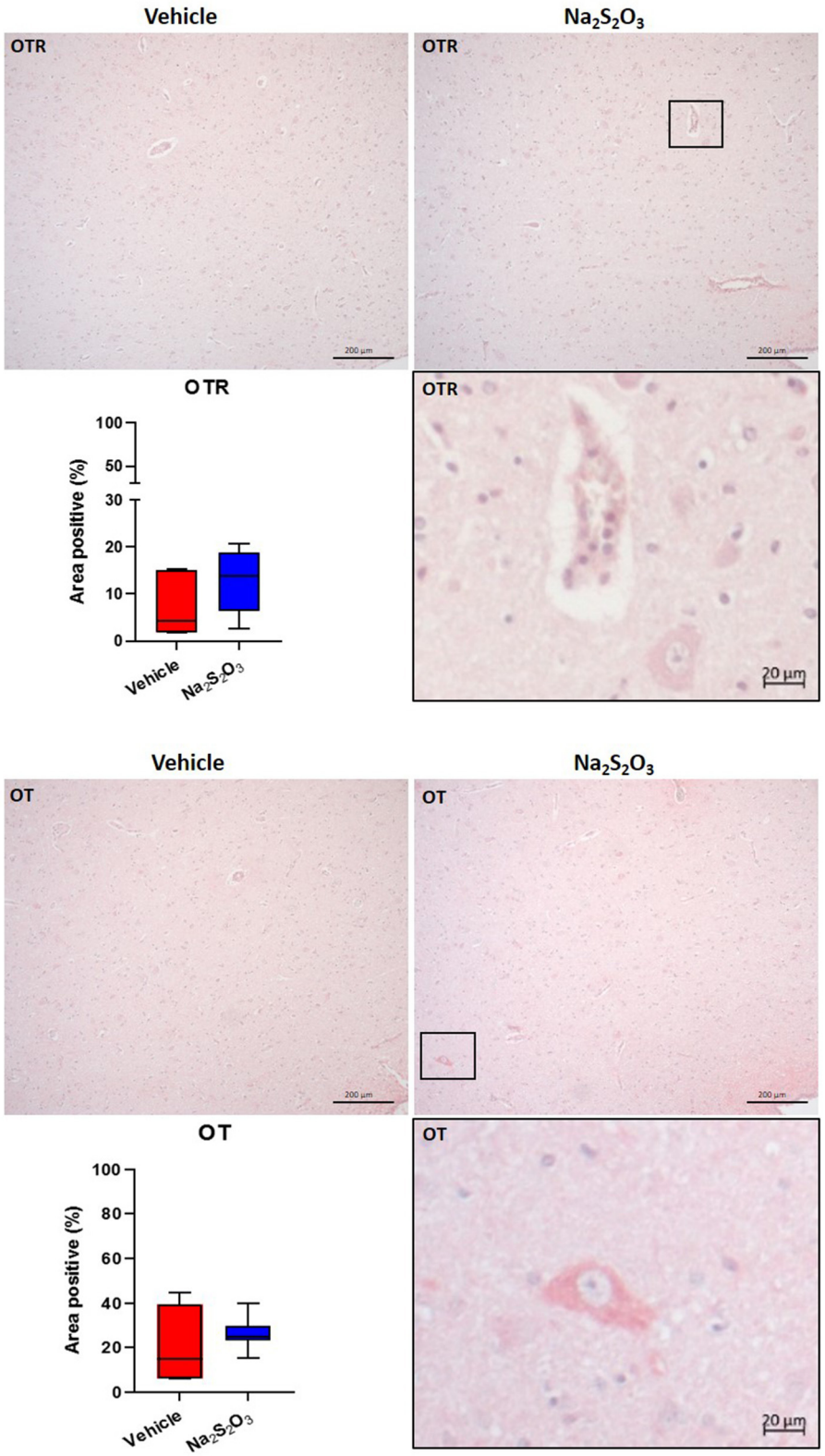

FIGURE 3 | OTR and OT in the porcine PVN. Quantification of the immunohistochemical stainings as positive percentage area in the PVN for the OTR (vehicle: $n = 5$; $Na_2S_2O_3$: $n = 7$) and OT (vehicle: $n = 5$; $Na_2S_2O_3$: $n = 7$). Boxes represent the interquartile ranges with the median (black line), whiskers represent minimum and maximum values. Exemplary immunohistochemical pictures of the OTR and OT in the PVN of vehicle and $Na_2S_2O_3$ treated animals (10X). Higher magnification pictures of the OTR and OT originate from the black box in the respective 10X picture. OT, oxytocin; OTR, oxytocin receptor; $Na_2S_2O_3$, sodium thiosulfate.

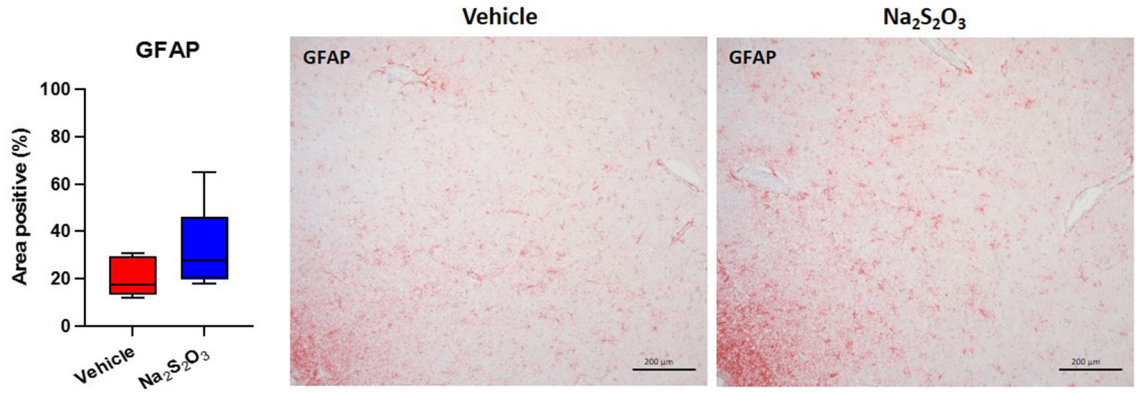

FIGURE 4 | GFAP in the porcine PVN. Quantification of the immunohistochemical stainings as positive percentage area in the PVN for GFAP (vehicle: $n = 5$; $Na_2S_2O_3$: $n = 8$). Boxes represent the interquartile ranges with the median (black line), whiskers represent minimum and maximum values. Exemplary immunohistochemical pictures of GFAP in the PVN of vehicle and $Na_2S_2O_3$ treated animals (10X). PVN, paraventricular nucleus; GFAP, glial fibrillary acidic protein; $Na_2S_2O_3$, sodium thiosulfate.

this study revealed generally uninjured brain tissue morphology with only minor perivascular edema in cortico-subcortical brain regions.

Hypoxia-induced cellular injury can start immediately with hemodynamic decompensation (18, 20) and may cause damage that is first visible on protein level. We recently characterized the gyrencephalic porcine brain after acute subdural hematoma with concomitant pressure-induced brain injury and BBB disruption (15). CBS, OT and the OTR were more localized at the injury site, whereas CSE was constitutively expressed in the uninjured brain tissue and reduced at the injury site (15). In the present study we now quantified protein levels in the PVN after a massive drop in blood volume, which revealed that OT and the OTR are present in the porcine PVN, and that CBS is generally expressed in higher quantity than CSE.

Limitations of the Study

The present study was a *post-hoc* analysis of brain tissue from a previous experiment. The brain was not a target organ to be investigated in the original study. Thus, no brain monitoring was performed and we cannot comment on how the cerebral perfusion pressure and/or cerebral blood flow have been affected by the hemorrhagic shock. It may well-be, that cerebral autoregulation prevented any effect of the lower MAP on cerebral perfusion.

CONCLUSION

We found neither neuro-histopathological differences, nor differences in the pattern or levels of CSE, CBS, OT, OTR, GFAP nor nitrotyrosine in the porcine PVN between $Na_2S_2O_3$ and vehicle administration after HS-and resuscitation. These findings are in contrast to the findings in unresuscitated rodents and may be indicative of the reason the neurotrauma pre-clinical trials in rodents have failed to translate to the clinic. The presence of CSE, CBS, OTR and OT in magnocellular neurons of the porcine hypothalamus may reflect their interaction in response to HS-induced hypovolemia (35). The lack of inter-group differences in the PVN may be attributed to the organ-specific compartmentalization due to preserved impermeability of the intact BBB for $Na_2S_2O_3$ as observed in humans. Nonetheless, our results do not preclude that $Na_2S_2O_3$ could have a therapeutic benefit in the brain in an injury that disrupts the BBB, e.g., traumatic brain injury (TBI), acute subdural hematoma (ASDH), asphyxiation or "no flow" scenarios such as cardiopulmonary resuscitation.

DATA AVAILABILITY STATEMENT

The raw data supporting the conclusions of this article will be made available by the authors, without undue reservation.

ETHICS STATEMENT

The animal study was reviewed and approved by Regierungspräsidium Tübingen; Reg.-Nr. 1341, date of approval May 2, 2017.

AUTHOR CONTRIBUTIONS

ND performed the immunohistochemistry, data analysis and interpretation, and drafting of the manuscript. AH performed animal experiments and removal of the brain during the necropsy. AS performed the neuro-histopathological evaluation with ND and helped with data interpretation, critical comments, and expert feedback on the manuscript. CS, CW, HG, and TK contributed critical comments and expert feedback on the manuscript. OM and TM contributed to the experimental design, supervising immunohistochemistry, data interpretation, and writing of the manuscript. PR contributed to the study design and edited and approved the final version of the

manuscript. All authors read and approved the final version of the manuscript.

FUNDING

This research was funded by the Deutsche Forschungsgemeinschaft (DFG), grant number Project-ID 251293561 – Collaborative Research Center (CRC) 1149, the German Ministry of Defense, and an unrestricted research grant from the Dr. Franz Köhler Chemie GmbH, Bensheim, Germany. The funder was not involved in the study design, collection, analysis, interpretation of data, the writing of this article, or the decision to submit it for publication. All authors declare no other competing interests.

ACKNOWLEDGMENTS

We thank Rosy Engelhardt and Andrea Seifritz for their skillful technical assistance.

REFERENCES

1. Datzmann T, Hoffmann A, McCook O, Merz T, Wachter U, Preuss J, et al. Effects of sodium thiosulfate ($Na_2S_2O_3$) during resuscitation from hemorrhagic shock in swine with preexisting atherosclerosis. *Pharmacol Res.* (2020) 151:104536. doi: 10.1016/j.phrs.2019.104536
2. Marutani E, Ichinose F: Emerging pharmacological tools to control hydrogen sulfide signaling in critical illness. *Intensive Care Med Exp.* (2020). 8:5. doi: 10.1186/s40635-020-0296-4
3. Neuwelt EA, Gilmer-Knight K, Lacy C, Nicholson HS, Kraemer DF, Doolittle ND. Hornig GW,: Toxicity profile of delayed high dose sodium thiosulfate in children treated with carboplatin in conjunction with blood-brain-barrier disruption. *Pediatr Blood Cancer.* (2006) 47:174–82. doi: 10.1002/pbc.20529
4. Marutani E, Yamada M, Ida T, Tokuda K, Ikeda K, Kai S, et al. Thiosulfate mediates cytoprotective effects of hydrogen sulfide against neuronal ischemia. *J Am Heart Assoc.* (2015) 4:e002125. doi: 10.1161/JAHA.115.002125
5. Shan H, Qiu J, Chang P, Chu Y, Gao C. Wang Het al: Exogenous hydrogen sulfide offers neuroprotection on intracerebral hemorrhage injury through modulating endogenous H[[sb]]2[[/s]]S metabolism in mice. *Front Cell Neurosci.* (2019) 13:349. doi: 10.3389/fncel.2019.00349
6. Bucci M, Vellecco V, Cantalupo A, Brancaleone V, Zhou Z, Evangelista S, et al. Hydrogen sulfide accounts for the peripheral vascular effects of zofenopril independently of ACE inhibition. *Cardiovasc Res.* (2014) 102:138–47. doi: 10.1093/cvr/cvu026
7. McCook O, Radermacher P, Volani C, Asfar P, Ignatius A, Kemmler J, et al. H_2S during circulatory shock: some unresolved questions. *Nitric Oxide.* (2014) 41:48–61. doi: 10.1016/j.niox.2014.03.163
8. Merz T, Stenzel T, Nußbaum B, Wepler M, Szabo C, Wang R, et al. Cardiovascular disease and resuscitated septic shock lead to the downregulation of the H_2S-producing enzyme cystathionine-γ-lyase in the porcine coronary artery. *Intensive Care Med Exp.* (2017) 5:17. doi: 10.1186/s40635-017-0131-8
9. Stenzel T, Weidgang C, Wagner K, Wagner F, Gröger M, Weber S, et al. Association of kidney tissue barrier disrupture and renal dysfunction in resuscitated murine septic shock. *Shock.* (2016) 46:398–404. doi: 10.1097/SHK.0000000000000599
10. Merz T, Wepler M, Nußbaum B, Vogt J, Calzia E, Wang R, et al. Cystathionine-γ-lyase expression is associated with mitochondrial respiration during sepsis-induced acute kidney injury in swine with atherosclerosis. *Intensive Care Med Exp.* (2018) 6:43. doi: 10.1186/s40635-018-0208-z
11. Merz T, Lukaschewski B, Wigger D, Rupprecht A, Wepler M, Gröger M, et al. Interaction of the hydrogen sulfide system with the oxytocin system in the injured mouse heart. *Intensive Care Med Exp.* (2018) 6:41. doi: 10.1186/s40635-018-0207-0
12. Wigger DC, Gröger N, Lesse A, Krause S, Merz T, Gündel H, et al. Maternal separation induces long-term alterations in the cardiac oxytocin receptor and cystathionine γ-lyase expression in mice. *Oxid Med Cell Longev.* (2020) 2020:4309605. doi: 10.1155/2020/4309605
13. Nußbaum BL, McCook O, Hartmann C, Matallo J, Wepler M, Antonucci E, et al. Left ventricular function during porcine-resuscitated septic shock with pre-existing atherosclerosis. Intensive care Med Exp 4:14, 2016 erratum in: Intensive Care. *Med Exp.* (2016) 4:18. doi: 10.1186/s40635-016-0092-3
14. Merz T, Denoix N, Wigger D, Waller C, Wepler M, Vettorazzi S, et al. The role of glucocorticoid receptor and oxytocin receptor in the septic heart in a clinically relevant, resuscitated porcine model with underlying atherosclerosis. *Front Endocrinol.* (2020) 11:299. doi: 10.3389/fendo.2020.00299
15. Denoix N, Merz T, Unmuth S, Hoffmann A, Nespoli E, Scheuerle A, et al. Cerebral immunohistochemical characterization of the H_2S and the oxytocin systems in a porcine model of acute subdural hematoma. *Front Neurol.* (2020) 11:649. doi: 10.3389/fneur.2020.00649
16. Taccone FS, De Backer D. Is cerebral microcirculation really preserved in shock states? *Crit Care Med.* (2010) 38:1008–9. doi: 10.1097/CCM.0b013e3181d16958
17. Nistor M, Behringer W, Schmidt M, Schiffner R. A systematic review of neuroprotective strategies during hypovolemia and hemorrhagic shock. *Int J Mol Sci.* (2017) 18:2247. doi: 10.3390/ijms18112247
18. Ida KK, Otsuki DA, Sasaki AT, Borges ES, Castro LU, Sanches TR, et al. Effects of terlipressin as early treatment for protection of brain in a model of haemorrhagic shock. *Crit Care.* (2015) 19:107. doi: 10.1186/s13054-015-0825-9
19. Jakobsen RP, Nielsen TH. Mølstrøm, S, Nordström CH, Granfeldt A, Toft P: Moderately prolonged permissive hypotension results in reversible metabolic perturbation evaluated by intracerebral microdialysis - an experimental animal study. *Intensive Care Med Exp.* (2019) 7:67. doi: 10.1186/s40635-019-0282-x
20. Ida KK, Chisholm KI, Malbouisson LMS, Papkovsky DB, Dyson A, Singer M, et al. Protection of cerebral microcirculation, mitochondrial function, and electrocortical activity by small-volume resuscitation with terlipressin in a rat model of haemorrhagic shock. *Br J Anaesth.* (2018) 120:1245–54. doi: 10.1016/j.bja.2017.11.074
21. Lin KH, Liu CL, Kuo WW, Paul CR, Chen WK, Wen SY, et al. Early fluid resuscitation by lactated Ringer's solution alleviate the cardiac apoptosis in rats with trauma-hemorrhagic shock. PLoS One 11:e0165406, 2016 Erratum for. *PLoS ONE.* (2016) 11:e0168419. doi: 10.1371/journal.pone.0168419
22. Schiffner R, Bischoff SJ, Lehmann T, Rakers F, Rupprecht S, Reiche J, et al. Redistribution of cerebral blood flow during severe hypovolemia and reperfusion in a sheep model: critical role of α1-adrenergic signaling. *Int J Mol Sci.* (2017) 18:1031. doi: 10.3390/ijms18051031
23. Coletti R, Almeida-Pereira G, Elias LL, Antunes-Rodrigues J. Effects of hydrogen sulfide (H_2S) on water intake and vasopressin and oxytocin secretion induced by fluid deprivation. *Horm Behav.* (2015) 67:12–20. doi: 10.1016/j.yhbeh.2014.11.008
24. Coletti R, de Lima JBM, Vechiato FMV, de Oliveira FL, Debarba LK, Almeida-Pereira G, et al. Nitric oxide acutely modulates hypothalamic and neurohypophyseal carbon monoxide and hydrogen sulphide production to control vasopressin, oxytocin and atrial natriuretic peptide release in rats. *J Neuroendocrinol.* (2019) 31:e12686. doi: 10.1111/jne.12686
25. Rankin SL, Partlow GD, McCurdy RD, Giles ED, Fisher KR. Postnatal neurogenesis in the vasopressin and oxytocin-containing nucleus of the pig hypothalamus. *Brain Res.* (2003) 971:189–96. doi: 10.1016/S0006-8993(03)02350-3
26. Zhu XY, Gu H, Ni X. Hydrogen sulfide in the endocrine and reproductive systems. *Expert Rev Clin Pharmacol.* (2011) 4:75–82. doi: 10.1586/ecp.10.125

27. Ruginsk SG, Mecawi AS, da Silva MP, Reis WL, Coletti R, de Lima JB, et al. Gaseous modulators in the control of the hypothalamic neurohypophyseal system. *Physiology (Bethesda).* (2015) 30:127–38. doi: 10.1152/physiol.00040.2014
28. Horn EM, Waldrop TG. Oxygen-sensing neurons in the caudal hypothalamus and their role in cardiorespiratory control. *Respir Physiol.* (1997) 110:219–28. doi: 10.1016/S0034-5687(97)00086-8
29. Snijder PM, Frenay AR, de Boer RA, Pasch A, Hillebrands JL, Leuvenink HG, et al. Exogenous administration of thiosulfate, a donor of hydrogen sulfide, attenuates angiotensin II-induced hypertensive heart disease in rats. *Br J Pharmacol.* (2015) 172:1494–504. doi: 10.1111/bph.12825
30. Merz T, Denoix N, Wepler M, Gäßler H, Messerer DAC, Hartmann C, et al. H_2S in acute lung injury: a therapeutic dead end(?). *Intensive Care Med Exp*. (2020). 8:33. doi: 10.1186/s40635-020-00324-0
31. Szabo C, Papapetropoulos A. Pharmacological modulation of H_2S levels: H_2S donors and H_2S biosynthesis inhibitors. *Pharmacol Rev.* (2017) 69:497–564. doi: 10.1124/pr.117.014050
32. Sakaguchi M, Marutani E, Shin HS, Chen W, Hanaoka K, Xian M, et al. Sodium thiosulfate attenuates acute lung injury in mice. *Anesthesiology.* (2014) 121:1248–57. doi: 10.1097/ALN.0000000000000456
33. Hartmann C, Loconte M, Antonucci E, Holzhauser M, Hölle T, Katzsch D, et al. Effects of hyperoxia during resuscitation from hemorrhagic shock in swine with preexisting coronary artery disease. *Crit Care Med.* (2017) 45:e1270–1279. doi: 10.1097/CCM.0000000000002767
34. Matějková Š, Scheuerle A, Wagner F, McCook O, Matallo J, Gröger M, et al. Carbamylated erythropoietin-FC fusion protein and recombinant human erythropoietin during porcine kidney ischemia/reperfusion injury. *Intensive Care Med.* (2013) 39:497–510. doi: 10.1007/s00134-012-2766-y
35. Denoix N, McCook O, Ecker S, Wang R, Waller C, Radermacher P, et al. The interaction of the endogenous hydrogen sulfide and oxytocin systems in fluid regulation and the cardiovascular system. *Antioxidants (Basel).* (2020) 9:748. doi: 10.3390/antiox9080748
36. McCook O, Scheuerle A, Denoix N, Kapapa T, Radermacher P, Merz T: Localization of the hydrogen sulfide and oxytocin systems at the depth of the sulci in a porcine model of acute subdural hematoma. *Neural Regen Res*. (2021) 16:2376–82. doi: 10.4103/1673-5374.313018
37. Cavaillon JM, Annane D. Compartmentalization of the inflammatory response in sepsis and SIRS. *J Endotoxin Res.* (2006) 12:151–70. doi: 10.1179/096805106X102246
38. Neuwelt EA, Brummett RE, Doolittle ND, Muldoon LL, Kroll RA, Pagel MA, et al. First evidence of otoprotection against carboplatin-induced hearing loss with a two-compartment system in patients with central nervous system malignancy using sodium thiosulfate. *J Pharmacol Exp Ther.* (1998) 286:77–84.
39. Rise IR, Kirkeby OJ. Effect of cerebral ischaemia on the cerebrovascular and cardiovascular response to haemorrhage. *Acta Neurochir (Wien).* (1998) 140:699–706. doi: 10.1007/s007010050165
40. Sharma HS, Miclescu A, Wiklund L. Cardiac arrest-induced regional blood-brain barrier breakdown, edema formation and brain pathology: a light and electron microscopic study on a new model for neurodegeneration and neuroprotection in porcine brain. *J Neural Transm.* (2011) 118:87–114. doi: 10.1007/s00702-010-0486-4
41. Nikolian VC, Georgoff PE, Pai MP, Dennahy IS, Chtraklin K, Eidy H, et al. Valproic acid decreases brain lesion size and improves neurologic recovery in swine subjected to traumatic brain injury, hemorrhagic shock, and polytrauma. *J Trauma Acute Care Surg.* (2017) 83:1066–73. doi: 10.1097/TA.0000000000001612
42. Bronshvag MM. Cerebral pathophysiology in hemorrhagic shock. Nuclide scan data, fluorescence microscopy, and anatomic correlations. *Stroke.* (1980) 11:50–9. doi: 10.1161/01.STR.11.1.50
43. Meybohm P, Gruenewald M, Zacharowski KD, Albrecht M, Lucius R, Fösel N, et al. Mild hypothermia alone or in combination with anesthetic post-conditioning reduces expression of inflammatory cytokines in the cerebral cortex of pigs after cardiopulmonary resuscitation. *Crit Care.* (2010) 14:R21. doi: 10.1186/cc8879

Conflict of Interest: The authors declare that the research was conducted in the absence of any commercial or financial relationships that could be construed as a potential conflict of interest.

Publisher's Note: All claims expressed in this article are solely those of the authors and do not necessarily represent those of their affiliated organizations, or those of the publisher, the editors and the reviewers. Any product that may be evaluated in this article, or claim that may be made by its manufacturer, is not guaranteed or endorsed by the publisher.

Advantages of publishing in Frontiers

OPEN ACCESS
Articles are free to read for greatest visibility and readership

FAST PUBLICATION
Around 90 days from submission to decision

HIGH QUALITY PEER-REVIEW
Rigorous, collaborative, and constructive peer-review

TRANSPARENT PEER-REVIEW
Editors and reviewers acknowledged by name on published articles

Frontiers
Avenue du Tribunal-Fédéral 34
1005 Lausanne | Switzerland

Visit us: www.frontiersin.org
Contact us: frontiersin.org/about/contact

REPRODUCIBILITY OF RESEARCH
Support open data and methods to enhance research reproducibility

DIGITAL PUBLISHING
Articles designed for optimal readership across devices

FOLLOW US
@frontiersin

IMPACT METRICS
Advanced article metrics track visibility across digital media

EXTENSIVE PROMOTION
Marketing and promotion of impactful research

LOOP RESEARCH NETWORK
Our network increases your article's readership